

---

# DEVELOPING NEUROIMAGING BIOMARKERS OF BLAST- INDUCED TRAUMATIC BRAIN INJURY

---

**Adriana M. Azor**

**Imperial College London**

Dyson School of Design Engineering

&

The Computational, Cognitive and Clinical Neuroimaging Laboratory (C<sup>3</sup>NL) –

Department of Brain Sciences

*This thesis is submitted for the degree of Doctor of Philosophy*

## **Copyright declaration**

The copyright of this thesis rests with the author. Unless otherwise indicated, its contents are licensed under a Creative Commons Attribution-NonCommercial 4.0 International Licence (CC BY-NC).

Under this licence, you may copy and redistribute the material in any medium or format. You may also create and distribute modified versions of the work. This is on the condition that: you credit the author and do not use it, or any derivative works, for a commercial purpose.

When reusing or sharing this work, ensure you make the licence terms clear to others by naming the licence and linking to the licence text.

Where a work has been adapted, you should indicate that the work has been changed and describe those changes. Please seek permission from the copyright holder for uses of this work that are not included in this licence or permitted under UK Copyright Law.

## **Statement of originality**

The work within this thesis is my own except where otherwise referenced.

The data presented in chapter 3 and 6 are a collation of data collected as part of work conducted within C<sup>3</sup>NL and provided by Dr Amy Jolly who helped collect the data.

The data presented in chapter 4 and 5 are a collection of data previously presented in Dr David Baxter's PhD thesis and collected through the BIOSAP (Blast Injury Outcome Study in Armed Forces Personnel) project at C<sup>3</sup>NL. Immunohistochemistry results included in the discussion of the chapters were obtained from Prof Gentleman's lab.

*This thesis is dedicated to the memory of the victims of the Beirut explosion that tragically shook our beautiful city on August 4<sup>th</sup>, 2020.*

*May you find eternal peace.*

Do not be afraid of those who kill the  
body but cannot kill the soul.  
- Matthew 10:28

## Acknowledgment

To my supervisors Mazdak and Dave, for welcoming me into your teams, for guiding me and advising me, for your knowledge and your support throughout my PhD, and for all the opportunities you gave me and the trust you put in me, thank you, and to Pete, for being a mentor and for always pushing me forward, for being an ear and a brain when I needed one, and for always trying to help me reach my goal, thank you.

To the teams of C3NL and Head Lab (Siamak, Harry, Hazel, Amy, you know yourselves) and to the new team at KCL, for your support, the friendships, the lunches, conversations, and sometimes even tears we shared, thank you.

To my parents, who have been the reason for everything and the driving force behind every single one of my accomplishments, for giving me strength and the chance to reach for the stars and chase my dreams, no matter where it takes me, for teaching me to be faithful and hopeful, and for your unwavering love, thank you. You have made me who I am today, and who I thrive to be every day.

To my younger siblings, Sabrina and Georges, for being my biggest source of inspiration, and for being the reason I always try to be a better person and never give up on my dreams, for our virtual game nights during the pandemic, our laughs and even our small fights, thank you. I hope to always make you proud.

To my grandmother, who's the source of my curiosity and creativity, who's been inspiring me and encouraging me since day 1, who has taught me to always find a beautiful story in every single thing I do, who encourages me to be a strong and independent woman, thank you.

And to Carl, words are never enough. You have been my rock and my support through the years. You give me something to look forward to. Your strength, your optimism and your ambitions have inspired me every minute of every day. It hurt to be apart for more than 5 years, but wherever you were on this planet, it always felt like you were right here holding my hand. Thank you for everything, and I can't wait for the next chapter of our lives together. I love you.

To all of you, who have made this journey possible, I am eternally indebted and grateful, from the bottom of my heart.

# ABSTRACT

---

In the past two decades, the awareness of the physical and emotional effects and sequelae of traumatic brain injuries (TBI) has grown considerably, especially in the case of soldiers returning from their deployment in Iraq and Afghanistan, after sustaining blast-induced TBI (bTBI). While the understanding of bTBI and how it compares to civilian non-blast TBI is essential for proper prevention, diagnosis and treatment, it is currently limited, especially in human in-vivo studies.

Developing neuroimaging biomarkers of bTBI is key in understanding primary blast injury mechanism. I therefore investigated the patterns of white matter and grey matter injuries that are specific to bTBI and aren't commonly seen in civilians who suffered from head trauma using advanced neuroimaging techniques. However, because of significant methodological issues and limitations, I developed and tested a new pipeline capable of running the analysis of white matter abnormalities in soldiers, called subject-specific diffusion segmentation (SSDS). I also used standard methodologies to investigate changes at the level of the grey matter structures, and more particularly the limbic system. Finally, I trained a machine learning algorithm that builds decision trees with the aim of classifying between patients with TBI and controls, and between different TBI mechanisms as an example of what could potentially be applied in the context of bTBI.

I found three main neuroimaging biomarkers specific to bTBI. The first one is a microstructural white matter abnormality at the level of the middle cerebellar peduncle, characterized by a decrease of diffusivity measures. The second is also a decrease in diffusivity properties, at the level of the white matter boundary, and the third one is a loss of hippocampal volume, with no association to post-traumatic stress disorder. Finally, I demonstrated that SSDS can be used in tandem with a machine learning algorithm for potential diagnosis of TBI with high accuracy. These findings provide mechanistic insights into bTBI and the effect of primary blast injuries on the human brain. This work also identifies important neuroimaging biomarkers that might facilitate prevention and diagnosis in soldiers who suffered from bTBI.

## List of abbreviations

AIS	Abbreviated injury scale
BBR	Boundary-based registration
BCC	Body of the corpus callosum
BET	Brain-extraction tool
bTBI	Blast-related traumatic brain injury
COV	Coefficient of variation
CSF	Cerebral spinal fluid
CT	Computed tomography
CTE	Chronic traumatic encephalopathy
DAI	Diffuse axonal injury
DOF	Degrees of freedom
DSC	Dice similarity coefficient
DTI	Diffusion tensor imaging
DWI	Diffusion-weighted imaging
FA	Fractional anisotropy
GCC	Genu of the corpus callosum
GLM	General linear model
GM	Grey matter
HPA	Hypothalamic pituitary adrenal
IED	Improvised explosive device
ISS	Injury severity score
L	Left
MCP	Middle cerebellar peduncle
nbTBI	Non-blast related traumatic brain injury
P	Posterior
PTSD	Post-traumatic stress disorder
R	Right
ROI	Region of interest
RTA	Road traffic accident
S	Superior
SCC	Splenium of the corpus callosum
SNR	Signal-to-noise ratio
SSDS	Subject-specific diffusion segmentation
SVM	Support vector machine
T1	T1-weighted imaging
TBI	Traumatic brain injury
TBSS	Tract-based spatial statistics
TCV	Total corrected volume
VBA	Voxel-based analysis
VBM	Vertex-based morphometry
WM	White matter



# Table of Contents

<b>CHAPTER 1 Introduction .....</b>	<b>17</b>
<b>1.1. Aims and Objectives.....</b>	<b>18</b>
<b>1.2. Hypotheses .....</b>	<b>19</b>
<b>1.3. Summary of Chapters.....</b>	<b>20</b>
<b>1.4. Traumatic Brain Injury (TBI) .....</b>	<b>21</b>
1.4.1. Definition of TBI.....	21
1.4.2. Classification System of TBI Severity.....	21
<b>1.5. Blast-Induced TBI .....</b>	<b>23</b>
1.5.1. Definition of Blast TBI.....	23
1.5.2. Mechanism of Blast TBI.....	24
1.5.3. Clinical Presentation of bTBI .....	27
<b>1.6. Pathophysiology of TBI.....</b>	<b>29</b>
1.6.1. Dynamic Neurobiological Changes Following bTBI .....	29
1.6.2. How the Grey Matter is Impacted.....	29
1.6.3. How the White Matter is impacted .....	30
<b>1.7. Research and Findings in blast TBI – A Literature Review .....</b>	<b>31</b>
1.7.1. In-Vitro Investigations .....	31
1.7.2. Animal Models and Modelling .....	32
1.7.3. Post-Mortem Investigations and Serum Measures .....	34
1.7.4. Clinical and Cognitive Observations Following Blast-Induced TBI .....	35
<b>1.8. Current Limitations in the Neuroimaging Detection of Blast-Induced TBI.....</b>	<b>45</b>
1.8.1. Issues with Controlling Factors .....	45
1.8.2. Issues with Homogeneity of Studies and Neuroimaging Analyses .....	45
1.8.3. Civilian Considerations .....	46
<b>CHAPTER 2 Materials &amp; Methods.....</b>	<b>47</b>
<b>2.1. Structural Imaging of the Brain .....</b>	<b>48</b>
2.1.1. Historical Background .....	48
2.1.2. MRI Definition, Physics and Principles .....	48
2.1.3. Anatomy in Neuroimaging .....	51
2.1.4. Overview of Structural MRI Analysis.....	52
<b>2.2. Diffusion Imaging of the Brain.....</b>	<b>55</b>
2.2.1. Principles of dMRI .....	55
2.2.2. Acquisition of dMRI .....	56
2.2.3. Analysis of dMRI .....	57
<b>2.3. Neuropsychology and Endocrinology.....</b>	<b>58</b>
2.3.1. Neuropsychology Testing .....	58
2.3.2. Endocrinology Testing .....	60
<b>2.4. Registration in Neuroimaging Studies .....</b>	<b>62</b>
2.4.1. Linear Transformations .....	62
2.4.2. Non-linear Transformations .....	63
2.4.3. Cost Functions .....	63
2.4.4. Interpolation and Resampling.....	64
<b>2.5. Principles of Group-Level Analysis .....</b>	<b>66</b>
2.5.1. Templates and Atlases .....	66
2.5.2. Voxel-Based Morphometry.....	66
2.5.3. Vertex Analysis .....	67
2.5.4. Tract-Based Spatial Statistics (TBSS) .....	68

<b>2.6. Machine Learning and Predictions in Neuroimaging Studies.....</b>	<b>69</b>
2.6.1. Multiple Linear Regression.....	69
2.6.2. Classification, Decision Trees, and Non-Linear Regression Models.....	69
2.6.3. Validations and Evaluation of Performance.....	71
<b>2.7. Statistical analyses.....</b>	<b>74</b>
<b>2.8. Pitfalls in Current Diffusion Neuroimaging Studies.....</b>	<b>76</b>
2.8.1. Acquisition artifacts for EPI images.....	76
2.8.2. Issues with ROI analyses.....	76
2.8.3. Partial Volume.....	76
2.8.4. Inter-Subject Analyses and Normalization.....	77
2.8.5. Issues with TBSS.....	77
<b>CHAPTER 3 Development &amp; Validation of the Subject-Specific Diffusion Segmentation (SSDS) pipeline.....</b>	<b>79</b>
<b>3.1. Abstract.....</b>	<b>80</b>
<b>3.2. Introduction.....</b>	<b>81</b>
<b>3.3. Methods: Subject-Specific Diffusion Segmentation.....</b>	<b>87</b>
3.3.1. Participants.....	87
3.3.2. Imaging Acquisition.....	87
3.3.3. Imaging Analysis.....	88
3.3.4. Exemplar applications.....	96
<b>3.4. Results.....</b>	<b>99</b>
3.4.1. Registration.....	99
3.4.2. Tract segmentation and estimation of fractional anisotropy.....	101
3.4.3. Test-retest reliability.....	103
3.4.4. SSDS vs other common methods.....	106
3.4.5. Example – TBI patients vs healthy controls.....	110
<b>3.5. Discussion.....</b>	<b>116</b>
<b>CHAPTER 4 Detecting White Matter Abnormality in Blast-Related Traumatic Brain Injury.....</b>	<b>121</b>
<b>4.1. Abstract.....</b>	<b>122</b>
<b>4.2. Introduction.....</b>	<b>123</b>
<b>4.3. Methods.....</b>	<b>127</b>
4.3.1. Participants.....	127
4.3.2. Neuropsychological Assessment.....	127
4.3.3. Imaging Acquisition.....	127
4.3.4. Imaging Analysis.....	128
4.3.5. Statistical analysis.....	132
<b>4.4. Results.....</b>	<b>133</b>
4.4.1. Patients' Characteristics.....	133
4.4.2. WM Abnormalities in Skeletonised Tracts Following Group-Level Analysis.....	136
4.4.3. WM Abnormalities Following Subject-Specific Diffusion Segmentation.....	138
4.4.4. WM Abnormalities at the Boundaries of ROIs.....	140
4.4.5. Individual Comparison of Soldiers to the Normal Distribution.....	141
<b>4.5. Discussion.....</b>	<b>144</b>
<b>CHAPTER 5 Morphometry, Volumetry, Diffusivity, and the Limbic System in bTBI.....</b>	<b>148</b>
<b>5.1. Abstract.....</b>	<b>149</b>
<b>5.2. Introduction.....</b>	<b>150</b>
<b>5.3. Methods.....</b>	<b>153</b>
5.3.1. Participants.....	153
5.3.2. Imaging Acquisition.....	154
5.3.3. Imaging Analysis.....	154

5.3.4. Statistics .....	155
<b>5.4. Results .....</b>	<b>157</b>
5.4.1. Demographics.....	157
5.4.2. Neuroimaging Findings.....	158
5.4.3. Relationship Between GM and WM abnormalities .....	161
5.4.4. Relationship Between Neuroimaging Findings and Clinical Characteristics .....	162
5.4.5. Prediction Model of Hippocampal TCV .....	163
<b>5.5. Discussion .....</b>	<b>164</b>
<b>CHAPTER 6 Traumatic Brain Injury and the Use of Classification Decision Trees Following SSDS.....</b>	<b>169</b>
6.1. Abstract.....	170
6.2. Introduction .....	171
6.3. Methods.....	174
6.3.1. Participants.....	174
6.3.2. Imaging Acquisition .....	175
6.3.3. Decision Tree Training and Testing .....	176
6.3.4. Statistical Analysis .....	179
6.4. Results .....	180
6.4.1. Results from SSDS Pipeline.....	180
6.4.2. Results from Decision Tree Classification of TBI vs Controls .....	183
6.4.3. Results from Decision Tree Classification of RTA vs Other Mechanisms.....	186
6.4.4. Comparing Results.....	188
6.5. Discussion .....	190
6.5.1. Important Next Steps for this Analysis.....	192
<b>CHAPTER 7 Discussion .....</b>	<b>193</b>
7.1. Summary of Chapters.....	194
1.8.5. 7.1.2. Chapter 3 .....	195
1.8.6. 7.1.3. Chapter 4 .....	196
1.8.7. 7.1.4. Chapter 5 .....	196
1.8.8. 7.1.5. Chapter 6 .....	197
7.2. Conclusion & Interpretation.....	199
7.3. Limitations & Recommendations .....	202
<b>APPENDIX.....</b>	<b>216</b>
<b>A.3. Appendix of Chapter 3 .....</b>	<b>217</b>
1.8.9. A.3.1. Code of SSDS .....	217
1.8.10. A.3.2. Tracts from the JHU atlas .....	221
1.8.11. A.3.3. Segmentation example.....	222
<b>A.4. Appendix of Chapter 4 .....</b>	<b>223</b>
1.8.12. A.4.1. ROI mean FA results .....	223
<b>A.5. Appendix of Chapter 5 .....</b>	<b>225</b>
1.8.13. A.5.1. Effect of clinical characteristics on ROI measures.....	225
1.8.14. A.5.2. Medication Details .....	226
<b>A.5. Appendix of Chapter 6 .....</b>	<b>227</b>
1.8.15. A.5.1. Demographics of TBI patients .....	227
1.8.16. A.5.2. Results from SSDS .....	229
1.8.17. A.5.3. Decision Tree Statistics for TBI vs Controls .....	231
1.8.18. A.5.4. Decision Tree Statistics for RTA vs Other Types of Injuries .....	233
<b>Note from the Author.....</b>	<b>236</b>

# Table of Figures

FIGURE 1: EXAMPLE OF AN IED .....	23
FIGURE 2: FRIEDLANDER WAVE.....	24
FIGURE 3: VARIATION OF POSITIVE AND NEGATIVE PRESSURE ASSOCIATED WITH BLAST .....	24
FIGURE 4: DIFFERENT MECHANISMS OF BTBI .....	25
FIGURE 5: SOME OF THE HYPOTHESIZED MECHANISMS OF PRIMARY BLAST-INDUCED TBI. ....	26
FIGURE 6: EXAMPLE OF A BASIC FINITE ELEMENT MODEL OF THE HUMAN HEAD .....	34
FIGURE 7: TRENDS OF INTEREST. ....	39
FIGURE 8 HYDROGEN ATOMS IN A WATER MOLECULE.....	49
FIGURE 9 HARDWARE AND COMPOSITION OF AN MRI SCANNER .....	49
FIGURE 10 MACROSCOPIC MAGNETIZATION OF HYDROGEN NUCLEI ALIGNING WITH THE B0 FIELD. ....	50
FIGURE 11 EXAMPLE OF HYDROGEN NUCLEUS ALIGNING TO AN EXTERNAL FIELD AND ITS PRECESSION PROPERTIES. ....	50
FIGURE 12 DIFFERENT RELAXATION PROPERTIES OF TISSUES, AND RESULTING IMAGES. ....	51
FIGURE 13: ILLUSTRATION OF GM AND WM TISSUES. ....	52
FIGURE 14 MAIN FEATURES AND SUBCORTICAL STRUCTURES OF THE BRAIN ANATOMY AS SEEN IN T1-WEIGHTED MRI.....	52
FIGURE 15 EXAMPLE OF BRAIN EXTRACTION. BEFORE (LEFT) AND AFTER (RIGHT).....	53
FIGURE 16: EXAMPLE OF TISSUE-TYPE SEGMENTATION YIELDING THE CSF (LEFT), GM (MIDDLE) AND WM (RIGHT) MAPS. ....	54
FIGURE 17 EXAMPLES OF WATER MOLECULE MOVEMENT.. ....	55
FIGURE 18: TENSOR ESTIMATION MODEL.....	56
FIGURE 19: EXAMPLE FROM THE MATRIX REASONING TEST. ....	59
FIGURE 20: EXAMPLE OF THE COLOUR-WORD INTERFERENCE TEST.....	60
FIGURE 21: REPRESENTATION OF BBR COST FUNCTION ESTIMATION AT A VERTEX V. ....	64
FIGURE 22: STEPS FOR THE VBM PIPELINE SPECIFIC THE GM. ....	67
FIGURE 23: EXAMPLE OF FA PROJECTION IN THE SKELETON.....	68
FIGURE 24: EXAMPLE OF HYPERPLANE GENERATION BETWEEN TWO DATASETS GROUP. ....	70
FIGURE 25: AN EXAMPLE OF DECISION TREE CLASSIFIER. ....	71
FIGURE 26: EXAMPLE OF K-FOLD CROSS-VALIDATION WITH K=5.....	72
FIGURE 27: EXAMPLE OF PARTIAL VOLUME VOXELS ON DIFFUSION IMAGE. ....	77
FIGURE 28: EXAMPLE OF LINEAR DISPLACEMENT AND SKELETON INACCURACY .....	78
FIGURE 29: OVERVIEW OF THE VALIDATION STEPS AND THE RESULTS PRESENTED IN THE CURRENT STUDY.....	88
FIGURE 30: OVERVIEW OF THE SSDS PIPELINE. ....	90
FIGURE 31: BOUNDARY OF THE WM.....	94
FIGURE 32: BOUNDARY OF THE WM/CSF AND WM/GM.....	94
FIGURE 33: VISUAL QUALITY CHECK FOR COST FUNCTION ON BRAIN OF PATIENT WITH SEVERE TBI.....	99
FIGURE 34: EXAMPLES OF INDIVIDUAL REGISTRATION PERFORMANCE.. ....	101
FIGURE 35: EXAMPLE OF TRACT SEGMENTATION.....	102
FIGURE 36: THE HISTOGRAM DISTRIBUTION.. ....	103
FIGURE 37: EXAMPLES OF 1 AND 2 EROSIONS ON SEGMENTATION AND COV OF TRACTS.. ....	104
FIGURE 38: CORRELATION OF INTRA-SUBJECT, INTER-VISIT SSDS RESULTS. ....	106
FIGURE 39: COMPARING SSDS TO OTHER METHODS. ....	109
FIGURE 40: TRACT-SPECIFIC MEAN FA VALUE COMPARISON IN 3 GROUPS.....	111
FIGURE 41: VISUAL REPRESENTATION OF CASE STUDIES OF PATIENTS WITH SEVERE TBI. ....	115
FIGURE 42: ORIGINAL VS ERODED IMAGE.....	119
FIGURE 43: WORKFLOW FOR THIS STUDY.. ....	129
FIGURE 44:HOW BOUNDARY MASKS ARE CREATED. ....	131
FIGURE 45: RESULTS OF TBSS ANALYSIS AND SKELETONIZED ROI COMPARISONS. ....	137
FIGURE 46: RESULTS OF WHOLE TRACT SSDS ANALYSIS.....	139
FIGURE 47: RESULTS OF TRACT BOUNDARY SSDS ANALYSIS.. ....	141
FIGURE 48: EXAMPLE OF INDIVIDUAL PATIENT DIAGNOSTIC RESULTS ACROSS ALL TRACTS. ....	142
FIGURE 49: RESULTS OF THE INDIVIDUAL COMPARISONS OF BTBI PATIENTS TO THE CONTROL GROUPS. ....	143
FIGURE 50: EPENDYMAL STRIPPING IN PORCINE MODEL OF BTBI.....	146
FIGURE 51: EXAMPLE OF THE SEGMENTATION OF THE HIPPOCAMPUS (YELLOW) AND AMYGDALA (BLUE) BILATERALLY .....	154
FIGURE 52: DISTRIBUTION OF MEAN FA VALUES FOR FORNIX INVESTIGATED IN THE THREE GROUPS.. ....	160
FIGURE 53: RESULTS OF VERTEX-BASED ANALYSIS ON THE HIPPOCAMPUS COMPARING BTBI AND CONTROLS. ....	161
FIGURE 54: PEARSON’S CORRELATION HIPPOCAMPAL TCV WITH MEAN FA OF THE WHOLE FORNIX. ....	162

FIGURE 55: HIPPOCAMPAL OEDEMA WITH CONCURRENT MICROGLIAL ACTIVATION .....	165
FIGURE 56 : GROUPS DEMOGRAPHICS.....	175
FIGURE 57: CONFUSION MATRIX .....	178
FIGURE 58: BOXPLOT SHOWING THE DISTRIBUTION OF MEAN FA ACROSS CONTROLS (BLUE) AND TBI (PINK). ....	181
FIGURE 59: BOXPLOT SHOWING THE DISTRIBUTION OF MEAN FA ACROSS TBI FROM RTA (LIGHT ORANGE) AND TBI FROM OTHER MECHANISMS (DARK ORANGE).. ....	182
FIGURE 60: RESULTS OF CLASSIFICATION DECISION TREE BEFORE PRUNING.....	184
FIGURE 61: RESULTS OF CLASSIFICATION DECISION TREE AFTER PRUNING.....	185
FIGURE 62: RESULTS OF CLASSIFICATION DECISION TREE RTA VS OTHER TYPES OF INJURIES AFTER PRUNING .....	187

## Table of Tables

TABLE 1: CRITERIA FOR THE MAYO CLASSIFICATION SYSTEM OF TBI SEVERITY. ....	21
TABLE 2: CATEGORIZATION OF BLAST-INDUCED INJURIES .....	24
TABLE 3: PUBMED SEARCH FOR LITERATURE REVIEW .....	38
TABLE 4: RESULTS OF THE SYSTEMATIC REVIEW, REPORTING METHODS AND MAIN FINDINGS FOR THE DIFFERENT NEUROIMAGING MODALITIES USED .....	39
TABLE 5: DIAGNOSTIC METHODS FOR PITUITARY DYSFUNCTION .....	61
TABLE 6: LIST OF SOME OF THE MOST COMMON COST FUNCTIONS USED IN IMAGE REGISTRATION.....	63
TABLE 7: OVERVIEW OF THE DIFFERENT POST-PROCESSING APPROACHES FOR STATISTICAL ANALYSIS OF DTI MEASURES.....	86
TABLE 8: DEMOGRAPHICS OF PATIENTS AND HEALTHY CONTROLS USED IN THE VALIDATION AND TESTING OF THE SDSS PIPELINE. ...	87
TABLE 9: REPORTED RESULTS FOR VARIABILITY STATISTICS.....	103
TABLE 10: DESCRIPTION OF THE CASE STUDIES.....	111
TABLE 11: DEMOGRAPHICS OF THE THREE GROUPS TAKING PART IN THIS STUDY .....	133
TABLE 12: RESULTS OF NEUROPSYCHOLOGICAL TESTS ACROSS THREE GROUPS, FOR DIFFERENT COGNITIVE DOMAINS AND THEIR ASSOCIATED COGNITIVE VARIABLES. SIGNIFICANCE.....	135
TABLE 13: DEMOGRAPHICS OF THE THREE COHORTS INCLUDED IN THIS STUDY.. ..	157
TABLE 14: CLINICAL DETAILS OF THE BTBI GROUP. ....	158
TABLE 15: MEASURES OF DIFFERENT ROIS INVESTIGATED.....	158
TABLE 16: FEATURE IMPORTANCE FROM PRUNED DECISION TREE CLASSIFYING BETWEEN TBI AND CONTROLS.....	184
TABLE 17: CONFUSION MATRIX OF DECISION TREE CLASSIFICATION. ....	186
TABLE 18: FEATURE IMPORTANCE FROM PRUNED DECISION TREE CLASSIFYING BETWEEN RTA AND OTHER INJURIES. ....	187
TABLE 19: CONFUSION MATRIX OF DECISION TREE CLASSIFICATION. ....	188
TABLE 20: COMPARING RESULTS BETWEEN T-TEST AND DECISION TREES IN TBI VS CONTROLS .....	188

## Table of Supplementary Tables

SUPPLEMENTARY TABLE 1: TRACTS FROM THE JHU ATLAS AND THEIR ABBREVIATION.....	221
SUPPLEMENTARY TABLE 2: MEAN FA RESULTS FOR ALL ROI FOLLOWING TBSS, SSDS, AND BOUNDARY SEGMENTATION.....	223
SUPPLEMENTARY TABLE 3: EFFECT OF CLINICAL CHARACTERISTICS ON ROI MEASURES WITHIN THE bTBI GROUP. ....	225
SUPPLEMENTARY TABLE 4: LIST OF MEDICATIONS USED BY SOLDIERS.....	226
SUPPLEMENTARY TABLE 5: RESULTS FROM SSDS IN TBI (N=85) VS CONTROLS(N=100).....	229
SUPPLEMENTARY TABLE 6: RESULTS FROM SSDS WITHIN THE TBI FOR RTA (N=43) VS OTHER TYPES OF INJURIES (N=42).....	230
SUPPLEMENTARY TABLE 7: RESULTS FROM SSDS WITHIN THE TBI FOR PRESENCE OF FOCAL INJURIES (CONTUSIONS/MICROBLEEDS) (N=14) VS NO FOCAL INJURIES (N=71). ....	230

## Statement of publications

The following manuscripts have been published or are being prepared for publication. Not all collaborative work in which I participated was used in this thesis, as publications in which I am a co-author do not constitute part of my thesis.

Yu, Xiancheng & **Azor, Adriana** & Sharp, David & Ghajari, Mazdak. (2020). Mechanisms of tensile failure of cerebrospinal fluid in blast traumatic brain injury. *Extreme Mechanics Letters*. 38. 100739. 10.1016/j.eml.2020.100739.

Jolly AE, Bălăeș M, **Azor A**, Friedland D, Sandrone S, Graham NSN, Zimmerman K, Sharp DJ. Detecting axonal injury in individual patients after traumatic brain injury. *Brain*. 2021 Feb 12;144(1):92-113. doi: 10.1093/brain/awaa372. PMID: 33257929; PMCID: PMC7880666.

Chapter 3:

**Azor A.M.**, Sharp D.J., Jolly A.E., Bourke N.J., Hellyer P.J. Automation and Standardization of Subject-Specific Region-of-Interest Segmentation for Investigation of Diffusion Imaging in Clinical Populations – Manuscript resubmitted after first round of revision for PlosOne

Chapter 4:

**Azor A.M.**, Ghajari M., Baxter D., Hellyer P.J., Leech R., Sagar J., Ham T., McGilloway E., Hughes E., Mistlin A., Bennett A., Midwinter M., Sharp D.J., Detecting White Matter Abnormalities in Blast-Related Traumatic Brain Injury in U.K. Military Personnel – Manuscript prepared for submission in Translational Medicine

Chapter 5:

**Azor A.M.**, [...], Goldstone T., Hippocampal Volume Loss in Combat-Related Traumatic Brain Injury in Veterans with no History of Post-Traumatic Stress Disorder – Manuscript prepared for submission in Brain



# CHAPTER 1

---

## Introduction

*In this chapter, I present the background concepts relevant to this thesis. I provide a summary of results from literature reviews, and the current limitations and questions still at the heart of the field.*

## 1.1. AIMS AND OBJECTIVES

The aim of this thesis was to investigate neuroimaging biomarkers of blast-induced traumatic brain injury (TBI) in military personnel post-deployment, with a focus on the structural and microstructural changes in the brain associated with blast TBI but not civilian TBI, as well as their association to clinical findings and neuropsychiatric measures. I used a combination of structural and diffusion magnetic resonance imaging, the development and validation of a new diffusion analysis technique, statistical predictions and machine learning algorithms.

***The objectives of this thesis were as follows:***

- 1- To develop, test and validate a new technique that would enable identification of patterns of white matter damage using an automated and standardized pipeline in the subject-level native diffusion space.
- 2- To implement the new pipeline with the aim of identifying patterns of white matter injury associated with blast-related TBI.
- 3- To investigate changes in cortical/subcortical structure in blast TBI and the difference in comparison to non-blast TBI using standard group-level analysis techniques.
- 4- To use the results of the new pipeline to train a decision tree classification algorithm to classify between A) TBI and healthy controls, B) road traffic accidents vs other injury mechanisms as a first step towards machine-learning based identification of blast TBI.

## 1.2. HYPOTHESES

*The hypotheses put forward in this thesis were:*

1. Group-level investigations of white matter microstructural damage cannot detect a pattern of injury specific to blast-related TBI due to the subtlety of group differences.
2. There will be specific patterns of white matter damage following blast-related TBI at the boundary of the white matter and the grey matter, and the white matter and fluid-filled cavities, as well as at the level of the middle cerebellar.
3. Blast-related TBI will be differentiated by a decrease of hippocampal volume in subject-level investigations, and hippocampal atrophy can be predicted by clinical variables.
4. It is possible to discern with high accuracy between TBI/controls and road traffic accidents/ other mechanisms of TBI using decision trees, in a way that might be reproduced on military TBI data in future work.

### 1.3. SUMMARY OF CHAPTERS

- Chapter 2 | I present and describe in details the methods and materials used throughout my experimental studies and chapters.
- Chapter 3 | I develop an individual, standardized, and automated pipeline, subject-specific diffusion segmentation (SSDS) to accurately measure changes in white matter microstructure in the subject's native diffusion space on an untransformed parametric map. I validate the pipeline against manual segmentation of white matter tracts and the widespread group-level analysis technique tract-based spatial statistics. I test the pipeline in a cohort of civilians with a diagnosis of TBI.
- Chapter 4 | I investigate injury at the subject-level in different white matter tracts and the boundary of the white matter using SSDS to detect a white matter-derived neuroimaging biomarker of blast TBI. I used two control groups: a non-blast TBI group and a group of healthy civilians.
- Chapter 5 | I investigate neuroimaging biomarkers of blast-induced TBI using common neuroimaging analysis techniques including volumetric measures of cortical and subcortical structures. I explain the changes observed using clinical, neuroradiological and neuropsychological measures.
- Chapter 6 | I derive mean FA measures from 47 white matter tracts by implementing SSDS in a large cohort of civilians with TBI and controls. I train a decision tree to classify between TBI and controls, and between different injury mechanisms within the TBI group. I test the decision tree and derive measures of the performance of the classification.
- Chapter 7 | I summarise the results of my thesis and discuss the findings and conclusions that would contribute to our understanding of blast-induced TBI and specifically how this mechanism and neurological underpinning differ from civilian TBI. I conclude by describing probable limitations and future directions in the field based on my work.

## 1.4. TRAUMATIC BRAIN INJURY (TBI)

### 1.4.1. Definition of TBI

Traumatic brain injury (TBI) is defined as a disruption in typical brain function caused by external force(s) such as a bump, blow, jolt or penetrating head injury (Prevention, 2020). In the U.K., TBI is the commonest cause of disability and death in people aged between 0 and 40 years, with a third to half of these being children under the age of 15. The leading causes of TBI are falls, assaults and road traffic accidents with alcohol being involved in 65% of adult cases (Mistry J., 2017).

### 1.4.2. Classification System of TBI Severity

There are different ways of assessing and classifying TBI. Because TBI presents with such heterogenous causes, mechanisms, severity, prognosis, and pathoanatomic changes, categorisation is essential. One of the main classification system, and the one I used to describe the patients in this thesis is the Mayo classification (Malec et al., 2007). It comprises three main categories: moderate-severe (definite), mild (probable), and symptomatic (probable). The classification of TBI is made based on imaging and clinical presentation (Table 1).

**Table 1: Criteria for the Mayo classification system of TBI severity.**

	Moderate / Severe	Mild	Symptomatic
<b>GCS</b>	< 13 in the initial 24 hrs	> 12	-
<b>PTA</b>	> 24 hrs	< 24 hrs	-
<b>LOC</b>	> 30min	< 30min	-
<b>Imaging</b>	Intracerebral haemorrhage Subdural haemorrhage Epidural haemorrhage Subarachnoid haemorrhage Contusion Penetrating injury through the dura Brainstem injury	Depressed, basilar or linear skull fracture	-
<b>Other</b>	Death		Other clinical symptoms including blurred vision, confusion, headache, nausea, dizziness or focal neurological changes

Other measures I also use in this thesis are the Abbreviated Injury Score (AIS) and Injury Severity Score (ISS). In both civilian and military trauma, head injuries frequently occur in the context of polytrauma (where there is an injury to more than one body system), especially in the context of exposure to blast, which I will detail in the next section. The ISS is an anatomical scoring that provides an overall score for patients with multiple injuries. Each injury is assigned an Abbreviated Injury Scale (AIS) score and assigned to one of the nine regions (face, neck, head, chest, spine, pelvis, abdomen, extremities (upper/lower) and external (skin)). The ISS score is the sum of square of the 3 highest AIS scores (from 0 to 6). ISS scores range from 0 to 75 and correlates with severity, mortality, morbidity, etc.. (Injury Severity Score, Trauma.org 2015).

### ***Focal vs diffuse injuries***

I talk about focal and diffuse injuries throughout the thesis, and this is a common way of describing TBI based on clinical and radiological examination (Silver, 2005). The mechanisms are not mutually exclusive but aren't always found together.

Focal injuries usually result from inertial forces, including blunt force trauma or rotational/translational movements of the brain, which can cause it to hit the skull, and lead to microbleeds and contusions that can be seen on diagnostic neuroradiology (Ommaya and Gennarelli, 1974).

Diffuse injury, and more specifically diffuse axonal injury (DAI) in the context of TBI, refers to a range of microstructural WM abnormalities, with the most severe being tearing of axons and axonal death. DAI is a common pathological finding of TBI (Gentry et al., 1988), and can occur even in the absence of impact to the head. It is hypothesized to be caused by the rapid acceleration- deceleration of the head (Adams et al., 1989). If the forces causing DAI are sufficiently strong, damage to the blood vessels within the WM can lead to petechial haemorrhages (or microbleeds), used as a diagnostic symptom of TBI in routine neuroradiology (Bigler, 2001).

## 1.5. BLAST-INDUCED TBI

### 1.5.1. Definition of Blast TBI

Blast injuries, including blast-induced traumatic brain injuries (bTBI) are triggered by blast waves generated by an explosion. Even though histories of explosions and bTBI incidence coincide, our knowledge of bTBI and its pathology is still very shallow even after a thousand years of using explosive devices. Over the decades, explosive devices have been designed to maximize efficiency and propel metal fragments to induce more damage. However, more recently, a shift from blunt and penetrating injuries to blast injury is being observed and this might be due to new types of explosives used in combat fields (Dearden, 2001), known as improvised explosive devices (IED). IEDs are designed to destroy vehicles and often contain ballistic fragments, causing injuries at greater distance than the blast alone would. They can be either triggered by the victim (trip wires, pressure sensitive plates or magnetic triggers) or by an attacker (command wire, remote control, and infrared).

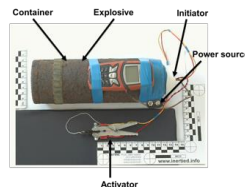


Figure 1: Example of an IED. Source: <http://www.inertproducts.com>

An explosion will generate a pulse of increased air pressure, the blast overpressure (BOP), which lasts a few milliseconds and rapidly expands from the point of detonation. The BOP is quickly followed by an area of negative pressure, and together they are known as the shock wave, the magnitude of which dissipates rapidly while expending away from the point of detonation (Kirkman et al., 2011). The gases released by the explosion displace an equal volume of air with an outward expansion at very high velocity, a phenomenon referred to as the blast wind (Cernak et al., 1996). The blast wind is a high-velocity and destructive movement of air with the ability of causing extreme damage (DePalma et al., 2005).

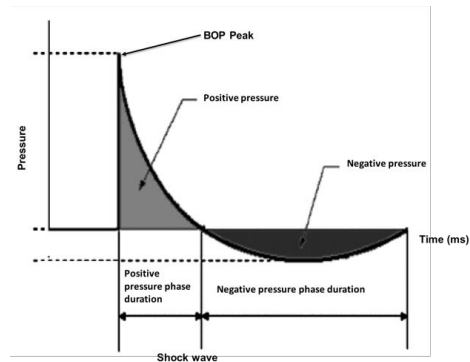


Figure 2: Friedlander wave. Shows the peak pressure, positive and negative pressure.  
Adapted from (Bauman et al., 2009).

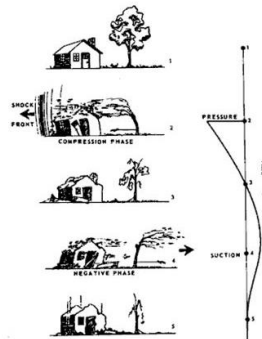


Figure 3: Variation of positive and negative pressure associated with blast. 1) Typical scene, 2) compression phase (positive pressure), 3) after positive pressure, 4) negative pressure, 5) after negative pressure. Source: [www.mega.nu](http://www.mega.nu)

### 1.5.2. Mechanism of Blast TBI

The effects of blast on the body can be categorized in 5 folds (Table 2). Primary blast injuries are typically a result of the BOP peak. The blast wind that follows can propel objects and other debris into the body, causing secondary effects. Rapid acceleration and deceleration of the head can lead to tertiary injuries as the victim is thrown and impacts surrounding objects. Other effects including heat, toxins, chemicals and radiations are classified as quaternary injuries (DeWitt and Prough, 2009).

Table 2: Categorization of blast-induced injuries

Category	Cause	Consequences
Primary	Blast wave (overpressure followed by under pressure) and blast winds.	Primary blast injuries
Secondary	Propelled fragments and debris.	Blunt and/or penetrating injuries



<b>Tertiary</b>	Acceleration/deceleration of the head when body is projected against hard surface.	Translational, rotational and impact injuries.
<b>Quaternary</b>	Usually heat and/or chemicals	Most commonly burns
<b>Quinary</b>	Other factors released during an explosion such as gases, radiation, biological material, etc.	Poisoning, asphyxiation of hypoxia, radiation, burns, infections

Primary blast injuries are rarely, if not ever present in isolation during TBI sustained in the battlefield. In a report from the Department of Defense, of 200,000 soldiers with a head injury, 150,000 were diagnosed with mild TBI and Post-Traumatic Stress Disorder (PTSD) (Vanderploeg et al., 2012). Among deployed soldiers, mild blast TBI is the most prevalent form of trauma and has therefore been labelled as the invisible signature wound of modern conflict (Okie, 2005).

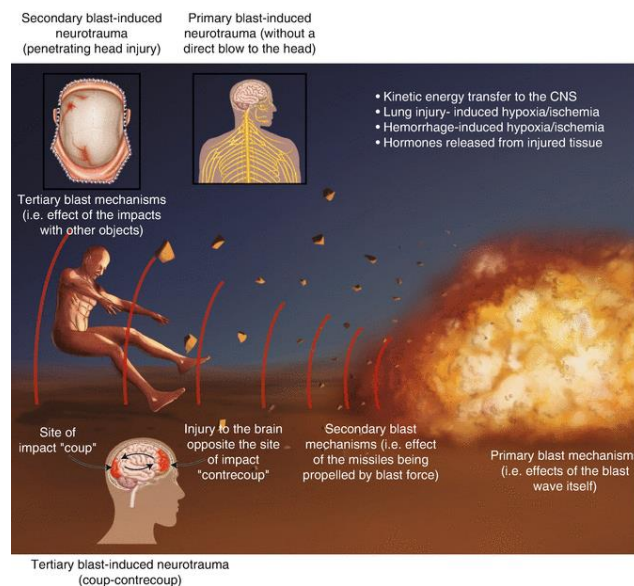


**Figure 4: Different mechanisms of bTBI. Source:(Cernak and Noble-Haeusslein, 2010)**

As mentioned previously, classification of TBI is challenging due to the heterogeneity of the condition. In the military setting, this classification is even more hindered given the countless variables that are difficult to control for: mechanism of injury, strength of blast, meaningful clinical acute, subacute, and chronic assessments (Bryden et al., 2019). The 3 most common mechanisms sustained by military personnel (primary, secondary, and tertiary) have largely overlapping mechanisms, and often happen simultaneously.

### ***Primary blast-related head trauma***

Head trauma due to the blast overpressure is still misunderstood, and there is still insufficient data to support a single mechanism that might be causing neurological sequelae. However, based on pre-clinical and post-mortem research, as well as injuries to other organs and cavities, many mechanisms have been proposed and hypothesized (Rosenfeld et al., 2013).

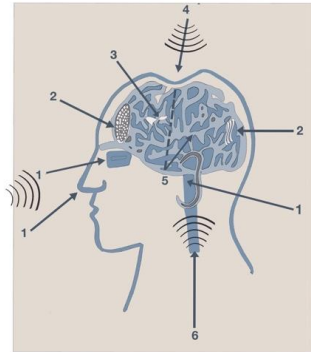


**Figure 5: Some of the hypothesized mechanisms of primary blast-induced TBI. 1) Direct stress wave reaching the brain through cavities, 2) coup/contre-coup resulting from translational and rotational movements of the brain, 3) shearing of WM tissue resulting in diffuse axonal injury, 4) skull flexure and direct trauma to the underlying tissue, 5) amplification of the wave by the skull, 6) vascular surge. Source: adapted from (Rosenfeld et al., 2013)**

**Spallation** is the transmission of a shock wave from higher to lower density (Wolf et al., 2009). **Cavitation** occurs when the dissolved gases form bubbles in fluids during the negative pressure phase (Wolf et al., 2009). The negative pressure then causes the bubbles to implode and expand explosively (Nakagawa et al., 2011). **Inertial forces** are mainly concentrated around the boundaries of tissues with different material properties, and create shearing forces, which have mainly been suggested by computerized studies and physical models of blast (Goeller et al., 2012). Other possible mechanisms also include **abrupt acceleration** of the brain, causing impact with the skull and leading to contusions, hematoma, micro-haemorrhaging or axonal injury (Lissner et al., 1960), similar to the mechanism seen in road traffic accidents (RTA). Finally, **vascular surge** is a more controversial mechanism that hypothesizes transmission of the pressure through the thoracic cavities, causing increased blood pressure within the cerebral vasculature (Bauman et al., 2009, Cernak et al., 2001, Simard et al., 2014).

### ***Ballistic head trauma***

Also referred to as secondary blast injuries, ballistic head traumas are injuries sustained from ballistic materials projected through the air and impacting the head resulting in a penetrating injury. Military helmets are primarily designed to reduce injuries resulting from projectiles.

### ***Blunt head trauma***

These are injuries resulting from the impact of the head with a blunt object, also categorized as tertiary blast injuries. They often cause skull deformations and focal damage to the underlying brain tissue at the site of impact, which leads to contusions and hematoma, as well as in contrecoup lesions. Blunt trauma triggers rotation and acceleration of the brain which can induce strain and shearing to tissues throughout the brain.

## **1.5.3. Clinical Presentation of bTBI**

It is often easier to diagnose PTSD in returning soldiers than it is to diagnose a history of TBI in retrospect. However, even with overlapping symptomatology for the two conditions, each one also presents with specific symptoms (Lash, 2013).

Fatigue, sleep disturbance, memory and attention deficits, depression, anxiety, and irritability can be experienced in both cases of PTSD and/or TBI.

TBI can be characterized, among other symptoms, by headaches, dizziness, nausea, vision changes and impulsivity.

PTSD can be diagnosed through the presence of alertness and fearfulness, flashbacks, paranoia and nightmares, and self-destructive behaviours.

In bTBI specifically, the literature and my work have focused on the middle cerebellar peduncle as a structure that might be susceptible to the effect of blast (Bigler et al., 2007). If the middle cerebellar peduncle is differentially affected in soldiers, then the clinical manifestations can include difficulty with motor movements, speech ataxia, vertigo, facial weaknesses and deafness among other symptoms.



## 1.6. PATHOPHYSIOLOGY OF TBI

### 1.6.1. Dynamic Neurobiological Changes Following bTBI

Both animal and human studies show that TBI is not a static insult to the brain, but rather an initial insult that leads to a cascade of processes (Werner and Engelhard, 2007). Neurobiological events following TBI might help explain the heterogeneity of clinical and cognitive symptomatology seen in patients (Gorgoraptis et al., 2019). In the context of dynamic changes, focal damage refers to contusions, haematomas, skull deformation or fractures, which arise from the initial impact. Diffuse injuries such as axonal injuries or damage to the vasculature are usually due to the acceleration/deceleration movement of the head.

Following the initial insult, dynamic neurobiological changes can be immediate, such as ischaemia or increased intracranial pressure (Pinto et al., 2021, Vespa et al., 2016). On the long-term, neuroinflammation and neurodegeneration can also arise because of TBI, with a clear association with cognitive decline (Schimmel et al., 2017, Graham et al., 1995, Graham, 2019). To understand the neurobiological changes in the brain following TBI, it is crucial to recognise the mechanisms of injuries and time since injury following TBI in any studied population.

### 1.6.2. How the Grey Matter is Impacted

The cortical GM structures of the brain can exhibit focal contusions following impact TBI, especially in regions closest to bony protrusions of the skull, namely the temporal, orbito-frontal and occipital lobes (Bigler, 2007, Gurdjian, 1975). When focal lesions are severe, mortality rate can be as high as 40%, and survivors develop cognitive and emotional problems, such as working memory impairment, apathy, and decreased awareness (Cicerone et al., 2006, Spikman and van der Naalt, 2010, Andersson et al., 1999). Months to years after a TBI, patients can exhibit GM atrophy, with research suggesting a strong association between TBI and the development of dementia symptoms, which further illustrate the long-term sequelae of the injury, with accelerated tissue atrophy compared to normal aging (Graham, 2019, Krueger et al., 2011, Fleminger et al., 2003, Ross, 2011, Sidaros et al., 2009, Cole et al., 2015). Although mild TBI does not show a specific pattern of atrophy, moderate-severe TBI have more robust generalized and focal patterns of atrophy, with the most commonly

affected areas being subcortical GM including the thalamus, hippocampus, and cerebellum (Harris et al., 2019).

### **1.6.3. How the White Matter is impacted**

Tissue atrophy following TBI is not limited to the GM, with the WM exhibiting greater rates of volume reduction with strong association to overall cerebral volume loss, and a higher impact on cognition compared to focal GM contusions (Cole et al., 2015, Ding et al., 2008). The most common WM regions exhibiting patterns of atrophy are the corpus callosum, corona radiata, and brainstem (Harris et al., 2019, Aoki et al., 2012). Both anatomical and diffusivity changes in the WM have been extensively investigated in patients with TBI. Techniques for diffusion imaging analyses mainly include the tensor model, but also diffusion kurtosis imaging (DKI) which assess the non-Gaussian behaviour of water molecules (Steven et al., 2014), as well as high angular resolution diffusion imaging (HARDI) to resolve issues and limitations related to crossing fibres (Tefera et al., 2013). Most tensor-based studies report diffusion abnormalities following TBI as a decrease in FA, and an increase in mean diffusivity (MD) (Shenton et al., 2012). While this pattern of injury is interpreted as a sign of cytotoxic oedema<sup>1</sup>, this hypothesis has been challenged (Lipton et al., 2012). Microhaemorrhages in the WM are usually a sign of diffuse axonal injury (DAI)(Bigler and Maxwell, 2012) , and WM lesions observed as hyperintensities on FLAIR sequences can be seen in patients with mild TBI (Bigler et al., 2016), but are much more common in cases of moderate-severe TBI. In mild cases of bTBI, lesions were shown to influence verbal memory, independently of a diagnosis of PTSD (Clark et al., 2016).

Inter-subject variations in FA are considerable in clinical studies of TBI, which directly reflects differences in vulnerability, genetics, anatomy, and mechanism (Petrie et al., 2014, Kim et al., 2013, Lipton et al., 2012, Shenton et al., 2012).

---

<sup>1</sup> Accumulation of intracellular fluid leading to cell swelling.

## 1.7. RESEARCH AND FINDINGS IN BLAST TBI – A LITERATURE REVIEW

Routine imaging and clinical assessments are typically unrevealing in mild TBI. Advanced neuroimaging and analysis techniques, however, enable quantification of structural and functional changes in the brain, at a certain time point or over time, following injury. It is believed that the mechanism of bTBI may be different from blunt or impact TBI, but still incorporates the rotational and translational aspects known to cause damage to the brain in civilian TBI. **Does the blast wave itself cause damage to brain tissues?** It has already been shown to cause damage to the respiratory and auditory systems, where cavities are filled with air (DePalma et al., 2005). However, very little is known about the effects of the blast's overpressure/under pressure on the central nervous system. This is a question that neuroscientists have been trying to answer.

### 1.7.1. In-Vitro Investigations

The first three categories of blast injuries (primary, secondary and tertiary) are biomechanically distinct. Therefore, they can be studied independently. In a reduced and simplified form, primary injury involves pressure wave transmission. However, the portion that converts into injury is unknown. Secondary injuries can translate to a direct shearing or section of the tissue and tertiary injuries are modelled by inducing stretch actions on the cells. In vitro models enable the study of each mechanism independently or together in a controlled environment. Tertiary models of bTBI suggest that exposure of brain cells to acceleration/deceleration-like mechanisms leads to enhanced or abnormal  $\text{Ca}^{2+}$  signalling following **astrocytic deformation**, (key process in the pathogenesis of neurodegenerative diseases) (Lamb et al., 1997, Charles et al., 1991, Floyd et al., 2004), (Rzigalinski et al., 1998, Rzigalinski et al., 1997), **free radical generation** (Hoffman et al., 2000, Floyd et al., 2001), **changes in polarization and ions movement** (Floyd et al., 2005, Di et al., 2000), **increased cell death** (Glass et al., 2002), and others. Secondary injury models are increasingly studied, due to the high mortality rate of penetrating injuries. In vitro, these types of injuries are mimicked by direct lacerations of cells, leading to damage of the cytoskeleton and microtubules (Lucas and Wolf, 1991, Lucas et al., 1985, Emery et

al., 1987) and **chemical imbalance** (Rosenberg and Lucas, 1996, Rosenberg et al., 2001) amongst others. As mentioned earlier, the initial phase of the blast consists of a wave pressure transmission, followed by the wind force. The transmission of a wave through the different tissues of the head is complex to model. The limited research available reveals **membrane damage and cytokines production** (Hariri et al., 1994, Howard and Sturtevant, 1997, Murphy and Horrocks, 1993). Just as there is no consensus on a single in-vitro model to investigate civilian TBI, it is as, if not more challenging to isolate the effects of bTBI for cellular and molecular studies, especially for primary blast injuries. The limited literature seems to point at significant intracranial pressures transmitting through tissues without shedding light on how this affects biological functions.

### 1.7.2. Animal Models and Modelling

Animal models are an essential part of TBI research given the controlled nature of the studies. Mechanisms can be isolated and examined, and variables can be investigated in a way that can't be done for soldiers returning from the battlefield. Animal models of bTBI usually include mice, rats, pigs, and non-human primate. However, the main issue with animal models is interspecies scaling and anatomical differences when translating to possible findings on humans (Goldstein et al., 2014). For non-human primates and pigs, translation is easier given that they have large, gyrencephalic brains. However, these models are less cost-effective and require more ethical guidelines. The location, nature, and severity of the primary injury as well as all the other factors such as age, health, gender, medical conditions, genetics and substance abuse explain the heterogeneity of pathophysiology of TBI. To overcome this and confidently study the effect of each variable, animal models of TBI are designed to reflect a homogeneous injury. The problem however remains the limited possibility to fully exhibit all aspects of the injuries as observed in humans. This may also explain why drugs and protective equipment that might seem promising in pre-clinical studies fail translation (Marklund et al., 2006). Unquestionably, however, preclinical studies are essential to understand the biomechanical, cellular, and molecular properties of bTBI in human, which are challenging to address in deployment or even clinical setting. Animal models of the injuries can also assist in the development of protection or treatment strategies. In the context of bTBI, models of rodents (Long et al., 2009, Cheng et al., 2010, Wang et al., 2011) and swine (de Lanerolle et al., 2011, Bauman



et al., 2009) are commonly used, even when investigating changes in cognition and addiction behaviours (Muelbl et al., 2018). Non-impact models develop **diffuse oedema, vasospasm and hypermia** (Cernak et al., 1996). **Diffuse axonal injury** and **cognitive deficits** were the most noticeable aspects of longitudinal follow-up findings (Saljo et al., 2009, Kuehn et al., 2011). The main concern with animal models of bTBI however is the focus on tissue destruction, while clinically the most prominent effect is not structural but functional (DeWitt and Prough, 2009). To replicate blasts in controlled lab environments, shock tubes are most used. However, these also present heterogeneity, especially across studies, rendering aggregation and evaluation of bTBI research difficult (Agoston and Kamnaksh, 2015). Shock tube experiments cause TBI-like symptoms with **hypotension** and possible internal **haemorrhage** and lung injuries (DeWitt and Prough, 2009), as well as post-trauma **seizures** and increased **neuronal excitability** (Bugay et al., 2020). Although it is challenging to validate bTBI animal models without more precise human data, these studies reproduce many of the known neuropathological and behavioural outcomes clinically described in humans after sustaining bTBI, such as **vasospasm, contusion, axonal injuries, oedema, and haemorrhage** (Armonda et al., 2006, Schwartz et al., 2008).

Computational modelling and mathematical techniques also allow us to overcome the complexity of studies involving humans and animals. Computational models of the blast wave as well as that of the human head/brain can predict how different blast parameters will affect neurological changes. These models usually rely on a deep understanding of the human brain anatomy, long term potential outcome, as well as the physics of blast waves. This field is still relatively new, and the intricacy of associated and interdependent variables can hinder such investigations (Przekwas et al., 2016, Gupta and Przekwas, 2013). Finite element modelling <sup>2</sup> (FEM) is one of the popular computational methods used to replicate bTBI in controlled experiments.

---

<sup>2</sup> FEM subdivides an element into its smaller constituents or finite elements by reconstructing the mesh of the element.

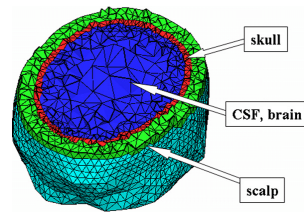


Figure 6: Example of a basic finite element model of the human head. Source: (Im et al., 2008)

High strain-rates generated by blast waves affect the anisotropy of **WM tracts** (Chen WW, 2010), in similar patterns to that seen in contact sports-related TBI (Zhang et al., 2004, Casson et al., 2008). A high-fidelity FEM model (skull, skin, grey and white matter) and an MRI based semi-automatic image segmentation (Lagravere et al., 2008, Moore et al., 2009) show a direct **propagation of the wave** into the brain in all blast cases, with stresses developing around areas known to be vulnerable in other non-blast TBI at an exposure to 0.324 kg TNT and 0.6 m from the source (Moore et al., 2009). **Shear stresses, strains and tissue displacements**, but also the duration of the blast load play a major role in brain tissue injuries, with the first peak causing maximum damage, and subsequent fluctuations being able to cause severe injuries, and trauma being lower in closed and confined spaces (Chaloner, 2005, Rezaei et al., 2014, Ommaya, 1995). More recently, it was shown that **CSF cavitation** leads to strain rate increase which is caused by the rapid head motion and rarefaction waves (Yu et al., 2020).

### 1.7.3. Post-Mortem Investigations and Serum Measures

Getting closer to what happens to the human brain during and after exposure to blast, a post-mortem case study published in Lancet (Shively et al., 2016) claimed to characterize a unique biomarker of bTBI. Analysing brain specimens from five deceased veterans with histories of chronic exposure to blasts and PTSD diagnosis, they revealed a pattern of **astroglial scarring at the boundary** between brain tissues and fluids. This has yet to be validated, but research from our group on a porcine model of bTBI reveals similar findings. Before this study, very few cases of bTBI described a chronic traumatic encephalopathy (**CTE**)-like **pathology** (Omalu et al., 2011, Goldstein et al., 2012). Contradictory findings reveal axonal pathology but no evidence of CTE (Ryu et al., 2014). Disruptions caused by blast-TBI can cause short- and long-term changes at the cellular and molecular level (Gupta and Przekwas, 2013, Przekwas et al., 2016) which can in turn lead to changes in the concentration of

circulating biomolecules available for detection. Longitudinal blood analysis of soldiers pre- and post-deployment investigating the association between inflammatory cytokines and mild/moderate-severe TBI reveal a **decrease in pro-inflammatory interleukins and glycoprotein** during the chronic phase of bTBI (Rusiecki et al., 2020). Developing a fluid biomarker of blast TBI can help with the rapid diagnosis or to track the progression of the underlying neurophysiological changes, especially in the context of battlefields where acute interventions are limited.

#### **1.7.4. Clinical and Cognitive Observations Following Blast-Induced TBI**

Understanding how bTBI translates into clinical, neurobehavioral, and cognitive symptoms is an essential part of the development of protective equipment, treatment, prognosis, management, and establishing a framework for rehabilitation for returning soldiers. However, specific long-term outcomes and their biological underpinnings in the military populations are not fully understood. Although research effort is being devoted to this area, it is still far behind compared to TBI in civilian populations (Lamberty et al., 2013). Therefore, most of our knowledge related to the effects of bTBI come from studies of civilian non-blast TBI.

##### ***Neuroradiological and sensory impairments***

Exposure to blast can lead to injuries ranging from mild to fatal. Neuroradiological abnormalities include **contusions, oedema, hematomas, swelling, and haemorrhage** (Schwartz et al., 2008, Levi et al., 1990, Ling et al., 2009). During deployment, CT scans might be available, but MRI scans cannot be transported to the battlefield. Although CT scans can reliably detect gross structural brain damage, it cannot detect abnormalities related to mild TBI (Borg et al., 2004), while MRI is much more sensitive to abnormalities such as diffuse axonal injury and cerebral contusions. This limits acute diagnostic or imaging data from soldiers. There have also been clinical observational studies on visual deficits, many of which reported abnormalities in soldiers having sustained bTBI (Pogoda et al., 2012, Magone et al., 2014, Lew et al., 2011, Goodrich et al., 2013). Several studies also reported **dual sensory impairment**, which describes both visual and auditory deficits in soldiers with a history of bTBI (Lew et al., 2009, Saunders and Echt, 2012, Lew et al., 2011).

### ***Cognitive impairments***

The issue with neuropsychological assessment is the lack of homogenous longitudinal approach. Early evidence suggests a pattern of cognitive **impairment similar to civilian** TBI (Belanger et al., 2009). As mentioned previously, primary blast injury mostly occurs concurrently to other types of TBI, commonly seen in civilians, rendering causal factors for differential neurological impairments challenging to assign to a specific mechanism of injury. Some studies have examined cognition at the acute stage of bTBI (Kennedy et al., 2012, Coldren et al., 2010), but there were no follow-up investigations that systematically followed performance trajectories chronically to uncover long-term recovery patterns. Other studies have looked at pre-deployment neuropsychological performance as a control for post-deployment measures (Vasterling et al., 2012, Roebuck-Spencer et al., 2012), and reported **no lasting cognitive impairments** in soldiers having sustained a bTBI. Reported cognitive performance (or subject performance) was much more affected in soldiers than in civilians with TBI. However, objective measures obtained from cognitive test scores were almost similar between the two groups (Nelson NW, 2015). When comparing soldiers with bTBI but no ongoing psychological or emotional disturbances to soldiers with no TBI, there is no evidence of lasting cognitive impairments (Shandera-Ochsner et al., 2013). However, there is evidence that PTSD or other psychopathology impact cognitive measures (Vasterling et al., 2012, Nelson et al., 2015, Shandera-Ochsner et al., 2013). Most impairments were seen in complex **attention, executive function** and **memory** and **learning**, (Vanderploeg et al., 2005, Ruff and Jurica, 1999, Bogdanova and Verfaellie, 2012).

### ***Stress and other comorbidities***

Stress-related symptoms, particularly **PTSD** are amongst the most common problems in soldiers post-deployment (Hoge et al., 2008), with anywhere between 4% and 33% of returning soldiers being affected (Gates et al., 2012). Because PTSD is easier to diagnose than bTBI, especially in the chronic phase, there are much more studies focused on PTSD in soldiers than those focused on bTBI. PTSD is mostly expressed by re-experiencing, avoidance, and hyperarousal, as well as cognitive deficiencies also seen in soldiers with bTBI including attention, memory and executive function. PTSD is also associated with cognitive inefficiencies in the domains of attention,

executive function, and memory (JJ Vasterling, 2005, Vasterling et al., 2012). A hypothesis suggests that bTBI increases the susceptibility of brain regions that lead to a greater expression of PTSD (Averill et al., 2018), and that deployment-related stress has lasting effects on the brain, creating heightened vulnerability. Even in the absence of a diagnosis for PTSD, neuropsychological functioning can be impacted due to prolonged stress exposure (Vasterling et al., 2006, Vasterling and Proctor, 2011). Activation of the autonomic and endocrine systems are usually involved in detection and reaction to threats, and the production and release of corticosteroids (eg, cortisone, hydrocortisone, & prednisone) following the normal hypothalamic–pituitary–adrenal (HPA) axis response (van Bodegom et al., 2017). Corticosteroids can bind to receptors primarily located in the limbic region, particularly the hippocampus. **Stress hormones** can impact different neurobiological processes such as cognition, emotion, and behaviour (Yaribeygi et al., 2017), as well as widespread inflammation and **chronic pain** (Kinlein et al., 2015).

Other common issues are related to **sleep** disturbances such as nightmares or insomnia, which overlap with PTSD symptoms, and these disturbances increase in the presence of PTSD (McLay et al., 2010, Seelig et al., 2010). As many as 70% of returning soldiers can experience insomnia (Germain et al., 2014). It is important to note that clinically significant relationships have been established between cognitive impairment and chronic insomnia, especially related to attention and episodic memory (Fortier-Brochu and Morin, 2014). Soldiers with bTBI also report higher incidence of **headaches** and **chronic pain** (Finkel et al., 2017, Phipps et al., 2020, Seelig et al., 2010).

### ***Set-up of literature review***

Since this thesis will be focusing mainly on neuroimaging analysis of human brain scans, I carried out a systematic review of the literature to underline the weaknesses and challenges to set up an impactful research on overlooked aspects and fill in the missing gaps in human bTBI investigations. The literature review spanned the most common neuroimaging techniques: structural and functional magnetic resonance imaging (fMRI), diffusion-weighted imaging (DWI), positron emission tomography (PET), electroencephalography (EEG), magnetoencephalography (MEG), magnetic resonance spectroscopy (MRS) and single-photon emission computed tomography (SPECT). Below is a description of the studies found, as well as an assessment of

the conclusion, what is missing and the best practices to move the field of bTBI imaging forward. The search was carried out for published articles on PubMed, between 2009 and 2020 (Table 3). Exclusion criteria included: non-human imaging and non-clinical studies, languages other than English, studies without a stand-alone military group, military studies without a focus on traumatic brain injuries, reviews, case reports and abstracts. A total of 77 articles (Table 4) met the search criteria.

**Table 3: PubMed search for literature review**

OR		OR		OR
Blast	AND	Traumatic brain injury	AND	Imaging
Explosion		TBI		Neuroimaging
Explosive		Concussion		MRI
IED		Brain Injury		DTI
Improvised	explosive	mTBI		fMRI
device		mild traumatic brain injury		PET
Veteran				SPECT
Military				MEG
Combat				EEG
				CT

Using google trends for analysis (<https://www.google.com/trends>), trends for publication dates show an increase in research focusing on bTBI imaging between 2013 and 2016. This corresponds to a worldwide interest in the terms “bombs” and “explosion”, peaking in April 2013 and reflected by the google searches of these terms (Figure 7). The highest percentage of searches is in the United States, which also sees the highest numbers of publications relating to bTBI. The United Kingdom’s search is 4<sup>th</sup> worldwide. The sudden increased interest similarly maps to the total number of terrorism-related episodes that peaks in 2009 and serves as the cut-off year for my literature review (Figure 7). This clearly illustrates the need for medical and scientific research in the field of blast injuries.

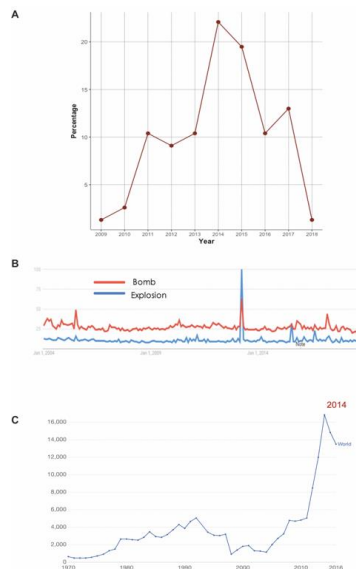


**Figure 7: Trends of interest. A) Trends of neuroimaging publications with a focus on blast traumatic brain injury, B) Google trends data: worldwide civilian search for terms “Bomb” and “Explosion” since 2004, C) Number of terrorism incidents per year. Terrorism defined as threat or use of illegal violence, fear or intimidation for political, social, religious or economic gain. Source: Terrorism incidents – Global Terrorism Database (<https://ourworldindata.org/terrorism>)**

I have grouped the findings of the literature review based on the different imaging techniques, the analysis methods and the main findings (Table 4).

**Table 4: Results of the literature review, reporting methods and main findings for the different neuroimaging modalities used (number of publications (n) & reference)**

	MRI	DWI	fMRI	PET	EEG	MEG	SPECT and/or MRS
Number of studies	13	33	20	5	2	3	3
<b>Techniques</b>							
Subcortical segmentations	3 (Lopez-Larson et al., 2013, Tate et al., 2016, Davenport et al., 2018)	1 (Waltzman et al., 2017)	-	-	-	-	2 (Kontos et al., 2017, Hetherington et al., 2014)
Cortical thickness	3 (Lindemer et al., 2013, Michael et al., 2015, Clark et al., 2018)		-	-	-	-	-
Multimodality	4 (Lopez-Larson et al., 2013, Yurgelun-Todd et al., 2011, Bazarian et al., 2013, Tate et al., 2017)	7 (Mac Donald et al., 2011, Costanzo et al., 2014, Matthews et al., 2011b, Petrie et al., 2014, Huang et al., 2009, Sponheim et al., 2011, Waltzman et al., 2017)	-	1 (Petrie et al., 2014)	1 (Sponheim et al., 2011)	-	-

Cognitive and/or behaviour tests	2 (Clark et al., 2016, Depue et al., 2014)	2 (Miller et al., 2017, Sorg et al., 2014)	3 (Matthews et al., 2011a, Scheibel et al., 2012, Matthews et al., 2011b)	3 (Stocker et al., 2014, Peskind et al., 2011, Mendez et al., 2013)	1 (Shu et al., 2014)	1 (Huang et al., 2014)	-
Voxel-based	1 (Depue et al., 2014)	1 (Trotter et al., 2015)	-	-	-	1 (Huang et al., 2017)	-
Freesurfer	2 (Michael et al., 2015, Tate et al., 2016)	-	-	-	-	-	-
Neuroradiological evaluation	1 (Tate et al., 2017, Clark et al., 2016, Savjani et al., 2017, Davenport et al., 2018)	-	-	-	-	-	-
Tensor-based	2 (Lopez-Larson et al., 2013, Yurgelun-Todd et al., 2011)	14 (Kamnaksh et al., 2014, Hayes et al., 2015, Davenport et al., 2015b, Levin et al., 2010, MacDonald et al., 2013, Matthews et al., 2012b, Sorg et al., 2016, Taber et al., 2015, Delano-Wood et al., 2015, Ware et al., 2016, Davenport et al., 2015a, Petrie et al., 2014, Venkatasubramanian et al., 2020, Adam et al., 2015)	-	1 (Petrie et al., 2014)	-	-	-
Tractography	-	2 (Clark et al., 2017, Yeh et al., 2017, Main et al., 2017)	-	-	-	-	-
HARDI	-	1 (Morey et al., 2013)	-	-	-	-	-
Resting-state	-	2 (Costanzo et al., 2014, Matthews et al., 2011a)	5 (Han et al., 2014, Gilmore et al., 2016, Newsome et al., 2016, Spielberg et al., 2015, Robinson et al., 2017)	-	-	-	1 (Raji et al., 2015)
Task-based	-	-	7 (Matthews et al., 2012a, Fischer et al., 2014, Scheibel et al., 2012, Roy et al., 2010, Newsome et al., 2015, McGlade et al., 2015, van Rooij et al., 2015)	-	-	-	-
FDG-PET	-	1 (Petrie et al., 2014)	-	3 (Stocker et al., 2014, Buchsbaum et al., 2015, Peskind et al., 2011)	-	-	-
Other	2 (Cheng et al., 2010, Tate et al., 2017)	3 (Miller et al., 2017, Jorge et al., 2012, Main et al., 2017)	2 (McGlade et al., 2015, Robinson et al., 2017)	1 (Mendez et al., 2013)	-	1 (Huang et al., 2012)	-
<b>Results</b>							
Volume change	5 (Lopez-Larson et al., 2013, Depue et al., 2014, Michael et al., 2015, Tate et al., 2016, Savjani et al., 2017)	-	-	-	-	-	-
No Volume change	2 (Davenport et al., 2018, Kamnaksh et al., 2014)	1 (Waltzman et al., 2017)	-	-	-	-	-
Reduced FA	1	14	-	1	1	-	-



	(Yurgelun-Todd et al., 2011)	(Hayes et al., 2015, Sorg et al., 2016, Taber et al., 2015, Yeh et al., 2014, Petrie et al., 2014, Delano-Wood et al., 2015, Ware et al., 2016, Yeh et al., 2017, Isaac et al., 2015, Matthews et al., 2012a, Mac Donald et al., 2013, Costanzo et al., 2014, Waltzman et al., 2017, Main et al., 2017, Adam et al., 2015)		(Petrie et al., 2014)	(Sponheim et al., 2011)		
Lesions	3 (Clark et al., 2016, Riedy et al., 2016, Tate et al., 2017)	1 (Levin et al., 2010)	-	-	-	-	-
No FA change	-	3 (Kamnaksh et al., 2014, Levin et al., 2010, Davenport et al., 2015b)	-	-	-	-	-
Altered connectivity and/or activation	-	4 (Clark et al., 2017, Costanzo et al., 2014, Huang et al., 2009, Sponheim et al., 2011)	11 (Han et al., 2014, Matthews et al., 2012a, Matthews et al., 2011a, Scheibel et al., 2012, Gilmore et al., 2016, Newsome et al., 2015, Spielberg et al., 2015, van Rooij et al., 2014, van Rooij et al., 2015, Brashers-Krug and Jorge, 2015, Fischer et al., 2014)	-	2 (Shu et al., 2014, Sponheim et al., 2011)	3 (Goldstein et al., 2012, Lopez-Larson et al., 2013, Scheibel et al., 2012)	1 (Kamnaksh et al., 2014)
Normal activation	-	-	2 (Newsome et al., 2015, van Rooij et al., 2015)	-	-	-	-
Abnormal metabolites and/or metabolism	-	1 (Petrie et al., 2014)	-	4 (Petrie et al., 2014, Buchsbaum et al., 2015, Peskind et al., 2011, Mendez et al., 2013)	-	-	2 (Kontos et al., 2017, Hetherington et al., 2014)
Other	1 (Bazarian et al., 2013)	5 (Miller et al., 2017, Jorge et al., 2012, Huang et al., 2009, Trotter et al., 2015, Mac Donald et al., 2019)	3 (Michael et al., 2015, Newsome et al., 2015, Robinson et al., 2017)	-	-	-	-

### Structural findings

Most of the reported cases of civilian and military TBI are mild, as compared to moderate or severe. In the case of mild TBI, acute scans are usually unremarkable, and visual inspection by neuroradiologists do not reveal much about structural or functional damage. Across 12 structural MRI reports, regions with volume change include mainly the **frontal and temporal lobes** (Tate et al., 2014, Lindemer et al., 2013, Clark et al., 2018), as well as subcortical areas mainly **amygdala and thalamus** (Lopez-Larson et al., 2013, Depue et al., 2014). Other studies did not find any

volumetric changes (Davenport et al., 2018). The widespread nature of volumetric changes is consistent with the diffuse aspect of blast wave. Changes to cortical and sub-cortical structures can either be a lasting effect of direct trauma to the head, or a latent effect due to microstructural damage to the WM. This can be studied by understanding the interaction between structure change and connectivity simultaneously.

### ***Diffusion findings***

Most DTI studies report measures of fractional anisotropy (FA), which describes the movement of water molecules within tracts. FA typically decreases when tracts are damaged. This quantification of microstructural changes in the WM is well-established and commonly used in clinical studies (Hulkower et al., 2013). Other metrics can be calculated from the tensor model, including axial, radial and mean diffusivity (AD, RD, MD). However, very few of the 31 DWI papers report them. Is it because of negative results or because of lack of investigations? It is therefore difficult to draw definitive conclusions about diffusivity patterns before further investigations. In the cases where metrics other than FA are used, there is an overlap. Studies looked at either whole-brain spatial statistics, or tracts-specific statistics, or both approaches (Venkatasubramanian et al., 2020, Levin et al., 2010, Yeh et al., 2014, Huang et al., 2009). Tracts commonly affected in bTBI are the **superior longitudinal fasciculus** (SLF) (Yeh et al., 2017, Matthews et al., 2011b, Petrie et al., 2014, Matthews et al., 2012b), the different regions of **the corpus callosum** (CC) (Venkatasubramanian et al., 2020, Mac Donald et al., 2011, Yeh et al., 2017, Morey et al., 2013), **thalamic radiations and internal capsule** (Yeh et al., 2017, Sponheim et al., 2011, Mac Donald et al., 2013, Sorg et al., 2014). Most of the studies performed comparisons at group level, which is common in DTI investigations. A few studies performed subject-level assessments, an approach that needs to be even more incorporated in future studies to understand how the biomechanics of the injury are associated with the neurological outcomes (Mac Donald et al., 2011, Mac Donald et al., 2013). As mentioned earlier, a clearer image of why certain areas are more vulnerable can be understood by using multi-modality comparisons, or even computational simulation of injury predictions. Longitudinal follow-up studies are also essential to uncover the long-term impact of bTBI (Mac Donald et al., 2019).

Among the studies that directly compared soldiers with bTBI to deployed soldiers without bTBI, (Bazarian et al., 2013, Davenport et al., 2012, Jorge et al., 2012, Levin et al., 2010, Mac Donald et al., 2011, Morey et al., 2013, Sorg et al., 2016), only two reported group differences, with no overlap in the reported regions with WM abnormalities. A possible explanation for the low findings that detect group differences in FA measures using standard neuroimaging techniques such as voxel-wise comparisons is that the effects of bTBI are spatially heterogeneous in subjects. Some studies already seem to support this hypothesis, showing that soldiers with bTBI have more ROIs or voxels with a decrease in anisotropy (Mac Donald et al., 2011, Mac Donald et al., 2013, Davenport et al., 2012, Jorge et al., 2012) which points to bTBI being associated with WM abnormalities, varying in location and intensity, even if a definite pattern does not emerge consistently.

### ***Functional findings***

20 of the reported studies used functional neuroimaging for their investigations. fMRI measures blood flow to specific areas of the brain, which represents the metabolic demand driven by neuronal activity. In other words, it reflects the activation or deactivation of certain areas of the brain in response to stimuli or in rest conditions. As with other techniques, the studies varied on different levels. 25% used resting-state fMRI, 35% used task-based fMRI, with heterogeneous tasks and dissimilar analysis methods (Costanzo et al., 2014, Han et al., 2014, Scheibel et al., 2012). Most of the studies however show abnormal activations of different brain regions. Difficulty with working memory is often reported following both blast and non-blast TBI (Rosenfeld and Ford, 2010, Vanderploeg et al., 2009). Studies suggest that the neural network associated with working memory include the pre-frontal cortex, temporal cortex, parietal cortex, and cerebellum (Drobyshevsky et al., 2006, Ranganath and D'Esposito, 2005, Owen, 2000).

### ***Brief conclusion***

The findings are not surprising since they are in line with the known biomechanical susceptibility of the brain when exposed to translational and rotational forces. What is still obscure is how the injuries caused by blast differ from other widely researched forms of TBI. This can only be accomplished by having a non-blast TBI group as a controlling factor to weaken the effect of secondary/tertiary insults. The importance of

distinguishing between the different forms of damage lies mainly in the understanding of mechanical properties of different insults for the development of protective equipment and treatment strategies. The nature of exposure to blasts is hard to assess given the lack of validated method for quantifying injury severity. Another challenge of bTBI research in humans is the circumstances in which injuries occur, 50% of which happen during active combat. Injuries are often under-reported, and it is highly exceptional to have acute neuroimaging data or neurological diagnosis. Adding to the complexity stated above, the comparison of existing studies is rendered tricky due to the small number of findings, the negligible overlap of results, the operational heterogeneity at the level of methodology, and the difficulty to control for the variations between cases. Drawing conclusions this early is still impossible. Therefore, methodological consistency as well as targeted controlling factors are essential in future studies aiming directly at understanding bTBI.

## 1.8. CURRENT LIMITATIONS IN THE NEUROIMAGING DETECTION OF BLAST-INDUCED TBI

### 1.8.1. Issues with Controlling Factors

There is an important variability regarding inclusion criteria among different studies, as well as a heterogeneity of the composition of the control groups (Phipps et al., 2020). However, it is crucial to note a main trend: the participants tend to be recently deployed and active or retired and with a diagnosis of PTSD and/or bTBI (Davenport et al., 2015a, Norris et al., 2014, Barlow-Ogden and Poynter, 2012).

Because of the nature and conditions in which bTBI tend to occur, different injury mechanisms (section 1.5.2) as well as comorbid conditions are common in soldiers with bTBI. However, more data and research is needed to understand the contributions of primary injuries exclusively, or pure blast wave in bTBI. It is therefore essential to evaluate and compare the effects of bTBI to other mechanisms of brain injuries, especially on military vs civilian population which is still scarce in the current literature

Going forward, it is important to control for

- 1) The difference between blast and civilian TBI to better understand neurological biomarkers exclusive to bTBI and introduce new hypotheses in relation to the contribution of primary injuries exclusively.
- 2) Understand how the absence of PTSD diagnosis can impact some of the results currently seen in the literature, mainly regarding neuropsychological and cognitive measures, as well as specific neuroimaging patterns that seem to be related to PTSD, such as a decrease in hippocampal volume (Logue et al., 2018). This is significant to better discriminate between bTBI and PTSD considering the similarity in clinical symptomatology.

### 1.8.2. Issues with Homogeneity of Studies and Neuroimaging Analyses

Blast-related TBI studies are plagued by inconsistent diagnostics and different assessment approach (Greer et al., 2018, Phipps et al., 2020), with many studies using self-report measures. In the context of neuroimaging analyses techniques, different approaches can lead to different results, therefore biasing interpretation of

the outcome. Although it is outside the scope of this thesis to standardize diagnostics and reporting of bTBI (Phipps et al., 2020), it is possible to improve the standardization of neuroimaging research protocols to encourage reproducibility in different cohorts and different demographics of patients with bTBI, and diagnostics technologies to detect injuries specific to blast exposure given the great need to understand outcome resulting from different types of blast exposures. DTI is of particular interest in this context because of the lack of detectable abnormalities with conventional CT or MRI imaging that used routinely for diagnosis. This is an aspect of the field I strongly focus on in this thesis.

### **1.8.3. Civilian Considerations**

In first world countries, what was formerly injuries confined to military personnel became a reality for their population when IEDs were deployed among civilian populations for terrorist attacks. Unfortunately, in other countries serving as the battlefield of both civil and proxy wars, this has always been a horrible reality. The absence of emergency care, as well as protective equipment such as helmets and body armour worsen the outcome and mortality of blast injuries in civilians, making extrapolation from military investigations flawed. However, the literature is almost non-existent to describe or understand bTBI in civilians. Resilience and community experience plays a big role in the recovery process and understanding the psychological and sociological implications of such events can also help military research.

# CHAPTER 2

---

## Materials & Methods

*In this chapter, I present the materials and methods used for my studies. I only describe relevant concepts that will be mentioned in subsequent chapters, without details of possible alternative protocols and methodologies. I begin by introducing the notions of structural and diffusion imaging, some of the main analyses used with these modalities, relevant neuropsychology and endocrinology measures, as well as some of the statistical methods used and the pitfalls of current methods.*

## 2.1. STRUCTURAL IMAGING OF THE BRAIN

### 2.1.1. Historical Background

For more than two centuries, scientists have been trying to map the brain's structure and understand its typical and pathological functions. In the early 19<sup>th</sup> century, phrenologists were the first to propose popular methods according to which the amount of brain tissue of a specific cognitive function influences the behaviour. Although, at the time, it was impossible to measure cortical volumes, the assumption was that increased brain size can be measured through bumps on the skull.

Fast forward to 1968, when the first nuclear magnetic resonance (NMR) signal was acquired from a rat. As by-products of wartime development of the radar, the injection of radiofrequency expertise as well as the availability of stable new frequency sources, made the demonstration of NMR possible. A few years later in 1971, Damadian reports on the capability of the NMR signal to differentiate tumours from normal tissues. Magnetic Resonance Imaging (MRI) was invented by physicist Paul C. Lauterbur who used magnetic field gradients to encode spatial information into the NMR signal and published his invention in March of 1973. Images acquired through MRI of the head provided excellent anatomical details with stronger grey/white matter contrast compared to images from other modalities. Other techniques soon followed, such as the flow-sensitive techniques, developed in the 1980s. These measures of the blood flow velocity were considered the first one not to be purely structural in nature. A major leap in neuroimaging happened with the development of functional MR imaging (fMRI), in 1990.

Although crucial work to develop the field has been occurring for over a century, it is fair to say that most of the research around the brain and its function and cognitive/behavioural neuroscience in general has transpired over the past few decades because of its prominence in the scientific literature for researchers in the field, as well as in the media for the general public, due mostly to the human fascination with the brain-mind questions. The field continues to grow, with practical applications of functional brain imaging becoming feasible in the 2000s with the development of brain-computer interfaces.

### 2.1.2. MRI Definition, Physics and Principles



The fundamental principle of MRI is that an atomic nucleus can act like a magnet, interacting with magnetic fields, thus allowing us to measure and even manipulate their magnetic state without damaging them and without interfering with any biological process that involves nuclei and molecules. Different elements can exhibit the necessary properties of magnetic resonance. However, MRI applications rely on the hydrogen atoms of the water molecules because of their abundance in the human body.

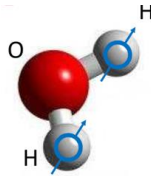


**Figure 8 Hydrogen atoms in a water molecule.**

A very strong magnetic field is required to interact with the hydrogen atoms. Just like a magnet, a hydrogen atom has an orientation with a north and south pole. In the absence of a magnetic field, the hydrogen atoms point in different and random directions, so the overall orientation of the magnetization from summing individual charge contribution is null, in which case, a signal can't be detected. In the presence of a strong magnetic field, the nuclei will start pointing in the same direction and along the main field. This strong magnetic field (**the B<sub>0</sub> field**) arise from a large superconducting coil that defines the strength of the MRI scanner, which is usually reported in tesla (**or T**). For example, the scanners used in the studies detailed below are 3T scanner: a scanner in which the B<sub>0</sub> field is 3 tesla.

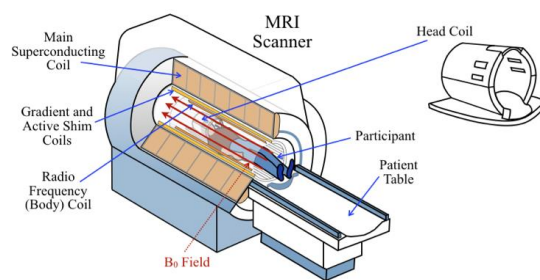


**Figure 9 Hardware and composition of an MRI scanner (Michael Chappell, 2018)**

Although alignment with the field is favoured in the presence of a strong magnetic field, at normal room temperature hydrogen atoms pointing in the opposite direction to the B<sub>0</sub> field is very low (in the order of one in one million).

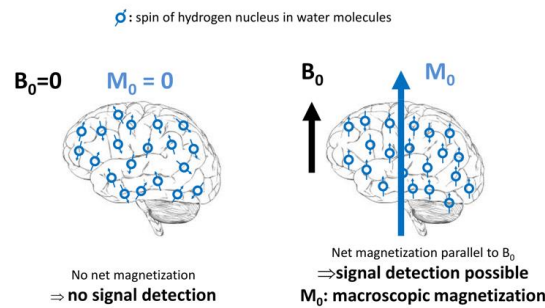


**Figure 10 Macroscopic magnetization of hydrogen nuclei aligning with the  $B_0$  field. Source: [unil.ch](http://unil.ch)**

When magnetization is achieved, the nuclei can be shifted out of alignment with the  $B_0$  field, leading to a precession, or rotation of the nucleus around the axis of the main field in a circular path. The frequency of this rotation is proportional to the strength of the main magnetic field (the  $B_0$  field), and the **Larmor Equation** governs the relationship between the frequency of the rotation of the nucleus and the field (Figure 11).

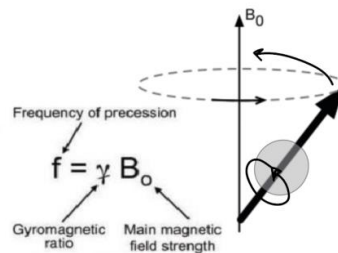


**Figure 11 Example of hydrogen nucleus aligning to an external field and its precession properties. The Larmor equation is described on the left. The grey sphere represents the hydrogen nucleus, the dashed line represents the precession around the  $B_0$  field axis.**

The net magnetization of hydrogen nuclei described above varies with time and generates a change in the magnetic field that can be measured by the head coil in the tens of MHz. As the magnetization loses its alignment with the  $B_0$  field through excitation, and varies with time at the Larmor frequency, the resulting magnetic field oscillates at the same frequency called **the  $B_1$  (or RF) field**, that, given the coil orientation, is perpendicular to the  $B_0$  field. The resulting effect is to change the orientation of magnetization away from  $B_0$  and into the transverse plane through excitation. For spatial localization of the signal, extra fields (**gradient fields**) are created by three different gradient coils (for the three orientations in space).

Excitation of atoms is thus used to disturb the magnetization and measure the signal created from the tissues that have been excited. The signal received by the coil can be separated through the **Fourier Transform**, to separate out the different parts of the signal and relate them to spatial positions. This is the **Gradient Recalled Echo** (GRE). In more simplistic terms: RF signal (excitation) + spatial gradient → readout signal (echo). To produce a readable image, we exploit the relaxation properties of the hydrogen nuclei. Relaxation is the return of the net magnetization to the B0 alignment following excitation by the B1 field. T1 (longitudinal) and T2 (transverse) relaxations are two processes that happen simultaneously. T2 is the time required for the transverse magnetization (perpendicular to the B0 field) to fall to approximately 37% of its initial value. The decay of this signal can generate a contrast since different brain tissues have different inherent T2 values. **Echo time** (or TE), is the time between excitation and measure of the signal. TE should be optimized for best contrast. T1 relaxation is the recovery of the component parallel to the main field. T1 decay is much slower than T2 decay and happens over a few seconds. The **repetition time** (TR) is the time between successive excitation, which impact largely on timing and contrast. TR needs to be optimized for greatest contrast between the different tissue types (GM, WM and CSF) possessing different relaxation times.

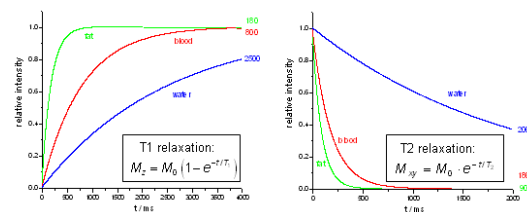
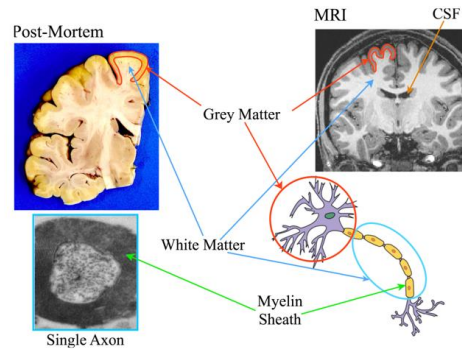


Figure 12 Different relaxation properties of tissues, and resulting images.

### 2.1.3. Anatomy in Neuroimaging

Major anatomical axes within the brain are named following a standard convention: superior–inferior, anterior–posterior, and left–right (or S-I, A-P, and L-R for short).



**Figure 13: Illustration of GM and WM tissues. As seen post mortem (up-left) and in a T1-weighted MRI image (up-right), with a microscopic transverse slice (down-left) of a myelinated WM axon and a schematic of a neuron (down-right). Source: [fmrib.ox](http://fmrib.ox.ac.uk/)**

Different planes resulting from the 3D imaging also have standard names: coronal (superior/inferior and left/right), sagittal (superior/inferior and anterior/posterior), and axial (anterior/posterior and left/right). Navigation around the brain images also rely on the different lobes: frontal, occipital, parietal, and temporal. Other than the major lobes, finer and more detailed structures are also distinguished on neuroimaging data: They include the lateral ventricles, the brainstem, the cortex, the corpus callosum, the cerebellum, the different types of tissues from WM, to CSF and cortical as well as subcortical GM structures - namely the thalamus, amygdala, hippocampus, globus pallidus, putamen, caudate, and nucleus accumbens.

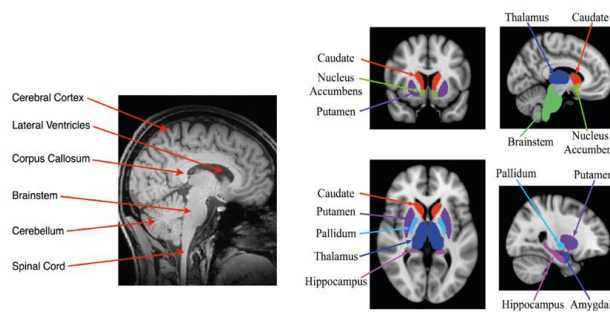


**Figure 14 Main features and subcortical structures of the brain anatomy as seen in T1-weighted MRI. Adapted from [fmrib.ox](http://fmrib.ox.ac.uk/)**

#### 2.1.4. Overview of Structural MRI Analysis

Applications of structural neuroimaging focuses mainly on determining the shape and size of brain structures. The basic principles of MRI analysis include brain extraction,

segmentation, spatial normalization (described in section 2.4) and methods of measurement (volumetry, voxel-based).

### ***Brain Extraction and Segmentations***

- The brain extraction tool (BET – FSL) (Smith, 2002) is used to strip away the skull, skin and facial features from an image based on the dark signal from the CSF between the skull and the brain, and CSF from the ventricles. This avoids wasting time on the analysis of unnecessary structures outside of the brain, as well as indication of which voxels are located inside the brain.

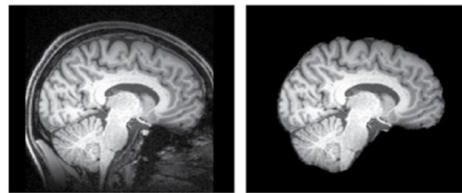


Figure 15 Example of brain extraction. Before (left) and after (right)

- Segmentations consist of labelling voxels based on their intensities and location, through machine-learning. In tissue-type segmentations, three labels are assigned to different locations: GM, WM and CSF, based on the intensity of the T1-weighted image. For most accurate segmentations, noise and bias field should be taken into consideration. However, some voxels contain a mixture of tissues, known as the **partial volume effect**. To overcome inaccuracies introduced by partial volumes, the automated tissue-type segmentation estimates the proportion of the different tissues in each voxel and gives the results in the form of partial volume estimates (**PVE**). An important application of tissue-type segmentation is the analysis of brain volume and tissue volume.



**Figure 16:** Example of tissue-type segmentation yielding the CSF (left), GM (middle) and WM (right) maps.

- The automatic segmentation of other structures, mainly subcortical GM structures, requires more information than intensity and location. These methods use information from prior labelled images (information about the shape and size) to determine which parts of the new image being segmented correspond to the label. The output of such segmentations can be a boundary mesh (coordinates of the outline of the structure), a labelled image or both.

#### ***Methods of Measurements***

- **Volumetry of subcortical GM structures:** following segmentation, volumes of specific tissues or structures can be computed by multiplying the number of voxels within the region and the voxel dimensions. This type of analysis requires a pre-defined region-of-interest (ROI).
- **Voxel-based morphometry (VBM)** tries to find differences in the local amount of a specific tissue between groups or in relation to a given covariate. This analysis follows a voxel-wise approach, and the resulting output is a 3D image of the local differences or associations.

## 2.2. DIFFUSION IMAGING OF THE BRAIN

### 2.2.1. Principles of dMRI

Images acquired through the diffusion MRI (dMRI) sequence are usually used to investigate the WM connectivity of the brain and its underlying microstructure. Water molecules provide most of the signal and are in constant random motion known as the **Brownian motion**. In the presence of bundles of axons, the movement of water molecules is restricted by the cell membranes, which means that the molecules move along the direction of the axons' orientation. The higher the density of the axons, the greater the diffusion along their axial plane rather than their radial plane.

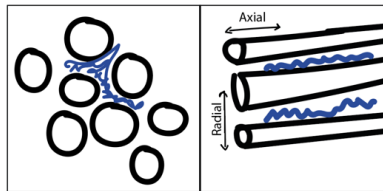


**Figure 17** Examples of water molecule movement. Movement of the water molecules (blue lines) along the axial plane of the axons (black representation) is restricted by the cell membrane of the axons when its microstructure is intact. *Image by author.*

The physical properties of the movement of water molecules within a given period are quantified through dMRI. dMRI uses a T2-weighted pulse sequence (long TR and long TE as opposed to the T1-weighted pulse described above), with two extra gradient pulses, equal in magnitude and opposite in direction, applied between excitation and data acquisition. These additional pulses render the imaging more sensitive to motion of water molecules by forcing protons out of phase and into phase again. When the protons diffuse, rephase is not complete, causing an attenuation in the signal's intensity, resulting in darker regions on diffusion-weighted images. In other words, higher diffusion of water molecules along the axis of the applied pulse yields lower signal intensity. Sensitivity to water diffusion is proportional to the gradient factor  $b$  ( $\text{sec}/\text{mm}^2$ ). One way to derive the physical properties of the diffusion process from the dMRI data is through a model called **diffusion tensor imaging (DTI)**. DTI assumes that there is a single direction of motion within each voxel and models the diffusion within an axon as a 3-D ellipsoid called a tensor (Figure 18).

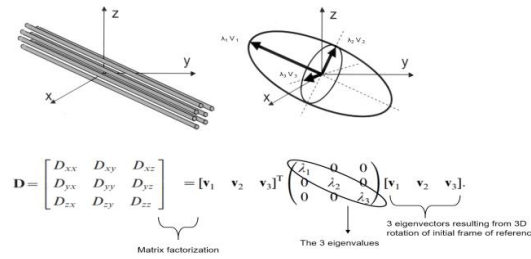


**Figure 18: Tensor estimation model. Top left: fibre tracts with orientation (x, y, z). Top right: 3D diffusivity modelled as an ellipsoid with specific 3x3 orientation matrix defined by the eigenvectors (V1, V2, V3) resulting from the transformation T, and shape ( $\lambda_1$ ,  $\lambda_2$ ,  $\lambda_3$ ), the three non-zero eigenvalues resulting from the matrix factorization. Bottom: transformation to scale up the vector from the initial frame of reference. Adapted from (Jellison et al., 2004)**

This diffusion tensor is a 3x3 matrix (from 6 directions) characterizing diffusion in 3D space, and assuming that the diffusion distribution is Gaussian. The mathematical properties of the tensor enable extraction of several scalar measures. The 3D orientation of tensor model is represented by three eigenvectors (V1, V2, V3) representing major, medium and minor axes, and the 3D shape is characterized by three eigenvalues ( $\lambda_1$ ,  $\lambda_2$ ,  $\lambda_3$ ) describing diffusivity in each direction. After transformation, the major eigenvector reflects the main direction of diffusivity within the voxel. This mathematical model describes the diffusion process in terms of quantities such as **fractional anisotropy (FA)**, **mean diffusivity (MD)**, as well as other measures. FA values can then be derived from eigenvalues and are an index of diffusion asymmetry within a voxel. FA values can vary between 0 and 1, with 0 being a perfect isotropy of equal eigenvalues (a sphere). As FA values tend to 1, progressive anisotropy describes an elongation of the ellipsoid and a more targeted diffusivity. The FA map is a representation of FA values (in greyscale) across the brain.

### 2.2.2.Acquisition of dMRI

The most common imaging sequence is known as **echo planar imaging (EPI)**, which is used in both diffusion and functional MRI. EPI is based on the principal of capturing all necessary information following a single RF excitation pulse. This is achieved by applying in both directions a series of different gradients in rapid succession, which results in a faster sequence (limitations are discussed in 2.8). To obtain an image of how diffusion varies in different directions, images with different diffusion-encoding directions need to be acquired. Typically, the number of 3D volumes and directions



vary between 60 and 200 to distinguish the fine details of the axons. The acquisition of the images is affected by both the orientation in space (usually distributed over the surface of a sphere), and the strength and timing of the diffusion-encoding gradient (**the b-value**), which typically range between 1000-1500 s/mm<sup>2</sup>. In a normal dMRI sequence, several images are acquired without using an encoding gradient, referred to as the **b0 image**, which defines the baseline for model estimation.

### 2.2.3. Analysis of dMRI

Before fitting any model to the dMRI image, several pre-processing steps are required. The main target of the pre-processing stages is to remove any motion or distortion-related artifacts, handled mostly through the following techniques:

- motion correction: correcting for head movement in the scanner
- eddy-current corrections: correcting for eddy currents resulting from the diffusion-encoding gradient causing spatial distortions in the image
- B0-induced distortion corrections: correcting the inhomogeneities induced by the B0 field

Following pre-processing, the result is a set of images in which changes in intensity between the images reflect changes of the diffusivity properties. After pre-processing and depending on the scope of the study and the chosen model, the model (*which in this case is the diffusion tensor model*) is fitted at every voxel.

The diffusion tensor model (described in 2.2.1), assumes that the diffusion in different directions follows a spatial Gaussian probability. At each voxel, the diffusion tensor is fitted to the intensity data as an estimation of the orientation along a sphere. Information derived from the tensor (such as FA or MD) can then be analysed depending on the hypothesis of the study, to extract indirect information reflecting the microstructural integrity of the WM. These can be done voxel wise (in group-level analyses) or region-based (for group and individual investigations). DTI can also enable tractography analysis, a 3D modelling of fibre orientation, directional information at each voxel, and delineation of WM tracts.

## 2.3. NEUROPSYCHOLOGY AND ENDOCRINOLOGY

### 2.3.1. Neuropsychology Testing

The patients and controls in the studies that follow performed a battery of standard pen and paper tests to measure cognitive function associated with memory, executive function, intellectual function and reasoning. The tests were previously used in TBI studies (Kinnunen et al., 2011, Jilka et al., 2014). The tests include:

1. The Wechsler Test of Adult Reading (WTAR) (Wechsler, 1945)
2. Matrix reasoning subtest from the Weschler Adult Intelligence Scale (WAIS-III) (Wechsler, 1945)
3. The peoples test (PT) from the Peoples and Door Test (Wechsler, 1945)
4. The logical memory subtest of the Weschler memory scale (Wechsler, 1945)
5. The colour-word interference (Stroop) test from the Delis-Kaplan executive function system (Delis et al., 2004)
6. The Trail-Making Test

#### **WTAR**

The WTAR measures levels of intellectual ability in individuals between the ages of 16 and 89 years. The test has a list of 50 words with atypical pronunciations to control for strategies. The score is based on the number of correctly pronounced words. Reading recognition is relatively intact following TBI and can be used as a premorbid marker in patients.

#### ***Matrix Reasoning***

The matrix reasoning subtest (part of WAIS-III) measures abstract reasoning and problem solving. The test has 26 trials with a 2x2 grid with  $\frac{3}{4}$  of the squares containing shapes, and the difficulty increasing over time. One of five shapes presented needs to be selected in a logic inferred in order to complete the grid (Figure 19). The scores reflect abstract reasoning/fluid intelligence.

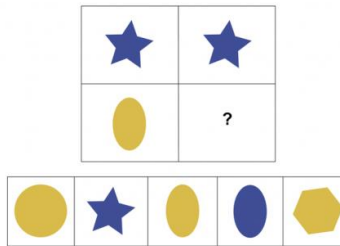


**Figure 19: Example from the matrix reasoning test.**

### ***Peoples Test***

The Peoples Test measures long-term memory associated with verbal recall. Four people with their profession and name are presented, and after delay, individuals are asked to recall the name prompted by their profession, three times for learning and after an extended delay (~20 minutes), individuals are to recall the names of the four people to measure forgetting.

### ***Logical Memory Test***

The logical memory test measures verbal-recall memory encoding. The test consists in reading a short story repeating it immediately and after a 20 minute delay. The scores reflect the immediate and delayed memory.

### ***Colour-Word Interference Test***

This test reflects executive function and is based on the classic Stroop effect (Stroop, 1935). It comprises of four increasingly difficult trials (Figure 20). Trial 1: name the colour of the squares displayed. Trial 2: Read words (in black ink) that describe colours. Trial 3: naming the colour in which the word is written, with the colour of the word with being incongruent to the colour it is describing. Trial 4: switching naming the ink colour of a word and reading the word (when it is framed in a box).


<b>Trial 1: Colour naming</b> 	<b>Trial 2: Word naming</b> Blue Red Green Green Green Blue Red Blue Red Green Blue Red
<b>Trial 3: Inhibition</b> Blue Red Green Red Green Green Blue Blue Red Blue Red Green	<b>Trial 4: Inhibition switching</b> Blue Red Green Red Green Green Blue Blue Red Blue Red Green

Figure 20: Example of the colour-word interference test.

Score is attributed based on time and error rate. The resulting measures are as follows:

**Equation 1: Measures of the Stroop test.**

$$\text{Baseline} = \frac{(\text{Colour naming} + \text{word reading})}{2}$$

$$\text{Inhibition} = \text{Inhibition (trial 3)} - \text{Baseline}$$

$$\text{Switching} = \text{Switch (trial 4)} - \text{Baseline}$$

$$\text{Inhibition Vs, Switching} = \text{Switching} - \text{Inhibition}$$

### ***Trail-Making test***

The Trail Making Test measures executive function and information processing. The first trail uses numbers from 1-25 – in which a line must be drawn between consecutive numbers starting from 1 - and the second uses both letters and numbers – in which numbers and letters must be alternatively connected in ascending (e.g. 1-A-2-B-3-C). Scores are based on completion time and reflect information processing performance (Trial 1) and executive function (Trial 2). Times from the first trial can be subtracted from times from the second trial to control for individual differences in information processing when examining executive function.

### **2.3.2. Endocrinology Testing**

Baseline measures of serum anterior pituitary hormones included: Cortisol, follicle stimulating hormone (FSH), luteinizing hormone (LH), testosterone, thyroid stimulating hormone (TSH), free thyroxine (T4), free triiodothyronine (T3), prolactin,

adrenocorticotrophic hormone (ACTH), growth hormone (GH), insulin-like growth factor 1 (IGF-I), sex hormone binding globulin (SHBG) and free androgen index (100xtestosterone/SHBG).

Endocrine dysfunction was reported on the basis on the following measures (Table 5):

- Hyperprolactinemia
- Gonadotrophin deficiency
- GH deficiency

**Table 5: Diagnostic methods for pituitary dysfunction**

Pituitary Axis	1 <sup>st</sup> Test	Confirmatory test
GH Deficiency	Glucagon Stimulation Test (Peak GH < 5µg/L)	GHRH-Arginine Test (GHD cut off based on age and BMI) or ITT peak GH < 3 µg/L (Colao)
ACTH Deficiency	Glucagon Stimulation Test (Cortisol < 350 nmol/L)	Metrapone Stimulation Test (ACTH < 60 ng/L and 11-DOC < 200 nmol/L) or peak cortisol ITT < 500 nmol/L
Prolactin	Prolactin > 375 mu/L	Repeat prolactin > 375 mu/L AND Macroprolactin Negative
Gonadotrophin Deficiency	Non-elevated LH (1.7-12.0) and FSH (1.7-8.0) AND Testosterone < 10 nmol/L or if SHBG low (< 15 nmol/L) FAI < 30	Non-elevated LH (1.7-12.0) and FSH (1.7-8.0) AND 9 am Testosterone < 10 nmol/L or if SHBG low (< 15 nmol/L) FAI < 30
TSH Deficiency	Non-elevated TSH (0.3-4.22) AND Free T4 < 9.0 pmol/L or free T3 < 2.5 pmol/L	Non-elevated TSH (0.3-4.22) AND Free T4 < 9.0 pmol/L or free T3 < 2.5 pmol/L
ADH Deficiency (Vasopressin)	Symptoms score	Water Deprivation Test

\*FAI=Free Androgen Index =100x free testosterone titre/SHBG

The **cortisol day curve** is measured as follows: blood samples are taken five times every three hours between 0900h and 2100 h (Immulite® 2000 assay (Siemens) or Architect i2000 (Abbott, UK)), and plasma ACTH at 0900h. ACTH deficiency was based on cortisol levels < 100 nmol/L or 3.62 µg/dL at 0900 or 1200h.

## 2.4. REGISTRATION IN NEUROIMAGING STUDIES

The following section describes **spatial transformations** used in neuroimaging studies. The aim of registration is to align the anatomy between different images by transforming images in space. Such changes can range from simple rotations and translations of the entire image, to changing the shape and size of specific structures within the image. Registrations can be intermodal (across different modalities), intramodal (within the same modality), Intra-subject (within the subject), Inter-subject (between different subjects), or a combination of these types. The important parameters of transformation, which will be mentioned in later chapters are 1) the type of transformation, 2) the cost function used, 3) The reference space and 4) the interpolation method. These four concepts are described in more details below.

### 2.4.1. Linear Transformations

#### *Rigid-body registrations*

This registration technique consists of **translations** and **rotations** and is called **rigid-body transformation**. In mathematics, a rigid transformation (or Euclidean transformation) is a transformation that preserves distance between two points (O. Bottema, 2018). Images keep the same shape and size following rigid transformations. In 3D imaging, rotations and translations happen along each of three axes – three independent translations / three independent rotations - so the combination results in six degrees of freedom (6-DOF), a [3x3] matrix where each DOF will correspond to a numerical parameter of the transformation. This transformation is mostly used when the anatomy remains the same (such as within-subject registrations), or as a first step alignment before more exhaustive transformations.

#### *Affine registration*

Affine transformations have 12-DOF, the same 6 DOFs as described above in rigid-body registrations, plus three DOF for scaling and shearing. These are mostly used to correct for acquisition errors such as eddy-current distortions (described in 2.2.2), or as a first step alignment before more exhaustive transformations. Affine registrations preserve collinearity (points on the same line remain on the same line) and parallelism. As in rigid-body registration, the change is applied to the entire image, and not to

specific voxels, so the output of such registration is the corresponding transformation matrix.

### 2.4.2. Non-linear Transformations

When the images have different anatomies, or anatomical abnormalities, linear transformation is not enough for accurate anatomical correspondence between the images. Non-linear transformations usually have more than 12 DOF, with the resulting output being a **warp** of voxel wise transformation rather than a matrix of the image transformation. Non-linear transformations result in a local change of geometry while preserving topology - a transformation known as **diffeomorphic registration**. Non-linear transformations also include smoothing (or regularization) to limit the change in geometry, as trade-off between anatomical correspondence and signal-to-noise ratio (SNR). This smoothing, however, might blur some anatomical details, with lower quality of images requiring higher amounts of regularization.

### 2.4.3. Cost Functions

Cost functions are a type of parameters that help achieve the best alignment of the images. The cost function searches for the lowest cost value associated with the different degrees of transformations, in order to choose the optimal transformation. There are different cost functions to choose from, depending on the situation. In this section, I only describe the **boundary-based registration** (BBR<sup>3</sup>) in more details, since I will be using this cost function in subsequent pipeline development as an essential element of image registration after trial and error of different mainstream cost functions.

**Table 6: List of some of the most common cost functions used in image registration.**

Cost Function	Use
Sum of Squared (SSD)	Intra-modality
Normalized correlation	Intra-modality (with intensity offset)
Correlation ratio	Inter-modality
Mutual Information	Any

---

<sup>3</sup> The BBR cost function can be applied with or without a field map. However, it performs better after distortion correction.

---

**Boundary-based registration (BBR)**


---



---

 Images with contrast across the  
tissue boundaries
 

---

Boundary-based registrations are most commonly applied to EPI images being registered to structural images (Greve and Fischl, 2009). BBR uses a reconstructed mesh of the white-grey matter (WM/GM) boundary to drive the alignment based on the difference in intensity along this mesh (Figure 21). Given that the anatomical boundary drives the alignment, the target data doesn't need to be of high quality if there can be a clear differentiation of tissue intensity across tissue boundaries. BBR is robust with respect to spatial intensity inhomogeneities and can allow alignment of EPI volumes to anatomical data. BBR calculates a cost function that integrates local calculations around vertices. A gradient value is calculated at each vertex by subtracting sampled intensity values on opposite perpendicular sides of the vertex, with the gradient at vertex  $v$  being:  $\text{grad}_v = g_v - w_v$ .

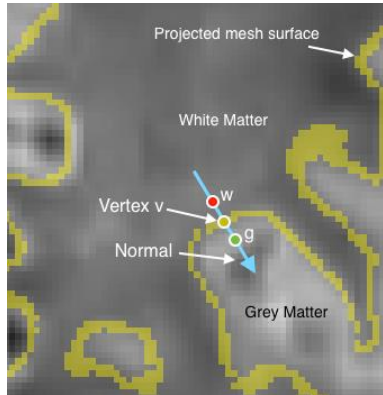


**Figure 21: Representation of BBR cost function estimation at a vertex  $V$ .**

#### 2.4.4. Interpolation and Resampling

Resampling is the process of using a transformation to move an image into another image's "space". The space of an image is the set of coordinates that determine the spatial location and orientation of the given image. Images in the same space will therefore share the same coordinate frame and are said to be aligned. Analyses can be performed in **native space** when the raw image is not resampled, or in a group space when images are resampled to a common average image or template. Resampling uses an interpolation method: intensities of voxels are calculated based on the combination of the intensities of the original voxels specified through the



interpolation function. The simplest and most common interpolation used in neuroimaging is the **nearest neighbour interpolation**, which copies the intensity value of the closest voxel to the one being interpolated while linear interpolation calculates the weighted average of neighbouring voxels.

## 2.5. PRINCIPLES OF GROUP-LEVEL ANALYSIS

Group-level studies are used to generalize the results to a wider population, unlike clinical practice where the interest lies in the results of a single subject's data. The pillars of group-level analyses are registration - to get accurate inter-subject alignment- and the use of appropriate statistical methods. The latter usually uses general linear models (GLM).

### 2.5.1. Templates and Atlases

In group-level analyses, all subjects are usually registered to a common **template space**. The template can be:

- Study-specific and created by averaging the images of the control population<sup>4</sup>.

The accurately represent a specific population, with the assumption that there are enough subjects.

- A standard template, publicly available, such as the **MNI152 template** derived from 152 averaged structural images of healthy young adults (Mazziotta et al., 1995).

**Atlases** are usually in a template's space (standard space), but the intensity usually encodes for information different than the standard data seen in structural imaging. For example, indexes can correspond to different structures, such as subcortical GM structures, or WM tracts. They are often used for the automatic labelling of ROIs in group-level or subject-level analyses. Atlases can be discrete (a label value corresponds to a structure) or probabilistic (a value of 0-1 at each voxel for the probability of the voxel being part of the structure).

The MNI152 template is the one I use for all my studies because all the atlases I required and utilized (WM, GM, subcortical structures) were derived from this template.

### 2.5.2. Voxel-Based Morphometry

VBM is a group-level computational method of neuroimaging analysis that measures voxel-wise differences in brain tissue concentration between multiple images (Ashburner and Friston, 2000). VBM requires many steps, most of which have been

---

<sup>4</sup> Some studies suggest the use of all images -controls or not- to create the template image in order not to bias the anatomy to a specific group.

described above. Fundamentally, it combines tissue-type segmentation and spatial normalization of the images from all the subjects in two or more different groups into the same space, usually a group-defined template. Registration to the template allows a calculation of the change in local volume of a given voxel – known as the Jacobian determinant. Another important aspect of the VBM pipeline is **smoothing**, which compensates for misalignments of the different images, renders noise distribution more Gaussian<sup>5</sup>, and improves sensitivity for subsequent statistical analysis.

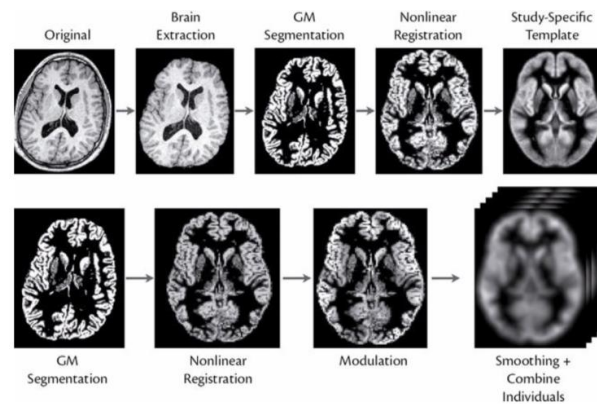


**Figure 22: Steps for the VBM pipeline specific the GM. Source: (Mark Jenkinson, 2018)**

The analysis usually relies on the GLM and standard parametric statistical procedures such as f-tests and t-tests with the assumptions of independent and normally distributed residuals. Following the application of the GLM, statistical significance of the difference between two groups is represented on a voxel-wise statistical parametric map (SPM).

VBM and ROI -based studies are most used when investigating volume differences between groups. However, the advantages of VBM can be explained by its automation and ease to use, time efficiency and whole-brain aspect, which has made it a popular tool in the neuroimaging community.

### 2.5.3. Vertex Analysis

Vertex analysis (or shape analysis) is like VBM in that it relies on segmentation, registration, and assessing group-differences on a per-vertex basis (instead of voxel-

---

<sup>5</sup> The Gaussian smoothing is a mathematical function that uses blurring to overcome noise and artifacts in a signal. The Gaussian kernel follows the normal distribution curve.

wise). Vertex analysis looks at how the shape of a particular structure differs between two groups based on the meshes of the structure. Using the mesh allows visualization of the area and the type of the morphometric difference.

#### 2.5.4. Tract-Based Spatial Statistics (TBSS)

TBSS is a suite of tool that enables group-level analyses of diffusion data (Smith et al., 2006). As mentioned previously, a common measure derived from the diffusion tensor is FA, which quantifies the **strength of directionality** of a given tract. Voxel wise statistical analyses of FA differences between groups can help localise brain changes related to development, aging and pathology. After standard pre-processing of the diffusion data and tensor estimation (described in 2.2.3), the FA maps are transformed to a high-resolution template space and are skeletonised before running the standard parametric statistical procedures such as f-tests and t-tests. Through the skeletonization process, each subject's transformed FA image is projected onto a mean skeleton to overcome transformation-induced misalignments. At each point in the skeleton, the maximum FA value perpendicular to the skeleton is assigned as the FA value of this point of the skeleton, creating an unbiased anatomical correspondence between subjects (Figure 23). The output is a binary skeleton mask that defines the voxels used for statistical analysis. The resulting image is a 4D of all the FA with the 4<sup>th</sup> dimension being that of the subjects. Similarly, to the VBM method, statistics will rely on the GLM and standard parametric statistical procedures such as f-tests and t-tests with the assumptions of independent and normally distributed residuals.

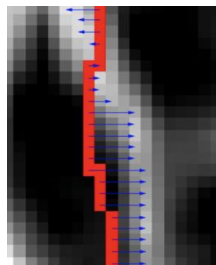


Figure 23: Example of FA projection in the skeleton. Source:(S.M.Smith, 2015)

## 2.6. MACHINE LEARNING AND PREDICTIONS IN NEUROIMAGING STUDIES

### 2.6.1. Multiple Linear Regression

Multiple regression is a statistical equation that predicts the outcome of a dependent variable based on several explanatory variables with the goal of modelling the linear relationship between the independent and dependent variables. The equation of multiple regression is the following:

$$y_i = \beta_0 + \beta_1 x_{i1} + \beta_2 x_{i2} + \dots + \beta_p x_{ip} + \epsilon$$

for  $i = n$  observations  
 $y_i$  = dependent variable  
 $x_i$  = explanatory variables  
 $\beta_0$  =  $y_i$ -intercept (constant term)  
 $\beta_p$  = slope coefficients of independent variables  
 $\epsilon$  = error term (residuals)

R-squared ( $R^2$ ) is the coefficient of determination. It measures how much of the variation the outcome of the dependent variable can be explained by the variation in the independent variables. The p-value determines the significance of the model, and the coefficients of each independent variable predict the size and direction of the effect that the given variable is having on the dependent variable.

When too many independent variables are present, or when the choice of predictive variables is not obvious, we can use a **stepwise regression**, which is a method that automatically identifies the predictive variables that can explain the regression equation (Efroymson, 1960).

### 2.6.2. Classification, Decision Trees, and Non-Linear Regression Models

#### *Classification*

In machine learning, classification is a type of supervised learning resulting in the categorization of a given set of data into classes. The main goal of a classification algorithm is to identify into which class or category a new data point will fall, with the output being categorical (or discrete). Several algorithms can be used in order to predict the most specific and accurate classifier. An example of common algorithm is

the support vector machine (SVM). SVM constructs a hyperplane that will maximize the separation between the group of data points with the greatest margin possible (Figure 24).

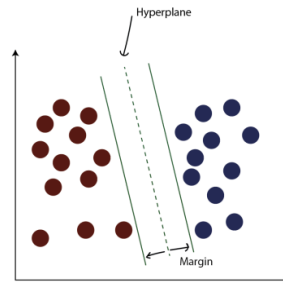


**Figure 24: Example of hyperplane generation between two datasets. Each colour of circle represents a separate group. The dashed line is the hyperplane.**

From a mathematical modelling perspective, the classifier requires a training set of data with many examples of inputs and outputs from which it learns which features best predict which category. Therefore, the training dataset should be exhaustive and sufficiently representative of the problem. The classification predictive model is then evaluated based on its results.

### ***Decision Trees Classification***

Decision trees are a type of classification that uses a non-parametric supervised learning, in which the model is built in the form of a tree structure and an “if-then” rule. Decision trees are constructed using a **recursive partitioning**, where each node is split into child nodes by following the largest Information Gain<sup>6</sup> (IG). The rules are learned sequentially by the algorithm using the training data until meeting a termination condition (or leaf nodes). It breaks down the data into increasingly smaller subsets. The attributes are all categorical, and the attributes that come highest in the top of the tree for earliest decisions have more impact towards the information. The deeper the tree, the higher the complexity of the decision rules. To reach a leaf node (or final result), each node has two or more branches (or decision nodes). The highest node is referred to as the root node and is usually the best predictor of the model (Figure 25).

---

<sup>6</sup> Function defined to optimize the tree learning algorithm at each split.

The tree selection is the process of finding the smallest tree fitting the data which usually yields the lowest cross-validation error.

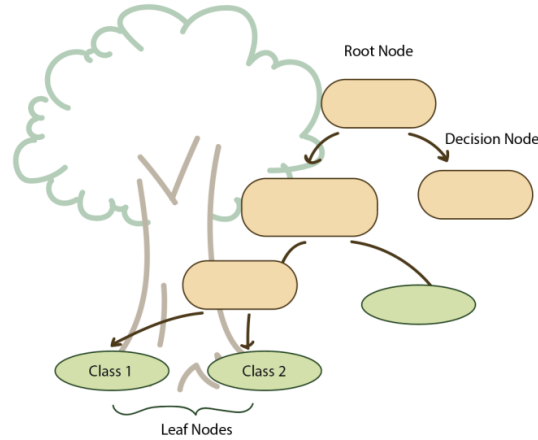


Figure 25: An example of decision tree classifier.

### 2.6.3. Validations and Evaluation of Performance

Before implementing and interpreting machine learning models, it is essential to properly validate them by estimating their error, bias and variance. After training of the model, the difference between the predicted outcome and the actual outcome is defined as “residuals” and reflects the error margin. However, residuals alone are not enough to examine the performance of the model and the training set.

#### **Cross-Validation**

Cross-validation is a technique commonly used to assess the accuracy of a model and how well it would generalise given a new dataset, by partitioning the current data into a training set and a test (or validation) set. For example, 80% of the data for training and 20% of the data for testing. However, given that the data used in the studies described later can be limited, splitting the data into two sets can lead to a small training set and therefore a higher error (or underfitting). To overcome this issue, one cross-validation method is known as the **K-fold cross-validation**. This method deals with this potential underfitting problem by ensuring a large proportion of data is partitioned into a training set with a large enough sample retained for validation.

The data is divided into  $k$  subsets, with one being used as the validation set and the remaining subsets ( $k-1$ ) being used as training sets. This process is repeated  $k$  times.

This means every data point is included in both the training and the validation process (Figure 26).

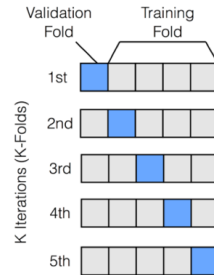


**Figure 26: Example of k-fold cross-validation with k=5. In each iteration, the training sets (grey) and validation set (blue) change so that all data points are included in testing of the model once. The process is repeated 5 times.**

The k-fold cross-validation method reduces the bias given that a maximum possible of the data is used to train the model. It also reduced the variance since a maximum possible of the data is used for validation. The overall model performance is an average of all folds.

### ***Evaluation of Classification Models***

Models can be evaluated on the basis of different metrics. A good performance means a greater likelihood of accurate prediction in new datasets. The most used metric in classification models is **accuracy**, which measures how well the model managed to classify the data in percentage.

$$\text{Accuracy (\%)} = 100 * \left( \frac{\text{Correct number of predictions}}{\text{Total number of predictions made}} \right)$$

This measure of accuracy should be used when the samples to classify have the similar size. If sizes vary greatly, a balanced accuracy should be calculated to account for the sample size variation. This is achieved by averaging the proportion of correct classifications for each class individually.

The Confusion Matrix is a matrix describing the complete performance of the model by modelling the number of true positives, true negatives, false positives and false negatives. This can help us understand which data points were most confusing to our classifier.

Another widely used matrix for binary classification problems is the area under the curve (AUC). The AUC of a classifier is defined as the probability of ranking a random positive higher than a random negative (or how well it can distinguish between the



different classes). A true positive rate is known as **sensitivity**, while a true negative rate is known as **specificity**. When plotting False Positive Rate vs True Positive Rate, the higher the AUC the better the performance of the model.

For decision trees, we use entropy as a measure of impurity, or uncertainty, which depends on the frequency of a certain element in the data and varies between 0 and 1. When all samples at the node belong to the same class, the entropy is equal to 0, and becomes maximal when there is a uniform class distribution.

### ***Evaluation of Regression Model***

The two main metrics for evaluation of regression-based predictive models are the **mean squared error** (MSE) and the  $R^2$  previously described (section 2.6.1).  $R^2$  measures how much of the variability in the dependent variable is explained by the model.

### ***Permutation***

To understand the significance of a model, or whether the classification or prediction is due to chance, we perform non-parametric permutation test to calculate confidence intervals and p values for the given model. Permutation testing consists in the random shuffling the data to cover as many ways as possible of rearranging the data and the distribution resulting from the random permutation is compared to the distribution of interest to determine whether there are significant differences. When the p-value  $< 0.5$ , the performance is determined to be significantly better than the null. In my thesis, I used 1000 permutations when non-parametric permutation is required to assess the significance of the model.

## 2.7. STATISTICAL ANALYSES

I conducted all statistical analysis using R v3.3.3 ([www.R-project.org](http://www.R-project.org)). When a p-value was required, I assessed significance at  $p\text{-value} < 0.05$  unless stated otherwise. I used Bonferroni when correcting for multiple comparisons.

Below are the statistical tests used across the chapters:

- **Dice similarity coefficients** (DSCs): compares the overlap of different ROIs as  $2 \times ((\text{overlapping voxels in X and Y}) / (\text{elements in X} + \text{elements in Y}))$ .
- Measures of test-retest included the **coefficient of variation (COV)** (the dispersion of data points around the mean) as  $(\frac{SD}{Mean} \times 100)$  with high COV being of 5% or higher, **intraclass correlation**, and **Pearson's correlation** of measures across visits.
- **Two-way ANOVA** tested for interactions between the different variables when comparing three or more groups. When the interaction was not significant, I used one-way ANOVA with one independent variable that was of interest.
- I used **one-way ANOVA** followed by a **Tukey HSD** post-hoc analysis in most cases. Tukey HSD is one of the more conservative post-hoc tests and it is therefore more difficult to find a difference than it is with other post-hoc analyses. If and when Tukey HSD failed, I used **Fisher LSD** as a post-hoc analysis. However, Fisher LSD does not have full control over Type I errors.
- I used a **t-tests** if comparing the mean of two groups. T-tests were paired if comparing the means of the same group under two different conditions. T-tests were unpaired if comparing the means of two independent groups.
- I use **Pearson's correlation coefficients** to understand the effect of an independent variable on the dependent variable being investigated.
- I calculated **Z-scores** when comparing an individual to the group's distribution.
- **Multiple linear regression** predicted the dependent variable based on a set of independent variables, based on the following assumptions: a linear relationship between dependent and independent variables, no high correlations between independent variable, the random selection of observations and the residuals distributed with a mean of 0 and variance  $\sigma$ . I also performed a stepwise selection in both directions to find the best predictors of the model.

- To calculate the confidence interval of the accuracy of the decision tree classifier, I used a **bootstrap resampling** technique (with  $n=500$ ).

## 2.8. PITFALLS IN CURRENT DIFFUSION NEUROIMAGING STUDIES

Most of the pitfalls mentioned in this section will be focused on DWI and its analyses techniques, which will be tackled later in this thesis. To obtain reliable result and draw significant and robust conclusions, we need to understand the limitations of the methods and how best to improve them.

### 2.8.1.Acquisition artifacts for EPI images

The first acquisition artifacts are eddy current distortions, which are electric currents generated by the magnets. Eddy current distortions vary with the diffusion encoding applied, causing mis-registration mostly at the edge of the brain. While eddy currents are not extremely problematic in most acquisition, it is still important to correct for them as a first step of the pre-processing of the image (section 2.2.3), using a global affine transformation, and correct the gradient encoding vector accordingly. Another issue during data acquisition is head motion in the scanner. Correcting for this motion and rotating the B matrix accordingly is crucial. Following pre-processing a tensor is usually fitted at every voxel. The use of different algorithms can lead to different results (Jones and Cercignani, 2010). For my studies, I use a standard tensor fitting model (weighted least squares).

### 2.8.2.Issues with ROI analyses

The gold standard of DTI metric extraction remains manual ROIs delineation. However, this approach has some limitations: it's time consuming, it requires specialist knowledge of the anatomy, and it can be subjective. Moreover, ROI positioning can be biased by values if performed directly of the parametric map. If the diffusion-free image and the DWI image are not properly registered, this can also cause subtle misregistration between the masks and the parametric image.

### 2.8.3.Partial Volume

With the low-resolution of the diffusion data, partial volume, particularly with CSF, remains a main concern. When a voxel is not 100% WM, it is affected by partial volume error. The key is to exclude voxels with the highest partial volume in a non-bias and homogenous way across the subjects. Patients with severe atrophy are more prone

to this type of diffusion bias given the possible damage to the microstructure of the WM.

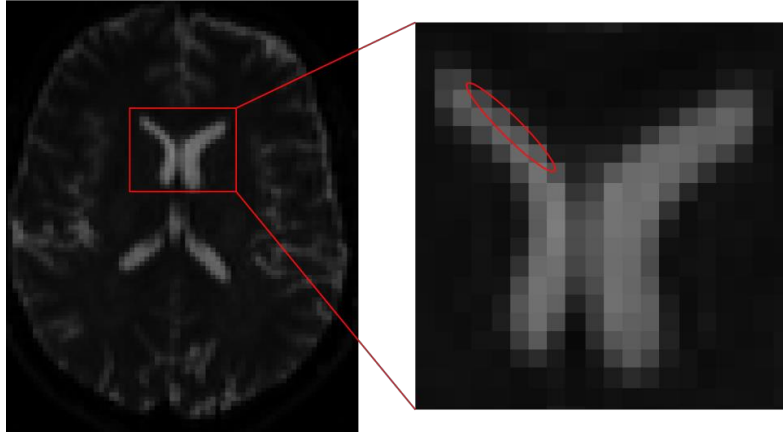


Figure 27: Example of partial volume voxels on diffusion image.

#### 2.8.4. Inter-Subject Analyses and Normalization

Group-level analyses are most popular in clinical neuroimaging studies. They are used to assess the association between diffusion and clinical variables. Some of the methods have been described previously (section 2.5.2) such as voxel-based analyses. A big component of successful voxel-based studies is the correct alignment of the images from different subjects to a common group or high-resolution template (section 2.5.1). Accurate normalisation of images is crucial, and registration errors can have a significant impact on the results. Unfortunately, thorough quality check or manual adjustments are not often performed. Moreover, structural abnormalities can seriously impact the transformations, and manual masking of such abnormalities is critical to allow for a better registration (Bookstein, 2001). Other factors that may impact the results are the choice of normalizations, the excessive warping of the image, as well as the smoothing used. Smoothing is a spatial filtering method that increases SNR, corrects for possible misalignments, and normalizes the data distribution using a 3D Gaussian kernel. The choice of the smoothing kernel also varies between studies, impacting the results.

#### 2.8.5. Issues with TBSS

TBSS is a method that tries to overcome these problems and homogenise diffusion studies (section 2.5.4). The projection of peak FA values from the tracts overcomes

the need to smooth data and decreases the effect of partial volume on the measurements. However, lesions, contusions and other structural brain abnormalities can lead to **inaccurate estimations** of the skeleton. Although TBSS achieves accurate correspondence between FA values, the anatomical alignment is less accurate. (Zalesky, 2011).

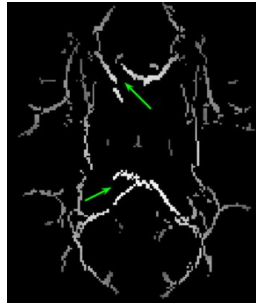


**Figure 28: Example of linear displacement and skeleton inaccuracy. Source: (Zalesky, 2011)**

There is a trade-off between alleviating post-registration misalignments and specificity of measurements. If the difference between clinical groups is not homogeneously distributed across the skeleton, and if the focal differences are located at the periphery of the WM, they do not form part of the estimated skeleton, and can therefore miss detection. And while the use of voxel-based analysis might increase the sensitivity of the measurement to the peripheral voxels, these analyses still use a smoothing correction, thus biasing the metric of interest.

# CHAPTER 3

---

## Development & Validation of the Subject-Specific Diffusion Segmentation (SSDS) pipeline

*In this chapter I present a new pipeline for the standardized automated subject-level segmentation for clinical investigations of diffusion imaging. I validate the method by showing good correspondence with manual segmentation of white matter tracts, demonstrate good test-retest reliability, show difference in performance to TBSS and demonstrate that the pipeline is robust to the effect of lesions and other structural abnormalities. I also provide recommendations for the use of this pipeline*

### 3.1. ABSTRACT

Diffusion weighted imaging (DWI) is key in clinical neuroimaging studies. In recent years, DWI has undergone rapid evolution and increasing applications. Diffusion magnetic resonance imaging (dMRI) is widely used to analyse group-level differences in white matter (WM) but suffers from limitations such as conservative measures or inaccurate transformation to group templates. These issues can be particularly impactful in clinical groups where 1) structural abnormalities may increase erroneous tensor fitting and registration and 2) subtle differences in WM microstructure within individuals can be missed. Region of Interest (ROI) segmentation of the WM in individual native space can help overcome these challenges, with manual segmentation still used as the gold standard. However, robust automated approaches for the analysis of ROI-extracted native diffusion characteristics are limited. Subject-Specific Diffusion Segmentation (SSDS) is an automated pipeline that uses pre-existing imaging analysis methods to carry out WM investigations in native diffusion space. SSDS overcomes the need to interpolate diffusion images and uses an intermediate T1 image to limit registration errors and guide segmentation using structural information. SSDS is validated in a cohort of healthy subjects scanned three times to derive test-retest reliability measures and compared to other methods, namely manual segmentation and tract-based spatial statistics as an example of group-level method. The performance of the pipeline is further tested in a clinical population of patients with traumatic brain injury and structural abnormalities. Mean FA values obtained from SSDS showed high test-retest reliability in 34 of the 47 tracts, with high correlation to the tract size, and were similar to FA values estimated from the manual segmentation of the same ROIs ( $p$ -value  $> 0.1$ ). Case studies of TBI patients showed robustness to the presence of significant structural abnormalities, overcoming the need for manual lesion masking indicating its potential clinical application in the identification and diagnosis of WM abnormalities. Further recommendation is given regarding the tracts used with SSDS.



### 3.2. INTRODUCTION

In recent years, diffusion magnetic resonance imaging (dMRI) has become widely used to investigate the white matter's (WM) microstructure (Huisman, 2010, Soares et al., 2013) in clinical studies. dMRI involves different analysis techniques (Table 7) which have proved extremely useful for determining the brain's structural connectivity as well as for the quantification of WM abnormalities based on diffusivity measures such as fractional anisotropy (FA) in a wide range of disorders (Le Bihan and Johansen-Berg, 2012, Assaf and Pasternak, 2008, Baliyan et al., 2016). Analyses based on region of interest (ROI) delineation are the most popular, but they are often combined with voxel-based analyses (VBA), a voxel-to-voxel correspondence method, usually carried out on images registered into standard space, and relying on t-test or ANOVA statistics to determine a spatial difference between two or more groups (Snook et al., 2007). In studies relying on individual subjects' native diffusion space, a rater usually draws ROIs manually on the parametric images such as FA maps. However, this approach can present several limitations; it is time-consuming depending on the number of subjects included in the analysis, it requires specialist anatomical knowledge, and it can lead to biased estimation of diffusion metrics if the rater chooses areas of high FA values for example, or if they rely on voxel intensity rather than location (Astrakas and Argyropoulou, 2010). In contrast, group-level analysis relies on the combined, standardized and automated analysis of diffusion images registered into group space (Astrakas and Argyropoulou, 2010). These techniques are specific and reproducible. However, inaccuracies introduced by the registration technique, such as misalignments or partial volume effects can lead to inaccuracies becoming particularly problematic where differences in microstructure is very subtle (e.g. different injury biomechanism) (Jones and Cercignani, 2010, Davatzikos, 2004), or when structural abnormalities are severe. In studies on populations with traumatic brain injuries (TBI), for example, DTI techniques are sensitive to WM damage at the group level. At the individual level, there is still insufficient evidence of WM structural abnormalities (Douglas et al., 2015), which hinders the association with injury biomechanics, severity, prognosis and outcome. When we define clear hypotheses about group differences in WM and in specific brain regions, or when the analysis should be carried out at the individual level if the groups are limited in power in clinically-relevant investigations, the study will include manual

segmentation of ROIs. This technique will also be utilized by researchers when structural abnormalities such as lesions, tumours, and others are present, and where group-level tract-based analyses which includes registration of the diffusion to a high resolution image become either very challenging or impossible (Martijn Froeling, 2016). The neuroimaging community has previously established that although interpolating DWI images by up-sampling it to a structural image with a higher resolution can improve the anatomical details of the manipulated diffusion data, the conventional methods we use for the registrations and interpolations can impact the results, more so in brain with atypical anatomy or structural abnormalities (Dyrby et al., 2014). This specific problem further highlights the need for a standardized and automated pipeline for diffusion studies in individual native space, to overcome the issue of user-dependent ROI measures, questions around reliability and quality of the results (Martijn Froeling, 2016).

The aim is therefore to develop a pipeline that can replicate the accuracy of manual ROI segmentation in diffusion space while maintaining the specificity of group-level analysis such as TBSS to enable investigation in a larger part of the tracts (such as boundaries). I have therefore worked on building an automated pipeline for the segmentation of diffusion images in native diffusion space and have named the pipeline Subject-Specific Diffusion Segmentation (SSDS). SSDS uses existing DTI analysis tools as well as ROIs from predefined atlas commonly used. The pipeline relies in the registration of a high-resolution template into a lower-resolution native T1 image, and the use of the anatomical T1 image to guide the registration of the high-resolution atlas-based ROIs to the diffusion image and the segmentation of the T1 image in native diffusion space. Through these steps, SSDS limits errors to the parametric map arising from any registration misalignment, partial volume errors, and anatomical inaccuracies when trying to fit lower resolution diffusion images into a higher resolution standard template (Aribisala et al., 2011). The pipeline also involves limited manipulation of raw diffusion data, which are now restricted to mainly movement correction and tensor fittings, excluding any need for interpolating diffusion images.

Through a combination of registration, segmentations, erosions and masking, my pipeline, enables fully automated structurally-driven ROI segmentation in native parametric maps, requires minimal intervention, and generates diffusion metrics with high reproducibility and the accuracy of manual segmentation. It can be used to

segment whole-brain WM maps, specific WM tracts, or any ROI based on a pre-existing atlas segmentation. SSDS overcomes the challenges presented by structural abnormalities such as lesions or tumours. Moreover, by eliminating the need for parameter changes, and with pre-calculated reliability and reproducibility, the pipeline can now be used as a homogenous and standard methodology in clinical studies involving diffusion imaging, which is still an important limitation of individual ROI-based DTI studies to date. SSDS will generate mean diffusion metrics values for a given ROI, or the distribution of values across the entire segmented tract when a single mean value is not enough to reflect information about the region being investigated. The novelty of the pipeline is in 1) using the T1 image as a mid-point reference for the registration and as a guide for the segmentation of the ROIs in the diffusion image, 2) overcoming the need to manually delineate and mask out anatomical abnormalities as to not bias the results, 3) combining a boundary-based registration with a non-linear warp to register ROIs into native diffusion space without interpolation of the parametric map and while obtaining the accuracy of manually segmented ROIs. Through back-projection of a template into native T1 space, and the use of the anatomical image as a guide for registration of a high-resolution atlas to the diffusion image and its segmentation, SSDS limits errors due to interpolating lower resolution diffusion images (Aribisala et al., 2011), and limits the manipulation of raw diffusion data (mainly movement correction and tensor fittings).

I validated SSDS using a control group scanned three times, and chose 47 tracts that are part of the JHU WM atlas (<https://identifiers.org/neurovault.collection:264>). In the following chapter, I present the performance of my registration pipeline, provide examples and show that FA can be estimated from segmented tracts in individual space with high reproducibility and with the accuracy of manual segmentation. I also apply the pipeline to a small clinical group of patients with moderate/severe traumatic brain injury (TBI) who present varying levels of focal and/or diffuse axonal injury. This type of brain injury can present challenges to traditional approaches of tract segmentation due to structural abnormalities, and we show that SSDS performs well in the estimation of tract FA in this situation. We also present further considerations and possible applications for use of this pipeline.

***Hypotheses of Chapter 3***

- Automated segmentation of WM tracts on the parametric map at the individual level can result in high test-retest reliability and a high correspondence with fractional anisotropy results obtained from manual segmentation
- Some smaller tracts will have to be excluded from the SSDS analysis due to higher variation in intra-subject measurements across different visits

***Tips on when to use SSDS***

- ⇒ The clinical group shows neuroanatomical abnormalities which might be challenging for the between-subject transformation/registration required in group-level analyses
- ⇒ The WM injury difference between groups is more subtle and/or not homogenously distributed across the skeleton
- ⇒ The work included individual clinical investigations and/or case studies compared to typical group distributions

***Current analysis methods, their use and their pitfalls*****Table 7: Overview of the different post-processing approaches for statistical analysis of DTI measures.**

Method	Principles	Strengths	Limitations
<b>Region of Interest (ROI)</b> (Astrakas and Argyropoulou, 2010, Jones and Cercignani, 2010, Snook et al., 2007)	Manual delineation of specific regions of the brain (most commonly on parametric map)	Good anatomical placement (spatially specific) and less partial volume effect	<ul style="list-style-type: none"> <li>- Time-consuming</li> <li>- Requires anatomical knowledge</li> <li>- Biased by parametric map</li> <li>- Difficulty of inter-modality registration for anatomical ROI</li> <li>- Reproducibility in longitudinal studies</li> <li>- If defined in standard space may include smoothed and partial volume voxels.</li> </ul>
<b>Histogram</b> (Zhou et al., 2011, Della Nave et al., 2007, Soares et al., 2013)	Frequency distribution within voxels of specific parameters of interest	Unbiased analysis of the whole brain without determining an ROI	<ul style="list-style-type: none"> <li>- Requires removal of non-WM tissues.</li> <li>- No anatomical information</li> <li>- Sensitive to partial volume in structurally atypical brain</li> </ul>
<b>Voxel-Based analysis</b> (Mukherjee et al., 2008, Abe et al., 2010, Astrakas and Argyropoulou, 2010, Van Hecke et al., 2010)	Voxel-by-voxel analysis and group-level comparison via normalization to a standard template	Automated, reproducible and requires minimal intervention. Anatomically specific and unbiased	<ul style="list-style-type: none"> <li>- Accuracy of registration</li> <li>- Accuracy of anatomy following normalization</li> <li>- Partial volume if using pre-defined ROIs</li> </ul>
<b>Tract-Based Spatial Statistics (TBSS)</b> (Smith et al., 2006, Zalesky, 2011, Jones and Cercignani, 2010)	Detect group voxel-wise differences based on skeletonization of the parametric map registered to a template	Removes the need for spatial smoothing & reduces the number of voxels included in the analysis, thus increasing statistical power	<ul style="list-style-type: none"> <li>- Accuracy of registration</li> <li>- Danger of inaccuracy of skeletonization</li> <li>- Cannot recognize structural abnormalities following skeletonization</li> <li>- Cannot back-project to native space</li> </ul>

### 3.3. METHODS: SUBJECT-SPECIFIC DIFFUSION SEGMENTATION

#### 3.3.1. Participants

All participants gave informed consent according to the declaration of Helsinki (Table 8). Healthy controls were scanned three times, at three separate visits at the same scanner. The fully automated pipeline was independently tested on all three scans for 17 subjects. The clinical population was scanned once. The same scanner was used for both cohorts.

**Table 8: Demographics of patients and healthy controls used in the validation and testing of the SDSS pipeline.**

	n (count)	Male: Female (ratio)	Mean Age $\pm$ SD (years)	Presence of Lesions
<b>Healthy Controls</b>				
	17	11:6	32.1 $\pm$ 4.2	NA
<b>Clinical Population</b>				
Controls	10	5:5	32.8 $\pm$ 6.3	NA
TBI patients	19	15:4	43 $\pm$ 9.16	52%

#### 3.3.2. Imaging Acquisition

Scanning used a 3T Siemens Magnetom Verio Syngo with a 32-channel head coil. Scanning session for each participant generated a structural high resolution image T1-weighted MPRAGE image (106 1-mm thick transverse slices, TR=2300ms, TE=2.98ms, FA=9°, inplane resolution= 1x1mm, matrix size=256x256, field of view=25.6cmx25.6cm), a diffusion-weighted image (64 directions, b=1000s/mm<sup>2</sup>, 4xb=0s/mm, TE/TR=103/9500ms, 64 contiguous slices, FoV=256mm, voxel size=2mm<sup>3</sup>) and a fluid-attenuated inversion recovery (FLAIR) image for lesion identification. The b0 volume used consequently is an average.

### 3.3.3. Imaging Analysis

I carry out development and validation of the SSDS pipeline on two separate cohorts: a healthy control group (3 scans for 17 individuals) and a clinical group comprising 3 subgroups: TBI with lesions, TBI without lesions, healthy controls (Figure 29).

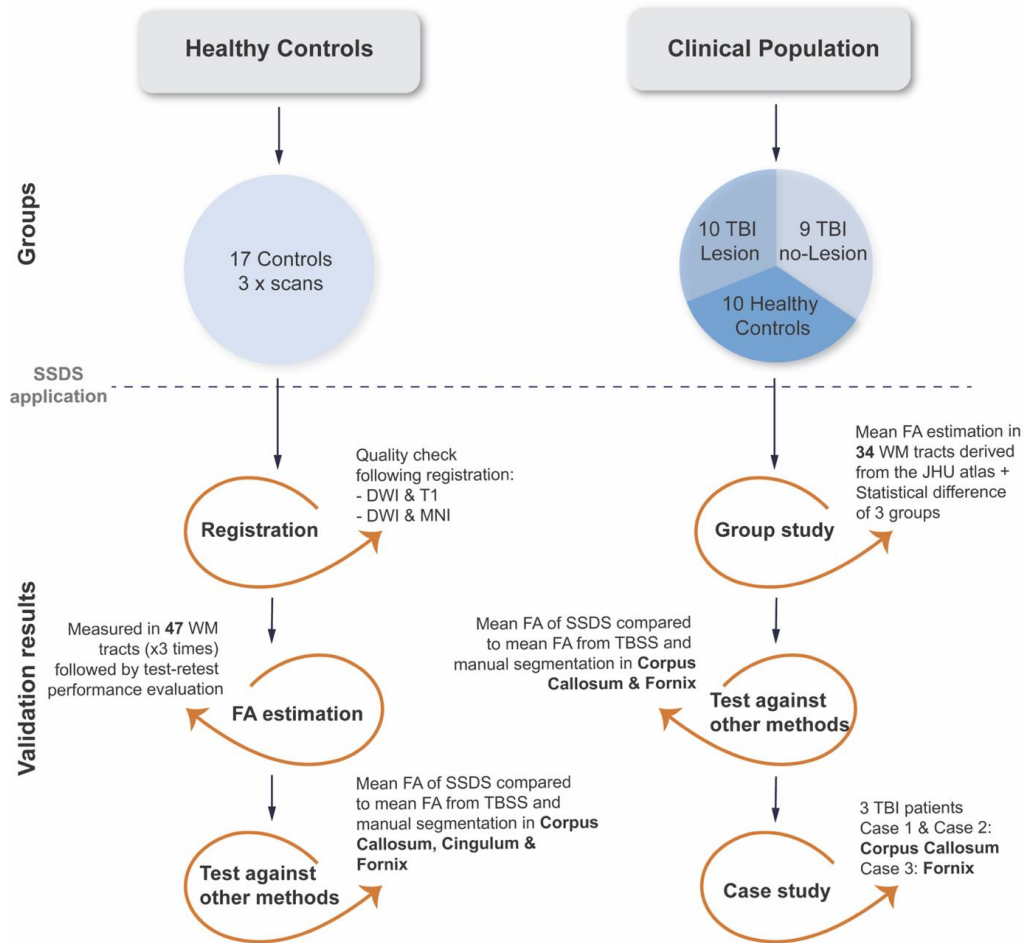


**Figure 29: Overview of the validation steps and the results presented in the current study.** Analyses on the two cohorts were done separately. The first validations were carried out on the healthy controls (scanned three times for test-retest validation). We present results from the different registration steps, estimation of FA values and test-retest measures, as well as a comparison to other methods. The clinical population (scanned once on the same scanner as the control population) was analysed first in a group-level study by comparing individually-obtained ROI measures, then the results of SSDS were compared to other methods. Finally, three subjects were chosen for case study comparative analyses.



### ***Overview of SSDS***

The requirements for running the Subject-Specific Diffusion Segmentation (SDSS) pipeline are for each subject: a pre-processed DTI image, a T1 image, a gradient field map image, a standard template and a set of atlas-based tracts or ROIs (Code is available in A.3.1. Code of SSDS).

To summarize the different steps included in the pipeline (Figure 30):

- Step 1: Pre-process the raw diffusion data and fit the tensor
- Step 2: Pre-process the structural data and run brain extraction. The structural image is used as a mid-point reference to limit registration errors and preserve anatomical details in lower-resolution diffusion space.
- Step 3: Make sure your diffusion data and the no diffusion slice are perfectly aligned
- Step 4: Register the T1 image to the diffusion image using a linear boundary-based registration as a cost function. This requires a prior segmentation of the T1 image and an estimation of the WM boundary mask. For all registrations, warps and matrices are estimated initially by moving images from low to high resolution then inverting the transformation.
- Step 5: Once registered to native diffusion space, segment the T1 image into different tissue types to drive anatomically correct ROI segmentation by restricting it to the underlying WM anatomy.
- Step 6: Use non-linear registration of the template of choice (in this case the MNI152 template) to the corresponding T1 image and combine the non-linear warp and the BBR matrix to obtain a transformation warp from standard template to native diffusion space.
- Step 7: Use the estimated warp to move the tracts from the standard template space to the native diffusion space.
- Step 8: Cross-mask whole WM map or from specific ROIs are cross masked with the T1 segmentation for further restriction to WM tissue.

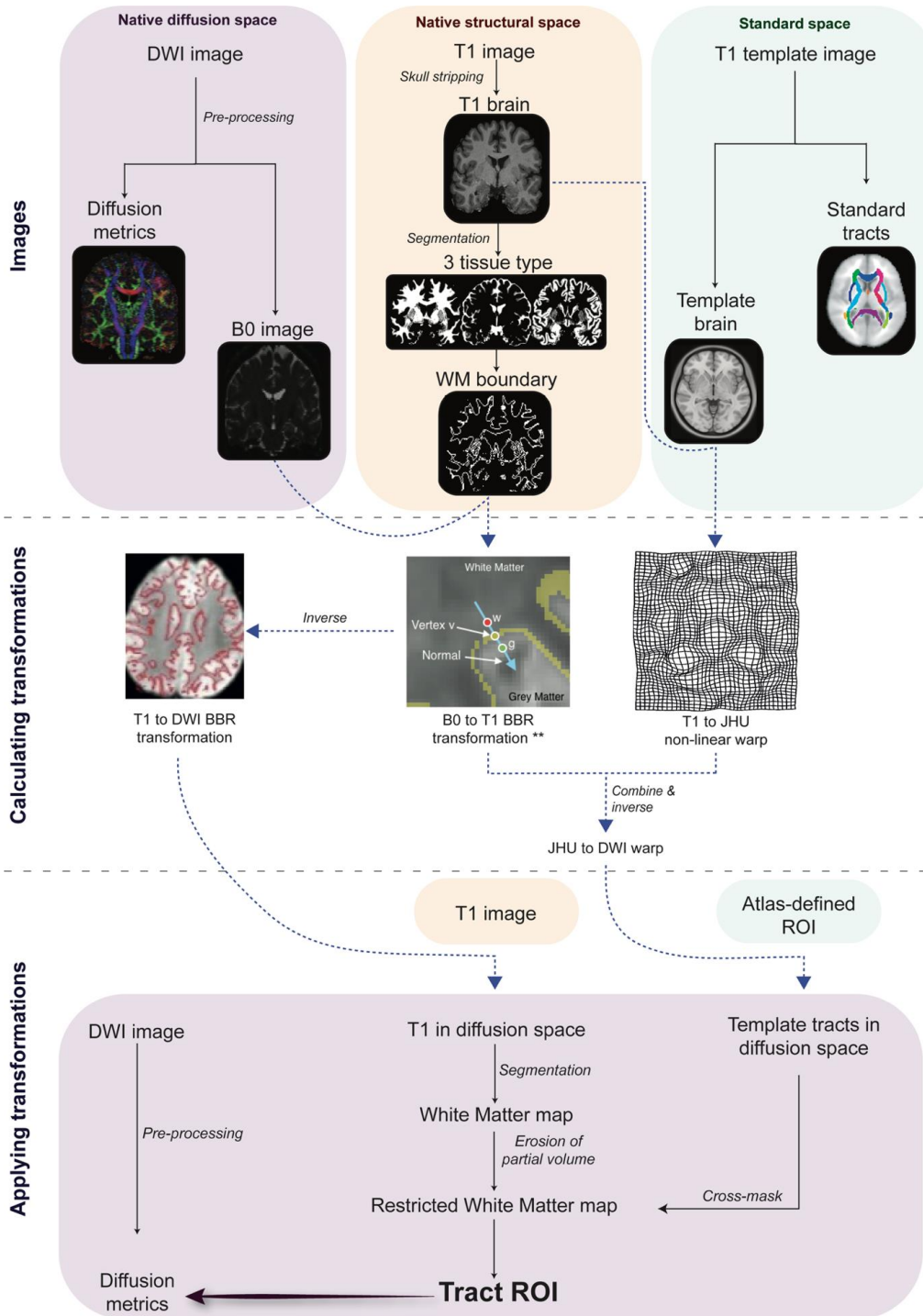


Figure 30: Overview of the SSDS pipeline. DWI images are pre-processed individually. 3D T1-weighted images are segmented, the mask of the WM boundary is estimated and used for a BBR of the diffusion image to the T1 image. Non-linear registration is estimated to move the

**T1 image to a pre-defined template space. The BBR matrix and the non-linear warp are then combined and reversed to estimate a transformation from the standard template to the individual diffusion image. The reverse BBR matrix is applied to the original T1-image, resulting in an inter-modality registration of the T1 to the DWI image. In the last steps, once all three images are in DWI space, the T1-image is segmented, the WM map is then used for cross-masking pre-defined ROIs which have been moved to the DWI image. \*\* image adapted from (16)**

## ***Pre-processing***

### *DWI images*

---

The two main artefacts when dealing with diffusion data are head motion and eddy currents from the gradient coil (more details in section Pitfalls in Current Diffusion Neuroimaging Studies). I align the images via registration to the non-diffusion-weighted (b0) image to correct for these distortions. I extract the B0 image to subsequently use as a reference image for registration, skull stripping and generation of a brain mask in diffusion space. I process the DWI images using FSL's FDT standard pre-processing technique (Behrens et al., 2003) and the brain extraction tool (BET) for skull-stripping (Smith, 2002). I apply motion parameters to the DTI B-vectors to compensate for the registration performed to correct for eddy current and motion effects. Finally, I estimate the diffusion tensor using the skull stripped DWI image to generate FA maps using the FSL DTIFIT algorithm (weighted least squares approach). The tensor is estimated at each voxel, using a simple least-square fit of the tensor model to the diffusion data. We could potentially calculate diffusion metrics other than the tensor such as fibre density and cross-section. For demonstration purposes in this chapter, I use Fractional Anisotropy (FA) as the metric of interest.

### *T1 images*

---

I performed brain extraction using the brain extraction tool FSL-BET, then segmented into different tissue types and corrected for spatial intensity variations using FSL FAST (Zhang et al., 2001). The WM map is used to generate a map of the WM boundary, using a surface model used subsequently for BBR (figure 2).

## ***Registrations***

### *T1 to native DWI*

---

To achieve optimized alignment we need to first up-sample the b0 image through registration to corresponding T1 image and calculating the inverse of the transformation to move the structural image to the subject's native diffusion space. This is done to preserve as much anatomical details from the T1 image as possible once we apply the transformation matrix to downsize it. The inter-modality, intra-subject registration of the T1 image to the B0 image requires four steps:

- 1) Initially, the EPI volume is aligned to the T1 skull-stripped brain image using 6 DOF (rigid) and a nearest-neighbour interpolation.
- 2) The field map (when available) is then registered to the T1 skull-stripped brain image. Using a field map is not required but does yield a better alignment. Because EPI causes geometric distortions, adding information from field maps results in a more accurate and efficient registration (Wang et al., 2017), thus leading to improvements in the geometry of the image. This was revealed to be an important but not essential aspect of accurate registration to the T1 image.
- 3) The BBR of the b0 image to the T1 image is guided by the pre-alignment matrix and the registered field map. BBR uses a reconstructed mesh along the WM boundary of the T1 image, which can be estimated by hand or automatically in the `epi_reg` script from the FSL toolbox. BBR drives the registration to the B0 image by spatially aligning the vertices of the mesh with the intensity gradient across the WM boundary (Greve and Fischl, 2009) (see section 2.4). Through this registration, the target image (diffusion) does not require high quality as long as grey and white matter are differentiated. The choice of BBR over alternative mainstream cost-functions of registrations is described in detailed in the next section (section 3.4.1)
- 4) We calculate the inverse of the output of this transformation. This is done to preserve the diffusion image in its native space and avoid any interpolation of the data for best estimation of diffusion metrics following segmentation of ROIs.
- 5) The final transformation matrix can be applied to the T1 image using the b0 image as a reference. The two main outputs of these registrations are a) the subject's T1

image down-sampled and registered to the subject's b0 image (i.e., the T1 image aligned to the DTI image), b) a subject-specific matrix for this transformation which will be subsequently required to drive the registration of the high-resolution ROIs.

### *Standard template to native DWI*

---

The next step is a non-linear registration of the standard template of interest was to the b0 image using the T1 image as a midpoint and the pre-calculated BBR matrix. In this case, my regions of interest (ROIs) are derived from the JHU WM atlas (see supplementary section A.3.2. *Tracts from the JHU atlas*). I use the MNI152 standard-space T1-weighted average structural template and estimate a subject-specific warp field to register the 54 tracts to the diffusion image. The tracts are all eroded by one voxel (single voxel, 3x3x3 box centred on target voxel) before any registration to ensure exclusion of partial volume effect once transformed to the native diffusion image. I achieve optimized alignment in three main steps. 1) Registration of the T1 structural image to MNI152 template through a non-linear warp. 2) Combining the non-linear warp and the BBR matrix to obtain a non-linear transformation of diffusion image to the high-resolution template. 3) Calculating the inverse of the transformation to move the template to the subject's native space in a one-step transformation.

Non-linear registration from native diffusion space to standard space is a two-step process that requires the T1 image as a mid-point reference. The final warp field of the transformation from the standard template to the native diffusion space will be the equivalent of the inverse of the following transformations: diffusion to T1 linear BBR + T1 to standard template non-linear transformation. The main output is a subject-specific transformation field to accurately move ROIs defined through the standard template to the b0 image (i.e., the MNI152 T1-weighted standard template aligned to the DTI image).

## **Segmentations**

### *Boundary segmentation*

---

To segment the boundaries of the WM, the T1 image is segmented into 3 tissue-types after registration to the B0 image. Once segmented, the WM map is thresholded and binarized, and can then be eroded from all inner voxels to give a binary mask of the

entire WM (Figure 31). Even with a lower resolution, the segmentation of the T1 image yields more accurate results than the transformation of segmented maps.

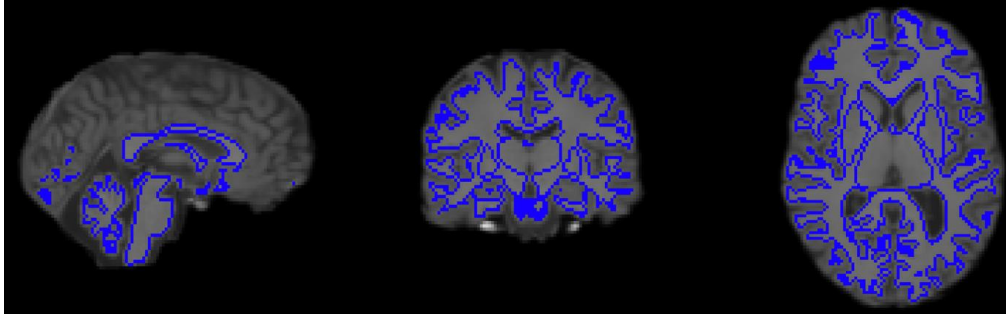


**Figure 31: Boundary of the WM. The blue line is the binary mask. The T1 image is in native diffusion space.**

The map of the CSF is then dilated and cross-masked with the whole-brain WM boundary map to create the map of the WM/CSF boundary, and this mask is subtracted from the whole-brain WM boundary map to create the map of the WM/GM boundary.

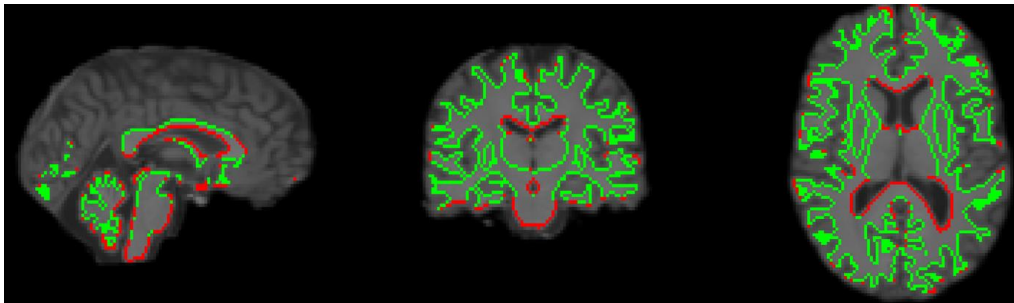


**Figure 32: Boundary of the WM/CSF and WM/GM. The red line is the mask of the WM/CSF boundary, and the green line is the mask of the WM/GM boundary. The T1 image is in native diffusion space.**

### *Tract segmentation*

---

Restriction of registered and down sampled tracts to the underlying WM anatomy helps avoid partial volume effects and improves the segmentation of the tracts in DWI space (Horbruegger et al., 2019).

Segmentation is achieved in six steps. 1) After registration to the b0 volume, the T1 image is segmented. Even with a lower resolution, the segmentation of the T1 image yields more accurate results than the transformation of segmented maps. 2) To optimize exclusion of partial volume voxels the WM map is thresholded to exclude all

boundary voxels with values below 0.8 (range 0-1) and binarized. 3) 47 tracts were selected from the ICBM-DTI-81 white-matter labels atlas (Oishi et al., 2008). 4) The tracts are initially eroded (single voxel, 3x3x3 box centred on target voxel) to limit overlap with partial volume voxels. 5) Using the previously estimated warp field ([see section 3.4.2](#)), the 47 WM tracts are then warped to subject-specific diffusion space to guide the segmentation of ROIs. 6) After registration to the b0 volume, each tract is cross masked with the estimated WM map and further thresholded and binarized to ensure exclusion of boundary voxels with partial volume errors (threshold 0.8, range 0-1). 6.b) However, I did not think this improved FA estimation, resulted in more variability and excluded relevant spatial details. I only use one erosion in all subsequent analyses.

### ***Validations***

For validation of the results obtained from the SSDS pipeline, I chose the body, splenium and genu of the corpus callosum, the right and left cingulum and the fornix as ROIs. I selected these tracts to test the performance of the pipeline on different anatomy and size for tracts with different reliability in the validation process. For the validation, I included a comparison against manual segmentation of the ROIs, ROIs obtained following skeletonization through the ENIGMA protocol (Jahanshad et al., 2013), and ROIs obtained from a one-step non-linear registration of a diffusion image to the high-resolution JHU template.

Dice similarity coefficients (DSCs) were calculated to compare the overlap of the automated ROI segmentation through SSDS and the manual segmentation using the following formula.

$$2 \times \frac{|X \cap Y|}{(|X| + |Y|)}$$

The DSC measures the overlap (or similarity) between two sets of data, X and Y, with |X| and |Y| being the number of elements in sets X and Y, and (X n Y) being the number of elements common to both sets X and Y. In neuroimaging terms, this translates to:

$2 \times ((\text{overlapping voxels in X and Y}) / (\text{elements in X} + \text{elements in Y}))$ .

#### *Manual segmentation of ROIs for validation*

---

Six tracts were manually traced on each parametric map, using the scans from the first visit of 15 healthy subjects selected at random. Each manually delineated ROI consisted of multiple slices fully covering the three-dimensional structure. The anatomical of the tracts were defined according to the definitions provided in a standard DTI atlas (Mori et al., 2008). I chose the ROIs to cover a) large and reliable tracts: the body, splenium and genu of the corpus callosum, b) thinner and longer tracts: the right and left cingulum c) small tracts prone to tensor estimation errors: the fornix (Plaisier et al., 2014). Manual segmentation is still considered the gold standard for ROI analysis. If SSDS can perform with similar accuracy to the manual segmentation on different tracts, the method can gain credibility for clinical investigations involving diffusion imaging.

#### *Mean FA from ROIs following non-linear registration to a template*

---

Following the method for the non-linear transformation of diffusion data to a standard template, I register the individual FA maps to the MNI152 standard template using the 1mm FRMIB FA atlas in TBSS (Smith et al., 2006). Following registration to the high-resolution template, I cross-mask the FA map with the tracts of interest and estimate the mean FA value for each ROI. I use this validation method to emphasize how normalizing tracts can increase their size and the contribution of partial volume. However, this method is not recommended for diffusion studies.

#### *Mean FA from ROIs following TBSS skeletonization – or the ENIGMA DTI method*

---

Following the standard TBSS protocol, I merge and skeletonize all the normalized FA maps using a 0.2 threshold to ensure exclusion of partial volume effect. I subsequently split the 4D image of concatenated FA maps to obtain the skeletonised FA for each participant separately. I mask the individual skeletonised FA maps with ROI masks to get individual mean FA for each ROI (Smith et al., 2006). This method is described as the ENIGMA DTI method (Jahanshad et al., 2013).

### **3.3.4. Exemplar applications**



### ***Group-level comparison: TBI vs healthy controls***

As an example of clinical application of the SSDS pipeline, I included three age and gender-matched groups: 10 healthy controls, 10 subjects with moderate/severe TBI and presence of structural abnormalities, and 9 subjects with mild TBI (Malec et al., 2007). Of the 47 tracts available in the JHU WM atlas, I included 34 tracts in this analysis as part of the validation process. The tracts were chosen because of their reliability (see section 3.4.3. Test-retest reliability). I extracted the mean FA as well as the histogram distributions of FA values for each of the 34 tracts. To further validate the pipeline in a clinical population, I selected 4 of the 34 tracts for comparison with manual segmentation and skeletonized FA estimation following TBSS (as described in section 3.3.3. *Imaging Analysis- Validations*). I chose the tracts used in the validation process to include different sizes, anatomy and reliability measures. The tracts were the three parts of the corpus callosum and the fornix.

### ***Case studies of patients with severe TBI and performance of SSDS pipeline***

I analysed three cases of patients with severe TBI separately (Table 10). All three patients presented with neuroanatomical abnormalities. For each case, I included the segmentation of a single tract and compared it to the three other methods: manual segmentation, ENIGMA-DTI protocol (Jahanshad et al., 2013) and masking from a high-resolution template. The segmented tract was chosen to reflect the atypicality of the structures.

### ***Statistical Analysis***

I performed all statistical analyses using Rstudio v. 3.5.1. I assessed test-retest reliability using the following three measures: intraclass correlation (Koo and Li, 2016), coefficient of variation and correlation of measures across visits. I used the results from the coefficient of variation to reject unreliable for use in the SSDS pipeline based on high intra-subject variation (>5%).

I first used a Tukey non-additivity test on the FA results I obtained from the first visit, with a two-factor factorial design  $\text{tracts} \times \text{subject} = 47 \times 16$ , with  $n=1$  replicate for each  $\text{tract} \times \text{subject}$  combination. Following this test, I ran a two-way mixed single measure consistency Intra-class correlation (ICC), with a design of  $\text{tracts} \times \text{subject} \times 3\text{visits}$  (47 tracts and 48 raters per tract). This was followed by a 2-level bootstrap with

Development & Validation of the Subject-Specific Diffusion Segmentation (SSDS) pipeline | A. A.

replacement, with 10,000 for our 47\*48 design. Following each replication, ICC is estimated to generate a bootstrapped confidence interval of 95%. The coefficient of variation (COV) was calculated using the following formula ( $\frac{SD}{Mean} \times 100$ ) to assess the variability of FA and tract size measures within each subject across all three visits (i.e. how similar are the values for each person for three different visits). Initially, I extracted a mean FA value and a tract size (voxel count) for each tract, for all 16 subjects and three visits. For each subject, I estimated a COV for every tract across the three visits (i.e. one measure per subject per tract). For each tract, I calculated an average of all 16 COV measures was then calculated for every tract. Lastly, I calculate a Pearson's correlation coefficients, including all tracts and all subjects for pairwise comparison across visits. Dice similarity coefficients (DSCs) was calculated to determine the similarity and spatial overlap of the manual segmentation and the ROIs resulting from SSDS.

## 3.4. RESULTS

### 3.4.1. Registration

I assessed different registrations and trial and errors before choosing the methods described above as most effective. The cross-modality intra-subject registration was more sensitive to inaccuracies than the non-linear template to subject alignment. Individual T1 images were registered to the lower resolution diffusion image using linear BBR (EPI to T1 image). For inter-modality registration, the results obtained using BBR were more accurate alternative methods. The use of a gradient map field increases slightly the registration accuracy but was not deemed necessary.

I tested the following alternative methods: linear FLIRT and non-linear FNIRT) with different cost function including the within-modality functions: least Squares and Normalised Correlation, as well as the between-modality functions: Correlation Ratio (which is the default with FLIRT), Mutual Information and Normalised Mutual Information. For each run with a different cost function, I performed a thorough quality check on a structurally typical brain and a brain with severe structural abnormalities after registration of the T1 to the DWI image. Although most cost functions provided accurate registration for the typical brain structures, BBR resulted in the most satisfying and accurate registration in the case of severe TBI. All other cost functions had misalignments.

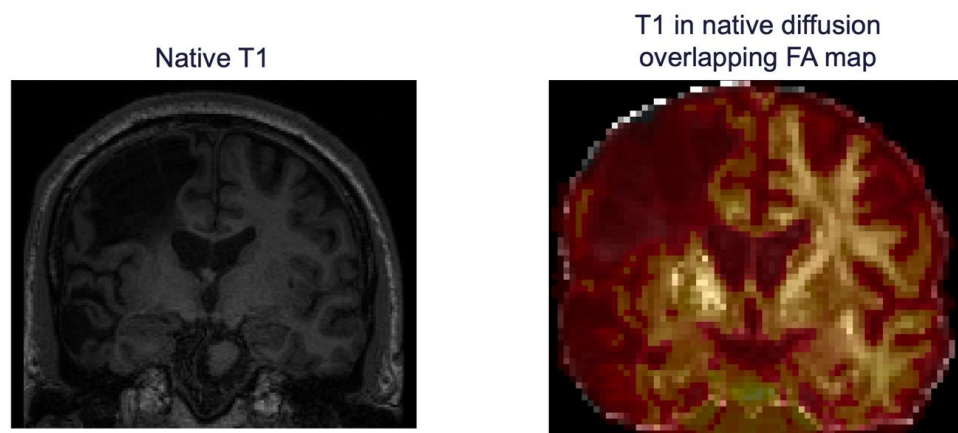
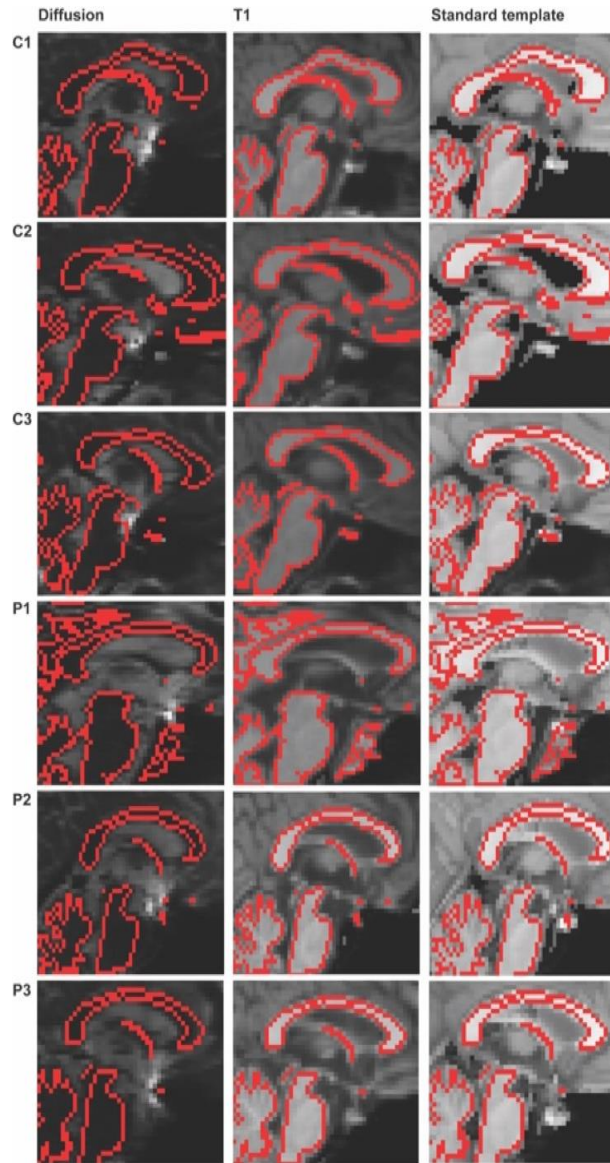


Figure 33: Visual quality check for cost function on brain of patient with severe TBI.

For visual quality check of the performance of the different registrations, I defined a WM boundary mask in the T1 image registered to the B0 image (as described in 3.3.3- Boundary segmentation). I overlaid the boundary mask was overlaid on the 3 images following registration in DWI space (diffusion, T1 JHU template). This visual assessment of the registration shows accurate alignment of the three images in 3 healthy subjects (C1,C2,C3) and 3 subjects with moderate/severe TBI (P1,P2,P3) (Figure 34). The overlay of the WM boundary mask shows a voxel-wise correspondence for the voxels of the boundary among all three images for all cases after being moved to the individual subject diffusion space.



**Figure 34: Examples of individual registration performance.** All images have been registered to the native diffusion space in 3 controls (C1, C2, C3) and 3 TBI patients (P1, P2, P3). The mask of the WM boundary (red) resulting from the segmentation of the T1 image in DWI space is used to indicate voxel-wise correspondence among all three images and the accurate structural overlay.

### 3.4.2. Tract segmentation and estimation of fractional anisotropy

An example of the segmented tracts can be seen in Figure 35.

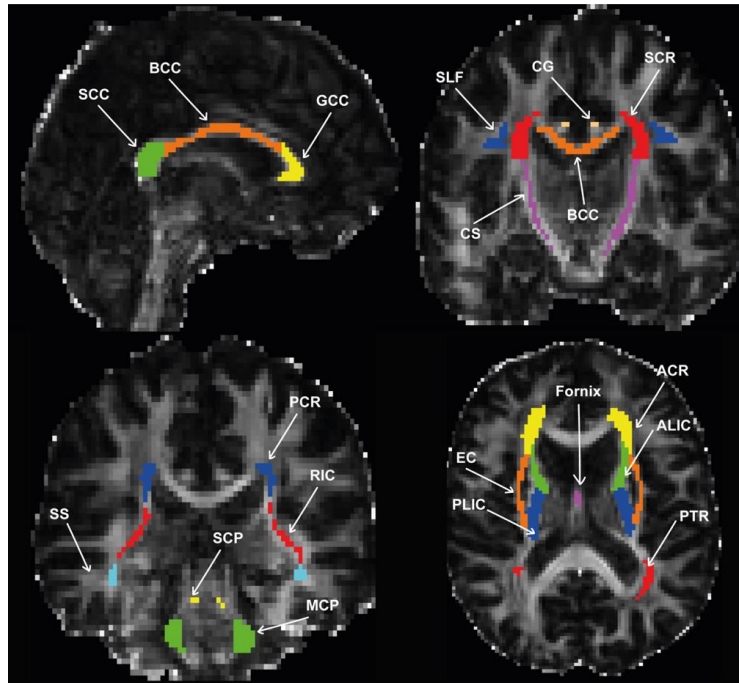


**Figure 35: Example of tract segmentation.** The FA map is in native diffusion space. Colours are selected at random. Subject is selected at random. SCC= splenium of the corpus callosum, BCC= body of the corpus callosum, GCC= genu of the corpus callosum, CS= corticospinal, SLF= superior longitudinal fasciculus, CG= cingulum bundle, SCR= superior corona radiata, SS= sagittal stratum, SCP= superior cerebellar peduncle, PCR= posterior corona radiata, RIC= retrolenticular part of the internal capsule, MCP= middle cerebellar peduncle, EC= external capsule, PLIC= posterior limb of the internal capsule, PTR= posterior thalamic radiation, ACR= anterior corona radiata, ALIC= anterior limb of internal capsule.

I used SSDS to segment 47 tracts and assess the performance of the pipeline. I carried out visual quality assessment by overlaying the segmented tracts on the parametric FA map and assessing voxel-wise correspondence (Supplementary Figure 1). The segmentation did not need manual intervention for correction. I extracted a histogram of FA values across the tract for each of the 47 ROIs. I plotted the distribution of FA values and the single mean value for a subset representation of 26 tracts for individual subjects (Figure 36).

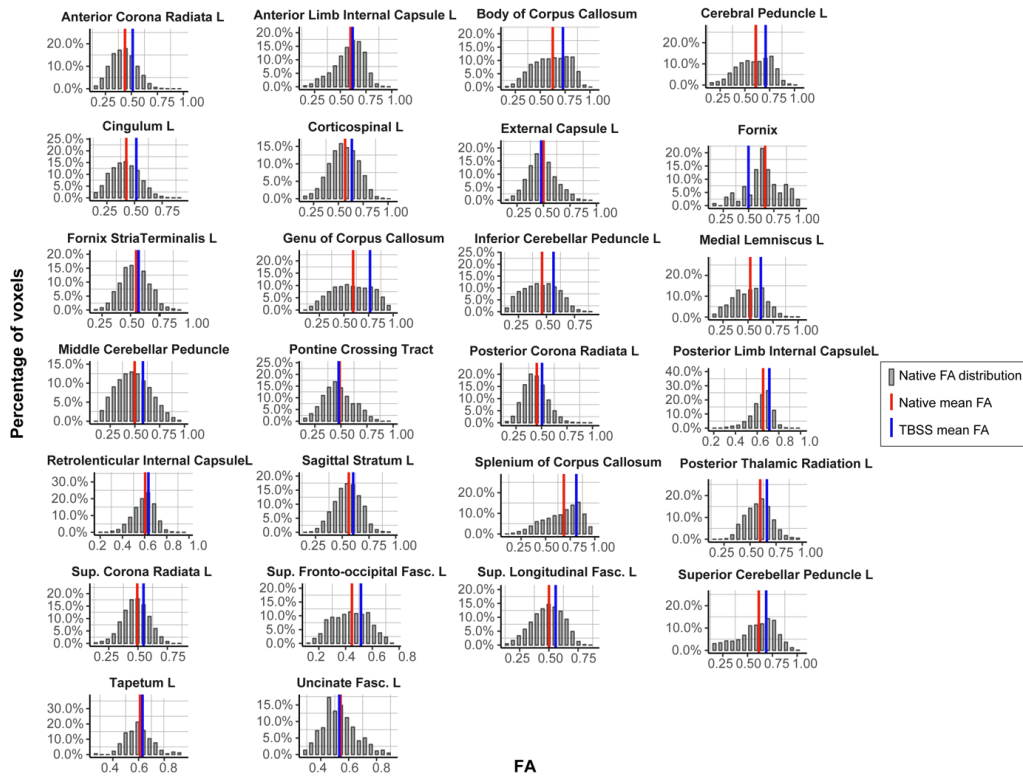


**Figure 36: The histogram distribution. Representation the frequency distribution of FA values for every voxel in a given tract following segmentation of the whole tract in native diffusion space. Only left hemisphere tracts are included, and tracts were selected at random. The native mean FA is plotted on the distribution (red), the mean skeletonised FA is used for comparison purposes (blue).**

### 3.4.3. Test-retest reliability

Tract diffusion measures generated using SSDS showed high test-retest reliability. Across the three visits the mean FA for each tract was generally very similar (Table 9):

- 1-erosion parameter: average COV was **2.7% ± 1.5%**
- 2-erosion parameter: average COV was **5.1% ± 8.6%**

**Table 9: Reported results for variability statistics. Mean intraclass correlation test (ICC), average coefficient of variation (COV) for within tracts and within-subject measurements, and pairwise FA correlation. ICC, COV and correlation analyses were carried on all 47 tracts, the**



average is reported. Boot ICC are results of the confidence interval following a bootstrap test on our data.

Category	ICC		F	Average COV		Correlation pairwise (FA)			
	Lower	Upper		Intra-subject	Intra-tract	Visits 1&2	Visits 1&3	Visits 2&3	
Values	0.742	0.870	0.808	203	2.61%	0.92%	0.95	0.94	0.94
P-value	<0.001			NA		<0.001	<0.001	<0.001	
Boot ICC	0.714 – 0.838			NA		NA	NA	NA	

13 tracts had a COV greater than 5% with either erosion parameters (Figure 37):

- The fornix
- The superior fronto-occipital fasciculus bilaterally
- The hippocampal cingulum bundle bilaterally
- The inferior cerebellar peduncle bilaterally
- The uncinate fasciculus bilaterally
- The fornix crescent bilaterally
- The tapetum bilaterally.

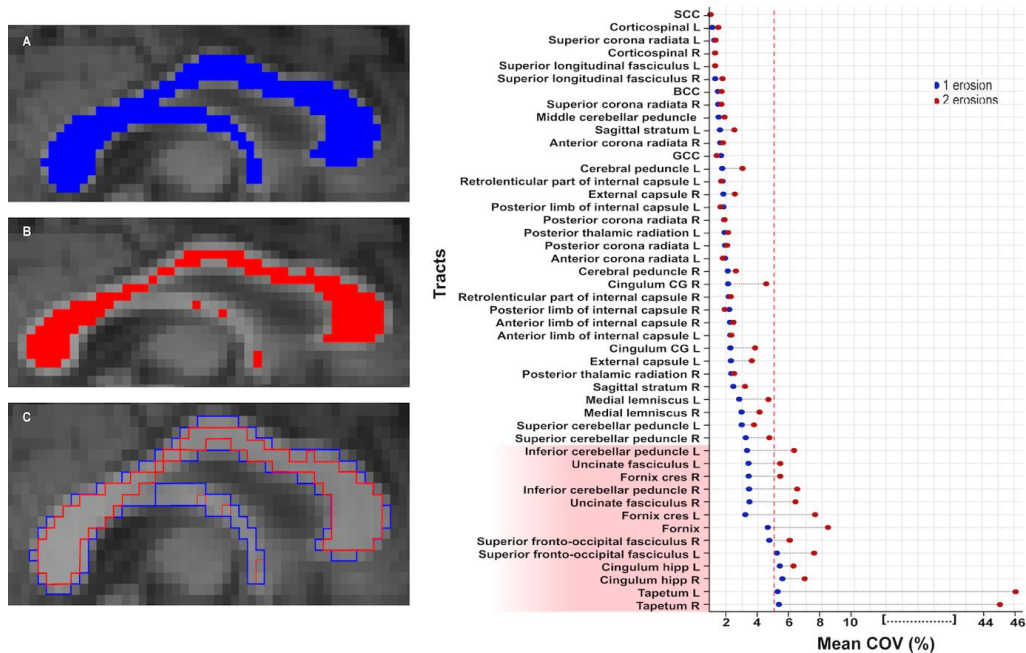


Figure 37: Examples of 1 and 2 erosions on segmentation and COV of tracts. (Left) Direct comparison of segmentation and voxel exclusion using an n-pass filter of 1 (A) or an n-pass



**filter of 2 (B) in the fornix and the three parts of the corpus callosum. (Right) Mean intra-subject COV per tract values following segmentation of 47 tracts using an n-pass filter of 1 (blue) or 2 (red). Cut-off (red dotted line) is at 5% variation for any of the two erosions (if variation of either 1 or 2 erosions is higher than 5%). Tracts highlighted in red are rejected. BCC= body of corpus callosum, GCC= genu of corpus callosum, SCC= splenium of corpus callosum.**

The 13 tracts with a higher COV tended to be smaller, with a strong correlation seen between the size of the tract, based on volume, and the COV (correlation coefficient  $r = -0.64$ ,  $p < 0.001$ ) (Table 9).

I have therefore decided to omit these tracts from subsequent analyses, in this chapter and the other chapters implementing the SSDS pipeline. However, I still used the fornix in this chapter for visualisation and comparison purposes, but I advise caution when segmenting any of the tracts mentioned above. For more conservative measures, I also suggest the use of a 2-erosion parameters. However, this increases variability and excludes important anatomical details. I therefore use 1 erosion whenever I use the SSDS pipeline (Figure 37).

I repeated SSDS analysis of each tract and each subject for each of the three visits (intra-subject, inter-visit). The three segmentations produced a similar number of voxels (correlation coefficient  $r = 1.0$ ,  $p < 0.001$ ) and very similar estimations of mean tract FA (correlation coefficient  $r = 0.94$ ,  $p < 0.001$ ) in all 17 subjects, for each of the three visits (Figure 38). Using a two-way mixed single measure consistency ICC, I calculated a mean value across all tracts and all visits of 0.87 (Table 9), considered excellent on the Cicchetti scale (Cicchetti, 1994).

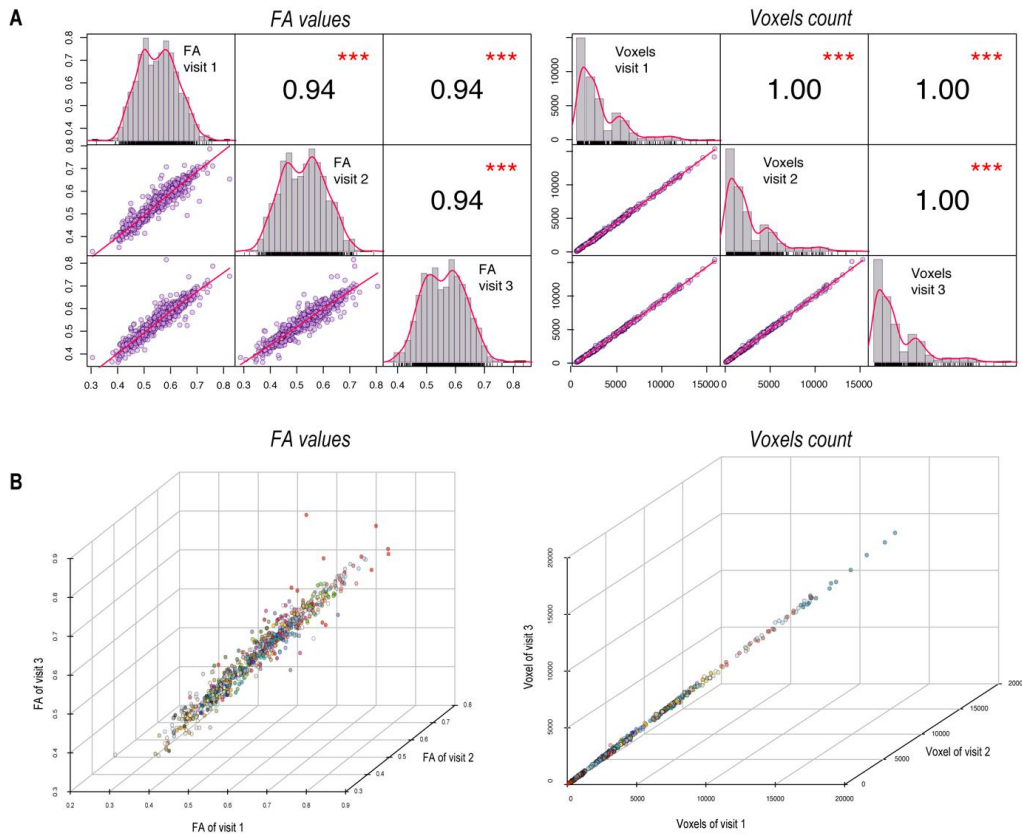


**Figure 38: Correlation of intra-subject, inter-visit SSDS results. (A) Pairwise correlation matrix of mean FA values and voxel count per tract per subject. Upper right values represent correlation coefficients  $r$ , histogram represent mean FA and voxel count distributions and scatterplot represent pairwise correlation of data points. P-values: \*\*\* $<0.01$ . (B) 3D correlation plot of mean FA value and number of voxels for all three visits per tract, per subject. Each colour represents a different tract, for all 47 tracts of the JHU atlas.**

### 3.4.4. SSDS vs other common methods

The pipeline needed validation above and beyond its ability to hold test-retest. I therefore compared to other commonly used methods in diffusion neuroimaging: Manual segmentation, registration to a template, and TBSS. For this validation step, I chose 6 tracts while trying to include different sizes and morphologies: the genu, body and splenium of the corpus callosum, the cingulum bundle left and right, and the fornix. Although I have previously suggested not using the Fornix as a tract in SSDS analysis (Section 3.4.2), I chose it as a validation tract to check if its segmentation fails with SSDS, or whether it is an unreliable tract while resorting to different methods as well. The mean FA resulting from SSDS were compared to:

- a) ROI analysis following manual segmentation on the parametric diffusion map
- b) ROI masking following registration to the high resolution MNI152 template
- c) skeletonized mean FA measures of ROI tracts after TBSS

Running a one-way ANOVA for the effect of the method used on the FA value, revealed statistically significant difference on all 6 tracts (Figure 39): the body of the corpus callosum ( $F=36.34$ ,  $p<0.001$ ), the genu of the corpus callosum ( $F=78.86$ ,  $p<0.001$ ), the splenium of the corpus callosum ( $F=38.3$ ,  $p<0.001$ ), the right and left cingulum bundles ( $F=22.88$ ,  $p<0.001$  and  $F=27.5$ ,  $p<0.001$  respectively) and the fornix ( $F=29.33$ ,  $p<0.001$ ).

I performed a pairwise comparison of each method with the results from manual segmentation: the paired t-test showed similar mean FA values for SSDS and manual segmentation for 5 tracts, while the mean FA value of the splenium of the corpus callosum is slightly higher using SSDS ( $t=1.75$ ,  $p=0.046$ ) (Figure 39-A).

This result further reflects the high levels of similarity between SSDS and the gold-standard of segmentation which is manual delineation of ROIs.

The average DSC value for all tracts comparing ROIs from manual segmentation and SSDS was  $0.8 \pm 0.1$ , ranging from 0.5 to 0.97, with the highest DSC average being for the segmentation of the splenium of the corpus callosum ( $0.81 \pm 0.06$ ), and the lowest being for the segmentation of the fornix ( $0.76 \pm 0.13$ ).

When I compared FA obtained from SSDS to the FA obtained from both registrations to a standard template (masked with a JHU tract in MNI152 space) and skeletonized tract following TBSS, there was a significant difference between mean FA of all tracts. As expected, the mean FA obtained using the SSDS pipeline were on average lower than mean FA extracted following skeletonization and using the ENIGMA DTI pipeline (Figure 39-A). This result is expected given that, as mentioned previously, the skeletonization process projects expected peak FA values onto the skeleton while ignoring neighbouring voxels. This further demonstrates the need for an automated pipeline with higher anatomical specificity and coverage.

One more method for extracting mean FA from ROIs that we commonly see in studies is the segmentation of the tract following non-linear registration of the parametric map to the standard template, and before skeletonization. This method has fundamental

flaws (see section 3.5. Discussion), but I used it as a comparative method to explain the problems that might arise from warping diffusion data.

The volume of each tract segmented, in  $\text{cm}^3$ , is on average 1.5 folds higher than the mean values for the corresponding tracts in native diffusion space for each individual (Figure 39-B). Moreover, while the volume of a given tract varies from an individual to another, it's a constant volume once warped to a standard template. This transformation to a higher resolution template will therefore inevitably include smoothed voxels and partial volume effect. This effect is further exacerbated when we look at the resulting mean FA values, which are consistently lower than value obtained from both SSDS and manual segmentation when all voxels are included to derive the mean value.

After skeletonization and exclusion of the partial volume to limit measurements to peak voxels and the centre of the tracts, the volume of the skeletonised ROI is on average 3 times smaller than that of the ROI segmented in native space (Figure 39-A). By sampling FA values from neighbouring voxels with peak signals by projecting values onto the skeleton, we end up with a higher mean FA value for each ROI. Even when outermost voxels are eroded, the diffusivity measures obtained from SSDS sample a larger volume without being skewed to peak values which are obtained from the skeletonization process. This reflects the limitation of only looking at peak FA values in samples where microstructural differences might not be homogenously distributed across the skeleton.

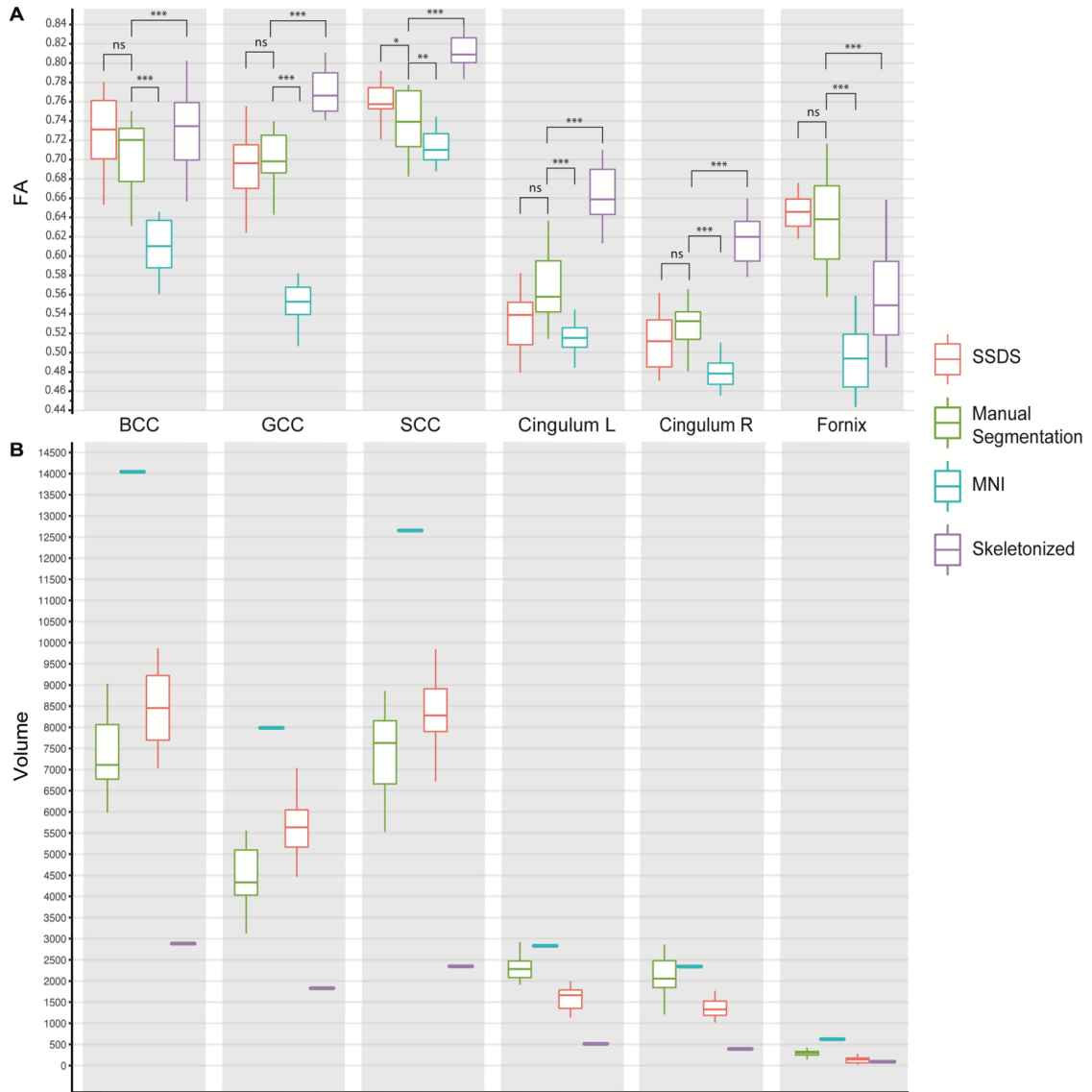


**Figure 39: Comparing SSDS to other methods. Boxplot comparing mean FA values (A) and volume in mm<sup>3</sup> (B) in n=15 healthy controls for 4 segmentation methods of the body, genu and splenium of the corpus callosum (BCC, GCC, SCC respectively), fornix and cingulum bilaterally. The four segmentation methods include SSDS, a manual segmentation on the parametric map, crossing ROI with normalized FA in MNI152 template space, and extracting the mean skeletonised FA value of each ROI mask. Although the fornix was omitted from analysis (because of a poor test -retest reliability), we included segmentation of the fornix to illustrate comparisons of the methods on a small tract. Ns= not significant, \*p < 0.05, \*\*p < 0.01, \*\*\*p < 0.001.**

A new method should have the same, or a better reliability measure to be adopted for future analyses. I compared reliability for FA values obtained from the different methods. The intra-tract (same tract, different subject) COV for the manual segmentation and TBSS stands at 6.60 % and 7.23% respectively, compared to 7.26% for SSDS. This indicates similar variation for SSDS to the methods commonly used.

### **3.4.5. Example – TBI patients vs healthy controls**

As an example of a clinical application of the SSDS pipeline, I looked at TBI patients with and without lesions, and compared the two groups to a third one of healthy controls. The mean FA derived from the whole brain WM map was significantly lower in both TBI groups (with and without lesions) compared to the healthy control group ( $t=6.59$ ,  $p<0.001$  and  $t=5.25$ ,  $p<0.001$  respectively), with the lowest WM mean FA recorded in TBI patients with lesions, but not significantly lower than mean FA of TBI patients with no lesions (respective mean  $X1=0.5 \pm 0.1$  and  $X2=0.51 \pm 0.08$ ,  $t=-1.62$   $p=0.053$ ).

I then looked at the different tracts and derived tract-specific mean FA values. The results showed a decrease in mean FA in the group with lesion compared to both the TBI group without lesions and the control group in the right anterior corona radiata, and the genu of the corpus callosum (Figure 39).

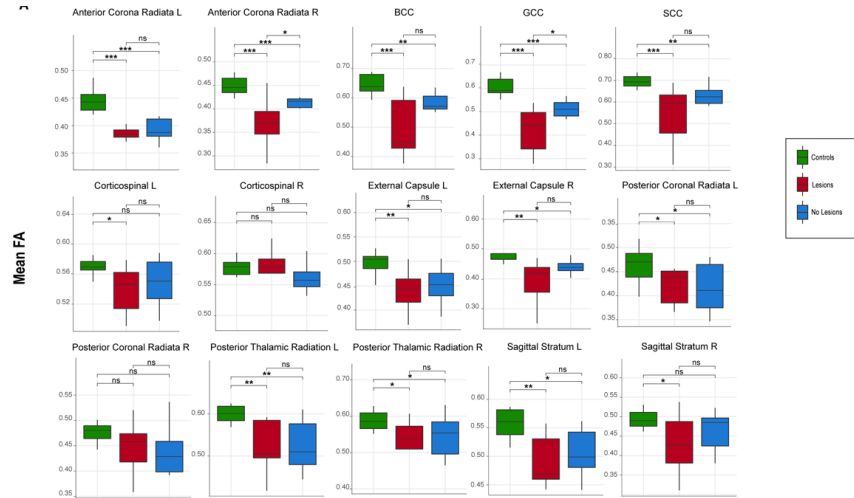


**Figure 40: Tract-specific mean FA value comparison in 3 groups. Healthy controls (green), TBI with lesions (orange), and TBI without lesions (purple). A subset of tracts is considered in this analysis, mainly when at least one of the bilateral tracts showed a difference. Ns=non-significant, \* $p<0.05$ , \*\* $p<0.01$ , \*\*\* $p<0.001$ .**

I then applied SSDS to three case studies to further demonstrate that SSDS provides robust FA estimations in cases of severe focal injuries and structural abnormalities following TBI (Table 10). I test it once again against the other common group-level methods.

**Table 10: Description of the case studies. PTA= post-traumatic amnesia.**

	Gender	Age	Time since injury (months)	Length of PTA (days)	Focal Abnormality	Mechanism
Case 1	Male	52	17	21	Contusions & Microbleeds	Fall
Case 2	Male	49	249	120	Contusions & Microbleeds	Sports
Case 3	Male	48	366	60	Contusions	Road traffic accident

#### Case 1:

The MRI of this patient shows a pronounced loss of volume within the corpus callosum, with enlargement of the ventricles. We can also see severe damage in the genu of the corpus callosum (Figure 41-case 1).

When manually segmented in native space, the affected WM region is not picked up by the rater given the lack of signal on the parametric FA map.

Similarly, the automated segmentation of SSDS returns an empty mask given the lack of signal from both the T1 and the diffusion image.

In contrast, the process of normalization to a standard space produces an estimated WM map in the damage region, and a subsequent skeleton within this location if TBSS is performed.

The results obtained with each method are as follow:

- Following TBSS and projection of peak voxels on the skeleton, the mean FA value is calculated as **0.514**.
- Following SSDS the mean FA value for the intact region of the corpus callosum is **0.364**.
- Following manual segmentation of the same ROI, mean FA is **0.382**.

### **Case 2:**

This case illustrates a similar case as the one mentioned above, with the MRI scan showing a thinning of the WM at the junction of the splenium and the body of the corpus callosum (Figure 41-case 2).

When performing a manual segmentation directly on the parametric map, this WM region is not segmented by the rater, nor the automated segmentation of SSDS.

In contrast, the process of normalization to a standard space (Case 2- C), and enlargement of the tract, produces an estimated WM map and subsequent skeleton within this location.

- Manual segmentation of the corpus callosum yields a mean FA value of **0.450**.
- SSDS segmentation of the corpus callosum yields a mean FA value of **0.425**.
- Following TBSS estimation of a skeleton at this region, the mean FA value is calculated as **0.532**.

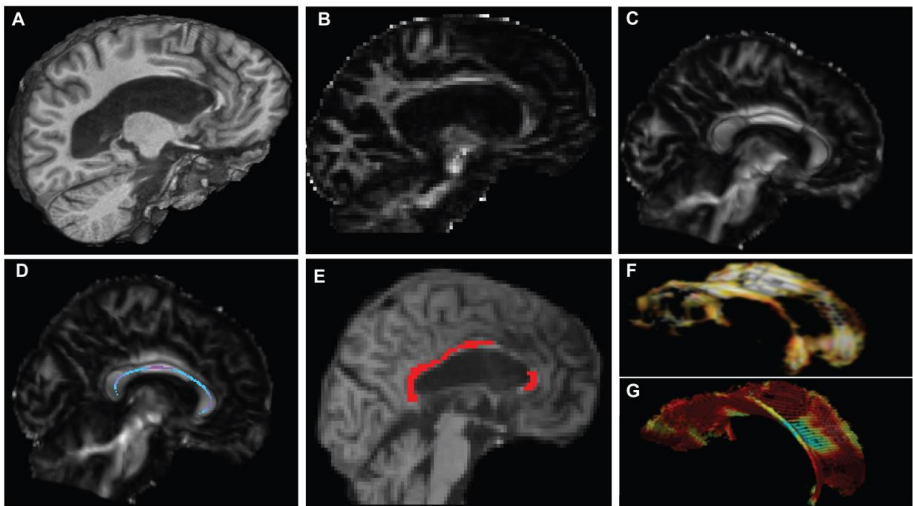
### **Case 3**

This case illustrates a brain with significant atrophy (Figure 41-case 3). This results in a loss of signal on the MRI, especially from small tracts around the ventricles such as the fornix. For this individual, the rater was unable to segment the fornix

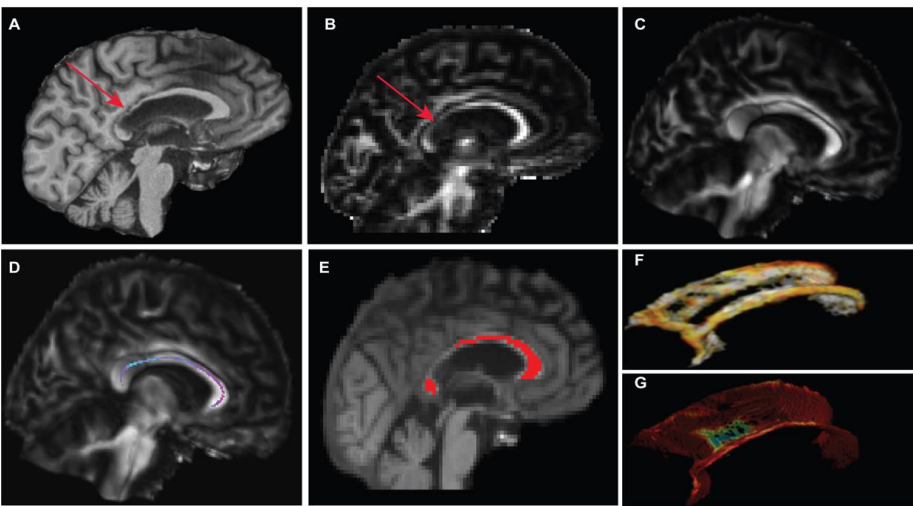


directly on the FA map. SSDS also returned an empty mask when trying to segment the fornix. However, registration to a high-resolution template normalizes the parametric map to a standard average, resulting in an estimate for the WM signal at the fornix, and a mean FA value of 0.15, and the skeletonized tract returned a mean FA value of 0.16.

CASE 1



CASE 2



CASE 3

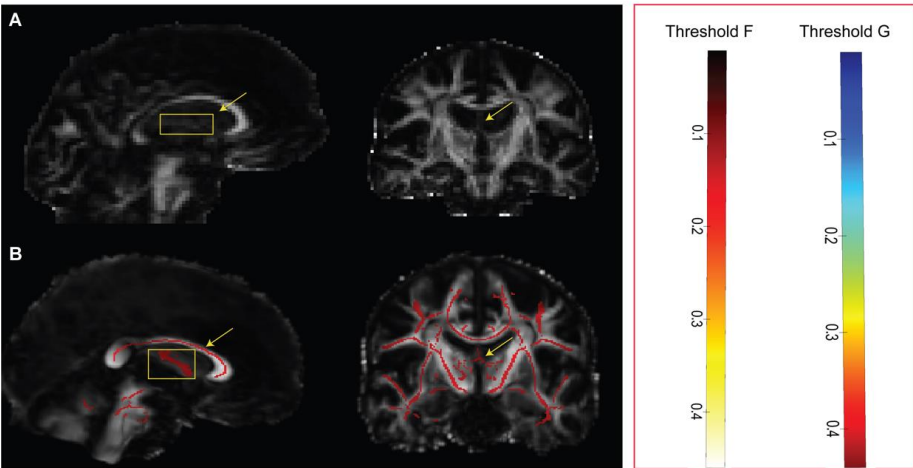


**Figure 41: Visual representation of case studies of patients with severe TBI. Cases 1 and 2 show the segmentation of the corpus callosum, and case 3 illustrates the robustness of the pipeline when a signal is not detected on the DWI image. A) native T1 image to illustrate structural abnormality before registration to the diffusion image, B) FA map in native diffusion space, C) FA map following registration to a higher resolution standard template through non-linear alignment, D) SSDS segmentation of corpus callosum and heatmap of FA values.**

### 3.5. DISCUSSION

I developed the Subject-Specific Diffusion Segmentation (SSDS) pipeline in the context of group studies where many subjects' MRI had to undergo segmentation in areas that might not be accessible with other methodologies, or in studies where group differences are relatively more subtle – both of which apply to my cohort of soldiers. The point of SSDS was to obtain a reliable method that combines both the spatial specificity of manual tract segmentation on native parametric maps, with the accuracy, standardization, automation, and reproducibility of group-level approaches. SSDS therefore overcomes the need for time-consuming manual segmentations in studies investigating individual changes in ROIs diffusion data, or in clinical groups with severe anatomical abnormalities in which registration of the diffusion image can yield inaccurate results.

One of the novelties of SSDS is that it relies on the underlying anatomy when deriving diffusion information. This is achieved by using the corresponding T1 structural image to guide both registration and segmentation.

The second strength of SSDS is that the diffusion image is never warped to the high-resolution template. If we look closely at what happens during warping to a higher resolution template, we can see that normalization results in artificial and smoothed voxels that both increase the volume of the ROI investigated and decrease the overall mean signal (Jones and Cercignani, 2010) (Section 3.4.4). Instead of relying on normalization, SSDS was optimized by using the T1 image to iteratively drive the intra-subject registration of the high-resolution template into the native diffusion space and preserve the anatomical details of the standard templates and the T1 image and the integrity of the diffusion information.

A third edge of SSDS is the use of boundary-based registration (BBR), which is based on the definition of a WM boundary and the difference of intensity across the boundary in both structural and diffusion images (Greve and Fischl, 2009). For the accurate intra-subject, inter-modality registration, integrating BBR and the 'up sampling-combine-inverse' technique (see section 3.3.3) resulted in an accurate registration of both the template and the T1 image in the lower-resolution DWI space in structurally typical as well as atypical brains suffering from anatomical abnormalities.

We could argue that SSDS is not the “first automated method for measuring ROI-specific in diffusion information (Ressel et al., 2018)”, citing methods such as TBSS and the ENIGMA-DTI pipeline. And although this is true, most standardized and commonly used pipelines still perform analyses in group space, still normalize diffusion data, and still register images across subjects (Soares et al., 2013), and are therefore not suitable to the problem I’m tackling – which, to reiterate, is the automated investigation at the individual level or regions that are not accessible once diffusion data is normalized and warped. In fact, standardized and publicly available simple protocols with pre-defined test-retest reliability and parameter normalization for more homogenous diffusion investigations at the individual level are still lacking. SSDS uses common registration techniques and predefined atlases to make automated segmentation stable in native diffusion space, maintaining high correspondence with FA values obtained from manual segmentation of ROI, and providing a reproducible pipeline capable of replacing manual segmentation of ROIs on parametric maps in clinical subject-level investigations.

SSDS shows high test-retest reliability across subjects and visits, for both the FA value calculated and the size of the tracts. Out of the 47 tracts segmented and tested, I eliminated all the tracts with a COV value higher than 5% - which resulted in the exclusion of 27% of the tracts. The excluded tracts were the fornix, superior fronto-occipital fasciculus bilaterally, hippocampal cingulum bundle bilaterally, the inferior cerebellar peduncle bilaterally, the uncinate fasciculus bilaterally, the fornix crescent bilaterally, and the tapetum bilaterally. There was a strong negative correlation between size and variability, with smaller tracts being the ones with a COV higher than 5%. I have also used 1-erosion of tracts for all subsequent analysis. Although adding a second erosion allows for more conservative segmentation, it increases the variation in measured FA and excludes important spatial information from the tracts.

SSDS also seems to reflect manual segmentation more accurately than the other methods and shows a high dice similarity coefficients (DSC) score on tracts studied. Like manual segmentation, SSDS retains the size and the morphology of the ROI, while in group-level analysis, spatial normalization of the parametric map

to a higher resolution template means warping and smoothing, and normalizing anatomy to achieve voxel-to-voxel correspondence for the subjects studied (Soares et al., 2013). Warping and non-linear registration can result in errors when moving images of low resolution and poorer contrast (such as DWI) to high template resolution (Jones and Cercignani, 2010). Smoothing is also often used to increase signal-to-noise ratio and compensate for possible misalignment, creates a normal distribution of the data (Worsley et al., 1996). Although spatial normalization is reliable and has been shown to preserve micro and macro-structural properties of large WM tracts, we can't say the same about smaller structures and/or structurally atypical brains (Adluru et al., 2013, Jones and Cercignani, 2010). To overcome the effect of normalization, TBSS successfully measures FA values at the centre of the tract via projection of the peak FA values onto a skeleton (Smith et al., 2006), which was revealed to be a valuable tool for DTI investigation. To achieve this projection, the algorithm searches for the maximum value, assumed to represent the centre, perpendicular to the midline skeleton structure (Zalesky, 2011). However, it is important to note that not all differences in signal are homogeneously distributed to the centre of the tracts, and differences between groups can be too subtle to detect with more conservative techniques where only peak voxels are reflected, and can be affected by anatomical shifts, WM structural abnormalities and registration errors (Zalesky, 2011). But on the other hand, if ROIs are investigated following spatial normalization by masking with atlas-derived pre-defined tracts, the estimated tracts are much larger tracts (~1.5 fold increase), compared to native WM tracts through normalization and up sampling, which leads to inclusion of smoothed voxels and partial volume effects, and can bias the results. Other approaches to investigating ROIs include fibre tractography, with its main advantage, from a clinical perspective, being the possibility to derive measures from the entire fibre bundle, instead of one of its segments, and as a discovery technique for WM connectivity (Hulkower et al., 2013). However, such measurements can be challenged by the presence of structural abnormalities leading to false positive bundles (Schilling et al., 2019), and different approaches should be used when specific and predefined ROIs are investigated.

This brings us back to the novelty of SSDS. We can now carry out longitudinal studies of volume changes in WM ROIs over time in both group and individual investigations. SSDS also eliminates the need to manually delineate and mask structural abnormalities (lesions, tumours, etc...), which, up to this point, was still a routine step in our lab for diffusion studies of TBI. This is possible given that the technique relies on a WM map to guide the segmentation; and WM map estimation excludes low-intensity signals from the T1 image (Horbruegger et al., 2019). Several steps in the pipeline also curb the issues arising from partial volume, reducing their effect on the results. These steps include using a T1 WM binary map as an anatomical guide, eroding the WM map, and adding optional erosions of the tracts before and after registering them to native space. It is important to note that the kernel used for erosion only excludes the outermost voxels (Figure 42). The partial volume is therefore limited to the resolution of the diffusion image.

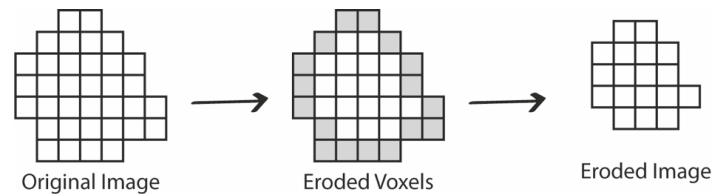


**Figure 42: Original vs eroded image. In grey: simplistic representation of outermost voxels excluded during the erosion process.**

This pipeline can be applied to any measure derived from diffusion images, although we have demonstrated its utility in the analysis of FA data. However, the resolution and performance of the algorithm will ultimately be determined by the resolution and performance of the underlying DWI acquisition: the higher the quality of the diffusion data, the more accurate the segmentation process. My approach can either be used independently or can complement group-level analysis such as VBA or TBSS. SSDS also has significant advantages if specific parts of WM tracts need to be sampled, for example WM boundaries or tract-specific boundaries. I mention this because investigation of the boundaries of the WM is the reason I developed SSDS. Such investigations would be of interest for a variety of conditions, including TBI and autism (Andrews et al., 2017, Narayana, 2017).

As with any imaging technique, SSDS has its pitfalls which I'm hoping to improve in future implementations. The main limitations of SSDS relate to its application to smaller tracts, which tend to have higher variation (e.g. the superior Fronto-Occipital Fasciculus and the hippocampal projection of the Cingulum). To reduce this variation, we could either improve on the quality of the acquisition, the registration, or the structural image. The effect of noise on FA measures has well been documented (Pierpaoli and Basser, 1996) and impacts on the variance in anisotropy. This, however, is not exclusive to SSDS, and implies high error rates when using alternative methods. Another limitation would be the performance of registration if and when gradient field maps have not been acquired, or the quality of the structural image segmentation in case abnormalities are present.

Future investigations using SSDS will have to determine the minimal angular resolution, spatial resolution, and signal to noise ratio for SSDS to still be able to perform, as well as the applicability in small white matter tracts when using higher spatial resolution diffusion imaging.

In summary, I describe a novel pipeline for diffusion MRI investigations of WM abnormality at the individual level, and provide the code for use by other studies, as well as test-retest measures of reliability and information on best practice when implementing SSDS. I showed that it is robust to the presence of structural abnormalities, reliable, and most importantly shows high correspondence to manual segmentation of WM tracts which remains the gold standard for ROI-driven diffusion analyses. Validating the pipeline was a crucial step for its implementation in bTBI investigation in the next chapter.

### ***In the next chapter***

In chapter 4, I will investigate diffusion abnormalities in bTBI, and the difference at the level of the WM microstructure between blast and nbTBI. I will do this by first using a standard group-level analysis, TBSS, and then by implementing SSDS in the same cohort at the individual level, and in regions where diffusion-related metrics can't be measures with TBSS.



# CHAPTER 4

---

## Detecting White Matter Abnormality in Blast-Related Traumatic Brain Injury

*In this chapter I use two different techniques to investigate white matter abnormality in blast-related traumatic brain injury. I first perform a TBSS approach on a subset of white matter tracts on the three groups: a healthy control group, a group of civilians with non-blast traumatic brain injury, and a group of soldiers with blast-induced traumatic brain injury. I then apply the SSDS approach to examine whether increasing specificity at the individual level can help uncover a pattern of microstructural white matter abnormality specific to blast injury.*

#### 4.1. ABSTRACT

Investigating the effect of primary blast injury on the brain, and how it compares to civilian traumatic brain injuries (TBI) and other injury mechanisms can help understand the symptoms and sequelae of blast-related TBI (bTBI), as well as improve prevention and diagnosis. Based on previous neuroimaging studies showing damage at level of the middle cerebellar peduncle (MCP), and on post-mortem investigations, pre-clinical studies and computational simulation suggesting susceptibility to blast at the interface of different tissue types, a direct comparison to civilians with non-blast TBI and analysis of tissue boundaries in vivo are still lacking. It has already been determined that primary blast-related TBI leads to diffusion tensor MRI abnormalities consistent with diffuse axonal injury and microstructural damage of the white matter (WM). To further examine the difference in WM injuries between blast and non-blast TBI in specific tracts and the boundary of the WM, we compared 19 U.K. military personnel with a history of blast-related TBI, to age and gender-matched healthy controls (n=30) and civilians with non-blast TBI (n=20) matched for the time since injury and injury severity. I used diffusion tensor imaging (DTI) data to perform three distinct analyses: group-level tract-based spatial statistics (TBSS), followed by an automated and individual segmentation of whole WM tracts using subject-specific diffusion segmentation (SSDS) to increase the specificity of the measurements, and a segmentation of the boundary of the WM in the whole brain, and in specific tracts. While group-level TBSS showed a similar pattern of widespread WM abnormalities in both injured groups relative to controls when comparing skeletonised mean FA across tracts ( $p>0.05$ ), subject-level SSDS measures revealed differential injury at the level of the MCP tract in the soldiers compared to civilians with TBI ( $p=0.02$ ) and healthy controls ( $p=0.02$ ). The pattern of damage specific to the blast group was also concentrated around the boundary of the WM and the cerebrospinal fluid in the whole brain ( $F=2.98$ ,  $p=0.05$  one-way ANOVA) and the MCP more specifically ( $F=4.79$ ,  $p=0.01$  one-way ANOVA). DTI findings in U.K. military personnel support the hypothesis that primary blast TBI can involve a differential pattern of WM injury in soldiers.

## 4.2. INTRODUCTION

The number of U.K. and US military personnel affected by blast-related TBI (bTBI) is estimated to stand at around 15.2% - 22.8% (McKee and Robinson, 2014, Masel et al., 2012, Hoge et al., 2008). As I mentioned in earlier chapters, previous studies across different disciplines suggest that there may be differences in the pathophysiology of blast-related and non-blast related TBI (Robinson et al., 2019, Shively and Perl, 2017, Hoffer et al., 2010, Moore et al., 2009), and this is the main hypothesis that my thesis has been tackling. However, blast-related injuries are rarely present in isolation (Kirkman et al., 2011) given that the different types of injuries mostly coexist in soldiers, which renders assessing primary blast injuries a challenge because of the spectra of clinical manifestations following blast waves (Thompson et al., 2008), direct blows to the head (Ryan and Warden, 2003), or both, when they happen simultaneously (Hoffer et al., 2009).

Head trauma resulting from blast overpressure is still incompletely understood. In vitro investigations, pre-clinical animal studies, computational simulations and modeling, as well as clinical research are still trying to elucidate the pathophysiology of primary blast injuries, and although many mechanisms have been hypothesized, evidence supporting one or the other is still insufficient. In this chapter I focus on the damage to the white matter (WM) microstructure, and how it can be a signature of primary blast injury.

A finite element model of the effects of blast on the brain suggests that the primary blast wave may produce direct WM injury, in locations that are unusual for non-blast TBI (Taylor and Ford, 2009a), while another model shows that the rapid head motion caused by blast could result in strain on tissues surrounding CSF cavities (Yu et al., 2020). In the latter study, to which I contributed during my PhD, a finite element head model was exposed to a frontal blast wave and predicted the strain and strain rate distribution in the cortex<sup>7</sup>. The conclusion was that strain and strain rate were significantly increased in the cortex, and that this change was mainly caused by head

---

<sup>7</sup> Strain is the deformation of a tissue and strain rate is the rate of this deformation caused by the strain over a period of time.

motion, while the strain rate increase was caused by both rapid head motion and rarefaction waves. The study also shows that rapid motion of the head as a result of the blast wave is the key mechanism for CSF tensile failure and subsequent cavitation, which seems to be the cause of strain and strain rate increase.

In line with this hypothesis, a post-mortem histopathological investigation of bTBI showed evidence of interface astroglia scarring at boundaries between brain and fluids, but the findings were also seen at the boundaries of the WM and grey matter (GM) (Shively et al., 2016). The biomechanical prevailing hypothesis is that when the waves are transmitted from a type of tissue to another, the refraction waves amplify the effect, possibly causing the damage at the boundaries (Courtney and Courtney, 2015).

As already mentioned, moderate and severe bTBI are often associated with obvious injuries such as severe cerebral oedema, intracranial haemorrhage, and vascular injury in neuroradiological assessments (Mutch et al., 2016). However, the variations in the samples and their sizes, the study designs and the measurements across neuroimaging studies and reports, as well as the heterogeneity of TBI and causes of TBI in general, present a major challenge to generalizable results and conclusions. Even in the absence of abnormalities on brain CT and MRI, investigations have revealed other neuroimaging findings such as morphological and volumetric abnormalities or changes in diffusivity properties reflecting diffuse axonal injuries (DAI), which are not typically seen in standard CT and MRI imaging (Benzinger et al., 2009, Mu et al., 2017), shedding light on the importance of advanced neuroimaging techniques and standardized analyses. Diffusion tensor imaging (DTI) has been widely and successfully used in the assessment of DAI in civilian with mild TBI. DTI measures the fractional anisotropy (FA) of diffusion, as a dynamic indicator of the underlying WM microstructure (O'Donnell and Westin, 2011). In the context of military brain injuries, previous DTI studies have reported abnormalities in soldiers, consistent with traumatic axonal injury (Mac Donald et al., 2011), and a correlation between those abnormalities and worsening performance on executive tasks (Jorge et al., 2012) following bTBI (see Table 4).

However, the main question is yet unanswered: **to what extent neuroimaging abnormalities produced by blast exposure are specific to the primary injury?**

Since it is rare for soldiers to suffer from isolated blast injuries, the neuroimaging abnormalities are likely to be the combination of several different mechanisms, including what is more commonly seen in civilians suffering from non-blast TBI.

This chapter was inspired by a previous prestigious in-vivo neuroimaging investigation showing the presence of axonal injury through microstructural damage at the level of the cingulum bundle, uncinate fasciculus, and anterior limb of the internal capsule, and most prominent abnormalities were found in the middle cerebellar peduncle (Mac Donald et al., 2011). They predicted this region to be most vulnerable to primary blast injury (Taylor and Ford, 2009b). However, the contribution of primary blast injury specifically could not be determined given that the soldiers included in the study sustained different mechanism of injuries, and that no control group for different injury mechanisms was included.

If parts of the WM are specifically vulnerable to blast injuries, and in line with the hypothesis of stress changes at the boundaries of different tissues and cavitation effects at the edges of CSF-filled cavities, then damage of the microstructure at the WM boundary of these tracts might be driving the changes observed.

In this study, I use two control groups, a civilian nbTBI as well as a healthy control group to understand how WM injuries differ between bTBI and nbTBI. I implement both a group-level and a subject-level analysis to identify widespread WM damage and to investigate whether a pattern of WM injury specific to bTBI emerges. I apply the subject-specific diffusion segmentation (SSDS) pipeline to detect more subtle changes in the WM that might not be homogeneously distributed across the skeleton of tract and across individuals in group-level analysis. I also extend the method to look more specifically at boundaries of the WM tracts.

#### ***Hypotheses of Chapter 4***

- Using group-level tract-based spatial statistics (TBSS) (Smith et al., 2006) on a reliable subset of WM tracts, the pattern of injury reflected by DTI abnormalities will be present in both bTBI and nbTBI groups.
- When increasing the specificity of measurements with subject-level investigations, bTBI will be associated with abnormalities in the posterior fossa, specifically the middle cerebellar peduncle, with greater damage seen at the boundary of the WM.

### **4.3. METHODS**

#### **4.3.1. Participants**

Data from 19 soldiers (mean age  $\pm$ SD:  $29.8 \pm 5.9$  years) with moderate to severe blast traumatic brain injury (bTBI) in the post-acute phase were included in this study. The two control groups consisted of 20 civilians with non-blast TBI (mean age  $\pm$ SD:  $30.3 \pm 7.6$  years), as well as 31 healthy controls (mean age  $\pm$ SD:  $30.6 \pm 6.7$  years). The bTBI and nbTBI groups were matched time since injury (mean  $\pm$  SD  $14.6 \pm 5.9$  and  $12 \pm 12.7$  months respectively). All participants gave written informed consent according to the Declaration of Helsinki.

All cases of military and civilian injury were categorised as moderate or severe based on the Mayo Classification System for Traumatic Brain Injury Severity, relating to the duration of loss of consciousness, the length of PTA, the lowest recorded GCS in the first 24 hrs and/or CT or MRI result (Malec et al., 2007). Exclusion criteria were as follows: penetrating brain injury, neurosurgery, except for intracranial pressure monitoring; a history of psychiatric or neurological illness prior to head injury; a history of previous TBI; anti-epileptic medication; current or previous drug or alcohol abuse; or contraindications to MRI.

#### **4.3.2. Neuropsychological Assessment**

All participants completed a standardised neuropsychological test battery sensitive to cognitive impairment associated with TBI (Kinnunen et al., 2011). The cognitive functions assessed were: Verbal and non-verbal reasoning ability via the Wechsler Abbreviated Scale of Intelligence (WASI) Similarities and Matrix Reasoning subtests, associative learning and memory via the immediate recall score on the People Test, executive functions, inhibitory control, cognitive flexibility and word generation fluency via the Trail Making Test, alternating-switch cost index, and two indices from the Delis–Kaplan Executive Function System (Delis 2001), and the total score on Letter Fluency; and information processing speed via a simple computerised choice reaction task.

#### **4.3.3. Imaging Acquisition**

Each patient had standard high-resolution T1 and gradient-echo (T2\*) imaging. MRI was performed on Philips 3T Achieva scanner (Philips Medical Systems, The

Netherlands) using a body coil. For DWI, diffusion-weighted volumes with gradients were applied in 16 non-collinear directions in each of the four DTI runs, resulting in a total of 64 directions. The following parameters were used: 73 contiguous slices, slice thickness = 2mm, field of view 224 mm, matrix 128 X 128 (voxel size = 1.75 X 1.75 X 2 mm<sup>3</sup>), b value = 1000 and four images with no diffusion weighting (b=0s/mm<sup>2</sup>).

#### **4.3.4. Imaging Analysis**

##### ***Pre-processing***

The workflow of this study is outlined in Figure 43. I pre-processed DWI images using FSL's FDT standard pre-processing technique (Behrens et al., 2003) and the brain extraction tool (BET) for skull-stripping (Smith, 2002). I applied motion parameters to the DTI b-vectors to compensate for the eddy current and motion corrections. I estimated the diffusion tensor using the skull stripped DWI image to generate fractional anisotropy (FA) maps using the FSL DTIFIT algorithm (weighted least squares approach). I subsequently used FA maps in the analysis as an indicator of the microstructural integrity of the underlying WM structure.

For the T1 image, I performed brain extraction using FSL-BET, then segmented the brains into different tissue types and corrected for spatial intensity variations using FSL FAST (Zhang et al., 2001). I used the WM segmented tissue to generate a map of the WM boundary, subsequently used in SSDS analysis.



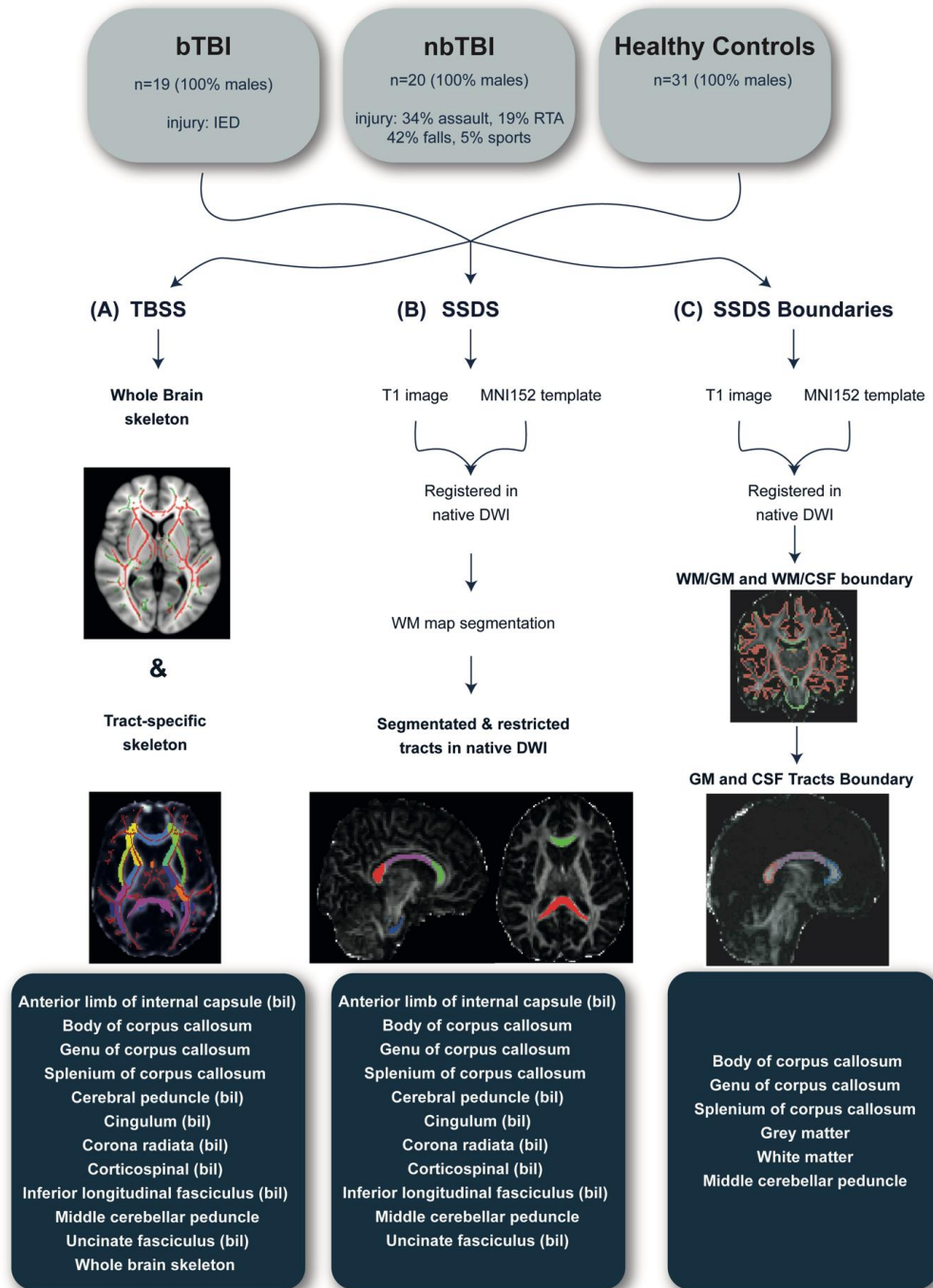


**Figure 43: Workflow for this study. A) TBSS and skeletonized mean FA of ROI B) SSDS overview of methodology and tracts used for mean FA estimation in native diffusion space C) SSDS boundary segmentation overview of methodology and tracts used to estimate mean FA at the boundary of the WM/GM and WM/CSF. For whole brain boundary, red is the WM/GM**

boundary, green is WM/CSF boundary. IED= improvised explosive device, RTA= road traffic accident, bil= bilaterally.

### **TBSS**

I performed voxel wise analysis of the FA maps using TBSS (Smith et al., 2006) in the FMRIB Software Library. Following estimation of the mean FA skeleton, I used non-parametric permutation-based statistics with randomize and threshold-free cluster enhancement and 5000 permutations while correcting for multiple comparison. I included age as a covariate, and I assessed significance at P-value<0.05. Using a region of interest (ROI) approach to investigate FA within a specified WM region, I created ROI masks in the MNI152 1mm space and then applied them to the TBSS skeletonised images to extract mean skeletonised FA from each ROI (Figure 43-A).

### **SSDS**

I implemented and extended the method described in the subject-specific diffusion segmentation (SSDS) pipeline (CHAPTER 3) (Figure 43-B). As a brief overview, tracts segmented through SSDS allow an estimation of FA from the entire tract in native diffusion, reflecting manual segmentation of the tracts on the parametric FA map, and more tracts with high reliability can therefore be including in the analysis. SSDS overcomes the need to interpolate diffusion data and enables measurements from the whole tract instead of the skeleton. I registered the T1 image to the native DWI through alignment of the EPI volume to the T1 brain image using a boundary-based registration (BBR) (Goebel, 2020), then segmented the T1 image into three tissue type following registration to the B0 image. I thresholded the WM map to 0.99 and binarized to exclude partial volume voxels. To register the ROIs to the diffusion image, I calculated an inverse of the non-linear warp of the T1 to the MNI152 template. I then concatenated the non-linear registration and the linear BBR transforms and used the resulting transformation to register the ROIs to the native diffusion image. The tracts are then cross masked with the WM map to ensure restriction to the underlying anatomy.

### ***Segmentation of the tract boundaries***

I calculated mean FA at the boundary of the whole-brain WM as well as the WM/GM and WM/CSF boundaries of the following tracts (Figure 43-C).

The boundary mask consists of the outermost voxels of an ROI. To generate a boundary mask, I eroded the mask of the ROI by 1 voxel when non-zero are found in the kernel and subtracted the eroded mask from the initial mask to generate a 1-voxel thick boundary that excludes partial volume by being limited to the underlying anatomy (Figure 44). I then dilated the map of both the cerebrospinal fluid (CSF) and the grey matter (GM) to create an overlay with the eroded WM map. I transformed the overlay into binary masks: WM/GM boundary and WM/CSF boundary.

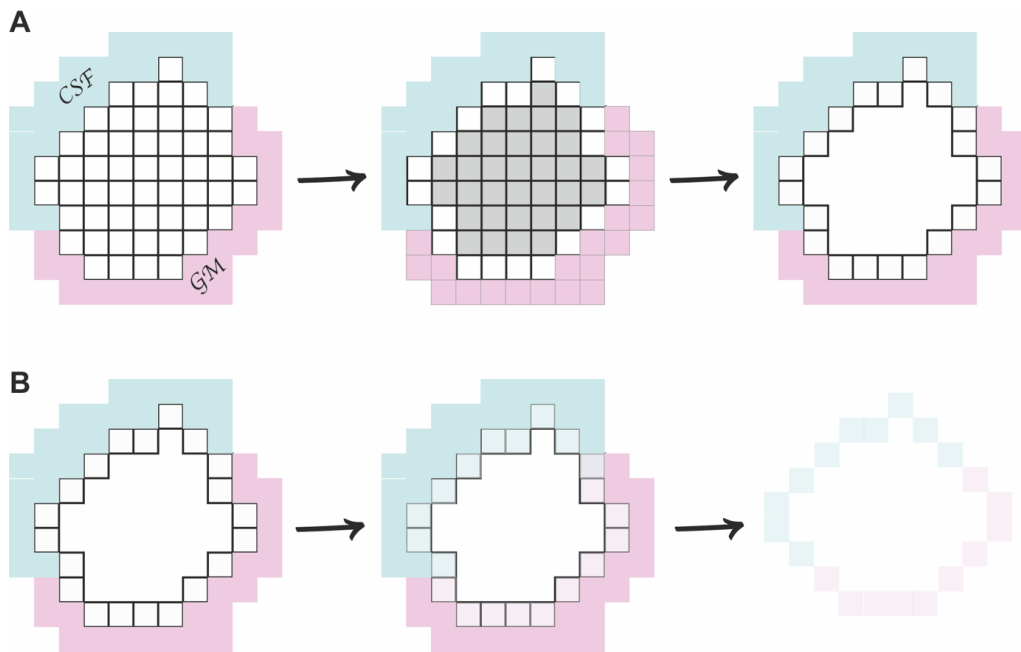


**Figure 44:**How boundary masks are created. Blue area represents the CSF, pink area represents the GM, and pixelated area represents the WM. A) the initial image is eroded, resulting in the inner voxels being preserved. Inner voxels are then used to mask out the corresponding voxels on the initial image to end up with the outermost voxels. B) Voxels from both the CSF and GM are dilated, resulting in an overlap with the adjacent WM boundary voxels. Dilated maps of the CSF and GM are then used to mask out the boundaries specifically associated with either GM, or CSF.

To validate measures obtained from these masks, I manually segmented the WM/CSF boundary of the whole corpus callosum and compared to the results obtained following SSDS and boundary segmentation of the whole corpus callosum. Each manually delineated ROI consisted of multiple slices fully covering the 3D structure. The

anatomical structures were defined according to the definitions provided in a standard DTI atlas (Oishi et al., 2008). I chose at random five subjects from each of the three groups (bTBI, nbTBI, controls) for a total of n=15 individuals.

### ***Regions of interest***

For both the TBSS and SSDS analyses, I chose the ROIs based on the following criteria: 1) the most reliable tracts to use in the individual diagnostic pipeline, as well as their importance in TBI diagnosis (Jolly et al., 2020): the genu, body and splenium of the corpus callosum, the corticospinal tract bilaterally, the corona radiata bilaterally, the inferior longitudinal fasciculus bilaterally and the middle cerebellar peduncle, and 2) the tracts of interest for bTBI based on previous in-vivo findings (Mac Donald et al., 2011) including the cerebellar peduncle bilaterally, the cingulum bilaterally, the anterior limb of the internal capsule bilaterally, and the uncinate fasciculus bilaterally.

For the analysis of the boundary of the WM, tracts fitting the following characteristics were chosen: 1) Large/wide tracts for accurate segmentation of the boundary, 2) sharing a boundary with both the GM and the CSF, and 3) tracts of interest for bTBI. Therefore, four different regions were investigated, including the body, splenium and genu of the corpus callosum, and the middle cerebellar peduncle.

### **4.3.5. Statistical analysis**

I conducted all statistical analysis using R v3.3.3 ([www.R-project.org](http://www.R-project.org)) to assess normality relationships between variables and compare experimental groups. I used one-way ANOVA followed by a Tukey HSD post-hoc analysis as well as two-sample t-tests if comparing the mean of two groups. To study the effect of a cognitive variable on FA measures within the bTBI group, I report Pearson's correlation coefficients. I assessed significance at  $p\text{-value} < 0.05$ . To compare an individual's FA value to the distribution of the control group, I calculated a Z-score for each ROI. Negative Z-scores indicate a lower FA value compared to the control's mean. I calculated P-values of the Z-scores [two-tailed, with 95% confidence interval (CI)] and corrected for multiple comparisons (false discovery rate). Bonferroni correction was used to correct for multiple comparison.

## 4.4. RESULTS

### 4.4.1. Patients' Characteristics

#### *Clinical demographics*

Soldiers with bTBI were all injured by improvised explosive devices (IEDs) during deployment, were wearing full personal protective equipment and were immediately transferred to Camp Bastion to receive emergency care, then repatriated to the United Kingdom within 48 hours (Table 11: Demographics of the three groups taking part in this study. Results for age, time between injury and scan are in mean  $\pm$  SD. PTA= post traumatic amnesia, ISS = Injury severity score, Mounted: in a vehicle or room corner, Unmounted= in open field.).

For the non-blast TBI (nbTBI) group, all civilians were diagnosed with TBI after being referred to the local TBI service because of functional impairments following injuries. In the nbTBI group, injuries were caused by assaults (34%), road traffic accidents (19%), falls (42%) or sports related injuries (5%).

**Table 11: Demographics of the three groups taking part in this study. Results for age, time between injury and scan are in mean  $\pm$  SD. PTA= post traumatic amnesia, ISS = Injury severity score, Mounted: in a vehicle or room corner, Unmounted= in open field.**

	Controls	nbTBI	bTBI
<b>n</b>	31	20	19
<b>Gender (% males)</b>	100 %	100 %	100 %
<b>Age at scan (years)</b>	30.6 $\pm$ 6.7	28.7 $\pm$ 6.3	29.8 $\pm$ 5.9
<b>Time between injury and scan (months)</b>	NA	12 $\pm$ 12.7	14.6 $\pm$ 5.9
<b>Presence of contusions and/or microbleeds</b>	NA	95 %	63 %
<b>PTA (&gt;24 hours)</b>	NA	35 %	68 %
<b>ISS [1-75]</b>	NA		33.0
<b>Biomechanics (% mounted)</b>	NA	NA	64 %

#### *Focal injuries following TBI*

In the bTBI group, focal damage was concentrated on the frontal and temporal lobes. In the nbTBI group, focal damage had a similar fronto-temporal distribution, although there was no overlap in location of contusions at the voxel level between the two groups. The mean volume of contusions in the bTBI group was  $2.7\text{cm}^3$  compared to  $5.3\text{cm}^3$  in the nbTBI group, but although the nbTBI group seemed to have more focal damage, the difference between groups was not significant ( $p=0.07$ ).

Standard T1 MRI was normal in 70% of soldiers with bTBI, and in 40% of civilians with nbTBI. Gradient echo imaging showed intraparenchymal microbleeds, indicative of DAI in 45% of those suffering bTBI and 50% of the nbTBI group. Only 20% (4 soldiers) of the bTBI group had evidence of focal damage on T1/Flair imaging. This was located mainly in the left frontal and temporal lobes. In contrast, 60% of the nbTBI group, had evidence of focal damage which was in a similar fronto-temporal distribution. There was no overlap in location of contusions between the two groups.

### ***Impaired cognitive function in TBI groups***

Both TBI groups showed a pattern of cognitive impairment characteristic of traumatic brain injury (Ponsford and Kinsella, 1992). Compared to the healthy control group, soldiers showed cognitive impairments across:

- (i) processing speed: through the Trail Making Test A (bTBI:  $24.8\pm6.0$  controls:  $20.5\pm6.8$ ,  $p=0.03$ )
- (ii) impaired executive functioning: assessed using inhibition switching minus a baseline of colour naming and word reading (bTBI:  $46.6\pm198$  controls:  $25.2\pm4.1$ ,  $p=0.0001$ ), and the word generation fluency task (bTBI:  $37.8\pm11.4$  controls:  $45.3\pm12.9$ ,  $p=0.036$ ) (Table 12).
- (iii) intellectual ability: with lower score on WASI similarities test (bTBI:  $31.2\pm6.2$  controls:  $35.1\pm6.0$ ,  $p=0.037$ ).

The nbTBI group showed evidence of impairments, compared to healthy controls in:

- (i) memory: people test immediate recall (bTBI:  $31.2\pm6.2$  controls:  $35.1\pm6.0$ ,  $p=0.037$ ), and naming/reading as measured by the STROOP colour naming task

- (ii) impaired executive functioning assessed using the Trail Making Test B minus A, inhibition switching minus a baseline of colour naming and word reading and word generation fluency (Table 12).

Despite the focal damage being more pronounced in the nbTBI group, the bTBI group showed more impaired cognitive function relative to the nbTBI group. A comparison of the blast and non-blast groups revealed lower current intellectual ability in the blast group using the Wechsler Abbreviated Scale of Intelligence (WASI) Similarities test (nbTBI: 37.72±4.01, bTBI: 31.21±6.24,  $p=0.0003$ ). Additionally, the blast group showed lower performance on: (i) processing speed: naming/reading demonstrated using the STROOP word reading task; (ii) executive functioning assessed with the Trail Making Test B minus A; and (iii) impaired information processing speed tested on the choice reaction task (Table 12).

**Table 12: Results of neuropsychological tests across three groups, for different cognitive domains and their associated cognitive variables. T-test were performed pairwise to assess difference between groups. ns= no significance, \* $p<0.05$ , \*\* $p<0.01$ , \*\*\* $p<0.001$ .**

Cognitive Domain	Cognitive Variable	bTBI	nbTBI	Control s	bTBI vs nbTBI	bTBI vs Control	nbTBI vs Control s
		Mean SD	Mean SD	Mean SD	P-value	P-value	P-value
Intellectual ability: verbal/non-verbal	WASI similarities	31.211 6.241	37.722 4.012	35.133 6.034	***	*	ns
	WASI matrix reasoning	24.842 6.752	26.471 5.780	27.867 4.533	ns	ns	ns
Memory: associative memory	People Test immediate recall	24.158 7.042	24.444 6.061	29.067 5.325	ns	*	*
Processing speed: visual search/complex	Trail Making Test Trail A (s)	24.842 6.039	23.961 7.976	20.533 6.850	ns	*	ns
	Trail Making Test Trail B (s)	49.789 13.742	60.356 30.656	50.122 46.037	ns	ns	ns
Processing speed: naming/reading	Colour naming (s)	38.316 19.451	33.889 10.643	29.600 40.050	ns	ns	ns
	Word reading (s)	28.368 10.915	21.389 4.046	27.730 5.990	**	ns	***
Executive function: alternating-switch cost	Trail Making Test Trails B minus A (s)	24.947 11.956	36.394 27.763	19.420 7.540	*	ns	**
Executive function: cognitive flexibility	Inhibition/switching (s)	75.526 26.692	63.611 17.429	51.630 20.400	ns	**	*
	Inhibition switching minus a baseline of colour naming and word reading (s)	46.630 19.770	28.300 6.390	25.200 4.110	*	***	ns
Executive function: word generation fluency	Letter Fluency F+A+S total	37.789 11.360	40.611 11.325	45.330 12.860	ns	*	ns
Processing: choice reaction time	Choice reaction task median reaction time (ms)	482.000 136.000	416.000 62.000	380.000 53.000	*	ns	*

#### **4.4.2. WM Abnormalities in Skeletonised Tracts Following Group-Level Analysis**

Soldiers exposed to blast showed evidence of widespread WM abnormalities compared to healthy controls (Figure 45-A). When I examined ROIs, the comparison of bTBI and healthy control groups showed reductions in FA in several WM tracts including the genu of the corpus callosum, the left corticospinal tract and corona radiata, and the inferior longitudinal fasciculus bilaterally (Figure 45-B).

Similarly, comparing whole brain voxel wise measures of FA between nbTBI and healthy controls following TBSS demonstrated evidence of widespread WM disruption as indicated by a lower FA (Figure 45-A). Reductions in FA were seen within the genu of the corpus callosum, the left corticospinal tract and corona radiata, and the inferior longitudinal fasciculus bilaterally (Figure 45-B). The patterns of WM abnormalities were the same in both injury groups compared to healthy controls, and there was no significant difference in the whole-brain skeletonised FA between the two injury groups.



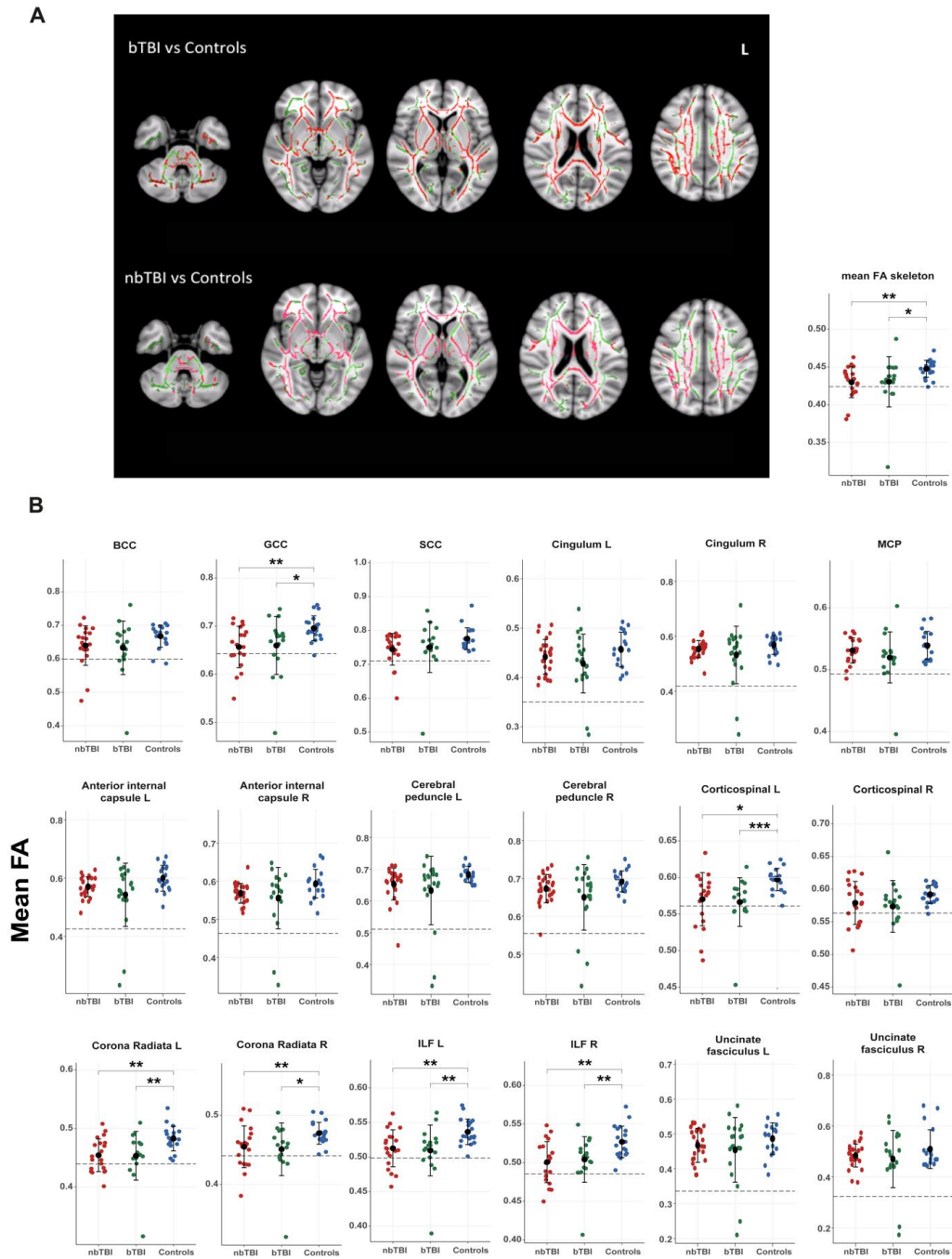


**Figure 45: Results of TBSS analysis and skeletonized ROI comparisons. A) Results of TBSS in different slices of the average group template. Red indicates area of the skeleton with significantly lower FA values at  $p < 0.05$ , and green indicate skeleton with similar mean FA values. B) Jitter plot with mean and standard deviation (black circle and solid line) of mean skeletonized FA in 18 tracts and the whole brain skeleton for each of the three groups: nbTBI**

(red), bTBI (green), controls (blue). The dotted line indicates 2SD below the mean of the control group. Pairwise comparisons p-values are based on post hoc Tukey HSD analysis: ns no significant difference, \* $p < 0.05$ , \*\* $p < 0.01$ , \*\*\* $p < 0.001$ . BCC= body of the corpus callosum, GCC= genu of the corpus callosum, SCC= splenium of the corpus callosum, MCP= middle cerebellar peduncle, ILF= inferior longitudinal fasciculus.

Following TBSS and skeletonization of the WM, an ROI analysis was performed on the tracts. There was no significant group x ROI interaction on Mean FA ( $p = 0.99$ ). To understand which tracts are most affected, a one-way ANOVA was performed on each ROI, followed by a post-hoc Tukey HSD analysis. One-way ANOVA showed a significant difference for mean FA for the following ROIs: the **genu of the corpus callosum** ( $F = 4.37$ ,  $p = 0.02$ ), the **left corticospinal tract** ( $F = 4.27$ ,  $p = 0.02$ ), the **inferior longitudinal fasciculus left** ( $F = 5.00$ ,  $p = 0.01$ ) and **right** ( $F = 5.66$ ,  $p = 0.006$ ), the **corona radiata left** ( $F = 5.25$ ,  $p = 0.008$ ) and **right** ( $F = 3.30$ ,  $p = 0.04$ ) and the **whole brain skeleton** ( $F = 3.50$ ,  $p = 0.04$ ) (Supplementary Table 2).

Following pairwise comparisons between groups, both bTBI and nbTBI showed significant decrease in mean FA compared to healthy controls in the affected tracts (Supplementary Table 2). Comparing both TBI groups, there was no difference in skeletonized mean FA in any of the tracts studied.

#### 4.4.3. WM Abnormalities Following Subject-Specific Diffusion Segmentation

I next investigated whether bTBI produced specific patterns of WM tract damage when measuring FA directly from the parametric map and across the whole tract (i.e., not skeletonized, and not normalized) using subject-specific diffusion segmentation (SSDS). This estimation of FA increases sensitivity and anatomical coverage of the ROI (Figure 46).

In whole tract investigations, there was no significant group x ROI interaction on Mean FA ( $p = 0.88$ ). To understand which tracts are most affected, I performed a one-way ANOVA on each ROI, followed by a post-hoc Tukey HSD analysis. One-way ANOVA showed a significant difference for mean FA for most ROIs except the cerebral peduncles ( $F(2,115) = 1.96$ ,  $p = 0.14$ ) and the uncinate fasciculi ( $F(2,115) = 2.91$ ,  $p = 0.06$ ) (Supplementary Table 2).

However, compared to results obtained in SSDS, some tracts were only significantly affected in the bTBI group, but not the nbTBI compared to controls following the post-hoc pairwise analysis. These tracts included the **body of the corpus callosum** ( $p=0.02$  and  $p=0.23$ ) **splenum of the corpus callosum** ( $p=0.03$  and  $p=0.09$ ), **the anterior limb of the internal capsule left** ( $p=0.03$  and  $p=0.46$ ) **and right** ( $p=0.01$  and  $p=0.20$ ), **the corticospinal left** ( $p=0.01$  and  $p=0.49$ ) **and right** ( $p=0.04$  and  $p=0.91$ ), **the left inferior longitudinal fasciculus** ( $p=0.007$  and  $p=0.3$ ), and **the corona radiata left** ( $p<0.001$  and  $p=0.12$ ) **and right** ( $p<0.001$  and  $p=0.16$ ) (supplementary table 1).

**The middle cerebellar peduncle** was the only tract that showed an abnormal FA measure in the blast group compared to both the nbTBI group ( $p=0.02$ ) and the control group ( $p=0.02$ ). The middle cerebellar peduncle was not affected in nbTBI relative to controls ( $p=0.99$ ) (Figure 46).

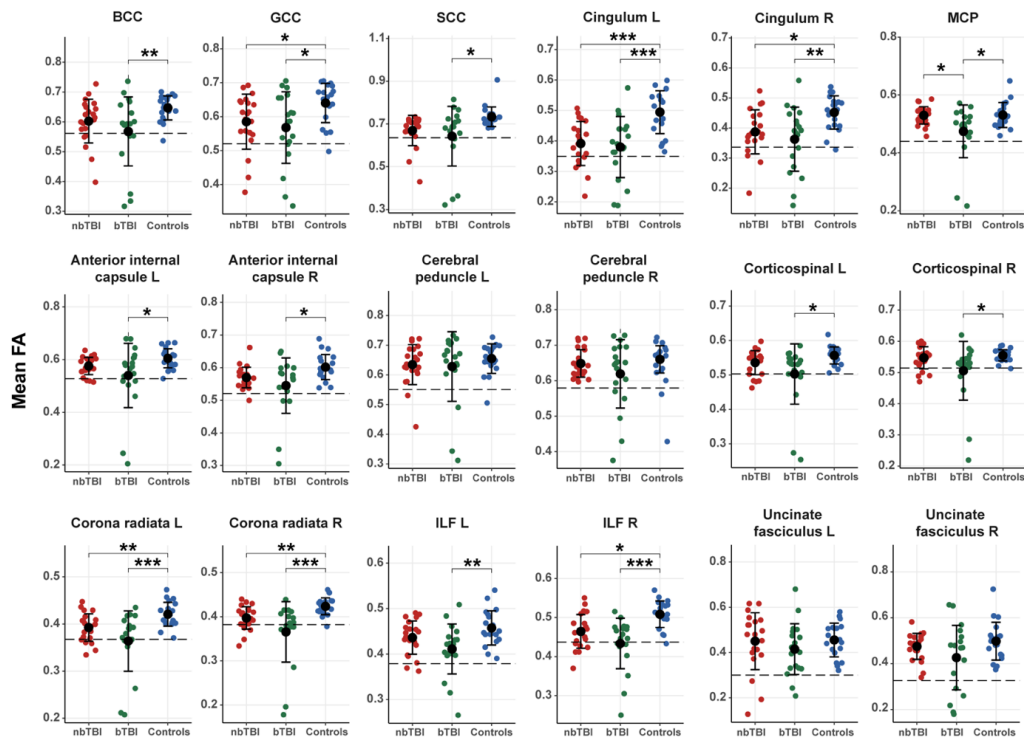


**Figure 46: Results of whole tract SSDS analysis. Jitter plot with mean and standard deviation (black circle and solid line) of mean native FA in 12 tracts for each of the three groups: nbTBI (red), bTBI (green), controls (blue). The dotted line indicates 2SD below the mean of the**

control group. Pairwise comparisons p-values are based on post hoc Tukey HSD analysis: ns no significant difference, \* $p < 0.05$ , \*\* $p < 0.01$ , \*\*\* $p < 0.001$ . BCC= body of the corpus callosum, GCC= genu of the corpus callosum, SCC= splenium of the corpus callosum, MCP= middle cerebellar peduncle, ILF= inferior longitudinal fasciculus.

When I compared patients with and without structural abnormalities (contusions, microbleeds or both) within the bTBI group I found no significant difference in the mean FA for any of the tracts investigated.

#### 4.4.4. WM Abnormalities at the Boundaries of ROIs

In my next analysis, I wanted to understand what was driving the difference I was observing using SSDS in the whole ROI. If my hypotheses were correct, I could see damage at the boundary of the WM, which might be explaining the differences I saw between the bTBI and nbTBI group.

I investigated FA values at the boundary of the WM using the SSDS pipeline. For this analysis, I split ROIs as follows (check *Regions of interest* -page 126- for more information): whole-brain boundary of WM/GM, whole brain boundary of WM/CSF (Figure 47), the WM/GM boundary of the middle cerebellar peduncle, genu, body and splenium of the corpus callosum (Figure 47-A) as well as the WM/CSF boundary of the middle cerebellar peduncle, genu, body and splenium of the corpus callosum (Figure 47-B). The volume of the chosen ROIs were all larger than the volume of the ROIs previously shown to be too small for accurate and reliable measures (see section 3.4.3.).

There was no significant group x ROI interaction on Mean FA ( $p = 0.84$ ). Using a one-way ANOVA, the bTBI group, but not the nbTBI group shows a decrease in global WM/GM and WM/CSF boundaries relative to controls (Supplementary Table 2). In the bTBI group, all three parts of the corpus callosum have a significantly lower FA compared to controls at the WM/GM boundary (Figure 47-A). Measures at the boundary of the WM/CSF shows no decrease in mean FA in any part of the corpus callosum for either injury groups relative to controls. However, the WM/CSF boundary of the middle cerebellar peduncle is affected in the bTBI group compared to both the nbTBI group and the controls ( $p = 0.04$ ,  $p = 0.02$  respectively), but not between the nbTBI group and the controls ( $p = 0.86$ ) (Figure 47-B).

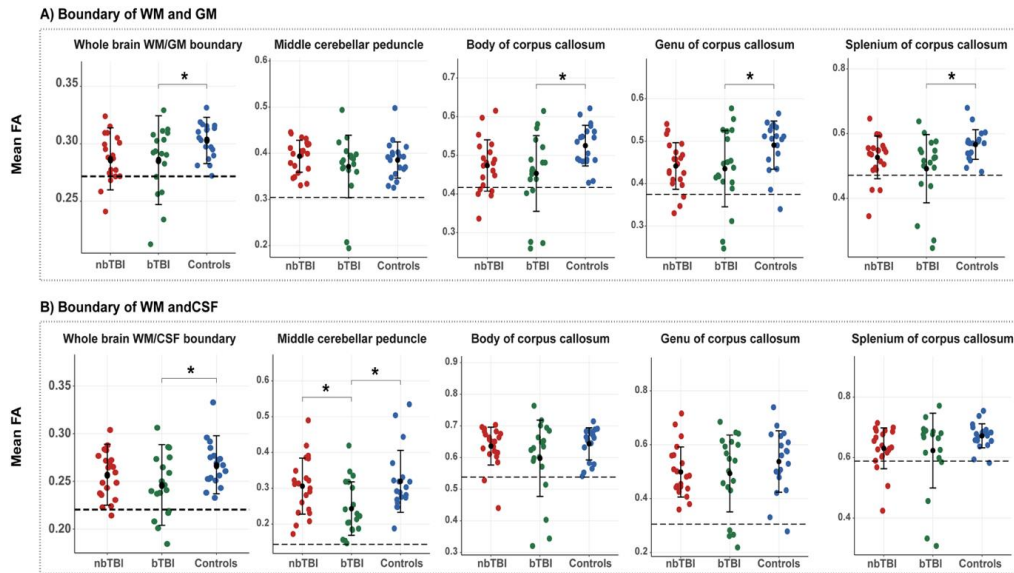


**Figure 47: Results of tract boundary SSDS analysis. Jitter plot with mean and standard deviation (black circle and solid line) of mean native FA at the boundary of the (A) WM/GM and (B) WM/CSF in 4 tracts for each of the three groups: nbTBI (red), bTBI (green), controls (blue). The dotted line indicates 2SD below the mean of the control group. Pairwise comparisons p-values are based on post hoc Tukey HSD analysis: <sup>ns</sup> no significant difference, \* $p < 0.05$ , \*\* $p < 0.01$ , \*\*\* $p < 0.001$ .**

To further validate the results, I obtained from the boundaries of the WM tracts, I manually segmented the boundary of the whole corpus callosum (all three parts), and compared the results obtained from the SSDS boundary segmentation to those from the manual segmentation. There was no difference in the mean FA values of the boundaries of the whole corpus callosum (genu, body, and splenium) between the manual and SSDS methods ( $t = -1.612$ ,  $p = 0.061$ ).

#### 4.4.5. Individual Comparison of Soldiers to the Normal Distribution

To understand the individual abnormalities on the DTI findings of soldiers, I compared the mean FA of ROIs in the bTBI group to the control's normal range following each of the three analyses and based on their Z-score and its significance at  $p < 0.05$ . Each bTBI patient's FA is plotted against the distribution of the control group for each ROI, and abnormal tracts are highlighted in red (Figure 48).

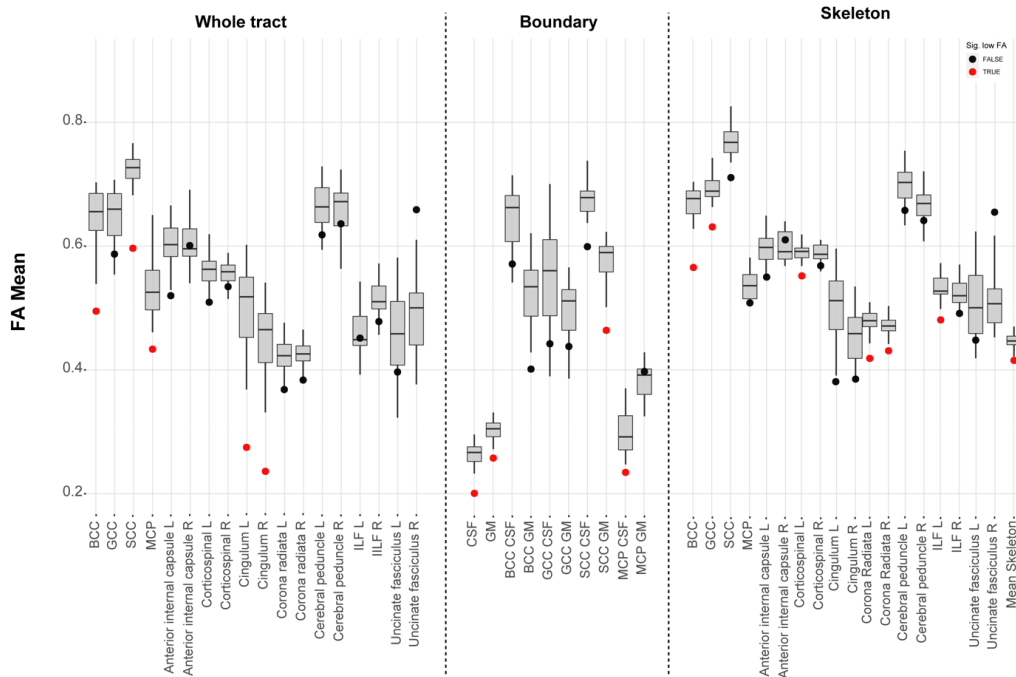


**Figure 48: Example of individual patient diagnostic results across all tracts. The dots represent the individual patient FA. Boxplots represent the distribution and median value of mean FA across the control group. Red dots indicate a significantly abnormal individual FA value ( $p < 0.05$ , 95% confidence interval, FDR corrected). Black dots represent patients mean FA value within normal ranges compared to healthy controls. CSF= cerebral spinal fluid, GM= grey matter, BCC= body of the corpus callosum, GCC= genu of the corpus callosum, SCC= splenium of the corpus callosum, MCP=middle cerebellar peduncle, ILF= inferior longitudinal fasciculus, sig= significant.**

Of the 19 military personnel that make up the bTBI group and that have been individually compared to the healthy control population, a total of 10 (or 52%) have at least one tract abnormality.

Of the 10 patients classified as abnormal, six (or 31.5%) had abnormalities in two or more tracts (Figure 49).

When I performed TBSS, the highest rates of abnormalities were seen in the genu of the corpus callosum (6/19 soldiers), while the highest rate of abnormalities in native FA following SSDS was in the body and genu of the corpus callosum, as well as in the left and right cingulum bundles, and the middle cerebellar peduncle (4/19 soldiers).

The highest rate of abnormalities for FA measures at the boundaries was seen at the WM/CSF boundary of the middle cerebellar peduncle, and the whole brain WM/GM boundary (5/19 soldiers).

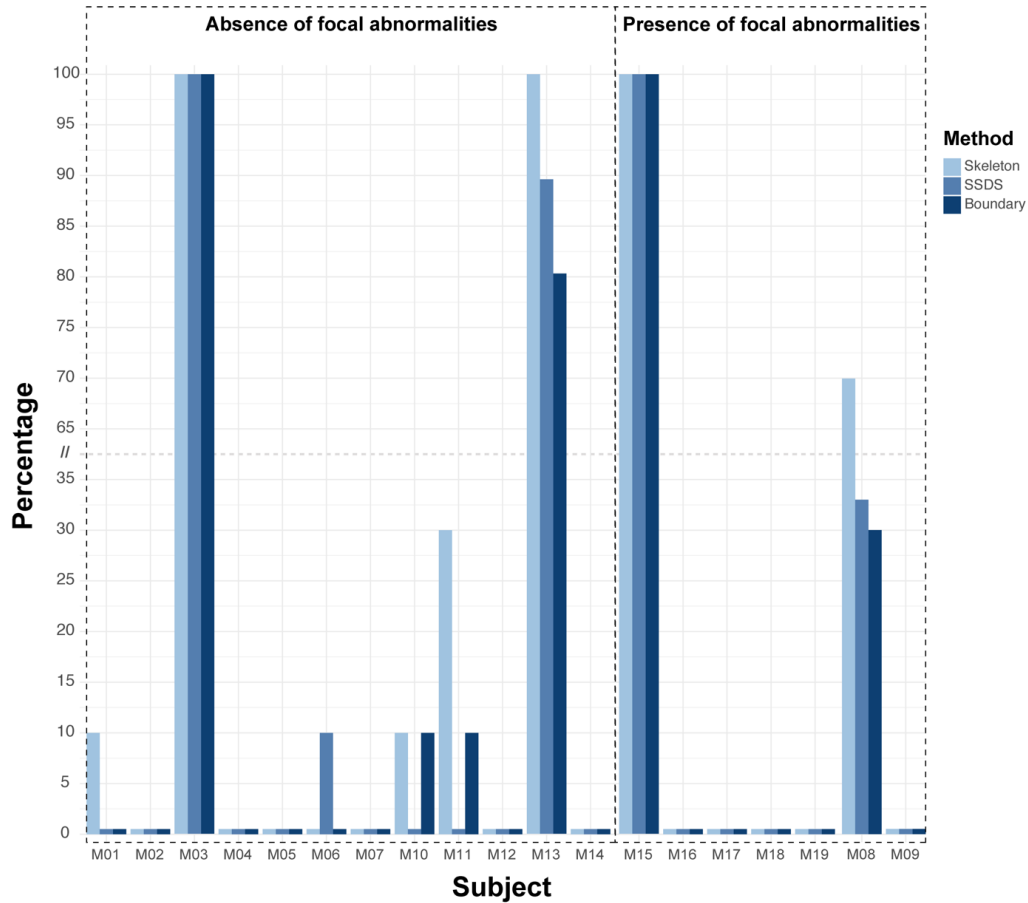


**Figure 49: Results of the individual comparisons of bTBI patients to the control groups.** Percentage of tracts affected in each patient for all three analysis methods (blue): TBSS: 19 tracts, SSDS 18 tracts, FA at the boundary 10 tracts. Each subject is labelled as having neuroradiological abnormalities (microbleeds and/or contusions) (red) or no radiological abnormalities (green).

Of the six soldiers with two or more affected tracts, the ratio of those with neuroradiological abnormalities to those without was 2:1, but there was no difference in mean FA measures when comparing groups with and without microbleeds and/or contusions.

There were no significant differences in mean FA measures when comparing groups of mounted (in a vehicle) vs unmounted (in open field) soldiers.



## 4.5. DISCUSSION

Soldiers who have suffered blast-induced traumatic brain injury (bTBI) often have persistent cognitive problems despite relatively normal standard magnetic resonance imaging (MRI). This was the case in our cohort of soldiers with bTBI, who showed cognitive impairments across processing speed, executive function, memory, and intellectual ability when compared to healthy controls. Despite the lesser extent of abnormalities seen on the routine neuroradiological assessment of soldiers, they seem to have higher abnormalities than civilians with bTBI, more specifically for cognitive domains such as intellectual ability, processing speed, executive function, and information processing.

In the absence of abnormalities on standard structural imaging it is difficult to determine neurological underpinnings of the symptoms, and the difference blast and non-blast TBI might have on the brain. However, the discrepancy seen at the clinical/behavioural level leads us to believe there might be a difference at the neurological level. The presence of diffuse axonal injury (DAI) might be an important contributing factor to the long-term cognitive problems that the soldiers face (McKee and Robinson, 2014). Therefore, understanding how these types of injuries differ or are similar is crucial to the question of bTBI given the wide research progression and understanding of non-blast TBI in the civilian population (Blennow et al., 2016).

My work in this chapter (Chapter 4) focuses specifically on the white matter (WM) microstructure, since my next chapter (Chapter 5) will examine grey matter (GM) changes more closely. The investigation I performed in this chapter provides evidence that microstructural WM injury examined through diffusion neuroimaging is common after moderate/severe bTBI. The bTBI patient group showed lower fractional anisotropy (FA) in large parts of the WM, indicating a widespread pattern of DAI similar to what is commonly seen in civilian TBI (Humble et al., 2018). The extent of WM damage also seems to be heterogeneous. However, this trend wasn't a significant enough to draw conclusions regarding the association between WM damage and neuroradiological focal abnormalities. This might be due to the limited number of soldiers in our group, and more work needs to be carried out.



Although the bTBI group demonstrates WM abnormalities compared to the healthy control group at the standard group-level analysis, in this case using tract-based spatial statistics (TBSS) (Jolly et al., 2020, Smith et al., 2006), there is no difference in skeletonised FA values between the two injury groups following group-level analyses, and the patterns of abnormalities in comparison to the control group were similar.

I previously developed the subject-specific diffusion segmentation (SSDS) pipeline to increase the specificity of diffusion analysis without compromising the accuracy of group-level analyses (CHAPTER 3). SSDS enabled me to look at the whole WM tract (not just the skeletonised tract), as well as the boundary of specific tracts to better compare injury groups.

The SSDS analysis revealed a more pronounced pattern of WM injury compared to healthy controls than what is seen in nbTBI. SSDS also uncovered a significant difference between the two injury groups at the level of the middle cerebellar peduncle (MCP). This was an area that had previously been shown to be impacted in bTBI relative to healthy controls, while a hypothesis of being specific to bTBI had been raised (Mac Donald et al., 2011).

My study also managed to locate differential damage in the blast group but not in the civilians with TBI, mainly concentrated at the boundary between the WM and the corticospinal fluid (CSF) in the whole brain and at the level of the MCP, as well as damage common to both injury groups (civilian and military) at the boundary between the WM and the grey matter (GM). The hypothesis according to which bTBI causes damage at the boundary of the WM had previously been demonstrated in a post-mortem investigation of military case studies (Shively et al., 2016), as well as in a porcine model of bTBI, which was part of an experiment conducted at C3NL and has yet to be published.

The porcine model of bTBI showed that all animals exposed to blast had ependymal stripping, with sub-ependymal microglial activation, which was not observed in the sham or control groups (Figure 49), and which was unrelated to other experimental factors.

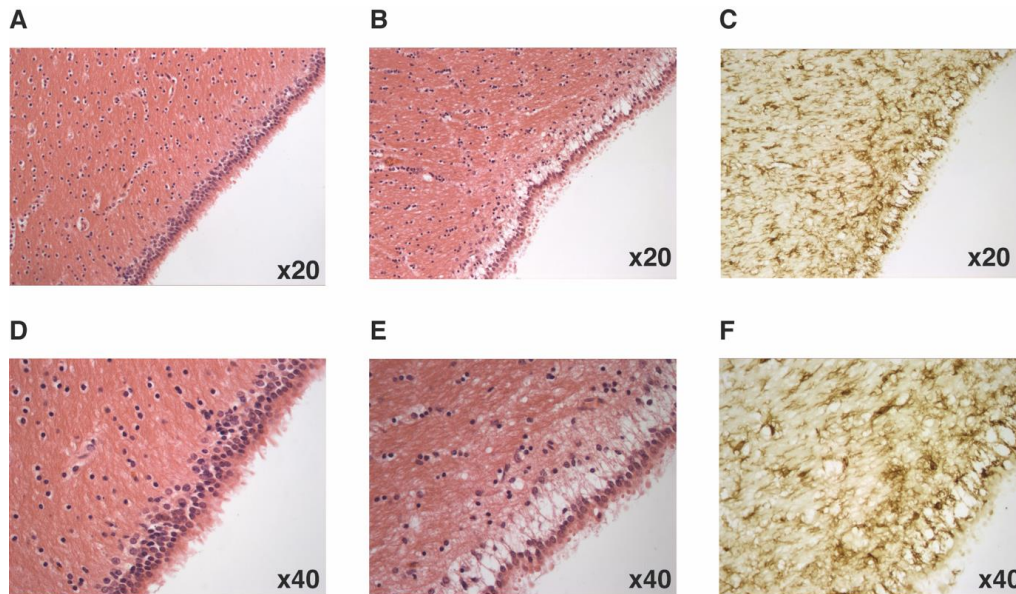


**Figure 50: Ependymal stripping in porcine model of bTBI. Staining on controls (A&D). B) and E) show abnormal staining of the ventricular ependyma in the bTBI group. C) and F) evidence of sub-ependymal activation of microglia using Iba-1 staining in the bTBI group. Taken from**  
[https://discovery.ucl.ac.uk/id/eprint/1546198/1/Baxter\\_David\\_e-thesisPhD.pdf](https://discovery.ucl.ac.uk/id/eprint/1546198/1/Baxter_David_e-thesisPhD.pdf)

Other high fidelity models of the human brain explain the biomechanical susceptibility of the tissue surrounding the CSF as a possible location for blast-related TBI through cavitation-induced strain (Yu et al., 2020). This study, which exposed a finite element head model to a frontal blast wave demonstrates that CSF tensile failure can significantly elevate strain and strain especially in the tissue adjacent to the CSF. Although these effects were mostly observed at the cortical level, it might be a possible mechanistic hypothesis for the damage we see at the interface of the WM and the CSF.

One limitation of human studies is the inability to isolate the possibility or extent of primary blast injuries, especially in cases of self-reported blast exposure and outcome during deployment. By including soldiers who have suffered moderate to severe injury because of a single exposure to an explosion, my study limits the impact of this problem. Information such as estimates obtained on the size of improvised explosive device used, the victims' proximity to the blast source, as well as medical reports demonstrate a significant blast exposure in each case. However, the soldiers still sustained heterogenous injuries caused by several different mechanisms (Mathews

and Koyfman, 2015), which means TBI was not exclusively related to blast waves, making it difficult to attribute a specific neurological outcome to primary blast injuries. However, by including a similarly injured civilian control group as well as uninjured controls, I curb this limitation and my investigation narrows down the patterns of neurological changes arising from bTBI specifically, although more controlled investigations are still needed. Leveraging two age and gender-matched control groups (with and without injury), I have shown that whilst there are many WM regions commonly injured in both blast and non-blast injury there are differences between the two groups which seem to relate to cognitive changes commonly seen in soldiers post-deployment. I also use a pipeline that can be useful for future studies to standardize the analyses for test-retest purposes.

To conclude, I found widespread WM damage in soldiers exposed to blast when compared to uninjured controls. Compared to civilians with TBI, soldiers who sustain bTBI have similar patterns of injury and overlapping areas of cognitive deficits except for the damage seen at the WM/CSF boundary, that seems to be exclusive bTBI when relying on a new pipeline that increases the specificity of the measurements in whole tracts and at the boundary of the tracts of interest. In the context of similar findings by computational models and human studies this may indicate that these areas are more vulnerable to blast injury. In future studies, it would be important to know whether changes in intellectual ability, processing speed and executive functions found in soldiers but not in injured civilians relate to WM damage, or if WM damage can be predicted based on clinical findings.

### ***In the next chapter***

In chapter 5, I investigate the limbic system, with emphasis on the hippocampus and amygdala, as well as two WM tracts: the cingulum bundle – results from the SSDS pipeline previously shown - and the fornix. For volume analysis, I use voxel-based morphometry as well as ROI-specific volumetry. I also investigate the relationship between neuroimaging findings and clinical/behavioural manifestations of bTBI.

# CHAPTER 5

---

## Morphometry, Volumetry, Diffusivity, and the Limbic System in bTBI

*In this chapter I investigate both grey and white matter abnormalities in the limbic system, mainly cortical, hippocampal and amygdala volumetry, as well as diffusivity in the fornix and the cingulum and the relationship between the different structures in blast-related TBI. I apply my analysis in three different groups: a healthy control group, a group of civilians with non-blast traumatic brain injury, and a group of soldiers with blast-induced traumatic brain injury. The purpose of this chapter is to show if an abnormality specific to blast-induced traumatic brain injury at the level of the hippocampus, the amygdala, the cingulum bundle and the fornix (i.e., the limbic system) can emerge, and if there is an association between neuroimaging findings and clinical/behavioural characteristics.*

## 5.1. ABSTRACT

As mentioned previously, blast-induced traumatic brain injury (bTBI), its proper diagnosis, its prevention, treatment, and long-term consequences are a major health concern among veterans. Despite all the work enhancing the knowledge about bTBI, we still know very little about the contribution of primary blast injuries alone to the observed sequelae. The literature also tends to focus mostly on post-traumatic stress disorder (PTSD), and associates the loss of hippocampal volumes, a hypothesized biomarker of bTBI, to PTSD outcomes, with no definite conclusion regarding the causality of the association. In this chapter, I focus on soldiers with a history of bTBI and no diagnosis of PTSD to understand if hippocampal atrophy is present following bTBI and in the absence of PTSD symptoms. I also compare the findings to healthy controls and to age and gender-matched civilians with non-blast TBI (nbTBI) to better control for the effect of primary blast injuries specifically. I also examine other parts of the limbic system, such as the fornix, amygdala, and cingulum.

Although the white matter of the fornix and cingulum shows a similar abnormality in both injury groups, hippocampal atrophy is only seen in soldiers with bTBI. However, there is a correlation between abnormalities of the fornix and the hippocampus, and hippocampal atrophy can be explained by TBI-derived variables such as the time since injury, the presence of focal abnormalities such as contusions and microbleeds, as well as abnormalities in the fornix. This study is the first to show the loss of hippocampal volume in the absence of PTSD as well as hippocampal atrophy being specific to bTBI. I also present potential hypotheses surrounding the cause/consequence of this biomarker of bTBI.

## 5.2. INTRODUCTION

Hundreds of thousands of soldiers are estimated to have suffered a brain injury from explosions ((DoD), 2020), and signs of TBI neuropathology were found in post-mortem brains of veterans who had been exposed to blast (Goldstein et al., 2012). Many returning veterans show no detectable neuropathology or physical injury, but suffer from persistent clinical sequelae such as headaches, insomnia and sleep disturbance, depression, blurred vision, and memory problems (see 1.7.4) (Tompkins et al., 2013), leading to a potential post-traumatic stress disorder (PTSD) diagnosis, which is found in 23% of veterans (Fulton et al., 2015).

Based on these clinical presentations, MRI studies of soldiers with cognitive/behavioural abnormalities have mostly focused on PTSD. These often report changes in the macrostructure of the limbic systems (Meng et al., 2014, Bremner, 2007, O'Doherty et al., 2015, Chao et al., 2013), which are brain regions thought to contribute to PTSD given their relevance in affective and cognitive processes. A relationship between the extent of PTSD severity and the magnitude of brain alterations at the level of the limbic system have also been reported (O'Doherty et al., 2017, Meng et al., 2016, Lindemer et al., 2013, Bing et al., 2013). For example, greater symptom severity correlated with reduction in hippocampal volumes (Nelson and Tumpap, 2017).

However, given the intense focus on the presence of a PTSD diagnosis, the question remains, how does the clinical/neuroimaging findings mentioned above relate to bTBI? It has been established that exposure to TBI in the context of deployment may impact PTSD severity. It is often a comorbidity and risk factor for PTSD (Yurgil et al., 2014, Lippa et al., 2015), and can aggravate its symptomatology (Spielberg et al., 2015, Lindemer et al., 2013, Vanderploeg et al., 2009). If we consider that around 12–35% of service members deployed to Iraq and Afghanistan have sustained a bTBI (Lindquist et al., 2017, Spielberg et al., 2015), and that head and neck trauma are now one of the most prevalent causes for disability in returning veterans (Schoenfeld et al., 2013), it is critical to consider the exposure and history of bTBI when trying to assess the neurological changes that might be contributing and exacerbating PTSD-like symptomatology, even in the absence of such a diagnosis to better understand the

long-term risk and outcomes of bTBI. Previous research has well established that individuals with TBI have widespread structural, microstructural, and functional brain alterations (Van Boven et al., 2009, Shenton et al., 2012, Ross, 2011, McDonald et al., 2012). Subcortical regions including bilateral hippocampus, amygdala, pallidum and thalamus show changes volume in individuals with TBI (Maller et al., 2014, Bigler et al., 2010, Anderson et al., 1996). The hippocampus plays a crucial role in learning, memory, fear conditioning and spatial navigation. In bTBI specifically, studies of animal models showed neuroinflammation in cerebral cortex, striatum and hippocampus following mild blast forces (Hernandez et al., 2018), as well as electrophysiological changes in the CA1 region of the hippocampus, and hippocampus-dependent behaviours (Beamer et al., 2016, Ratliff et al., 2020). Clinical research involving post-deployed veterans also showed that alterations in the CA1 region and subiculum subregions of the hippocampus may have a role in depression and PTSD (Bae et al., 2020, Kitayama et al., 2005). In investigations of hippocampal volume in relation to the absence of PTSD diagnosis, deployed veterans with PTSD as well as deployed veterans without PTSD, and non-deployed reservists all had significantly smaller whole hippocampal volumes when compared to a control group of healthy civilians (Vythilingam et al., 2005).

I want to understand if a diagnosis of bTBI leads to macrostructural abnormalities at the level of the limbic structure, like those seen in patients with PTSD diagnosis, but in the absence of PTSD. Although the epidemiology of bTBI is becoming clearer (Bryden et al., 2019), there is still significant debate over the difference between blast and non-blast TBI, with reviews of the existing literature showing conflicting reports. The unique nature of deployment presents obstacles to accurately reporting, assessing, and documenting injuries (Schwab et al., 2007), and the recruitment criteria when assessing macrostructural changes at the level of the limbic system include a diagnosis of PTSD but not necessarily a history of bTBI. It is therefore undetermined whether decreased volume at the level of the hippocampus, and abnormalities in other structures of the limbic system such as the fornix and the cingulum are a consequence of exposure to primary blast injury, given that studies do not control for the presence of other TBI mechanisms (Childress et al., 2013). Detecting differential injuries between blast and non-blast TBI may contribute to the development of protective equipment as well as objective methods to enhance the predictive accuracy of long-

term diagnoses and treatments, reducing costs, suffering and dependency on inaccurate self-reports. Moreover, it can pave the way to determining the neurological underpinnings of PTSD and the risk factors during deployment.

My study in this chapter investigates whether PTSD-free soldiers with a history of blast-induced TBI show differential patterns of volume loss compared to civilians with non-blast TBI in whole brain average, in cortical and WM volume, as well as variations of volume of the hippocampus in the absence of a diagnosis of PTSD. The study also explores how changes at the level of the hippocampus correlate with WM microstructural abnormalities in the fornix and the cingulum. Finally, I try to understand if the clinical and cognitive variables predict the patterns of volume change, to improve the understanding of the effect of blast and bTBI on neurological abnormalities specific to soldiers.

#### ***Hypotheses of chapter 5***

- The blast TBI group, but not the civilian TBI group, shows a decrease in hippocampal volume that correlates with abnormalities in the fornix.
- Loss of hippocampal volume does not correlate with measures of stress, or cognitive performance, but can be predicted based on the clinical characteristics of the soldiers.



## 5.3. METHODS

### 5.3.1. Participants

This study consisted of three groups:

- > 19 military bTBI patients were recruited using the Academic Department of Military Emergency Medicine (Birmingham, UK) trauma database to identify soldiers injured between December 2009 and March 2012.
- > The first control group consisted of 20 age- and gender-matched control group of civilians with non-blast TBI. This represented all the patients seen in our multidisciplinary Traumatic Brain Injury clinic at Charing Cross Hospital, London, United Kingdom between August 2009 and March 2012.
- > The second control group consisted of an age- and gender-matched group with 31 healthy controls civilians.

bTBI and nbTBI groups were matched for injury severity and time since injury (for soldiers mean  $\pm$  SD  $14.6 \pm 5.9$  months, for civilians  $12 \pm 12.7$ ).

All cases of TBI in both injury groups were categorized as moderate or severe based on the Mayo Classification System for Traumatic Brain Injury Severity (Malec et al., 2007). The classification relates to the length of post-traumatic amnesia, the duration of loss of consciousness, and lowest recorded GCS in the first day, and/or CT or MRI result. Exclusion criteria for both our TBI groups were the following: history of psychiatric or neurological illness (including PTSD), penetrating brain injury, anti-epileptic medication, neurosurgery (except intracranial pressure monitoring); current or previous substance abuse; any contraindications to MRI. All participants gave written informed consent according to the Declaration of Helsinki. The study was approved by the Hammersmith, Queen Charlotte's and Chelsea Research Ethics Committee.

Inclusion criteria for both bTBI and nbTBI were: 1) gender male, 2) between 2 and 48 months from a single TBI, 3) moderate/severe brain injury on Mayo classification criteria, 4) ongoing clinical or cognitive and/or psychological symptoms, and 5) completion of endocrine testing. Exclusion criteria for both bTBI and nbTBI participants

were: 1) diagnosis of diabetes mellitus, 2) history of psychiatric disorder (including PTSD), 3) previous or actual substance abuse, 4) craniotomy, neurosurgery or penetrating injury, 5) anti-epileptic medication, 6) any contraindications to MRI. Participants in both injury groups underwent clinical assessment for Abbreviated Injury Score (AIS) and total Injury Severity Score (ISS).

### 5.3.2. Imaging Acquisition

Each patient had standard high-resolution T1 and gradient-echo (T2\*) imaging. MRI was performed on Philips 3T Achieva scanner (Philips Medical Systems, The Netherlands) using a body coil. For DWI, diffusion-weighted volumes with gradients were applied in 16 non-collinear directions in each of the four DTI runs, resulting in a total of 64 directions. The following parameters were used: 73 contiguous slices, slice thickness = 2mm, field of view 224 mm, matrix 128 X 128 (voxel size = 1.75 X 1.75 X 2 mm<sup>3</sup>), b value = 1000 and four images with no diffusion weighting ( $b=0\text{s/mm}^2$ ).

### 5.3.3. Imaging Analysis

#### *Volumetry: segmentation of the hippocampus and amygdala*

I skull-stripped the T1 images using FSL-BET (Smith, 2002), and used FSL-FIRST (Patenaude, 2011) to segment the hippocampus and amygdala bilaterally for each subject. I then carried out thorough visual inspection of the initial registration step and the final segmentation to ensure all the structures of the hippocampus have been successfully segmented (Duvernoy, 1998) (Figure 51).

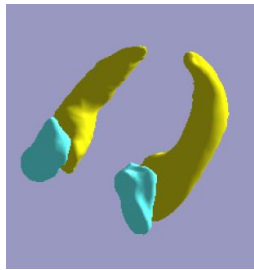


**Figure 51: Example of the segmentation of the hippocampus (yellow) and amygdala (blue) bilaterally.**

I also skull-stripped the T1 images and segmented them into the three different tissue types using FSL-FAST (Zhang, 2001) and visually inspected the segmentation. To obtain total grey matter (GM) volume, I multiplied the partial volume estimate of the

whole GM map and the total volume of the image (in mm<sup>3</sup>). I used the same method to obtain total white matter (WM) volume. By adding the total GM and total WM volumes, I estimated the total brain volume. The hippocampal volumes obtained through FSL-FIRST were normalized to the brain volume (Free et al., 1995) and the age, to obtain the total corrected volume (TCV).

***Diffusivity: Manual segmentation of the fornix, automated segmentation of the cingulum and FA estimation***

For manual segmentation of the fornix and the fornix crura, each ROI consisted of multiple brain slices fully covering three-dimensional anatomical structures of the whole fornix and the fornix crura bilaterally as defined in accordance with anatomical definitions provided in the fornix FMRIB 1mm template (Brown et al., 2017).

Fractional anisotropy (FA) was extracted from ROIs following pre-processing of diffusion data and estimation of the diffusion tensor using FSL's FDT software.

For the cingulum left and right, I used the results obtained in chapter 4, where I had already estimated the mean FA at the level of the cingulum (see section 3.3.3 for methods, and section 4.4.3 for results)

***Voxel-based morphometry (VBM) and vertex-based analysis (VBA)***

I performed the VBM analysis according to SPM12 guidelines (<https://www.fil.ion.ucl.ac.uk/~john/misc/VBMclass10.pdf>) - (see section 2.5.2 for more details regarding methodology of VBM).

I performed vertex-wise statistics to analyse localized 3D meshes and observe significant shape differences that occurred in the hippocampus of the military group compared to the healthy controls. For the vertex analysis I used *first\_utils* from the FSL-FIRST package (Patenaude, 2011), with age and group as regressors in the randomization of the t-test statistics. I overlaid the results of the vertex analysis on their respective group mean to further pinpoint the area where shape abnormality occurred.

#### **5.3.4. Statistics**

I analyse all data using R studio v3.3.3 ([www.R-project.org](http://www.R-project.org)). I used one-way ANOVA to assess the difference in group means among the three groups, followed by Tukey's

HSD post hoc test to assess the significance of differences between pairs of group means. Because the Tukey HSD post-hoc test was too conservative, I repeated and reported results using the Fisher LSD post-hoc analysis. However, unlike the Tukey HSD, the Fisher LSD does not have full control over type I error. I estimate significance at  $p\text{-value} < 0.05$ . I used Pearson's correlation to measure the dependence between hippocampal TCV and mean FA measures extracted from ROIs. I performed independent sample t-test pairwise comparison of the mean.

I utilized multiple linear regression to predict the hippocampal TCV based on clinical variables including: Age at injury, time between injury and scan, abbreviated injury scale (AIS) score, cortisol levels (nmol/L), presence/absence of microbleeds contusions, mean FA values from the fornix and the cingulum and pituitary dysfunction. I based the multiple linear regression on the following assumptions: a linear relationship between dependent and independent variables, no high correlations between independent variable, the random selection of observations and the residuals distributed with a mean of 0 and variance  $\sigma$ . To find the best predictors of our model, I performed a stepwise selection in both directions. The stepwise selection determines the contribution of each predictor previously entered in the regression equation to estimate the contribution of the one preceding it, to retain or ignore variables based on their statistical contribution. Based on the results of the stepwise selection, I estimate a new multiple regression model with the clinical variables that best explain the hippocampal TCV. I used Bonferroni correction for multiple comparison errors.

## 5.4. RESULTS

### 5.4.1. Demographics

The soldiers previously described (Baxter et al., 2013) (Table 13), were injured by IEDs while wearing full personal protective equipment. All required immediate transfer to Camp Bastion for emergency medical treatment, and repatriation to the United Kingdom within 48 hours. Although exposed to blast, TBI could have been the result of other mechanisms of injuries.

Civilians with a diagnosis of TBI were recruited for the non-blast TBI (nbTBI) group. In this group, injury was caused by assaults (34%), road traffic accidents (19%), falls (42%) and sports related injuries (5%). Civilians were referred to their local traumatic brain injury service because of the presence of functional impairments following their TBI.

**Table 13: Demographics of the three cohorts included in this study. Results for age, time between injury and scan are in mean  $\pm$  SD. PTA= post traumatic amnesia.**

	Controls	nbTBI	bTBI
<b>n</b>	31	20	19
<b>Gender (% males)</b>	100%	100%	100%
<b>Age at scan (years)</b>	30.6 $\pm$ 6.7	28.7 $\pm$ 6.3	29.8 $\pm$ 5.9
<b>Time between injury and scan (months)</b>	NA	12 $\pm$ 12.7	14.6 $\pm$ 5.9
<b>PTA (&gt;24 hours)</b>	NA	35 %	68 %
<b>Amputation</b>	NA	0 %	42 %

Within the bTBI group (Table 14), clinical neuroradiological reports showed that of the 19 soldiers, 11 had evidence of contusions and 8 had evidence of microbleeds on their gradient echo imaging. Details on the diagnosis of pituitary dysfunction, hypogonadism, limb amputation, PTS over 24 hours, and major organ damage, as well as medications such as antidepressants and opiates have been previously reported (Baxter et al., 2013)<sup>8</sup>. I used all measures with a prevalence of >20%, and with relevance to the hypothesis being investigated (i.e. trauma severity, pituitary

<sup>8</sup> Details of the medications can be found in A.5. Appendix of Chapter 5.

abnormality, stress levels) to test if clinical characteristics related to soldiers would have an impact on the neuroimaging analysis.

**Table 14: Clinical details of the bTBI group. PTA= post traumatic amnesia. Basal cortisol level was the serum concentration level.**

Characteristic	Presence (n)	Absence (n)
Microbleed	11	8
Contusion	8	11
Pituitary dysfunction	6	13
Hypogonadism	4	15
Antidepressants	9	10
Opiate	9	10
Limb amputation	8	11
PTA > 24hours	13	6
Major organ damage	11	8
Measure	Mean	SD
Basal cortisol (nmol/L)	310.26	123.23

## 5.4.2. Neuroimaging Findings

### *Results of ROI analysis*

For each participant, I estimated adjusted whole brain volume, white matter (WM) volume, grey matter (GM) volume and hippocampal volume, along with mean FA values of manually segmented whole fornix and the fornix crescent, and SSDS segmentation of the cingulum left and right<sup>9</sup> (Table 15). There was no significant difference in group means for the measures of the brain volume ( $p=0.77$ ), WM ( $p=0.41$ ) and GM ( $p=0.52$ ).

**Table 15: Measures of different ROIs investigated. Volumes are in  $\text{cm}^3$  and FA is the mean across the whole manually segmented tract. Results are presented as mean  $\pm$  SD. Hippocampal volume was corrected for total brain volume. Significance levels for one way ANOVA followed by post-hoc Fisher LSD are presented. Ns= not significant,  $.p<0.1$ ,  $*p<0.05$ ,  $**p<0.001$ .**

				One-way ANOVA	Post-hoc Fisher's LSD		
				F value p value	nbTBI vs Controls	bTBI vs Controls	bTBI vs nbTBI
	Controls	nbTBI	bTBI				

<sup>9</sup> Results of cingulum mean FA in this chapter were taken from chapter 4. See section 4.4.3 for mean FA ROI results following implementation of SSDS.

ROI volume (cm <sup>3</sup> )							
Brain Volume	1353.1 ± 106.5	1328.8 ± 121.9	1336.3 ± 104.4	0.26 0.77	ns	ns	ns
White Matter Volume	658.1 ± 61.9	641.2 ± 52.9	663.8 ± 47.0	0.94 0.39	ns	ns	ns
Grey Matter Volume	695 ± 49.3	687.5 ± 77.7	672.6 ± 67.1	0.60 0.55	ns	ns	ns
Total Corrected Hippocampal Volume	8.19 ± 0.76	8.16 ± 0.59	7.69 ± 0.64	2.54 0.04 *	ns	*	*
White matter tracts (mean FA)							
Fornix Mean FA	0.49 ± 0.03	0.44 ± 0.04	0.42 ± 0.09	5.29 0.007 **	*	**	ns
Fornix Crura Mean FA	0.57 ± 0.04	0.54 ± 0.06	0.51 ± 0.11	2.30 0.052 .	*	*	ns
Cingulum L	0.49 ± 0.07	0.39 ± 0.07	0.38 ± 0.10	10.85 <0.001 ***	***	***	ns
Cingulum R	0.45 ± 0.06	0.39 ± 0.07	0.46 ± 0.11	5.82 0.005 **	*	**	ns

When I compared group means using one-way ANOVA, I found a significant effect of group on hippocampal TCV at the [ $F(2, 58) = 3.38$ ,  $p = 0.04$ ], with post-hoc Fisher's LSD test indicating significant difference between the means of bTBI vs nbTBI ( $p=0.03$ ), and bTBI vs controls ( $p=0.02$ ).

When I compared group means using one-way ANOVA, I found a significant effect of group on the mean FA of the fornix at the [ $F(2, 58) = 5.29$ ,  $p = 0.008$ ], with post-hoc Fisher's LSD test indicating significant difference between the means of bTBI vs controls ( $p=0.002$ ), and nbTBI vs controls ( $p=0.03$ ).

When I compared group means using one-way ANOVA, I found a significant effect of group on the mean FA of the left cingulum [ $F(2, 56) = 10.85$ ,  $p<0.001$ ] and the right cingulum [ $F(2, 56) = 5.82$ ,  $p = 0.005$ ], with post-hoc Fisher's LSD test indicating significant difference between the means of bTBI vs controls ( $p<0.001$  and  $p=0.004$ ), and nbTBI vs controls ( $p<0.001$  and  $p=0.04$ ) on both the left and right side respectively.

I found a similar pattern when I compared measures of FA in the manual segmentation of the Fornix (body + crura bilaterally), and the crura bilaterally (Figure 52), there was a significant difference in the mean FA of the whole fornix in both bTBI and non-blast TBI groups compared to controls ( $p=0.004$  and  $p= 0.001$  respectively), with a trend towards atrophy in a subdivision of the fornix (crura bilaterally). I observed the same

results at the level of crura of the fornix bilaterally with both bTBI and nbTBI showing lower FA compared to controls ( $p=0.02$  and  $p=0.02$  respectively).

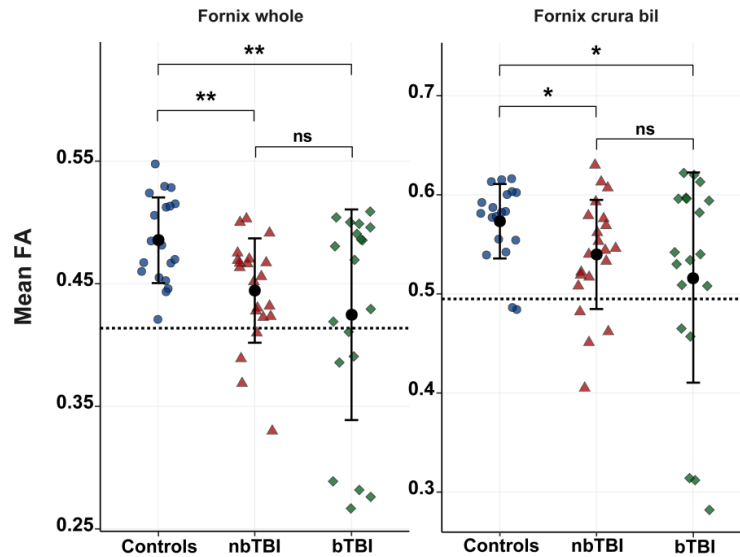


Figure 52: Distribution of mean FA values for fornix investigated in the three groups. nbTBI (red), bTBI (green) and controls (blue). Black distribution line represents the standard deviation, mean of each group is represented by the black circle. Significance levels represent results of unpaired t-test. Ns= non-significant, \* $p<0.05$ , \*\* $p<0.01$ .

### ***Results of voxel-based morphometry and vertex-based morphometry (VBA)***

VBM analysis applied to the standardized T1 images to quantify differences in GM across groups did not reveal any difference across all structures in pairwise comparisons: bTBI vs controls, nbTBI vs controls, and bTBI vs nbTBI (tfce corrected,  $p>0.05$  in all three analyses). No regions of increased or decreased volumes were observed in the injury groups relative to controls.

Vertex analysis shows probabilistically significant ( $p\text{-value}<0.05$ ) surface deformations of the hippocampus while using age and total brain volume as covariates. The analysis revealed reductions in volume of the following hippocampal structures in the military bTBI group compared to the healthy control population: anterior and posterior regions of the CA1 (Figure 53).



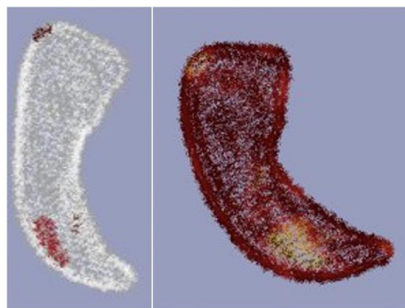


**Figure 53: Results of vertex-based analysis on the hippocampus comparing bTBI and controls. Areas in red on the left, and yellow on the right represent a decrease in volume in bTBI relative to the controls group.**

#### **5.4.3. Relationship Between GM and WM abnormalities**

To understand the relationship between hippocampal volume and measures of WM tracts of interests (fornix and bilateral cingulum), I applied Pearson's correlation. This analysis revealed a significant positive correlation in the bTBI group ( $R^2=0.40$ ,  $p=0.005$ ) between hippocampal size and mean FA measures of the whole fornix, but not in the nbTBI and the control groups ( $p>0.05$ ) (Figure 2). For the bTBI group, the positive correlation was also significant, between hippocampal TCV and mean FA of the crura bilaterally ( $R^2=0.25$ ,  $p=0.035$ ). This relationship was not observed in controls and nbTBI groups ( $p>0.05$ ) (Figure 54).

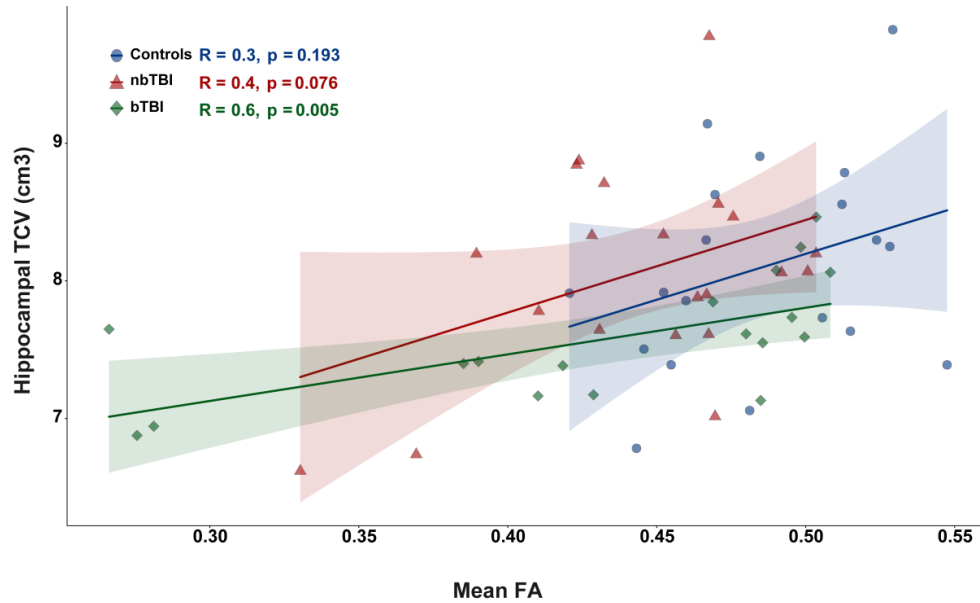


**Figure 54: Pearson's correlation hippocampal TCV with mean FA of the whole fornix. The three groups are controls (blue), nbTBI (red), bTBI (red), with results of Pearson's correlation and 95% confidence interval for each group.**

The correlation was not significant between hippocampal TCV and cingulum mean FA bilaterally ( $R^2=0.037$ ,  $p=0.43$ ). I also found this lack of significance when running a correlation between hippocampal TCV and cingulum mean FA bilaterally in both the nbTBI and control groups ( $p>0.05$ ).

#### 5.4.4. Relationship Between Neuroimaging Findings and Clinical Characteristics

Comparisons within the bTBI group revealed no significant difference in hippocampal TCV, cingulum mean FA, and fornix mean FA between soldiers with and without different clinical characteristics including: microbleeds, contusions, pituitary dysfunction, hypogonadism, limb amputation, as well as between soldiers using antidepressant or not, and opiate or not (Supplementary Table 3).

There was also no significant correlation between levels of cortisol (nmol/L) and hippocampal TCV ( $R^2=0.08$ ,  $p=0.76$ ).

There was no significant correlation between hippocampal TCV and injury severity based on AIS-head measures ( $R^2=0.10$ ,  $p=0.19$ ).

I used measures of associative memory measured by the People Test for immediate recall. Soldiers show a decrease in performance compared to healthy controls ( $24.2 \pm 7.0$ ,  $29.1 \pm 5.3$  respectively,  $p=0.032$ ). I found no correlation between measures of hippocampal TCV and performance on the associative memory test.

Mean FA for the whole fornix shows a significant correlation with immediate recall ( $R^2=0.30$ ,  $p=0.02$ ). Mean FA of the cingulum bilaterally also shows a significant association with immediate recall ( $R^2=0.37$ ,  $p=0.01$ ).

#### **5.4.5. Prediction Model of Hippocampal TCV**

Finally, I calculated a multiple linear regression to predict the hippocampal TCV based on the following measures: Age at injury, time between injury and scan, abbreviated injury scale (AIS) score, presence/absence of microbleeds and contusions, mean FA of the fornix and fornix crura bilaterally, the cingulum bilaterally, as well as the presence/absence of pituitary dysfunction. To optimize the model, we proceeded to run a stepwise selection in both directions to select a subset of best predictor variables and simplify the model. A significant regression equation was found ( $R^2 = 0.79$ ,  $F(5,12)=9.29$ ,  $p<0.001$ ), with five predictors explaining 71% of the variation in hippocampal TCV. There was a significant relationship between presence of microbleeds and hippocampal TCV ( $p = 0.006$ ), presence of contusions and hippocampal TCV ( $p = 0.003$ ), AIS score and hippocampal TCV ( $p=0.02$ ), and mean FA of the whole fornix and hippocampal TCV ( $p=0.007$ )

***Hippocampal TCV = 6.84 - 0.02 (Time since TBI) -0.53 (Presence of Microbleeds) + 0.62 (Presence of Contusions) – 0.10 (AIS- score) + 2.64 (Fornix Mean FA).***

## 5.5. DISCUSSION

Soldiers with a diagnosis of post-traumatic stress disorder (PTSD) often have macrostructural abnormalities at the level of the limbic/paralimbic system (Sydnor et al., 2020). This includes reduced hippocampal volume (Nelson and Tumpap, 2017, O'Doherty et al., 2017, Wrocklage et al., 2017, Bing et al., 2013), reduced thickness of the cingulate cortex, and association between the neurological abnormalities and neurocognitive deficits related to PTSD (Twamley et al., 2009, Cohen et al., 2013). It is unclear if and how exposure to blast-related traumatic brain injury (bTBI), relate to these findings. If primary bTBI (i.e. the blast wave/wind) causes neurological abnormalities to the brain's limbic system, even in the absence of a PTSD diagnosis, then there could be a rapport of causality between bTBI and PTSD-like symptomatology. Understanding this relationship can help with easier diagnosis, efficient treatment, and prognosis, but most importantly more effective protection.

In this study I wanted to answer two main questions, which remained to be tackled in the literature:

Does the absence of PTSD diagnosis, but the presence of bTBI lead to the same loss of hippocampal volume?

Do the findings differ from non-blast TBI?

What I was able to show was that the bTBI group shows a significant decrease of hippocampal volume compared to both the nbTBI and the healthy control groups, even in the absence of a clinical PTSD diagnosis. Vertex-based analysis showed that a specific area of the hippocampus, mainly around the CA1 has an atypical morphometry relative to controls. Both injury groups showed similar microstructural abnormalities of the fornix and cingulum, with a significant decrease of fractional anisotropy (FA) compared to controls. The fornix crura followed a similar trend of abnormality. Whole brain measures of atrophy, as well as voxel-based morphometry analysis did not reveal any loss of volume in the bTBI and nbTBI groups compared to controls. Therefore, the neuroimaging finding that seems to be specific to bTBI is the hippocampal atrophy, while other structural and diffusion abnormalities are consistent with general brain trauma.

Previous studies had already established that the hippocampi are particularly susceptible to the effects of blast exposure (de Lanerolle et al., 2011, Goldstein et al., 2012). Moreover, our lab had previously demonstrated in a porcine model of blast neurotrauma hippocampal oedema and microglial activation, coupled with a significantly lower fractional anisotropy in the hippocampi and fornices in animals exposed to blast, leading to the conclusion that of direct damage to limbic structures (Figure 55) (for more details on the experiment and results, see Ph.D. thesis of Dr Baxter D. [here](https://discovery.ucl.ac.uk/id/eprint/1546198/1/Baxter_David_e-thesisPhD.pdf)<sup>10</sup>).

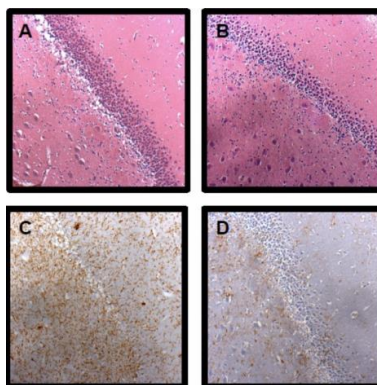


**Figure 55: Hippocampal oedema with concurrent microglial activation. (A) and (C) are section of the hippocampus in the same animal. (A) showing fibrous structural pathology denoting oedema and (C) show activation of microglia. (B) (D) Sections from a sham animal in which the oedema and microglial activation are not present. Taken from**

([https://discovery.ucl.ac.uk/id/eprint/1546198/1/Baxter\\_David\\_e-thesisPhD.pdf](https://discovery.ucl.ac.uk/id/eprint/1546198/1/Baxter_David_e-thesisPhD.pdf))

However, this is the first time that the findings of abnormalities in both the hippocampus and fornix in blast TBI regardless of neuropsychological diagnosis were verified in humans and in-vivo studies.

Based on the clinical and demographic information I had available, I tried to understand the association between clinical characteristics and the loss of hippocampal volume in the group of soldiers with bTBI. I found a significant correlation between measure of hippocampal total corrected volume (TCV) and mean FA measures of the fornix. However, particularly in this case, correlation does not imply causation in any direction, especially given that a similar abnormality of the WM microstructure in the fornix is found in nbTBI. I also focused on pituitary dysfunction

<sup>10</sup> Link to Ph.D. thesis of Dr David Baxter:

[https://discovery.ucl.ac.uk/id/eprint/1546198/1/Baxter\\_David\\_e-thesisPhD.pdf](https://discovery.ucl.ac.uk/id/eprint/1546198/1/Baxter_David_e-thesisPhD.pdf)

and hormonal abnormalities to understand if proximity of the structures, and damage of the limbic system shows correlation with pituitary abnormalities. A previous study with the same cohort showed greater diffusion abnormalities in the cerebellum and corpus callosum in soldiers with pituitary dysfunction compared to soldiers without. The cingulum did not show correlation between mean FA and pituitary abnormalities (Baxter, 2013). Although I did not focus on most WM tracts in this chapter, including the corpus callosum and the cerebellum – which I had shown to exhibit abnormalities in soldiers in Chapter 4 - I also did not find any association between measures of WM abnormalities in the cingulum and pituitary abnormalities or with hippocampal atrophy.

Future work needs to establish the hippocampus-fornix relation in bTBI, and whether chronic stress exposure, acute blast exposure, or another phenomenon specific to bTBI might be implicated. The hippocampus may be vulnerable to bTBI for several reasons: The structure of the CA1 region makes it more sensitive to trauma (Duvernoy 1988) and trauma to the fronto-basal parts of the brain, may therefore result in trans neuronal hippocampal cell death. In bTBI, damage to the hippocampi might be a direct result of the blast wave or could be secondary to hypoxia or impaired perfusion due to hypovolaemia.

Two main hypotheses arise in the case of bTBI and the hippocampal atrophy findings. The first hypothesis suggests that trauma to either of the structures arising from the blast could lead to a downstream neuropathological effect on the other structure. The fornix is one of the two major pathways into and out of the hippocampus. Through the fornix, the hippocampus receives input from the mamillary bodies and the hypothalamus. Therefore, because of this connection, integrity of the fornix is in-part linked to the integrity of the hippocampus. Many clinical studies on other types of disorders (eg. Dementia), show that fornix FA is lower in people with hippocampal atrophy, and that these changes correlate with memory function (Kantarci, 2014). It would also be important to mention biomechanistic consideration of the proximity of the fornix to the lateral ventricles, that were shown to be a major contributor based on the cavitation theory, with the ventricles representing the largest fluid-filled region in which cavitation could occur (Marsh, 2021).

The second hypothesis suggests that exposure to chronic stress in deployment settings could be causing hippocampal atrophy. The ventral part of the hippocampus is known to be important for stress regulation (Fanselow and Dong, 2010). Animal

studies have shown that stress can alter the synaptic plasticity and firing properties of hippocampal neurons (Kim et al., 2015), with the glucocorticoid hypothesis suggesting that the hippocampus having a dense concentration of corticosteroid receptors becomes susceptible to heightened cortisol secretion in response to stressors (McEwen and Sapolsky, 1995). I tried to verify this hypothesis by measuring the correlation between serum concentration basal cortisol levels<sup>11</sup> and hippocampal atrophy, but I found no significant correlation between the measures. However, these results do not completely reject this hypothesis, as further measures of cortisol (before/after deployment or during deployment) and other stress hormones will be more accurate and reliable.

No other measure seems to affect hippocampal TCV, including FA measures of the cingulum, measures of injury severity, basal cortisol levels, presence/absence of focal neuroradiological and endocrinological abnormalities as well as use of medications. Abnormality in the fornix seems to lead to memory impairment in our cohort, but there was no significant correlation between measures of memory and hippocampal TCV, even though the soldiers showed lower performance on immediate recall as measured by the people test. However, a multiple regression model did show that 71% of the variation in hippocampal TCV could be explained by focal neuroradiological abnormalities, injury severity, time since injury, and measures of FA in the fornix. This means that most of the variables explaining the reduction in hippocampal volume are directly related to the TBI event and given that abnormality in the hippocampus is only seen in bTBI, the assumption is that the variables are directly related to bTBI. This study was in part limited by the number of participants, but also by the availability of data. Longitudinal measures of hippocampal volume, cortisol levels, and cognitive or behavioural data could come a long way in determining the causal relationship of our findings, and their relation to clinical manifestations following bTBI.

In conclusion, soldiers with exposure to blast-related brain trauma show a loss of hippocampal volume, even in the absence of a PTSD diagnosis, and more severe than nbTBI. We can therefore assume that the hippocampus seems to be vulnerable to

---

<sup>11</sup> These measures of cortisol were obtained to confirm or exclude a diagnosis of adrenocorticotrophic hormone deficiency, and not in the context of stress research (Baxter et al., 2013).

blast exposure, as a direct result of the trauma, or as a downstream consequence, and this vulnerability seems to be linked to abnormalities in the fornix, in a relationship specific to bTBI.

***In the next chapter***

In chapter 6, I use the SSDS pipeline on a large cohort of TBI patients from the C3NL lab. I present descriptive statistics obtained, and train and test a decision tree classification model. The purpose of this decision tree is to classify between TBI and non-TBI patients with high accuracy by choosing the most relevant tracts to such a diagnosis.



## CHAPTER 6

---

# Traumatic Brain Injury and the Use of Classification Decision Trees Following SSDS

*In this chapter I use the SSDS pipeline to train a machine learning classification using decision trees. I apply the SSDS pipeline on a cohort of patients with TBI and on healthy controls on all the JHU tracts. By applying the decision tree model, I can classify subjects based on the presence or absence of TBI, but the novelty is in choosing the tracts that are most relevant for this classification.*

## 6.1. ABSTRACT

Traumatic brain injury (TBI) can often be difficult to identify using conventional imaging. And while diffusion tensor imaging (DTI) has previously been used to detect diffuse axonal injury in vivo and the underlying microstructural white matter (WM) abnormalities resulting from a trauma to the head, it is mainly used to investigate groups of patients and with an a priori knowledge of the hypothesis. To improve diagnosis based on imaging data, machine learning techniques are now increasingly used. However, in standard classification and regression problems, we still need to have a knowledge of the best features that differ from group to group to increase the accuracy of the output. In this chapter, I investigated whether decision tree machine learning applied to DTI data obtained from subject-specific diffusion segmentation (SSDS) can be used to diagnose WM damage following TBI and to predict the tracts that are most relevant in the differentiation between TBI and healthy controls, as well as TBI resulting from road traffic accidents (RTA) or other mechanisms. I train my decision tree classifier to predict the presence/absence of WM damage in 148 TBI patients and healthy controls. To test the performance of the algorithm, I applied it to a testing set of 37 participants with/without TBI. I repeated the same analysis to classify between RTA and non-RTA injuries within the TBI group with a training set of 69 subjects and a testing set of 16 subjects. The decision tree managed to discriminate between TBI and healthy controls with an 86% accuracy, while informing on the most important features (i.e. WM tracts) used for the classification. I also obtained similar results when classifying between different injury mechanisms within the TBI group, with a slightly lower accuracy of 69%. This work provides an initial approach to using decision trees in the diagnosis of TBI and should be extended to the diagnosis of blast-induced TBI in future.

## 6.2. INTRODUCTION

Traumatic brain injury (TBI) often results in diffuse axonal injury (DAI), regardless of the mechanism of the trauma. Patterns of DAI are usually investigated using diffusion tensor imaging (DTI) (Mac Donald et al., 2007). In the context of general TBI, when conventional neuroimaging diagnostic techniques fail to detect abnormalities, DTI can provide useful information regarding the microstructural integrity of the white matter (WM), usually through a measure of fractional anisotropy (FA) in specific WM tracts (Mac Donald et al., 2007, Kinnunen et al., 2011, Sidaros et al., 2008). DTI quantifies the directionality or change of directionality of water diffusion within tracts, therefore reflecting structural integrity (Beaulieu, 2002, Basser and Pierpaoli, 2011).

However, the translational aspect of DTI for diagnostic purposes is challenging, whether in the context of blast related TBI in soldiers, or non-blast TBI in civilians. The first problem is the need for individual investigations. I tackled this challenge of diagnostic DTI in CHAPTER 3, where I explain the issues with group-level analysis and develop a subject-level analysis to determine the presence of DAI and WM abnormalities in individuals. Subject-specific diffusion segmentation (SSDS) enables us to sensitively find differential patterns of injury in an individual compared to a healthy group of controls. The next step would be to use machine learning alongside SSDS to provide diagnostic information about TBI in a patient. Machine learning algorithms have been increasingly used to assist and even provide complex decisions of an outcome by finding patterns in the information and data available (Sajda, 2006). Classifiers are trained on data that are usually diagnostically labelled, so that when a new data point is undiagnosed, an individual prediction can be made.

Previous work has managed to successfully and accurately train a pattern support vector machine (SVM) classifier to predict the presence of WM microstructural damage following TBI (Hellyer et al., 2013). In such methods however, it is central to either know the importance of the features prior to training the model or calculate discriminant weights for WM tracts following the classification. Therefore, any comparison of individuals or groups still require a priori knowledge of hypotheses and anatomical regions to study. The challenge now becomes to be able to blindly determine the presence and significance of TBI with minimal interference and

undefined variables for efficient use in diagnostic pipelines, while learning about the weight attributed to every feature. This is where decision tree classifiers come into play, and the motivation of the use of decision tree classifications in this chapter. Machine learning tools using decision analysis applies evidence-based to inform unbiased clinical decisions in complex situations. Decision trees coupled with literature-derived probabilities, pre-set knowledge of the conditions and defined outcome values, can help determine the best diagnosis or course of action as well as an essential exploration of the important features and variables on the outcome. A decision-maker can thereafter establish a preferred method of treatment and explore variables which influence the final outcome.

The advantages of decision trees are that pre-processing, and assumptions of distributions are not requirements. This is essential in clinical research for two main reasons: 1) unifying methodologies becomes simpler and more efficient given the lack of arbitrary parameters in pre-processing protocols and 2) statistics to verify assumptions before running statistical analyses are no longer required. Decision trees are also able to handle collinearity (or correlation between predictors) efficiently, while providing understandable explanation over the prediction. This enables its use without a full understanding of the relationship between variables, which is often the case in clinical studies. Decision trees are usually better than SVM classifiers when dealing with categorical data – which is particularly the case in this study. The use of decision trees in clinical practice is becoming more common and involves the need to make complex decisions with crucial long-term consequences. Although it has been tested, developed and implemented in different clinical cases, it's yet to be tackled in the case of TBI given the complexity of the information used. For TBI generally and bTBI more specifically, training decision tree classifiers for accurate diagnosis would be an essential part of accurate classification and diagnosis in the absence of advanced tools and techniques.

In this chapter, I derive diffusion information from 47 WM tracts using SSDS from individuals with and without TBI, to train and then test a decision tree classifier. I also do the same analysis on TBI patients who suffered a road traffic accident (RTA), or other type of injuries to test if the decision tree can accurately discriminate between different injury mechanisms. I extract the most important features used for the classification for each decision tree and compare them to results obtained from group-

wise comparisons in each tract following SSDS to check whether decisions trees can yield more/different information regarding the most important WM tracts to consider in the case of TBI. This work provides a proof of principle that machine learning techniques, and more specifically decision trees, can be used with DTI-derived measures through SSDS to provide important diagnostic information.

### ***Hypotheses of chapter 6***

- Decision trees can classify between TBI patients and healthy controls using diffusion tensor imaging-derived metrics and while informing on important features to discriminate between groups.
- Decision trees can classify between TBI resulting from road-traffic accidents and TBI resulting from other mechanisms using DTI-derived metrics and while informing on important features to discriminate between groups.

## **6.3. METHODS**

### **6.3.1. Participants**

Data from 85 patients (mean  $\pm$  SD: 41.9  $\pm$  12.1 years, 17 females) and 100 healthy controls (mean  $\pm$  SD: 35.6  $\pm$  12.2 years, 30 female) were included in this study (Figure 56). Both groups had no history of psychiatric illness, substance dependence and were not undergoing any litigation. All TBI patients were classified as moderate-severe as defined by the Mayo criteria (Malec et al., 2007) and were recruited from Neurology outpatient clinics at St Mary's hospital, London, within the chronic phase of their injury (mean time since injury 130 months, range 6-497 months). All patients and controls underwent advanced structural and diffusion MRI. Of the 85 TBI patients included and based on the diagnostic reports of a consultant neuroradiologist, 14 had no visible focal injuries on routine neuroimaging (e.g. contusion or microbleeds), 10 had evidence of microbleeds, 33 had evidence of focal contusion and 28 patients had both contusions and microbleeds. Written informed consent was obtained from all participants in both groups in accordance with the Declaration of Helsinki. The studies were approved by the West London and GTAC Research Ethics Committee (14/LO/0067, 13/LO/1678, 14/LO/1998).

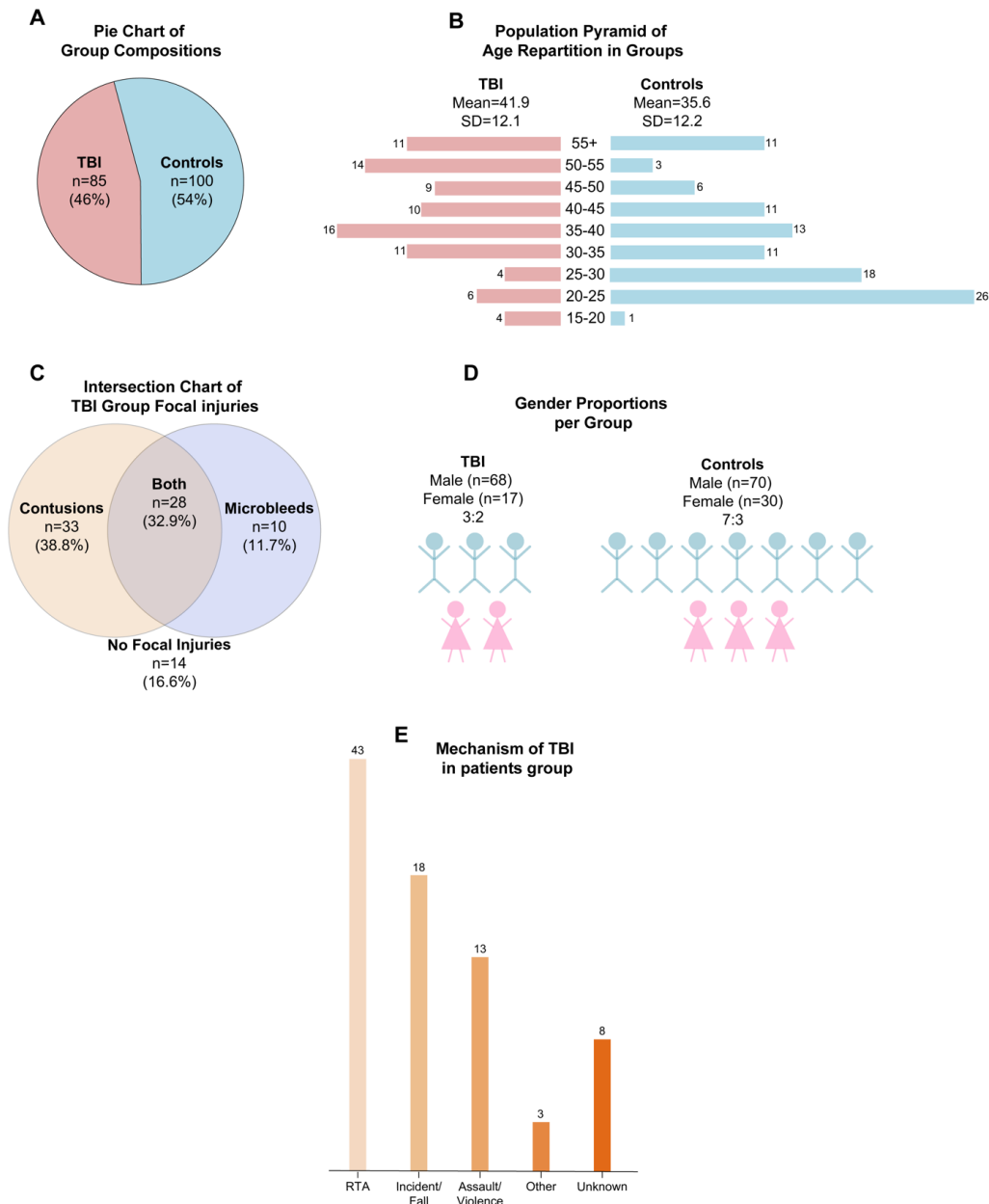


Figure 56 : Groups demographics. A) Pie chart showing the composition of each group, B) population pyramid graph showing the number of individuals in each group and each age category, C) number of TBI patients with microbleeds, contusions, both or none, D) Gender count and ratio in each group, E) Mechanism of TBI (not to scale), RTA= road traffic accident.

### 6.3.2. Imaging Acquisition

Structural MRI was acquired using a 3T Siemens Magnetom Verio Syngo with a 32-channel head coil. All participants in both groups were scanned using the same scanner and acquisition parameters. Structural MRI included a high-resolution T1-weighted MPRAGE106 1-mm-thick transverse slices, TR=2300ms, TE=2.98 ms, FA=9°, in-plane resolution=1x1mm, matrix size= 256x256, field of view=25.6x25.6cm), diffusion weighted imaging (64 directions, b=1000s/mm<sup>2</sup> with four interleaved b=0s/mm<sup>2</sup>, TE/TR 103/9,500ms, 64 contiguous slices, FoV 256mm, voxel size 2mm<sup>3</sup>). and fluid-attenuated inversion recovery (FLAIR) to identify focal lesions.

### 6.3.3. Decision Tree Training and Testing

#### *Applying SSDS*

For each patient, I made sure we had a raw T1-weighted image, a raw diffusion-weighted image, and a field map for optimal registration. I applied the SSDS pipeline as described in section 3.3.3. *Overview of SSDS*. All JHU tracts (n=47) were included in the analysis (more details in Supplementary Table 1). For each tract and each subject, the result of SSDS is a single mean FA value. For each of the 47 tracts, the mean FA result is extracted, resulting in a matrix of 185x47. The results of SSDS were used to compare groups in descriptive statistics using an unpaired t-test, then train the classifier to recognise TBI vs controls.

I repeated the analysis, but this time with 23 tracts. For every tract with a *left* and *right* mask, I created one bilateral mask, therefore reducing the input features. For each of the 23 tracts, the mean FA result is extracted, and used to train a decision tree to classify between TBI patients who suffered from road traffic accidents (RTA), and those who suffered from other injuries (85x23).

#### *Training the classifier*

I previously described the working theory of decision tree classifiers (see section 2.6.2). For the purpose of this chapter, decision tree is a type of supervised learning algorithm that will be used in a classification problem with a categorical output variable, and continuous input.



The initial dataset consisted of 185 subjects x 47 tracts. The root node represents this entire population, which will get divided into decision nodes, until it reaches a terminal node or a *leaf* that can no longer be split.

For training the decision tree, I randomly divided the data into 148 subjects for training and 37 subjects for testing (80% - 20%), while making sure both TBI and controls are included in both groups. I use the packages RPART (as the main workhorse for analysing and building the tree) and CARET (for splitting my data into training and testing sets) in Rstudio. The algorithm used to train this classification decision tree is Classification and Regression Trees (CART). CART creates a binary tree (two choices at each node) finding the best categorical feature to split using Gini impurity<sup>12</sup> as the impurity criterion.

(<https://cran.r-project.org/web/packages/caret/caret.pdf> )

(<https://cran.r-project.org/web/packages/rpart/rpart.pdf> )

With RPART package, we can use a formula call to build the tree. The *Group* variable is used as the y variable. The data to use to build the tree is the training set and since we are predicting categories (TBI or no TBI) the method is set to class. I use the same 47 tracts for prediction.

I repeated the training on a dataset of 85 subjects x 23 tracts (the bilateral tracts) to train a decision tree to classify within the TBI group between RTA injuries and other types of injuries. For training the decision tree, I randomly divided the data into 69 subjects for training and 16 subjects for testing (80% - 20%), while making sure both groups (with RTA and with other injuries) are included in both groups.

### ***Testing the classifier***

Once the tree is built, I check its predictive power by using it on the test data set I created earlier. For this, I calculate a confusion matrix (Figure 57), which gives the rate of false positive and false negatives and calculates five different metrics to measure the validity of the model.

---

<sup>12</sup> To choose the best split at a node, the Gini Impurity metric calculates the probability of wrong datapoint classification. The split is chosen to maximize the Gini Gain.

		True Class	
		Positive	Negative
Predicted Class	Positive	TP	FP
	Negative	FN	TN

**Figure 57: Confusion Matrix**

Validity metrics are calculated as follows:

$$\text{Accuracy} = (TP+TN) / (TP+TN+FP+FN)$$

$$\text{Misclassification} = (FP + FN) / (TP + TN + FP + FN)$$

$$\text{Precision} = TP / (TP + FP)$$

$$\text{Sensitivity} = TP / (TP+FN)$$

$$\text{Specificity} = TN / (TN+FP)$$

The accuracy determines how often the classifier is correct, and the misclassification determines how often the model gets it wrong.

The precision explains how often the model is correct when predicting positivity.

The sensitivity (true positive) determines how often the prediction is positive when the real outcome is positive.

The specificity (true negative) explains how often the prediction is negative when the real outcome is negative.

With decision trees, we could of course keep splitting until the tree has a maximum number of branches, but that of course is not best practice, even if it raises the accuracy of the decision tree. The tree in this case will be overfitted, slow and way too big to reveal anything relevant. Part of this classification problem is in fact determining which factors have most influence when categorising data. It is therefore important to set some predefined stopping criterion to halt the construction of the tree.

To overcome this problem of overfitting, it is essential to set the correct value for minimum number of instances per node using **tree pruning** technique. This allows us to avoid splitting redundancy. To prune my decision tree, I use a cost complexity prune of 0.03. I then calculated accuracy to see if the results are any better.

### ***Classifying different TBI mechanisms***

I train the same model on data from the TBI group, that were split as follows: TBI from road traffic accident (n=43) and TBI from other mechanisms (n=42). The point of this section is to test how well the algorithm would perform in classifying between different injury mechanism. Once again, the data is split in a training (n=68 subjects) and testing set (n=17 subjects) (80% - 20%). The method used is like the one described above.

### **6.3.4. Statistical Analysis**

I conducted all statistical analysis using R v3.3.3 ([www.R-project.org](http://www.R-project.org)) to assess normality relationships between variables and compare experimental groups. The groups to compare were TBI vs healthy controls first, then within the TBI group, road traffic accidents (RTA) vs other mechanism of injuries. I used a two-sample t-tests to compare groups. I assessed significance at  $p\text{-value} < 0.05$ . Details of statistical analysis related to training and testing of decision tree classifier are detailed above (section 6.3.3). To calculate the confidence interval of accuracy of the decision tree, I use a bootstrap resampling technique (with  $n=500$ ), which randomly samples from the dataset with re-selection to provide a variance of the model's performance.

## 6.4. RESULTS

### 6.4.1. Results from SSDS Pipeline

For the results, I use all tracts from the JHU, not just the tracts that passed the SSDS test-retest reliability measure. Reported results are for all 47 tracts in the first instance, and for concatenated bilateral tracts in the second analysis.

The purpose of this analysis is to draw a comparison between descriptive t-test statistics comparing both groups in order to find important features in each group, and using a classification decision tree that will run this analysis for us. Are the important features (or tracts in this case), similar in both approaches to dissociate between groups?

In the first instance, I compared healthy controls and patients with TBI. I obtained mean FA from SSDS for all 47 tracts for both groups and extracted the summary statistics (Supplementary Table 6). Tracts showing a decrease in mean FA in TBI patients compared to controls at  $p < 0.05$  were the anterior corona radiata bilaterally, the body, genu and splenium of the corpus callosum, the cerebral peduncle bilaterally, the cingulum and cingulum gyrus bilaterally, the corticospinal bilaterally, the external capsule bilaterally, the fornix stria terminalis bilaterally, the inferior longitudinal fasciculus bilaterally, the posterior corona radiata bilaterally, the posterior thalamic radiation bilaterally, the retro lenticular part of the internal capsule bilaterally, the inferior fronto-occipital fasciculus bilaterally, and the sagittal stratum bilaterally (Figure 58).

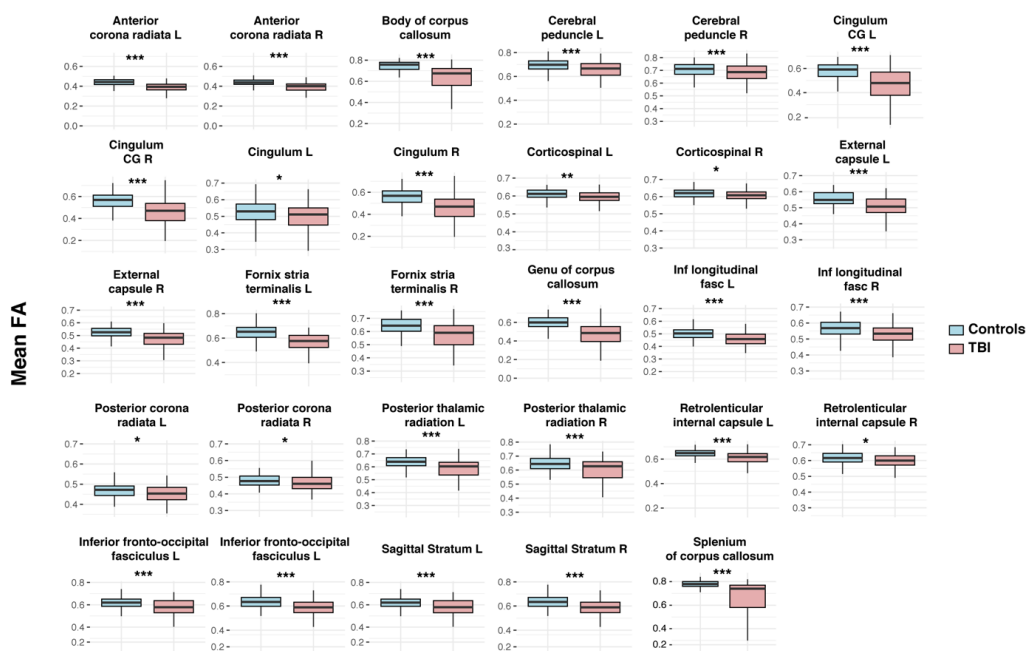


**Figure 58: Boxplot showing the distribution of mean FA across controls (blue) and TBI (pink).**

**Results are for significant tracts only (29 of 47 tracts) Mean and standard deviation are represented on the boxplots. Tracts are bilateral. \* $p<0.05$ , \*\* $p<0.01$ , \*\*\* $p<0.001$ . L= left, R= right. Only tracts with significant mean FA difference are shown**

I then looked at the differences in mean FA within the TBI group, comparing RTA injuries and other injuries (Supplementary Table 7) as well as the presence or absence of focal injuries (Figure 59). For this analysis, I used 23 masks, where bilateral tracts were concatenated to give a single mask for simplicity purpose. All ROIs are still covered, but instead of analysing left and right as two independent regions, I now analyse the structure as a whole. At a significance level of  $p<0.05$ , none of the tracts show a significantly different mean FA value between the two groups.

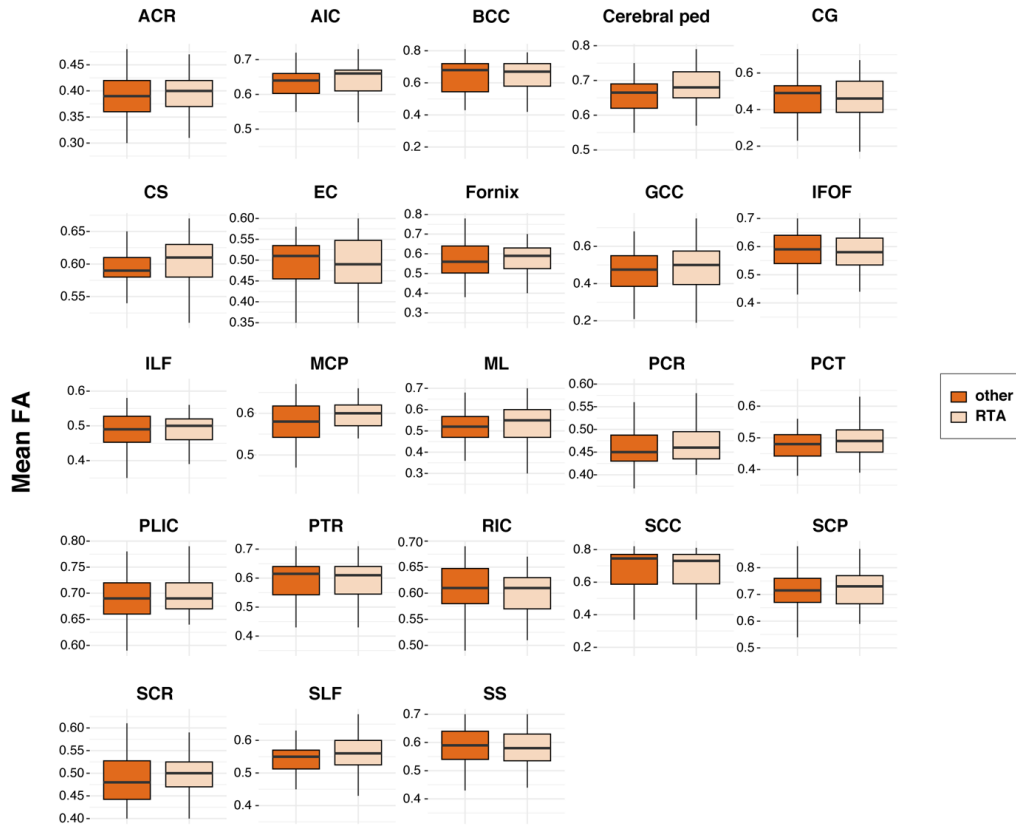


**Figure 59: Boxplot showing the distribution of mean FA across TBI from RTA (light orange) and TBI from other mechanisms (dark orange). Mean and standard deviation are represented on the boxplots. Tracts are bilateral. \* $p < 0.05$ , \*\* $p < 0.01$ , \*\*\* $p < 0.001$ . RTA= road traffic accident, ACR= anterior corona radiata, AIC= anterior limb of internal capsule, BCC= body of the corpus callosum, ped=peduncle, CG= cingulum gyrus, CS= corticospinal, EC=external capsule, GCC= genu of corpus callosum, IFOF=inferior fronto-occipital fasciculus, ILF= inferior longitudinal fasciculus, MCP= middle cerebellar peduncle, ML= medial lemniscus, PCR= posterior corona radiata, PCT= pontine crossing tract, PLIC= posterior limb of the internal capsule, PTR= posterior thalamic radiation, RIC= retrolenticular part of internal capsule, SCC= splenium of corpus callosum, SCP= superior cerebellar peduncle, SCR= superior corona radiata, SLF= superior longitudinal fasciculus, SS= sagittal stratum.**

Lastly, I also analysed the difference between TBI patients with focal neuroradiological abnormalities (microbleeds, contusions, or both) ( $n=71$ ), and TBI patients without any neuroradiological abnormality ( $n=14$ ). This analysis was not of particular interest for this chapter but was used as a way to compare methodologies and results obtained from a previous analysis on a similar cohort (Jolly et al., 2020). Although the number of subjects in each group was vastly different, I found the group with focal

abnormalities showed a significantly reduced FA in the following tracts: CG ( $p=0.024$ ), EC ( $p=0.012$ ), Fornix ( $p=0.016$ ), ILF ( $p=0.048$ ) and SCP ( $p=0.024$ ).

#### **6.4.2. Results from Decision Tree Classification of TBI vs Controls**

In this section, I use the raw data obtained from SSDS. These are not the results from processed data. They're the mean FA values as obtained from the SSDS analysis. First, I train a decision tree classifier to differentiate between TBI and healthy controls. The training set was composed of  $n=148$  subjects randomly selected. The groups were as follows: Controls  $n=80$  (80% of total controls) and TBI  $n=68$  (80% of total TBI patients) (Figure 56). When training the decision tree, and before pruning, the root node error was  $68/148=0.46$ . This means that 46% of subjects were correctly sorted at the first (root) splitting node.

I then looked at the feature importance for the classification. Feature importance is calculated as the decrease in node impurity weighted by the probability of reaching that node. The variables used in the tree construction were 22/49 tracts, including but not limited to the body, genu, and splenium of the corpus callosum, the cingulum gyrus bilaterally, the fornix stria terminalis bilaterally, the anterior corona radiata bilaterally, the left corticospinal, the left inferior longitudinal fasciculus, the right external capsule (Table 20). These results are obtained before any tree pruning, so they are not the final results.

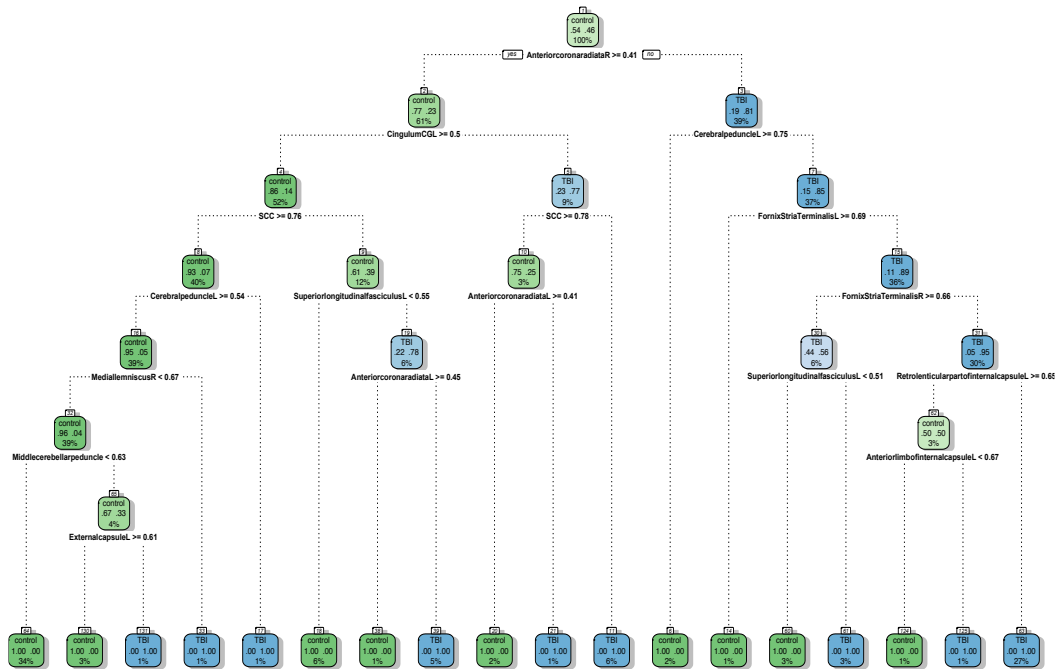


**Figure 60: Results of classification decision tree before pruning.** ‘Yes’ splits are on the left of every node, ‘No’ splits are on the right of every node. Node number is indicated above each node. More details about abbreviations can be found in (Supplementary Table 6). At every node, decimals on the left indicate the percentage of controls classified at this node, and decimal on the right indicate percentage of TBI patients classified at this node. The value near the tract name indicates the mean FA. L= left and R=right.

After tree pruning, the variables used in the tree construction were 16/49 of the tracts (Table 16). It is already clearer that the tree has less splits and nodes, and therefore less complexity. The root node error was 68/148=0.46. This means that 46% of subjects were correctly sorted at the first (root) splitting node. The feature importance was split as follows (see *section supplementary table 6* for all statistical details of the pruned decision tree).

**Table 16: Feature importance from pruned decision tree classifying between TBI and controls.**

BCC= body of corpus callosum, CG = cingulum gyrus, SCC= splenium of corpus callosum, GCC= genu of corpus callosum, FST= fornix stria terminalis, CS= corticospinal, ILF= inferior longitudinal fasciculus, EC- external capsule, ACR= anterior corona radiata, PCR= posterior corona radiata, SCR= superior corona radiata, PTR= posterior thalamic radiation, PCR= posterior cerebellar peduncle, L= left and R= right.

Feature	BCC	CG-R	CG-L	SCC	GCC	FST-L	CS-L	ILF-L
Importance	19	13	13	12	8	3	3	3



Feature	EC-R	ACR-L	PCR-R	PCR-L	SCR-R	PTR-L	Cerebral-ped-L	PCR-R
Importance	3	2	1	1	1	1	1	1

The final model after pruning uses the following features to classify between TBI and controls based on a series of decisions pertaining to mean FA measures (Figure 61).

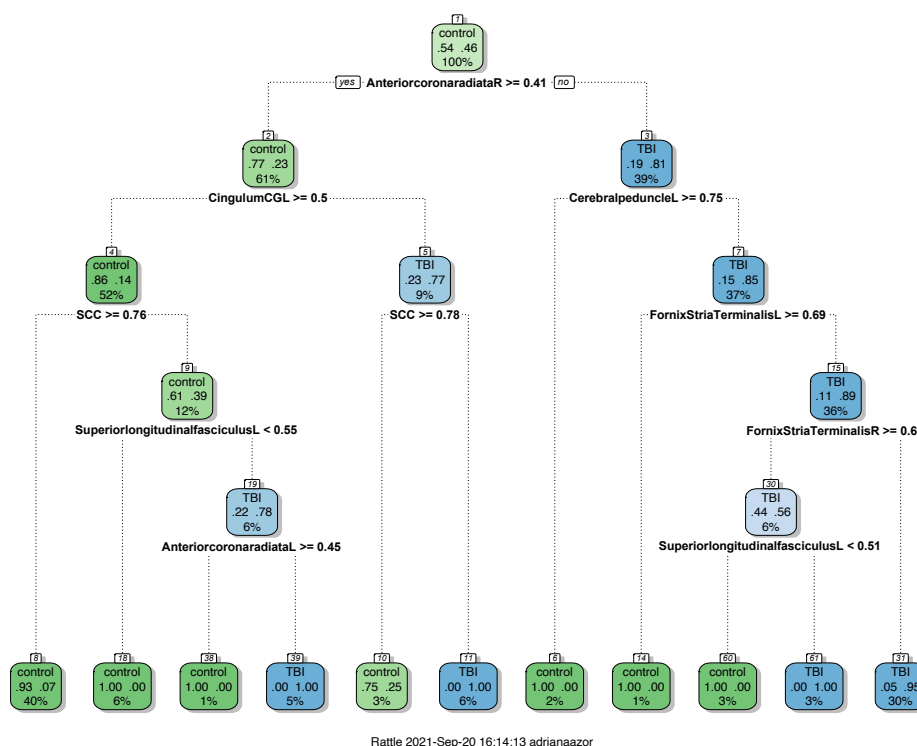


**Figure 61: Results of classification decision tree after pruning. ‘Yes’ splits are on the left of every node, ‘No’ splits are on the right of every node. Node number is indicated above each node. More details about abbreviations can be found in (Supplementary Table 1). At every node, decimals on the left indicate the percentage of controls classified at this node, and decimal on the right indicate percentage of TBI patients classified at this node. The value near the tract name indicates the mean FA. More details on this tree can be found in section (Supplementary Table 7). R= right and L=left.**

I then tested the tree on the testing set, which was not part of the training set. The testing set was composed of n=37 subjects, of which 20 healthy controls and 17 patients with TBI. Based on the confusion matrix resulting from running the classifier

on the testing set (Table 17), the accuracy was 86%, with a 95% confidence interval of 0.71 - 0.95, at  $p < 0.0001$ . The misclassification rate of 14%, a precision of 82%, a specificity of 85% and a sensitivity of 87%. The accuracy measure indicates that the model predicts 0.86 of the observations correctly.

**Table 17: Confusion matrix of decision tree classification.**

	<i>True Controls</i>	<i>True TBI</i>
<i>Predicted Controls</i>	18	3
<i>Predicted TBI</i>	2	14

### 6.4.3. Results from Decision Tree Classification of RTA vs Other Mechanisms

I tackled a similar decision tree classification problem in this section, but only within the TBI group to classify between RTAs and other types of injuries, and only for 23 tracts, after creating bilateral masks of each tract. The matrix used and resulting from SSDS is 85x23. The initial group of 85 patients (43 with RTA, 42 with other injuries) (Figure 56) was split into training and testing sets (80%-20%).

The training set was composed of  $n = 69$  subjects randomly selected. The groups were as follows: RTA  $n = 35$  (81% of RTA patients) and other injury  $n = 34$  (81% of patients with other injuries).

When training the decision tree, and before pruning, the root node error was  $34/69 = 0.49$ . This means that 49% of subjects were correctly sorted at the first (root) splitting node, with features used in tree construction (10/23 tracts): AIC, Cerebral ped, CG, GCC, PCR, PCT, PTR, SC and SCR. After tree pruning, the root node error was still  $34/69 = 0.49$  and the variables used in the tree construction were (4/23 tracts): Cerebral ped, PCT, SCP, SCR. The features importance can be seen below (see section A.5.4. *Decision Tree Statistics for RTA vs Other Types of Injuries* for more details on statistics):

**Table 18: Feature importance from pruned decision tree classifying between RTA and other injuries.**

Feature	SCP	Cerebral ped	SCR	AIC	CS	PCT	SCC	PCR	PLIC	Fornix
Importance	17	10	7	7	6	6	6	5	5	4
Feature	IFOF	RIC	SS	ACR	EC	GCC	ILF	ML	MCP	
Importance	4	4	4	4	3	3	3	3	2	

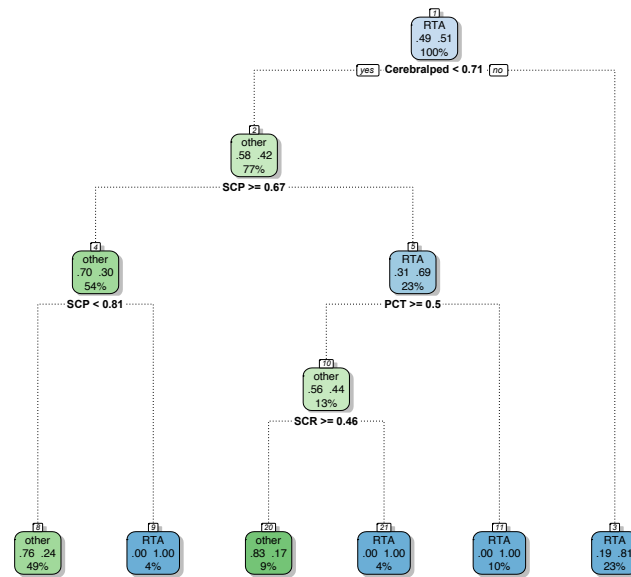


**Figure 62: Results of classification decision tree RTA vs other types of injuries after pruning.**

‘Yes’ splits are on the left of every node, ‘No’ splits are on the right of every node. Node number is indicated above each node. More details about abbreviations can be found in (Supplementary Table 1). At every node, decimals on the left indicate the percentage of controls classified at this node, and decimal on the right indicate percentage of TBI patients classified at this node. The value near the tract name indicates the mean FA. More details on this tree can be found in A.5.4. *Decision Tree Statistics for RTA vs Other Types of Injuries*. RTA= road traffic accident, PCT= pontine crossing tract, SCP= superior cerebellar peduncle, SCR= superior corona radiata.

I then tested the tree on the testing set, which was not part of the training set. The testing set was composed of n=16 subjects, of which 20 healthy controls and 17 patients with TBI. Based on the confusion matrix resulting from running the classifier on the testing set (Table 17), the accuracy was 69%, with a misclassification rate of 31%, a precision of 80%, a specificity of 88% and a sensitivity of 50%.

**Table 19: Confusion matrix of decision tree classification.**

	<i>True Other</i>	<i>True RTA</i>
<i>Predicted Other</i>	7	4
<i>Predicted RTA</i>	1	4

#### 6.4.4. Comparing Results

##### *TBI vs controls: Important tracts in t-test vs decision trees*

The final decision tree with a 73% accuracy used 7 of the 23 tracts as most important features to classify between the two groups. Of these tracts, 5 were shown to have a significantly lower mean FA when using a t-test on both groups, while the other two had similar mean FA distributions when using an unpaired t-test to compare between groups (Table 20).

**Table 20: Comparing results between t-test and decision trees in TBI vs controls.** ACR= anterior corona radiata, AIC= anterior limb of internal capsule, BCC= body of the corpus callosum, ped=peduncle, CG= cingulum gyrus, CS= corticospinal, EC=external capsule, GCC= genu of corpus callosum, IFOF=inferior fronto-occipital fasciculus, ILF= inferior longitudinal fasciculus, MCP= middle cerebellar peduncle, ML= medial lemniscus, PCR= posterior corona radiata, PCT= pontine crossing tract, PLIC= posterior limb of the internal capsule, PTR= posterior thalamic radiation, RIC= retrolenticular part of internal capsule, SCC= splenium of corpus callosum, SCP= superior cerebellar peduncle, SCR= superior corona radiata, SLF= superior longitudinal fasciculus, SS= sagittal stratum, RLIC= retro lenticular part of the internal capsule.

<b>T-test significant tracts</b>	<b>Decision tree important features – after pruning</b>
ACR	ACR
BCC	BCC
Cerebral ped	Cerebral ped
CG	CG
CS	CS
EC	EC
Fornix	Fornix
GCC	GCC
IFOF	IFOF
ILF	ILF
PCR	PCR
PTR	PTR
RIC	-
SCC	SCC
SCP	-
SS	-
RLIC	-
	+ PLIC and SCR

***RTA vs other injuries: Important tracts in t-test vs decision trees***

No tract came back significantly different in either group compared to the other when using a t-test. However, the final decision tree with an accuracy of 69% used 4 of the 23 tracts as most important features to classify between the three groups. The tracts were the following: Cerebral ped, PCT, SCP, SCR.

## 6.5. DISCUSSION

A faster and more efficient way to diagnose traumatic brain injury (TBI) or understand the difference between groups would be to train machine learning algorithms capable of detecting patterns associated with TBI. With this chapter, I tried to answer the following two questions: 1) Can I achieve high accuracy, specificity and precision with a decision tree classifying TBI patients from data obtained through SSDS? 2) What information can decision trees yield that aren't obtained from standard group comparison statistics?

Diffuse tensor imaging (DTI), and more specifically fractional anisotropy (FA) measures derived from DTI can give us important diagnostic information about TBI by providing quantitative measures of white matter (WM) microstructural integrity (Mac Donald et al., 2007). As seen throughout this thesis in the literature review and the experimental chapters, choosing pre-defined region of interest (ROI) and analysing them accordingly has been a technique widely used in clinical TBI investigations (Kennedy et al., 2009, Niogi et al., 2008b, Kraus et al., 2007, Niogi et al., 2008a). However, these approaches are limited to a priori hypotheses of which regions should be assessed, even when methods such as subject-specific diffusion segmentation, that try to curb these limitations, are used. The idea of using machine learning to detect TBI is not new (Hellyer et al., 2013). However, previous work has used support vector machine (SVM) classification algorithms to tackle this problem. The use of tree-based methods, on the other hand, is a novelty. Unlike other classification methods that typically use a set of features and a single decision step, decision trees are based on hierarchical decisions that follow tree-like structures, where each node makes the best binary choice to separate between classes.

In this study, I use a dataset composed of civilians with non-blast TBI. Running SSDS on the patients and controls returns a mean FA value for each tract and each subject. 80% of this output matrix is then used to build the decision tree, and 20% is used to test it. The recursive testing allows us to calculate a confidence interval for the accuracy of the tree. The model shows a high accuracy in its discrimination between TBI and no TBI (86%, 95 % CI: 0.71 - 0.95 ). With similar rates of precision, specificity, sensitivity and accuracy, the decision tree handles both TBI and control data well.

Using bootstrapping to calculate confidence interval of these measures also show that the rates aren't obtained by chance. An existing model using SVM to classify between TBI and controls had an accuracy of 86% to 92% (Hellyer, 2013). I have therefore managed to reach a similar accuracy, with an improved model of TBI classification. Moreover, instead of using a priori knowledge of tracts damage as is common in other classification problems, using decision trees enables us to test all tracts to see which ones give the most relevant information to discriminate between the two groups investigated.

I then looked at mechanisms of brain injury and trained a similar model to test whether classification between road traffic accidents (RTA) and other mechanisms of injuries (including falls, assaults, sports injuries, etc...) could be done with a similar accuracy rate. For this model however, accuracy was lower, at ~70%, and results show that the tree recognizes "other" injuries (88%) better than it recognizes RTAs (50%). Of course, the model is still young and should be trained on more data that are labelled by their proper mechanism if possible.

Interestingly, most of the tracts that were picked up by the group comparison statistics following SSDS as being significantly different between the control group and TBI patients were also defined by the decision tree as being important features in the decision process. However, not all significant tracts were used in the tree, while tracts that did not come up as significantly different between groups were. In the case of injury mechanism classification, although none of the tracts come up as significantly different using group comparisons, the tree still manages to discriminate between groups by using important features extracted from some of the tracts. This shows us that though we might think a particular WM area might be of interest in TBI, it isn't always the case when a machine learning algorithm tries to find patterns of abnormalities. On the other hand, group comparisons can sometimes omit information that seem to be relevant to the diagnostic outcome.

I made sure to tackle all the potential disadvantages of decision tree classifiers: while chances of overfitting the model is a concern, I use tree pruning to overcome this issue. The same technique also deals with the potential complexity and overgrowth of the tree while training complicated datasets. And although it is known that decision trees can potentially lose valuable information when handling continuous variables,

this chapter only works with categorical data, and more conservatively binary variables. Despite these steps, there are still some limitations to my approach. The first limitations lie in those of the DTI data pre-processing technique, already covered in CHAPTER 3. If SSDS fails in some aspect, the model will eventually be flawed. Second, it is important to note that the data used was heterogenous, and even though the participants were carefully selected after being scanned on the same scanner, there were differences in the age groups, and use of psychoactive drugs or other comorbidities were not taken into consideration. Lastly, it is important to remember that DTI changes remain dynamic after TBI, which renders the results specific to this phase of post-injury.

### **6.5.1. Important Next Steps for this Analysis**

This chapter should be relevant to the main hypotheses of this thesis, and therefore should lead to many more analyses into identifying biomarkers of bTBI and using them for a faster/more accurate diagnosis.

As a continuation of the analysis presented in this chapter, the first step would be to look at all the WM tracts instead of constraining the analysis to predefined atlas tracts. This, for example, would include the boundary of the tracts as described in chapter 4, that seemed to be relevant in bTBI. Then, a group with military TBI should be included to train a decision tree classification between blast and non-blast TBI. From there, we would know if the classifier used the boundary, or the MCP as important features in the classification, as demonstrated in chapter 4. Another possibility would be to include more metrics from the WM and other neuroimaging outputs such as the hippocampus for example into the classifier. Although not limited to application in bTBI, a good decision tree classifier would have important translational benefits, including but not limited to quicker and more accurate diagnosis – as this has repeatedly been problematic in bTBI.

Because of a limited number of soldiers in my cohort, I was not able to run a similar decision tree to classify between blast and non-blast TBI.



# CHAPTER 7

---

## Discussion

*In this chapter, I discuss the main findings from my thesis, their interpretation, limitations, as well as the potential impact and future directions of my research.*

## 7.1. SUMMARY OF CHAPTERS

In this thesis, I aimed to investigate and develop neuroimaging biomarkers of blast-induced traumatic brain injury (bTBI). I sought to use multimodal imaging with a particular focus on the development of a new pipeline, subjects-specific diffusion segmentation (SSDS), which enables us to carry out investigations at the subject-level. Developing biomarkers of bTBI would be essential for proper and more accurate diagnosis, prevention and treatment of long-term sequelae seen in soldiers post-deployment.

### **The main objectives of this thesis were:**

1. To develop, test and validate a new technique that would enable identification of patterns of white matter damage using an automated and standardized pipeline in the subject-level native diffusion space.
2. To investigate changes in cortical/subcortical structure and white matter (WM) microstructure in blast TBI and the difference in comparison to non-blast TBI using standard group-level analysis techniques.
3. To implement the new pipeline with the aim of identifying patterns of injury associated with blast-related TBI and the association with clinical and neuropsychological findings.
4. To use the results of the new pipeline to train a decision tree classification algorithm to classify between A) TBI and healthy controls, B) road traffic accidents vs other injury mechanisms

### **And the main hypotheses were:**

1. Group-level investigations of white matter microstructural damage cannot detect a pattern of injury specific to blast-related TBI.
2. Blast-related TBI will be differentiated by a decrease of subcortical structures volume in subject-level investigations, which can be explained by neuroradiological findings.
3. There will be specific patterns of white matter damage following blast-related TBI at the boundary between the WM and the fluid-filled cavities associated with neuropsychological measures impaired in soldiers with a diagnosis of blast TBI.

4. It is possible to discern with high accuracy between TBI/controls and road traffic accidents/ other mechanisms using decision trees, in a way that might be reproduced on military TBI data in future work.

For every chapter, I will revisit the specific hypotheses and present the main findings as bullet-point lists for clarity and simplicity.

### 1.8.5. 7.1.2. Chapter 3

#### **Main hypotheses:**

- Automated segmentation of WM tracts on the parametric map at the individual level can result in high test-retest reliability with a high correspondence with fractional anisotropy results obtained from manual segmentation.
- Some smaller tracts will have to be excluded from the subject-specific diffusion segmentation (SSDS) analysis due to higher variance in intra-subject measurements across different visits.

#### **Main findings:**

- ◆ I successfully developed SSDS using the following scans from healthy controls: T1-weighted images, diffusion-weighted images, field maps.
- ◆ Intra-subject and inter-modality registrations were accurate with the registration algorithms used.
- ◆ All tracts from the JHU atlas were successfully segmented through the pipeline, and the results were binary masks in individual diffusion space.
- ◆ I used 3 scans per subject for test-retest reliability measure, and a coefficient of variation of 5% as the cut-off point for tracts to use and not to use in SSDS analyses. The tracts with the lowest reliability were also the smallest tracts, with a high negative correlation between coefficient of variation and tract size. The tracts were: The fornix, the superior fronto-occipital fasciculus bilaterally, the hippocampal cingulum bundle bilaterally, the inferior cerebellar peduncle bilaterally, the uncinate fasciculus bilaterally, the fornix crescent bilaterally and the tapetum bilaterally.
- ◆ I compared SSDS to other standard diffusion imaging analyses. For mean fractional anisotropy (FA), SSDS had significantly similar results than manual

segmentation, and both methods had different results than SSDS. For tract volume, SSDS also outputs very similar tract volume than manual segmentation, but erosion of voxels with mixed intensity signals renders slightly smaller tracts. Tracts resulting from SSDS are always skeletonised, and therefore much smaller than the native ones.

- ◆ SSDS shows similar accuracy and higher specificity for investigations of WM abnormalities at the subject-level.

### 1.8.6. 7.1.3. Chapter 4

#### Main hypotheses:

- Using group-level tract-based spatial statistics (TBSS) on a reliable subset of WM tracts, the pattern of injury reflected by DTI abnormalities will be present in both bTBI and nbTBI groups.
- When increasing the specificity of measurements with subject-level investigations, bTBI will be associated with abnormalities in the posterior fossa, specifically the middle cerebellar peduncle, with greater damage seen at the boundary of the WM.

#### Main findings

- ◆ Group-level analysis, and more specifically TBSS derived skeletonised measures show a similar pattern of WM abnormalities in subjects with bTBI and civilians with non-blast TBI.
- ◆ Damage seen in both groups are consistent with TBI as we know it from previous studies and the literature, namely changes at the level of genu of the corpus callosum, the corticospinal tract, the inferior longitudinal fasciculus, the corona radiata, and the whole brain skeleton.
- ◆ SSDS uncovers abnormalities that seems to be specific to bTBI, at the level of the middle cerebellar peduncle, as well as at the boundary of the WM and grey matter (GM) in the whole brain, and WM and cerebrospinal fluid (CSF) in the whole brain as well as the middle cerebellar peduncle.
- ◆ Findings of WM abnormalities were heterogenous across soldiers, i.e. there were no significant differences between soldiers with/without focal injuries (microbleeds/contusions), or other abnormalities.

### 1.8.7. 7.1.4. Chapter 5

### **Main hypotheses:**

- The blast TBI group, but not the civilian TBI group, shows a decrease in hippocampal volume that correlates with abnormalities in the fornix.
- Loss of hippocampal volume does not correlate with measures of stress, or cognitive performance, but can be predicted based on the clinical characteristics of the soldiers.

### **Main findings**

- ◆ Hippocampal atrophy is only found in soldiers with bTBI, but not in healthy controls or civilians with nbTBI.
- ◆ FA abnormalities in the fornix, subdivision of the fornix, and cingulum are found in both injury groups relative to controls.
- ◆ Results of voxel-based morphometry shows no changes in whole brain WM and GM volumes in either injury groups compared to controls.
- ◆ Vertex-based morphometry focused on the hippocampi of soldiers compared to healthy controls shows changes in the anterior and posterior CA1 regions.
- ◆ There was a strong positive correlation between hippocampal volume and fornix mean FA in the bTBI group but not in the nbTBI group.
- ◆ None of the clinical characteristics investigated seemed to correlate with hippocampal volumes, and these include: level of cortisol level, injury severity, performance on cognitive tests of associative memory, presence of focal abnormalities (microbleeds/ contusions), pituitary dysfunction, hypogonadism, limb amputation, as well as between soldiers using antidepressant or not, and opiate or not.
- ◆ Measures of fornix and cingulum mean FA shows a correlation with performance on cognitive tests of associative memories.
- ◆ A multiple regression linear model reveals that 71% of the variation in hippocampal volume can be explained by the following variables: presence/absence of focal abnormalities, injury severity scores, and mean FA of the whole fornix.

### **1.8.8. 7.1.5. Chapter 6**

### **Main hypotheses:**

- Decision trees can classify between TBI patients and healthy controls using diffusion tensor imaging-derived metrics and while informing on important features to discriminate between groups.
- Decision trees can classify between TBI resulting from road-traffic accidents (RTA) and TBI resulting from other mechanisms using DTI-derived metrics and while informing on important features to discriminate between groups.

**Main findings:**

- ◆ SSDS was used to successfully segment all JHU tracts on 100 healthy controls and 85 patients with non-blast TBI. Left and right tracts were joined to create bilateral masks. Mean FA was extracted from a total of 47 tracts.
- ◆ Mean FA of the 47 tracts were used to train a decision tree to classify between patients with TBI and healthy controls.
- ◆ The most important tracts for the classification TBI vs controls were the anterior corona radiata, the body and genu of the corpus callosum, the inferior fronto-occipital fasciculus, the posterior limb of the internal capsule, the posterior thalamic radiation and the superior corona radiata.
- ◆ For the classification TBI vs controls, an 80%-20% training/testing revealed an accuracy of 86%, a specificity of 85% and a sensitivity of 87%.
- ◆ Mean FA of the 24 tracts (bilateral masks combined) were used to train a decision tree to classify between patients with who suffered from RTA, and those who suffered from other injury mechanisms.
- ◆ The most important tracts for the classification TBI vs controls were the cerebral peduncle, the pontine crossing tracts, the superior cerebellar peduncle and the superior corona radiata.
- ◆ For the classification RTA vs other mechanisms, an 80%-20% training/testing revealed an accuracy of 69%, a specificity of 88% and a sensitivity of 50%.

## 7.2. CONCLUSION & INTERPRETATION

### ***Investigations at the subject-level are essential in specific cases***

When the differences between groups being compared are very subtle, or when individual WM regions should be investigated at the level of every participant, group-level analyses become limiting (Soares et al., 2013, Zalesky, 2011). This is because such approaches deal with averages of images, which require normalization of data and images (Jones and Cercignani, 2010). This becomes problematic when the areas investigated can't be discerned or segmented at a group-level and need higher specificity. The subject-specific diffusion segmentation (SSDS) was developed for the particular purpose of investigating WM changes in soldiers in regions that cannot be attained by other methods such as tract-based spatial statistics, and that would have required manual segmentation (Soares et al., 2013). I managed to show that although biomarkers of bTBI cannot be determined using group-level techniques, SSDS manages to set the two injury groups (soldiers and civilians) apart.

However, the applications of SSDS extend beyond comparisons of groups or subjects to groups. One example is a project I am currently involved in, but that isn't part of this thesis, in which computational models and reconstructions of head injuries in specific cases are being compared to the abnormalities resulting from said injury. In this study, we are looking at 4 patients who suffered different mechanisms of falls. The team led by Dr Ghajari is reconstructing the falls using computations simulations, while I use SSDS to determine abnormalities in the underlying WM structure of the subject (Ghajari et al., 2017). We can then determine the relation between the strain/strain rate observed in a particular region on the model, and the change in diffusivity in the corresponding area using neuroimaging. In the context of bTBI, this interdisciplinary technique can help us reconstruct blast loads to the brain and the resulting injuries.

### ***White matter microstructural abnormalities at the level of the middle cerebellar peduncle and the boundary of the white matter are neuroimaging biomarkers of blast related TBI***

As mentioned previously, the hypothesis behind this conclusion came from previous post-mortem investigations, animal studies and neuroimaging. The idea that WM damage of the cerebellar peduncle and the boundary of the WM might be specific to blast exposure had been part of the literature for a few years (Shively et al., 2016, Mac

Donald et al., 2011, Kirkman et al., 2011). In a study that has yet to be published by the C3NL lab, a porcine model of blast neurotrauma showed signs of ependymal stripping in all animals following blast with astrocytic proliferation and axonal injury in the periventricular region, which had also been previously documented in a similar model (de Lanerolle et al., 2011). However, this is the first time that standardized in-vivo methods are used – which will be an essential part of result replication on a larger cohort - and a group of civilians with TBI is used to control for other injury mechanism. The hypotheses around why these areas are susceptible to damage following blast are still speculations. One of the explanations would be the nature of the blast wave, which causes refraction effects when it is transmitted between tissues with different properties (such as the WM and the fluid-filled cavities) (Yu et al., 2020). This might result in increasing forces between tissues. As for the middle cerebellar peduncle, the clinical and biomechanical relevance remains to be determined (Mac Donald et al., 2013). None of my subjects had clinical signs of cerebellar disturbances such as ataxia or gait disturbance, and although cognitive and behavioural measures were limited, we did not see any apparent correlation relevant to abnormalities in this region.

***Hippocampal atrophy is a grey matter neuroimaging biomarker of blast related TBI even in the absence of post-traumatic stress disorder***

Just as I did for WM investigations, I based investigation of the GM on previous post-mortem findings, animal studies and neuroimaging on soldiers (Sydnor et al., 2020, Nelson and Tumpap, 2017, Bremner, 2007, Lee et al., 2009). Investigations based on the same porcine model of blast neurotrauma as part of C3NL's research also found that animals had evidence of hippocampal oedema which was not seen in Sham animals or controls. One animal showed evidence of bilateral oedematous appearances in the dentate gyrus (DG) of the ventral hippocampi, another had unilateral changes in the DG of the ventral hippocampus. It is clear from the literature and previous work at our lab, that the hippocampus is a structure of interest regarding the neuropathology of blast injuries, but investigations of the hippocampus were always coupled with the presence of a post-traumatic stress disorder (PTSD) diagnosis in human analyses. From a neurological point of view, this raises the questions of causality; which comes first, PTSD or hippocampal atrophy? Showing that 1) hippocampal atrophy is present even in the absence of PTSD and 2) hippocampal atrophy is not seen in civilians, makes it another neuroimaging biomarker



of primary blast injury. The mechanism of this loss of volume however remains a mystery; Is it chronic stress? Is it brain trauma caused by blast? Or is it perhaps a decrease of cognitive activity during deployment?

Uncovering markers of blast neurotrauma is an essential building block in the development of more efficient prevention and the understanding of the mechanism of primary blast injuries.

***Training a decision tree classifier from diffusion data is a first step towards machine-learning driven diagnosis of TBI biomechanics***

Since bTBI seems to have particular biomarkers that are identifiable using in-vivo advanced neuroimaging techniques, and that decision trees can be used to recognize the presence of TBI, and potentially the mechanism behind TBI, it should be possible to leverage markers of bTBI, mainly abnormal diffusivity in the middle cerebellar peduncle, abnormal diffusivity at the boundary of the white matter, and grey matter hippocampal atrophy to train a diagnostic decision tree to classify between blast-induced TBI and non-blast induced TBI. This work lays all the required foundations for future research to test the clinical utility of such a diagnostic pipeline in a cohort of bTBI patients. The next logical progression would therefore be to apply SSDS and hippocampal volumetry in a larger cohort of soldiers with bTBI and civilians with non-blast TBI and use the multimodality decision tree to test whether groups could be discriminated with high accuracy when using these features.

### 7.3. LIMITATIONS & RECOMMENDATIONS

Limitations of each investigation have been covered in their corresponding chapters. The most important ones, which are common to all four experimental chapters, and which provide potential limitations to the overall conclusions are the following:

#### ***Group size and group selection***

My cohort of bTBI was limited to a small number of soldiers. Collaboration with other work carried out in the context of military TBI to include more participants and reproduce results using standardized techniques is essential.

Moreover, bTBI is a complex pathology that involves different injury mechanisms, and many of the imaging changes result from non-blast mechanisms such as head impact and rotational forces. The complexity is further exacerbated by the difficult circumstances during deployment to assess and report the conditions of the injury. Although my work supports the conclusion that there is a unique mechanism of injury associated with the blast itself, controlling for additional factors would be essential in future research.

#### ***The need for more mechanistic, cognitive, behavioural, and clinical data***

Unfortunately, I couldn't include enough behavioural and cognitive measures in my analysis. Although I report biomarkers of bTBI, it is important to understand if and how they provide neurological underpinnings of the symptomatology of bTBI. Future work should focus on the causality relationship between PTSD and hippocampal volume, the pathological downstream effects of trauma on the limbic system, the mechanistic importance of blast wave propagation on tissue boundaries, and how this translates to possible cognitive and behavioural disturbances, as well as the reason for the susceptibility of the middle cerebellar peduncle to the effects of blast. Knowledge of the strength, directionality, and nature of the forces that soldiers experience using accelerometers for example, that are placed inside the helmet, can provide valuable information about the mechanistic aspect of the individual experience. More relevant measures of cortisol level would be another example of crucial data. This would allow understanding of how stress might be implicated in hippocampal atrophy.

With this data, and on the clinical side, not only would we be able to build a diagnostic decision trees for bTBI, but it would potentially be possible to use machine learning regression analyses to predict long-term outcome and for accurate prognosis in

soldiers having sustained a bTBI. On the prevention side, uncovering why and how certain parts of the brain are more susceptible than others to blast wave forces could improve protective equipment and helmet designs.

### ***Importance of longitudinal studies***

As mentioned earlier, more information on clinical factors and cognition are essential, but a more effective approach would be a longitudinal investigation, with neuroimaging data, cognitive and behavioural tests, as well as endocrinology measures taken prior to deployment, and over different periods of time following bTBI. Measures such as cortisol, which would reflect stress levels, should also be collected throughout deployment even in the absence of bTBI. Such information can shed light on relationships of causality among all the different findings and serve as fluid biomarkers of neuropathology. Another important aspect of longitudinal study would be in the chronic phase following bTBI to understand the potential development of PTSD and its association with hippocampal atrophy.

### ***Other recommendations***

- Use white matter information other than fractional anisotropy. This would include performing pre-processing of diffusion imaging data with other packages such as MRtrix and estimate more complex diffusivity measures that would consider crossing fibres.
- Examine hippocampal volume and morphometry in soldiers with bTBI and compare differences in soldiers with and without PTSD.
- Focus on the development of homogenous longitudinal approach for cognitive and behavioural assessments.

## References

- (DOD), D. O. D. 2020. Data from "Worldwide numbers for traumatic brain injury".
- ABE, O., TAKAO, H., GONOI, W., SASAKI, H., MURAKAMI, M., KABASAWA, H., KAWAGUCHI, H., GOTO, M., YAMADA, H., YAMASUE, H., KASAI, K., AOKI, S. & OHTOMO, K. 2010. Voxel-based analysis of the diffusion tensor. *Neuroradiology*, 52, 699-710.
- ADAM, O., MAC DONALD, C. L., RIVET, D., RITTER, J., MAY, T., BAREFIELD, M., DUCKWORTH, J., LABARGE, D., ASHER, D., DRINKWINE, B., WOODS, Y., CONNOR, M. & BRODY, D. L. 2015. Clinical and imaging assessment of acute combat mild traumatic brain injury in Afghanistan. *Neurology*, 85, 219-27.
- ADAMS, J. H., DOYLE, D., FORD, I., GENNARELLI, T. A., GRAHAM, D. I. & MCLELLAN, D. R. 1989. Diffuse axonal injury in head injury: definition, diagnosis and grading. *Histopathology*, 15, 49-59.
- ADLURU, N., ZHANG, H., TROMP, D. P. & ALEXANDER, A. L. 2013. Effects of DTI spatial normalization on white matter tract reconstructions. *Proc SPIE Int Soc Opt Eng*, 8669.
- AGOSTON, D. V. & KAMNAKSH, A. 2015. Modeling the Neurobehavioral Consequences of Blast-Induced Traumatic Brain Injury Spectrum Disorder and Identifying Related Biomarkers. In: KOBEISSY, F. H. (ed.) *Brain Neurotrauma: Molecular, Neuropsychological, and Rehabilitation Aspects*. Boca Raton (FL).
- ANDERSON, C. V., WOOD, D. M., BIGLER, E. D. & BLATTER, D. D. 1996. Lesion volume, injury severity, and thalamic integrity following head injury. *J Neurotrauma*, 13, 59-65.
- ANDERSSON, S., KROGSTAD, J. M. & FINSET, A. 1999. Apathy and depressed mood in acquired brain damage: relationship to lesion localization and psychophysiological reactivity. *Psychol Med*, 29, 447-56.
- ANDREWS, D. S., AVINO, T. A., GUDBRANDSEN, M., DALY, E., MARQUAND, A., MURPHY, C. M., LAI, M. C., LOMBARDO, M. V., RUIGROK, A. N., WILLIAMS, S. C., BULLMORE, E. T., THE MRC AIMS, C., SUCKLING, J., BARON-COHEN, S., CRAIG, M. C., MURPHY, D. G. & ECKER, C. 2017. In Vivo Evidence of Reduced Integrity of the Gray-White Matter Boundary in Autism Spectrum Disorder. *Cereb Cortex*, 27, 877-887.
- AOKI, Y., INOKUCHI, R., GUNSHIN, M., YAHAGI, N. & SUWA, H. 2012. Diffusion tensor imaging studies of mild traumatic brain injury: a meta-analysis. *J Neurol Neurosurg Psychiatry*, 83, 870-6.
- ARIBISALA, B. S., HE, J. & BLAMIRE, A. M. 2011. Comparative study of standard space and real space analysis of quantitative MR brain data. *J Magn Reson Imaging*, 33, 1503-9.
- ARMONDA, R. A., BELL, R. S., VO, A. H., LING, G., DEGRABA, T. J., CRANDALL, B., ECKLUND, J. & CAMPBELL, W. W. 2006. Wartime traumatic cerebral vasospasm: recent review of combat casualties. *Neurosurgery*, 59, 1215-25; discussion 1225.
- ASHBURNER, J. & FRISTON, K. J. 2000. Voxel-based morphometry—the methods. *Neuroimage*, 11, 805-21.
- ASSAF, Y. & PASTERNAK, O. 2008. Diffusion tensor imaging (DTI)-based white matter mapping in brain research: a review. *J Mol Neurosci*, 34, 51-61.
- ASTRAKAS, L. G. & ARGYROPOULOU, M. I. 2010. Shifting from region of interest (ROI) to voxel-based analysis in human brain mapping. *Pediatr Radiol*, 40, 1857-67.
- AVERILL, C. L., AVERILL, L. A., WROCKLAGE, K. M., SCOTT, J. C., AKIKI, T. J., SCHWEINSBURG, B., SOUTHWICK, S. M., KRYSTAL, J. H. & ABDALLAH, C. G. 2018. Altered White Matter Diffusivity of the Cingulum Angular Bundle in Posttraumatic Stress Disorder. *Mol Neuropsychiatry*, 4, 75-82.
- BAE, S., SHEETH, C., LEGARRETA, M., MCGLADE, E., LYOO, I. K. & YURGELUN-TODD, D. A. 2020. Volume and shape analysis of the Hippocampus and amygdala in veterans with traumatic brain injury and posttraumatic stress disorder. *Brain Imaging Behav*, 14, 1850-1864.
- BALIYAN, V., DAS, C. J., SHARMA, R. & GUPTA, A. K. 2016. Diffusion weighted imaging: Technique and applications. *World J Radiol*, 8, 785-798.
- BARLOW-OGDEN, K. & POYNTER, W. 2012. Mild traumatic brain injury and posttraumatic stress disorder: investigation of visual attention in Operation Iraqi Freedom/Operation Enduring Freedom veterans. *J Rehabil Res Dev*, 49, 1101-14.
- BASSER, P. J. & PIERPAOLI, C. 2011. Microstructural and physiological features of tissues elucidated by quantitative-diffusion-tensor MRI. 1996. *J Magn Reson*, 213, 560-70.
- BAUMAN, R. A., LING, G., TONG, L., JANUSZKIEWICZ, A., AGOSTON, D., DELANEROLLE, N., KIM, Y., RITZEL, D., BELL, R., ECKLUND, J., ARMONDA, R., BANDAK, F. & PARKS, S. 2009. An introductory characterization of a combat-casualty-care relevant swine model of closed head injury resulting from exposure to explosive blast. *J Neurotrauma*, 26, 841-60.
- BAXTER, D., SHARP, D. J., FEENEY, C., PAPADOPOULOU, D., HAM, T. E., JILKA, S., HELLYER, P. J., PATEL, M. C., BENNETT, A. N., MISTLIN, A., MCGILLOWAY, E., MIDWINTER, M. & GOLDSTONE, A. P. 2013. Pituitary dysfunction after blast traumatic brain injury: The UK BIOSAP study. *Ann Neurol*, 74, 527-36.
- BAZARIAN, J. J., DONNELLY, K., PETERSON, D. R., WARNER, G. C., ZHU, T. & ZHONG, J. 2013. The relation between posttraumatic stress disorder and mild traumatic brain injury acquired during Operations Enduring Freedom and Iraqi Freedom. *J Head Trauma Rehabil*, 28, 1-12.
- BEAMER, M., TUMMALA, S. R., GULLOTTI, D., KOPIL, C., GORKA, S., TED, A., BASS, C. R., MORRISON, B., 3RD, COHEN, A. S. & MEANEY, D. F. 2016. Primary blast injury causes cognitive impairments and hippocampal circuit alterations. *Exp Neurol*, 283, 16-28.
- BEAULIEU, C. 2002. The basis of anisotropic water diffusion in the nervous system - a technical review. *NMR Biomed*, 15, 435-55.
- BEHRENS, T. E., WOOLRICH, M. W., JENKINSON, M., JOHANSEN-BERG, H., NUNES, R. G., CLARE, S., MATTHEWS, P. M., BRADY, J. M. & SMITH, S. M. 2003. Characterization and propagation of uncertainty in diffusion-weighted MR imaging. *Magn Reson Med*, 50, 1077-88.
- BELANGER, H. G., KRETZMER, T., YOASH-GANTZ, R., PICKETT, T. & TUPLER, L. A. 2009. Cognitive sequelae of blast-related versus other mechanisms of brain trauma. *J Int Neuropsychol Soc*, 15, 1-8.
- BENZINGER, T. L., BRODY, D., CARDIN, S., CURLEY, K. C., MINTUN, M. A., MUN, S. K., WONG, K. H. & WRATHALL, J. R. 2009. Blast-related brain injury: imaging for clinical and research applications: report of the 2008 st. Louis workshop. *J Neurotrauma*, 26, 2127-44.
- BIGLER, E. D. 2001. Distinguished Neuropsychologist Award Lecture 1999. The lesion(s) in traumatic brain injury: implications for clinical neuropsychology. *Arch Clin Neuropsychol*, 16, 95-131.

- BIGLER, E. D. 2007. Anterior and middle cranial fossa in traumatic brain injury: relevant neuroanatomy and neuropathology in the study of neuropsychological outcome. *Neuropsychology*, 21, 515-31.
- BIGLER, E. D., ABILDSKOV, T. J., GOODRICH-HUNSAKER, N. J., BLACK, G., CHRISTENSEN, Z. P., HUFF, T., WOOD, D. M., HESSELINK, J. R., WILDE, E. A. & MAX, J. E. 2016. Structural Neuroimaging Findings in Mild Traumatic Brain Injury. *Sports Med Arthrosc Rev*, 24, e42-52.
- BIGLER, E. D., ABILDSKOV, T. J., WILDE, E. A., MCCAULEY, S. R., LI, X., MERKLEY, T. L., FEARING, M. A., NEWSOME, M. R., SCHEIBEL, R. S., HUNTER, J. V., CHU, Z. & LEVIN, H. S. 2010. Diffuse damage in pediatric traumatic brain injury: a comparison of automated versus operator-controlled quantification methods. *Neuroimage*, 50, 1017-26.
- BIGLER, E. D. & MAXWELL, W. L. 2012. Neuropathology of mild traumatic brain injury: relationship to neuroimaging findings. *Brain Imaging Behav*, 6, 108-36.
- BING, X., MING-GUO, Q., YE, Z., JING-NA, Z., MIN, L., HAN, C., YU, Z., JIA-JIA, Z., JIAN, W., WEI, C., HAN-JIAN, D. & SHAO-XIANG, Z. 2013. Alterations in the cortical thickness and the amplitude of low-frequency fluctuation in patients with post-traumatic stress disorder. *Brain Res*, 1490, 225-32.
- BLENNOW, K., BRODY, D. L., KOCHANNEK, P. M., LEVIN, H., MCKEE, A., RIBBERS, G. M., YAFFE, K. & ZETTERBERG, H. 2016. Traumatic brain injuries. *Nat Rev Dis Primers*, 2, 16084.
- BOGDANOVA, Y. & VERFAELLIE, M. 2012. Cognitive sequelae of blast-induced traumatic brain injury: recovery and rehabilitation. *Neuropsychol Rev*, 22, 4-20.
- BOOKSTEIN, F. L. 2001. "Voxel-based morphometry" should not be used with imperfectly registered images. *Neuroimage*, 14, 1454-62.
- BORG, J., HOLM, L., CASSIDY, J. D., PELOSO, P. M., CARROLL, L. J., VON HOLST, H., ERICSON, K. & INJURY, W. H. O. C. C. T. F. O. M. T. B. 2004. Diagnostic procedures in mild traumatic brain injury: results of the WHO Collaborating Centre Task Force on Mild Traumatic Brain Injury. *J Rehabil Med*, 61-75.
- BRASHERS-KRUG, T. & JORGE, R. 2015. Bi-Directional Tuning of Amygdala Sensitivity in Combat Veterans Investigated with fMRI. *PLoS One*, 10, e0130246.
- BREMNER, J. D. 2007. Neuroimaging in posttraumatic stress disorder and other stress-related disorders. *Neuroimaging Clin N Am*, 17, 523-38, ix.
- BROWN, C. A., JOHNSON, N. F., ANDERSON-MOONEY, A. J., JICHA, G. A., SHAW, L. M., TROJANOWSKI, J. Q., VAN ELDIK, L. J., SCHMITT, F. A., SMITH, C. D. & GOLD, B. T. 2017. Development, validation and application of a new fornix template for studies of aging and preclinical Alzheimer's disease. *Neuroimage Clin*, 13, 106-115.
- BRYDEN, D. W., TILGHMAN, J. I. & HINDS, S. R., 2ND 2019. Blast-Related Traumatic Brain Injury: Current Concepts and Research Considerations. *J Exp Neurosci*, 13, 1179069519872213.
- BUCHSBAUM, M. S., SIMMONS, A. N., DECASTRO, A., FARID, N. & MATTHEWS, S. C. 2015. Clusters of Low (18)F-Fluorodeoxyglucose Uptake Voxels in Combat Veterans with Traumatic Brain Injury and Post-Traumatic Stress Disorder. *J Neurotrauma*, 32, 1736-50.
- BUGAY, V., BOZDEMIR, E., VIGIL, F. A., CHUN, S. H., HOLSTEIN, D. M., ELLIOTT, W. R., SPRAGUE, C. J., CAVAZOS, J. E., ZAMORA, D. O., RULE, G., SHAPIRO, M. S., LECHLEITER, J. D. & BRENNER, R. 2020. A Mouse Model of Repetitive Blast Traumatic Brain Injury Reveals Post-Trauma Seizures and Increased Neuronal Excitability. *J Neurotrauma*, 37, 248-261.
- CASSON, I. R., VIANO, D. C. & PELLMAN, E. J. 2008. Synopsis of the National Football League Player Health and Safety Meeting: Chicago, Illinois, June 19, 2007. *Neurosurgery*, 62, 204-9; discussion 209-10.
- CERNAK, I. & NOBLE-HAEUSSLEIN, L. J. 2010. Traumatic brain injury: an overview of pathobiology with emphasis on military populations. *J Cereb Blood Flow Metab*, 30, 255-66.
- CERNAK, I., SAVIC, J., MALICEVIC, Z., ZUNIC, G., RADOSEVIC, P., IVANOVIC, I. & DAVIDOVIC, L. 1996. Involvement of the central nervous system in the general response to pulmonary blast injury. *J Trauma*, 40, S100-4.
- CERNAK, I., WANG, Z., JIANG, J., BIAN, X. & SAVIC, J. 2001. Ultrastructural and functional characteristics of blast injury-induced neurotrauma. *J Trauma*, 50, 695-706.
- CHALONER, E. 2005. Blast injury in enclosed spaces. *BMJ*, 331, 119-20.
- CHAO, L., WEINER, M. & NEYLAN, T. 2013. Regional cerebral volumes in veterans with current versus remitted posttraumatic stress disorder. *Psychiatry Res*, 213, 193-201.
- CHARLES, A. C., MERRILL, J. E., DIRKSEN, E. R. & SANDERSON, M. J. 1991. Inter cellular signaling in glial cells: calcium waves and oscillations in response to mechanical stimulation and glutamate. *Neuron*, 6, 983-92.
- CHEN WW, S. B. 2010. *Split Hopkinson (Kolsky) bar: design, testing and applications.*, Springer
- CHENG, J., GU, J., MA, Y., YANG, T., KUANG, Y., LI, B. & KANG, J. 2010. Development of a rat model for studying blast-induced traumatic brain injury. *J Neurol Sci*, 294, 23-8.
- CHILDRESS, J. E., MCDOWELL, E. J., DALAI, V. V., BOGALE, S. R., RAMAMURTHY, C., JAWAID, A., KUNIK, M. E., QURESHI, S. U. & SCHULZ, P. E. 2013. Hippocampal volumes in patients with chronic combat-related posttraumatic stress disorder: a systematic review. *J Neuropsychiatry Clin Neurosci*, 25, 12-25.
- CICCHETTI, D. V. 1994. Multiple comparison methods: establishing guidelines for their valid application in neuropsychological research. *J Clin Exp Neuropsychol*, 16, 155-61.
- CICERONE, K., LEVIN, H., MALEC, J., STUSS, D. & WHYTE, J. 2006. Cognitive rehabilitation interventions for executive function: moving from bench to bedside in patients with traumatic brain injury. *J Cogn Neurosci*, 18, 1212-22.
- CLARK, A. L., DELANO-WOOD, L., SORG, S. F., WERHANE, M. L., HANSON, K. L. & SCHIEHSER, D. M. 2017. Cognitive fatigue is associated with reduced anterior internal capsule integrity in veterans with history of mild to moderate traumatic brain injury. *Brain Imaging Behav*, 11, 1548-1554.
- CLARK, A. L., MERRITT, V. C., BIGLER, E. D., BANGEN, K. J., WERHANE, M., SORG, S. F., BONDI, M. W., SCHIEHSER, D. M. & DELANO-WOOD, L. 2018. Blast-Exposed Veterans With Mild Traumatic Brain Injury Show Greater Frontal Cortical Thinning and Poorer Executive Functioning. *Front Neurol*, 9, 873.
- CLARK, A. L., SORG, S. F., SCHIEHSER, D. M., LUC, N., BONDI, M. W., SANDERSON, M., WERHANE, M. L. & DELANO-WOOD, L. 2016. Deep white matter hyperintensities affect verbal memory independent of PTSD symptoms in veterans with mild traumatic brain injury. *Brain Inj*, 30, 864-71.
- COHEN, B. E., NEYLAN, T. C., YAFFE, K., SAMUELSON, K. W., LI, Y. & BARNES, D. E. 2013. Posttraumatic stress disorder and cognitive function: findings from the mind your heart study. *J Clin Psychiatry*, 74, 1063-70.
- COLDREN, R. L., KELLY, M. P., PARISH, R. V., DRETSCH, M. & RUSSELL, M. L. 2010. Evaluation of the Military Acute Concussion Evaluation for use in combat operations more than 12 hours after injury. *Mil Med*, 175, 477-81.

- COLE, J. H., LEECH, R., SHARP, D. J. & ALZHEIMER'S DISEASE NEUROIMAGING, I. 2015. Prediction of brain age suggests accelerated atrophy after traumatic brain injury. *Ann Neurol*, 77, 571-81.
- COSTANZO, M. E., CHOU, Y. Y., LEAMAN, S., PHAM, D. L., KEYSER, D., NATHAN, D. E., COUGHLIN, M., RAPP, P. & ROY, M. J. 2014. Connecting combat-related mild traumatic brain injury with posttraumatic stress disorder symptoms through brain imaging. *Neurosci Lett*, 577, 11-5.
- COURTNEY, A. & COURTNEY, M. 2015. The Complexity of Biomechanics Causing Primary Blast-Induced Traumatic Brain Injury: A Review of Potential Mechanisms. *Front Neurol*, 6, 221.
- DAVATZIKOS, C. 2004. Why voxel-based morphometric analysis should be used with great caution when characterizing group differences. *Neuroimage*, 23, 17-20.
- DAVENPORT, N. D., GULLICKSON, J. T., GREY, S. F., HIRSCH, S., SPONHEIM, S. R. & CHRONIC EFFECTS OF NEUROTRAUMA, C. 2018. Longitudinal evaluation of ventricular volume changes associated with mild traumatic brain injury in military service members. *Brain Inj*, 32, 1245-1255.
- DAVENPORT, N. D., LIM, K. O., ARMSTRONG, M. T. & SPONHEIM, S. R. 2012. Diffuse and spatially variable white matter disruptions are associated with blast-related mild traumatic brain injury. *Neuroimage*, 59, 2017-24.
- DAVENPORT, N. D., LIM, K. O. & SPONHEIM, S. R. 2015a. Personality and neuroimaging measures differentiate PTSD from mTBI in veterans. *Brain Imaging Behav*, 9, 472-83.
- DAVENPORT, N. D., LIM, K. O. & SPONHEIM, S. R. 2015b. White matter abnormalities associated with military PTSD in the context of blast TBI. *Hum Brain Mapp*, 36, 1053-64.
- DE LANEROLLE, N. C., BANDAK, F., KANG, D., LI, A. Y., DU, F., SWAUGER, P., PARKS, S., LING, G. & KIM, J. H. 2011. Characteristics of an explosive blast-induced brain injury in an experimental model. *J Neuropathol Exp Neurol*, 70, 1046-57.
- DEARDEN, P. 2001. New blast weapons. *J R Army Med Corps*, 147, 80-6.
- DELANO-WOOD, L., BANGEN, K. J., SORG, S. F., CLARK, A. L., SCHIEHSE, D. M., LUC, N., BONDI, M. W., WERHANE, M., KIM, R. T. & BIGLER, E. D. 2015. Brainstem white matter integrity is related to loss of consciousness and postconcussive symptomatology in veterans with chronic mild to moderate traumatic brain injury. *Brain Imaging Behav*, 9, 500-12.
- DELIS, D. C., KRAMER, J. H., KAPLAN, E. & HOLDNACK, J. 2004. Reliability and validity of the Delis-Kaplan Executive Function System: an update. *J Int Neuropsychol Soc*, 10, 301-3.
- DELLA NAVE, R., FORESTI, S., PRATESI, A., GINESTRONI, A., INZITARI, M., SALVADORI, E., GIANNELLI, M., DICIOTTI, S., INZITARI, D. & MASCALCHI, M. 2007. Whole-brain histogram and voxel-based analyses of diffusion tensor imaging in patients with leukoaraiosis: correlation with motor and cognitive impairment. *AJNR Am J Neuroradiol*, 28, 1313-9.
- DEPALMA, R. G., BURRIS, D. G., CHAMPION, H. R. & HODGSON, M. J. 2005. Blast injuries. *N Engl J Med*, 352, 1335-42.
- DEPUE, B. E., OLSON-MADDEN, J. H., SMOLKER, H. R., RAJAMANI, M., BRENNER, L. A. & BANICH, M. T. 2014. Reduced amygdala volume is associated with deficits in inhibitory control: a voxel- and surface-based morphometric analysis of comorbid PTSD/mild TBI. *Biomed Res Int*, 2014, 691505.
- DEWITT, D. S. & PROUGH, D. S. 2009. Blast-induced brain injury and posttraumatic hypotension and hypoxemia. *J Neurotrauma*, 26, 877-87.
- DI, X., GOFORTH, P. B., BULLOCK, R., ELLIS, E. & SATIN, L. 2000. Mechanical injury alters volume activated ion channels in cortical astrocytes. *Acta Neurochir Suppl*, 76, 379-83.
- DING, K., MARQUEZ DE LA PLATA, C., WANG, J. Y., MUMPHREY, M., MOORE, C., HARPER, C., MADDEN, C. J., MCCOLL, R., WHITTEMORE, A., DEVOUS, M. D. & DIAZ-ARRASTIA, R. 2008. Cerebral atrophy after traumatic white matter injury: correlation with acute neuroimaging and outcome. *J Neurotrauma*, 25, 1433-40.
- DOUGLAS, D. B., IV, M., DOUGLAS, P. K., ANDERSON, A., VOS, S. B., BAMMER, R., ZEINEH, M. & WINTERMARK, M. 2015. Diffusion Tensor Imaging of TBI: Potentials and Challenges. *Top Magn Reson Imaging*, 24, 241-51.
- DROBYSHEVSKY, A., BAUMANN, S. B. & SCHNEIDER, W. 2006. A rapid fMRI task battery for mapping of visual, motor, cognitive, and emotional function. *Neuroimage*, 31, 732-44.
- DUVERNOY 1998. The Human Hippocampus Functional Anatomy, Vascularization and Serial Sections with MRI. *Springer*.
- DYRBY, T. B., LUNDELL, H., BURKE, M. W., REISLEV, N. L., PAULSON, O. B., PTITO, M. & SIEBNER, H. R. 2014. Interpolation of diffusion weighted imaging datasets. *Neuroimage*, 103, 202-213.
- EFROYMSON, M. A. 1960. Multiple regression analysis. *Mathematical Methods for Digital Computers*.
- EMERY, D. G., LUCAS, J. H. & GROSS, G. W. 1987. The sequence of ultrastructural changes in cultured neurons after dendrite transection. *Exp Brain Res*, 67, 41-51.
- FANSELOW, M. S. & DONG, H. W. 2010. Are the dorsal and ventral hippocampus functionally distinct structures? *Neuron*, 65, 7-19.
- FINKEL, A. G., YERRY, J. A., KLARIC, J. S., IVINS, B. J., SCHER, A. & CHOI, Y. S. 2017. Headache in military service members with a history of mild traumatic brain injury: A cohort study of diagnosis and classification. *Cephalalgia*, 37, 548-559.
- FISCHER, B. L., PARSONS, M., DURGERIAN, S., REECE, C., MOURANY, L., LOWE, M. J., BEALL, E. B., KOENIG, K. A., JONES, S. E., NEWSOME, M. R., SCHEIBEL, R. S., WILDE, E. A., TROYANSKAYA, M., MERKLEY, T. L., WALKER, M., LEVIN, H. S. & RAO, S. M. 2014. Neural activation during response inhibition differentiates blast from mechanical causes of mild to moderate traumatic brain injury. *J Neurotrauma*, 31, 169-79.
- FLEMINGER, S., OLIVER, D. L., LOVESTONE, S., RABE-HESKETH, S. & GIORA, A. 2003. Head injury as a risk factor for Alzheimer's disease: the evidence 10 years on; a partial replication. *J Neurol Neurosurg Psychiatry*, 74, 857-62.
- FLOYD, C. L., GORIN, F. A. & LYETH, B. G. 2005. Mechanical strain injury increases intracellular sodium and reverses Na<sup>+</sup>/Ca<sup>2+</sup> exchange in cortical astrocytes. *Glia*, 51, 35-46.
- FLOYD, C. L., RZIGALINSKI, B. A., SITTERDING, H. A., WILLOUGHBY, K. A. & ELLIS, E. F. 2004. Antagonism of group I metabotropic glutamate receptors and PLC attenuates increases in inositol trisphosphate and reduces reactive gliosis in strain-injured astrocytes. *J Neurotrauma*, 21, 205-16.
- FLOYD, C. L., RZIGALINSKI, B. A., WEBER, J. T., SITTERDING, H. A., WILLOUGHBY, K. A. & ELLIS, E. F. 2001. Traumatic injury of cultured astrocytes alters inositol (1,4,5)-trisphosphate-mediated signaling. *Glia*, 33, 12-23.
- FORTIER-BROCHU, E. & MORIN, C. M. 2014. Cognitive impairment in individuals with insomnia: clinical significance and correlates. *Sleep*, 37, 1787-98.
- FREE, S. L., BERGIN, P. S., FISH, D. R., COOK, M. J., SHORVON, S. D. & STEVENS, J. M. 1995. Methods for normalization of hippocampal volumes measured with MR. *AJNR Am J Neuroradiol*, 16, 637-43.



- FULTON, J. J., CALHOUN, P. S., WAGNER, H. R., SCHRY, A. R., HAIR, L. P., FEELING, N., ELBOGEN, E. & BECKHAM, J. C. 2015. The prevalence of posttraumatic stress disorder in Operation Enduring Freedom/Operation Iraqi Freedom (OEF/OIF) Veterans: a meta-analysis. *J Anxiety Disord*, 31, 98-107.
- GATES, M. A., HOLOWKA, D. W., VASTERLING, J. J., KEANE, T. M., MARX, B. P. & ROSEN, R. C. 2012. Posttraumatic stress disorder in veterans and military personnel: epidemiology, screening, and case recognition. *Psychol Serv*, 9, 361-82.
- GENTRY, L. R., GODERSKY, J. C. & THOMPSON, B. 1988. MR imaging of head trauma: review of the distribution and radiopathologic features of traumatic lesions. *AJR Am J Roentgenol*, 150, 663-72.
- GERMAIN, A., RICHARDSON, R., STOCKER, R., MAMMEN, O., HALL, M., BRAMOWETH, A. D., BEGLEY, A., RODE, N., FRANK, E., HAAS, G. & BUYSE, D. J. 2014. Treatment for insomnia in combat-exposed OEF/OIF/OND military veterans: preliminary randomized controlled trial. *Behav Res Ther*, 61, 78-88.
- GHAJARI, M., HELLYER, P. J. & SHARP, D. J. 2017. Computational modelling of traumatic brain injury predicts the location of chronic traumatic encephalopathy pathology. *Brain*, 140, 333-343.
- GILMORE, C. S., CAMCHONG, J., DAVENPORT, N. D., NELSON, N. W., KARDON, R. H., LIM, K. O. & SPONHEIM, S. R. 2016. Deficits in Visual System Functional Connectivity after Blast-Related Mild TBI are Associated with Injury Severity and Executive Dysfunction. *Brain Behav*, 6, e00454.
- GLASS, T. F., REEVES, B. & SHARP, F. R. 2002. Modeling both the mechanical and hypoxic features of traumatic brain injury in vitro in rats. *Neurosci Lett*, 328, 133-6.
- GOEBEL, R. 2020. Boundary-Based Registration. Available from: <https://download.brainvoyager.com/bv/doc/UsersGuide/Coregistration/Boundary-BasedRegistration.html>.
- GOELLER, J., WARDLAW, A., TREICHLER, D., O'BRUBA, J. & WEISS, G. 2012. Investigation of cavitation as a possible damage mechanism in blast-induced traumatic brain injury. *J Neurotrauma*, 29, 1970-81.
- GOLDSTEIN, L. E., FISHER, A. M., TAGGE, C. A., ZHANG, X. L., VELISEK, L., SULLIVAN, J. A., UPRETI, C., KRACHT, J. M., ERICSSON, M., WOJNAROWICZ, M. W., GOLETIANI, C. J., MAGLAKELIDZE, G. M., CASEY, N., MONCASTER, J. A., MINAEVA, O., MOIR, R. D., NOWINSKI, C. J., STERN, R. A., CANTU, R. C., GEILING, J., BLUSZTAJN, J. K., WOLOZIN, B. L., IKEZU, T., STEIN, T. D., BUDSON, A. E., KOWALL, N. W., CHARGIN, D., SHARON, A., SAMAN, S., HALL, G. F., MOSS, W. C., CLEVELAND, R. O., TANZI, R. E., STANTON, P. K. & MCKEE, A. C. 2012. Chronic traumatic encephalopathy in blast-exposed military veterans and a blast neurotrauma mouse model. *Sci Transl Med*, 4, 134ra60.
- GOLDSTEIN, L. E., MCKEE, A. C. & STANTON, P. K. 2014. Considerations for animal models of blast-related traumatic brain injury and chronic traumatic encephalopathy. *Alzheimers Res Ther*, 6, 64.
- GOODRICH, G. L., FLYG, H. M., KIRBY, J. E., CHANG, C. Y. & MARTINSEN, G. L. 2013. Mechanisms of TBI and visual consequences in military and veteran populations. *Optom Vis Sci*, 90, 105-12.
- GORGORAPTIS, N., ZAW-LINN, J., FEENEY, C., TENORIO-JIMENEZ, C., NIEMI, M., MALIK, A., HAM, T., GOLDSTONE, A. P. & SHARP, D. J. 2019. Cognitive impairment and health-related quality of life following traumatic brain injury. *NeuroRehabilitation*, 44, 321-331.
- GRAHAM, D. I., ADAMS, J. H., NICOLL, J. A., MAXWELL, W. L. & GENNARELLI, T. A. 1995. The nature, distribution and causes of traumatic brain injury. *Brain Pathol*, 5, 397-406.
- GRAHAM, N. S. S., D.J. 2019. Understanding neurodegeneration after traumatic brain injury: from mechanisms to clinical trials in dementia. *Journal of Neurology Neurosurgery Psychiatry*, 90, 1221-1233.
- GREER, N., SAYER, N., KOELLER, E., VELASQUEZ, T. & WILT, T. J. 2018. Outcomes Associated With Blast Versus Nonblast-Related Traumatic Brain Injury in US Military Service Members and Veterans: A Systematic Review. *J Head Trauma Rehabil*, 33, E16-E29.
- GREVE, D. N. & FISCHL, B. 2009. Accurate and robust brain image alignment using boundary-based registration. *Neuroimage*, 48, 63-72.
- GUPTA, R. K. & PRZEKAS, A. 2013. Mathematical Models of Blast-Induced TBI: Current Status, Challenges, and Prospects. *Front Neurol*, 4, 59.
- GURDJIAN, E. S. 1975. e-evaluation of the biomechanics of blunt impact injury of the head. *Surgery, gynecology, obstetrics*, 140, 845-850.
- HAN, K., MAC DONALD, C. L., JOHNSON, A. M., BARNES, Y., WIERZECZOWSKI, L., ZONIES, D., OH, J., FLAHERTY, S., FANG, R., RAICHLE, M. E. & BRODY, D. L. 2014. Disrupted modular organization of resting-state cortical functional connectivity in U.S. military personnel following concussive 'mild' blast-related traumatic brain injury. *Neuroimage*, 84, 76-96.
- HARIRI, R. J., CHANG, V. A., BARIE, P. S., WANG, R. S., SHARIF, S. F. & GHAJAR, J. B. 1994. Traumatic injury induces interleukin-6 production by human astrocytes. *Brain Res*, 636, 139-42.
- HARRIS, T. C., DE ROOIJ, R. & KUHL, E. 2019. The Shrinking Brain: Cerebral Atrophy Following Traumatic Brain Injury. *Ann Biomed Eng*, 47, 1941-1959.
- HAYES, J. P., MILLER, D. R., LAFLECHE, G., SALAT, D. H. & VERFAELLIE, M. 2015. The nature of white matter abnormalities in blast-related mild traumatic brain injury. *Neuroimage Clin*, 8, 148-56.
- HELLYER, P. J., LEECH, R., HAM, T. E., BONNELLE, V. & SHARP, D. J. 2013. Individual prediction of white matter injury following traumatic brain injury. *Ann Neurol*, 73, 489-99.
- HERNANDEZ, A., TAN, C., PLATTNER, F., LOGSDON, A. F., POZO, K., YOUSUF, M. A., SINGH, T., TURNER, R. C., LUKE-WOLD, B. P., HUBER, J. D., ROSEN, C. L. & BIBB, J. A. 2018. Exposure to mild blast forces induces neuropathological effects, neurophysiological deficits and biochemical changes. *Mol Brain*, 11, 64.
- HETHERINGTON, H. P., HAMID, H., KULAS, J., LING, G., BANDAK, F., DE LANEROLLE, N. C. & PAN, J. W. 2014. MRSI of the medial temporal lobe at 7 T in explosive blast mild traumatic brain injury. *Magn Reson Med*, 71, 1358-67.
- HOFFER, M. E., BALABAN, C., GOTTSALL, K., BALOUGH, B. J., MADDOX, M. R. & PENTA, J. R. 2010. Blast exposure: vestibular consequences and associated characteristics. *Otol Neurotol*, 31, 232-6.
- HOFFER, M. E., DONALDSON, C., GOTTSALL, K. R., BALABAN, C. & BALOUGH, B. J. 2009. Blunt and blast head trauma: different entities. *Int Tinnitus J*, 15, 115-8.
- HOFFMAN, S. W., RZIGALINSKI, B. A., WILLOUGHBY, K. A. & ELLIS, E. F. 2000. Astrocytes generate isoprostanes in response to trauma or oxygen radicals. *J Neurotrauma*, 17, 415-20.
- HOGUE, C. W., MCGURK, D., THOMAS, J. L., COX, A. L., ENGEL, C. C. & CASTRO, C. A. 2008. Mild traumatic brain injury in U.S. Soldiers returning from Iraq. *N Engl J Med*, 358, 453-63.

- HORBRUEGGER, M., LOEWE, K., KAUFMANN, J., WAGNER, M., SCHIPPLING, S., PAWLITZKI, M. & SCHOENFELD, M. A. 2019. Anatomically constrained tractography facilitates biologically plausible fiber reconstruction of the optic radiation in multiple sclerosis. *Neuroimage Clin*, 22, 101740.
- HOWARD, D. & STURTEVANT, B. 1997. In vitro study of the mechanical effects of shock-wave lithotripsy. *Ultrasound Med Biol*, 23, 1107-22.
- HUANG, M. X., HARRINGTON, D. L., ROBB SWAN, A., ANGELES QUINTO, A., NICHOLS, S., DRAKE, A., SONG, T., DIWAKAR, M., HUANG, C. W., RISBROUGH, V. B., DALE, A., BARTSCH, H., MATTHEWS, S., HUANG, J. W., LEE, R. R. & BAKER, D. G. 2017. Resting-State Magnetoencephalography Reveals Different Patterns of Aberrant Functional Connectivity in Combat-Related Mild Traumatic Brain Injury. *J Neurotrauma*, 34, 1412-1426.
- HUANG, M. X., NICHOLS, S., BAKER, D. G., ROBB, A., ANGELES, A., YURGIL, K. A., DRAKE, A., LEVY, M., SONG, T., MCLAY, R., THEILMANN, R. J., DIWAKAR, M., RISBROUGH, V. B., JI, Z., HUANG, C. W., CHANG, D. G., HARRINGTON, D. L., MUZZATTI, L., CANIVE, J. M., CHRISTOPHER EDGAR, J., CHEN, Y. H. & LEE, R. R. 2009. Single-subject-based whole-brain MEG slow-wave imaging approach for detecting abnormality in patients with mild traumatic brain injury. *Neuroimage Clin*, 5, 109-19.
- HUANG, M. X., NICHOLS, S., ROBB, A., ANGELES, A., DRAKE, A., HOLLAND, M., ASMUSSEN, S., D'ANDREA, J., CHUN, W., LEVY, M., CUI, L., SONG, T., BAKER, D. G., HAMMER, P., MCLAY, R., THEILMANN, R. J., COIMBRA, R., DIWAKAR, M., BOYD, C., NEFF, J., LIU, T. T., WEBB-MURPHY, J., FARINPOUR, R., CHEUNG, C., HARRINGTON, D. L., HEISTER, D. & LEE, R. R. 2012. An automatic MEG low-frequency source imaging approach for detecting injuries in mild and moderate TBI patients with blast and non-blast causes. *Neuroimage*, 61, 1067-82.
- HUANG, M. X., THEILMANN, R. J., ROBB, A., ANGELES, A., NICHOLS, S., DRAKE, A., D'ANDREA, J., LEVY, M., HOLLAND, M., SONG, T., GE, S., HWANG, E., YOO, K., CUI, L., BAKER, D. G., TRAUNER, D., COIMBRA, R. & LEE, R. R. 2009. Integrated imaging approach with MEG and DTI to detect mild traumatic brain injury in military and civilian patients. *J Neurotrauma*, 26, 1213-26.
- HUISMAN, T. A. 2010. Diffusion-weighted and diffusion tensor imaging of the brain, made easy. *Cancer Imaging*, 10 Spec no A, S163-71.
- HULKOWER, M. B., POLIAK, D. B., ROSENBAUM, S. B., ZIMMERMAN, M. E. & LIPTON, M. L. 2013. A decade of DTI in traumatic brain injury: 10 years and 100 articles later. *AJNR Am J Neuroradiol*, 34, 2064-74.
- HUMBLE, S. S., WILSON, L. D., WANG, L., LONG, D. A., SMITH, M. A., SIKTBERG, J. C., MIRHOSEINI, M. F., BHATIA, A., PRUTHI, S., DAY, M. A., MUEHLSCHLEGEL, S. & PATEL, M. B. 2018. Prognosis of diffuse axonal injury with traumatic brain injury. *J Trauma Acute Care Surg*, 85, 155-159.
- IM, C. H., JUNG, H. H., CHOI, J. D., LEE, S. Y. & JUNG, K. Y. 2008. Determination of optimal electrode positions for transcranial direct current stimulation (tDCS). *Phys Med Biol*, 53, N219-25.
- ISAAC, L., MAIN, K. L., SOMAN, S., GOTLIB, I. H., FURST, A. J., KINOSHITA, L. M., FAIRCHILD, J. K., YESAVAGE, J. A., ASHFORD, J. W., BAYLEY, P. J. & ADAMSON, M. M. 2015. The impact of depression on Veterans with PTSD and traumatic brain injury: a diffusion tensor imaging study. *Biol Psychol*, 105, 20-8.
- JAHANSHAD, N., KOCHUNOV, P. V., SPROOTEN, E., MANDL, R. C., NICHOLS, T. E., ALMASY, L., BLANGERO, J., BROUWER, R. M., CURRAN, J. E., DE ZUBICARAY, G. I., DUGGIRALA, R., FOX, P. T., HONG, L. E., LANDMAN, B. A., MARTIN, N. G., MCMAHON, K. L., MEDLAND, S. E., MITCHELL, B. D., OLVERA, R. L., PETERSON, C. P., STARR, J. M., SUSSMANN, J. E., TOGA, A. W., WARDLAW, J. M., WRIGHT, M. J., HULSHOFF POL, H. E., BASTIN, M. E., MCINTOSH, A. M., DEARY, I. J., THOMPSON, P. M. & GLAHN, D. C. 2013. Multi-site genetic analysis of diffusion images and voxelwise heritability analysis: a pilot project of the ENIGMA-DTI working group. *Neuroimage*, 81, 455-469.
- JELLISON, B. J., FIELD, A. S., MEDOW, J., LAZAR, M., SALAMAT, M. S. & ALEXANDER, A. L. 2004. Diffusion tensor imaging of cerebral white matter: a pictorial review of physics, fiber tract anatomy, and tumor imaging patterns. *AJNR Am J Neuroradiol*, 25, 356-69.
- JILKA, S. R., SCOTT, G., HAM, T., PICKERING, A., BONNELLE, V., BRAGA, R. M., LEECH, R. & SHARP, D. J. 2014. Damage to the Salience Network and interactions with the Default Mode Network. *J Neurosci*, 34, 10798-807.
- JJ VASTERLING, C. B. 2005. *Neuropsychology of PTSD: Biological, cognitive, and clinical perspectives*.
- JOLLY, A. E., BALLET, M., AZOR, A., FRIEDLAND, D., SANDRONE, S., GRAHAM, N. S. N., ZIMMERMAN, K. & SHARP, D. J. 2020. Detecting axonal injury in individual patients after traumatic brain injury. *Brain*.
- JONES, D. K. & CERCIGNANI, M. 2010. Twenty-five pitfalls in the analysis of diffusion MRI data. *NMR Biomed*, 23, 803-20.
- JORGE, R. E., ACION, L., WHITE, T., TORDESILLAS-GUTIERREZ, D., PIERSON, R., CRESPO-FACORRO, B. & MAGNOTTA, V. A. 2012. White matter abnormalities in veterans with mild traumatic brain injury. *Am J Psychiatry*, 169, 1284-91.
- KAMNAKSH, A., BUDDE, M. D., KOVESDI, E., LONG, J. B., FRANK, J. A. & AGOSTON, D. V. 2014. Diffusion tensor imaging reveals acute subcortical changes after mild blast-induced traumatic brain injury. *Sci Rep*, 4, 4809.
- KANTARCI, K. 2014. Fractional anisotropy of the fornix and hippocampal atrophy in Alzheimer's disease. *Front Aging Neurosci*, 6, 316.
- KENNEDY, C. H., PORTER EVANS, J., CHEE, S., MOORE, J. L., BARTH, J. T. & STUESSI, K. A. 2012. Return to combat duty after concussive blast injury. *Arch Clin Neuropsychol*, 27, 817-27.
- KENNEDY, M. R., WOZNIAK, J. R., MUETZEL, R. L., MUELLER, B. A., CHIOU, H. H., PANTEKOEK, K. & LIM, K. O. 2009. White matter and neurocognitive changes in adults with chronic traumatic brain injury. *J Int Neuropsychol Soc*, 15, 130-6.
- KIM, E. J., PELLMAN, B. & KIM, J. J. 2015. Stress effects on the hippocampus: a critical review. *Learn Mem*, 22, 411-6.
- KIM, N., BRANCH, C. A., KIM, M. & LIPTON, M. L. 2013. Whole brain approaches for identification of microstructural abnormalities in individual patients: comparison of techniques applied to mild traumatic brain injury. *PLoS One*, 8, e59382.
- KINLEIN, S. A., WILSON, C. D. & KARATSOREOS, I. N. 2015. Dysregulated hypothalamic-pituitary-adrenal axis function contributes to altered endocrine and neurobehavioral responses to acute stress. *Front Psychiatry*, 6, 31.
- KINNUNEN, K. M., GREENWOOD, R., POWELL, J. H., LEECH, R., HAWKINS, P. C., BONNELLE, V., PATEL, M. C., COUNSELL, S. J. & SHARP, D. J. 2011. White matter damage and cognitive impairment after traumatic brain injury. *Brain*, 134, 449-63.
- KIRKMAN, E., WATTS, S. & COOPER, G. 2011. Blast injury research models. *Philos Trans R Soc Lond B Biol Sci*, 366, 144-59.
- KITAYAMA, N., VACCARINO, V., KUTNER, M., WEISS, P. & BRENNER, J. D. 2005. Magnetic resonance imaging (MRI) measurement of hippocampal volume in posttraumatic stress disorder: a meta-analysis. *J Affect Disord*, 88, 79-86.



- KONTOS, A. P., VAN COTT, A. C., ROBERTS, J., PAN, J. W., KELLY, M. B., MCALLISTER-DEITRICK, J. & HETHERINGTON, H. P. 2017. Clinical and Magnetic Resonance Spectroscopic Imaging Findings in Veterans With Blast Mild Traumatic Brain Injury and Post-Traumatic Stress Disorder. *Mil Med*, 182, 99-104.
- KRAUS, M. F., SUSMARAS, T., CAUGHLIN, B. P., WALKER, C. J., SWEENEY, J. A. & LITTLE, D. M. 2007. White matter integrity and cognition in chronic traumatic brain injury: a diffusion tensor imaging study. *Brain*, 130, 2508-19.
- KRUEGER, F., PARDINI, M., HUEY, E. D., RAYMONT, V., SOLOMON, J., LIPSKY, R. H., HODGKINSON, C. A., GOLDMAN, D. & GRAFMAN, J. 2011. The role of the Met66 brain-derived neurotrophic factor allele in the recovery of executive functioning after combat-related traumatic brain injury. *J Neurosci*, 31, 598-606.
- KUEHN, R., SIMARD, P. F., DRISCOLL, I., KELEDJIAN, K., IVANOVA, S., TOSUN, C., WILLIAMS, A., BOCHICCHIO, G., GERZANICH, V. & SIMARD, J. M. 2011. Rodent model of direct cranial blast injury. *J Neurotrauma*, 28, 2155-69.
- LAGRAVERE, M. O., CAREY, J., TOOGOOD, R. W. & MAJOR, P. W. 2008. Three-dimensional accuracy of measurements made with software on cone-beam computed tomography images. *Am J Orthod Dentofacial Orthop*, 134, 112-6.
- LAMB, R. G., HARPER, C. C., MCKINNEY, J. S., RZIGALINSKI, B. A. & ELLIS, E. F. 1997. Alterations in phosphatidylcholine metabolism of stretch-injured cultured rat astrocytes. *J Neurochem*, 68, 1904-10.
- LAMBERTY, G. J., NELSON, N. W. & YAMADA, T. 2013. Effects and outcomes in civilian and military traumatic brain injury: similarities, differences, and forensic implications. *Behav Sci Law*, 31, 814-32.
- LE BIHAN, D. & JOHANSEN-BERG, H. 2012. Diffusion MRI at 25: exploring brain tissue structure and function. *Neuroimage*, 61, 324-41.
- LEE, T., JAROME, T., LI, S. J., KIM, J. J. & HELMSTETTER, F. J. 2009. Chronic stress selectively reduces hippocampal volume in rats: a longitudinal magnetic resonance imaging study. *Neuroreport*, 20, 1554-8.
- LEVI, L., BOROVICH, B., GUILBURD, J. N., GRUSHKIEWICZ, I., LEMBERGER, A., LINN, S., SCHACHTER, I., ZAAROR, M., BRAUN, J. & FEINSOD, M. 1990. Wartime neurosurgical experience in Lebanon, 1982-85. II: Closed craniocerebral injuries. *Isr J Med Sci*, 26, 555-8.
- LEVIN, H. S., WILDE, E., TROYANSKAYA, M., PETERSEN, N. J., SCHEIBEL, R., NEWSOME, M., RADAIDEH, M., WU, T., YALLAMPALLI, R., CHU, Z. & LI, X. 2010. Diffusion tensor imaging of mild to moderate blast-related traumatic brain injury and its sequelae. *J Neurotrauma*, 27, 683-94.
- LEW, H. L., GARVERT, D. W., POGODA, T. K., HSU, P. T., DEVINE, J. M., WHITE, D. K., MYERS, P. J. & GOODRICH, G. L. 2009. Auditory and visual impairments in patients with blast-related traumatic brain injury: Effect of dual sensory impairment on Functional Independence Measure. *J Rehabil Res Dev*, 46, 819-26.
- LEW, H. L., POGODA, T. K., BAKER, E., STOLZMANN, K. L., METERKO, M., CIFU, D. X., AMARA, J. & HENDRICKS, A. M. 2011. Prevalence of dual sensory impairment and its association with traumatic brain injury and blast exposure in OEF/OIF veterans. *J Head Trauma Rehabil*, 26, 489-96.
- LINDEMER, E. R., SALAT, D. H., LERITZ, E. C., MCGLINCHEY, R. E. & MILBERG, W. P. 2013. Reduced cortical thickness with increased lifetime burden of PTSD in OEF/OIF Veterans and the impact of comorbid TBI. *Neuroimage Clin*, 2, 601-11.
- LINDQUIST, L. K., LOVE, H. C. & ELBOGEN, E. B. 2017. Traumatic Brain Injury in Iraq and Afghanistan Veterans: New Results From a National Random Sample Study. *J Neuropsychiatry Clin Neurosci*, 29, 254-259.
- LING, G., BANDAK, F., ARMONDA, R., GRANT, G. & ECKLUND, J. 2009. Explosive blast neurotrauma. *J Neurotrauma*, 26, 815-25.
- LIPPA, S. M., FONDA, J. R., FORTIER, C. B., AMICK, M. A., KENNA, A., MILBERG, W. P. & MCGLINCHEY, R. E. 2015. Deployment-related psychiatric and behavioral conditions and their association with functional disability in OEF/OIF/OND veterans. *J Trauma Stress*, 28, 25-33.
- LIPTON, M. L., KIM, N., PARK, Y. K., HULKOWER, M. B., GARDIN, T. M., SHIFTEH, K., KIM, M., ZIMMERMAN, M. E., LIPTON, R. B. & BRANCH, C. A. 2012. Robust detection of traumatic axonal injury in individual mild traumatic brain injury patients: intersubject variation, change over time and bidirectional changes in anisotropy. *Brain Imaging Behav*, 6, 329-42.
- LISSNER, H. R., LEBOW, M. & EVANS, F. G. 1960. Experimental studies on the relation between acceleration and intracranial pressure changes in man. *Surg Gynecol Obstet*, 111, 329-38.
- LOGUE, M. W., VAN ROOIJ, S. J. H., DENNIS, E. L., DAVIS, S. L., HAYES, J. P., STEVENS, J. S., DENSMORE, M., HASWELL, C. C., IPSER, J., KOCH, S. B. J., KORGAONKAR, M., LEBOS, L. A. M., PEVERILL, M., BAKER, J. T., BOEDHOE, P. S. W., FRIJLING, J. L., GRUBER, S. A., HARPAZ-ROTEM, I., JAHANSHAD, N., KOPOWITZ, S., LEVY, I., NAWIJN, L., O'CONNOR, L., OLFF, M., SALAT, D. H., SHERIDAN, M. A., SPIELBERG, J. M., VAN ZUIDEN, M., WINTERITZ, S. R., WOLFF, J. D., WOLF, E. J., WANG, X., WROCKLAGE, K., ABDALLAH, C. G., BRYANT, R. A., GEUZE, E., JOVANOVIĆ, T., KAUFMAN, M. L., KING, A. P., KRYSTAL, J. H., LAGOPOULOS, J., BENNETT, M., LANIUS, R., LIBERZON, I., MCGLINCHEY, R. E., MCCLAUGHLIN, K. A., MILBERG, W. P., MILLER, M. W., RESSLER, K. J., VELTMAN, D. J., STEIN, D. J., THOMAS, K., THOMPSON, P. M. & MOREY, R. A. 2018. Smaller Hippocampal Volume in Posttraumatic Stress Disorder: A Multisite ENIGMA-PGC Study: Subcortical Volumetry Results From Posttraumatic Stress Disorder Consortia. *Biol Psychiatry*, 83, 244-253.
- LONG, J. B., BENTLEY, T. L., WESSNER, K. A., CERONE, C., SWEENEY, S. & BAUMAN, R. A. 2009. Blast overpressure in rats: recreating a battlefield injury in the laboratory. *J Neurotrauma*, 26, 827-40.
- LOPEZ-LARSON, M., KING, J. B., MCGLADE, E., BUELER, E., STOECKEL, A., EPSTEIN, D. J. & YURGELUN-TODD, D. 2013. Enlarged thalamic volumes and increased fractional anisotropy in the thalamic radiations in veterans with suicide behaviors. *Front Psychiatry*, 4, 83.
- LUCAS, J. H., GROSS, G. W., EMERY, D. G. & GARDNER, C. R. 1985. Neuronal survival or death after dendrite transection close to the perikaryon: correlation with electrophysiologic, morphologic, and ultrastructural changes. *Cent Nerv Syst Trauma*, 2, 231-55.
- LUCAS, J. H. & WOLF, A. 1991. In vitro studies of multiple impact injury to mammalian CNS neurons: prevention of perikaryal damage and death by ketamine. *Brain Res*, 543, 181-93.
- MAC DONALD, C., JOHNSON, A., COOPER, D., MALONE, T., SORRELL, J., SHIMONY, J., PARSONS, M., SNYDER, A., RAICHE, M., FANG, R., FLAHERTY, S., RUSSELL, M. & BRODY, D. L. 2013. Cerebellar white matter abnormalities following primary blast injury in US military personnel. *PLoS One*, 8, e55823.
- MAC DONALD, C. L., BARBER, J., ANDRE, J., PANKS, C., ZALEWSKI, K. & TEMKIN, N. 2019. Longitudinal neuroimaging following combat concussion: sub-acute, 1 year and 5 years post-injury. *Brain Commun*, 1, fcz031.
- MAC DONALD, C. L., DIKRANIAN, K., SONG, S. K., BAYLY, P. V., HOLTZMAN, D. M. & BRODY, D. L. 2007. Detection of traumatic axonal injury with diffusion tensor imaging in a mouse model of traumatic brain injury. *Exp Neurol*, 205, 116-31.

- MAC DONALD, C. L., JOHNSON, A. M., COOPER, D., NELSON, E. C., WERNER, N. J., SHIMONY, J. S., SNYDER, A. Z., RAICHLE, M. E., WITHEROW, J. R., FANG, R., FLAHERTY, S. F. & BRODY, D. L. 2011. Detection of blast-related traumatic brain injury in U.S. military personnel. *N Engl J Med*, 364, 2091-100.
- MAGONE, M. T., KWON, E. & SHIN, S. Y. 2014. Chronic visual dysfunction after blast-induced mild traumatic brain injury. *J Rehabil Res Dev*, 51, 71-80.
- MAIN, K. L., SOMAN, S., PESTILLI, F., FURST, A., NODA, A., HERNANDEZ, B., KONG, J., CHENG, J., FAIRCHILD, J. K., TAYLOR, J., YESAVAGE, J., WESSON ASHFORD, J., KRAEMER, H. & ADAMSON, M. M. 2017. DTI measures identify mild and moderate TBI cases among patients with complex health problems: A receiver operating characteristic analysis of U.S. veterans. *Neuroimage Clin*, 16, 1-16.
- MALEC, J. F., BROWN, A. W., LEIBSON, C. L., FLAADA, J. T., MANDREKAR, J. N., DIEHL, N. N. & PERKINS, P. K. 2007. The mayo classification system for traumatic brain injury severity. *J Neurotrauma*, 24, 1417-24.
- MALLER, J. J., THOMSON, R. H., PANNEK, K., BAILEY, N., LEWIS, P. M. & FITZGERALD, P. B. 2014. Volumetrics relate to the development of depression after traumatic brain injury. *Behav Brain Res*, 271, 147-53.
- MARK JENKINSON, M. C. 2018. *Introduction to Neuroimaging Analysis*, Oxford, Oxford University press.
- MARKLUND, N., BAKSHI, A., CASTELBUONO, D. J., CONTE, V. & MCINTOSH, T. K. 2006. Evaluation of pharmacological treatment strategies in traumatic brain injury. *Curr Pharm Des*, 12, 1645-80.
- MARTIJN FROELING, A. L. 2016. *Chapter 9: DTI Analysis Methods: Region of Interest Analysis*, Springer Science+Business Media New York 2016.
- MASEL, B. E., BELL, R. S., BROSSART, S., GRILL, R. J., HAYES, R. L., LEVIN, H. S., RASBAND, M. N., RITZEL, D. V., WADE, C. E. & DEWITT, D. S. 2012. Galveston Brain Injury Conference 2010: clinical and experimental aspects of blast injury. *J Neurotrauma*, 29, 2143-71.
- MATHEWS, Z. R. & KOYFMAN, A. 2015. Blast Injuries. *J Emerg Med*, 49, 573-87.
- MATTHEWS, S., SIMMONS, A. & STRIGO, I. 2011a. The effects of loss versus alteration of consciousness on inhibition-related brain activity among individuals with a history of blast-related concussion. *Psychiatry Res*, 191, 76-9.
- MATTHEWS, S., SPADONI, A., KNOX, K., STRIGO, I. & SIMMONS, A. 2012a. Combat-exposed war veterans at risk for suicide show hyperactivation of prefrontal cortex and anterior cingulate during error processing. *Psychosom Med*, 74, 471-5.
- MATTHEWS, S. C., SPADONI, A. D., LOHR, J. B., STRIGO, I. A. & SIMMONS, A. N. 2012b. Diffusion tensor imaging evidence of white matter disruption associated with loss versus alteration of consciousness in warfighters exposed to combat in Operations Enduring and Iraqi Freedom. *Psychiatry Res*, 204, 149-54.
- MATTHEWS, S. C., STRIGO, I. A., SIMMONS, A. N., O'CONNELL, R. M., REINHARDT, L. E. & MOSELEY, S. A. 2011b. A multimodal imaging study in U.S. veterans of Operations Iraqi and Enduring Freedom with and without major depression after blast-related concussion. *Neuroimage*, 54 Suppl 1, S69-75.
- MAZZIOTTA, J. C., TOGA, A. W., EVANS, A., FOX, P. & LANCASTER, J. 1995. A probabilistic atlas of the human brain: theory and rationale for its development. The International Consortium for Brain Mapping (ICBM). *Neuroimage*, 2, 89-101.
- MCDONALD, B. C., SAYKIN, A. J. & MCALLISTER, T. W. 2012. Functional MRI of mild traumatic brain injury (mTBI): progress and perspectives from the first decade of studies. *Brain Imaging Behav*, 6, 193-207.
- MCEWEN, B. S. & SAPOLSKY, R. M. 1995. Stress and cognitive function. *Curr Opin Neurobiol*, 5, 205-16.
- MCGLADE, E., ROGOWSKA, J. & YURGELUN-TODD, D. 2015. Sex differences in orbitofrontal connectivity in male and female veterans with TBI. *Brain Imaging Behav*, 9, 535-49.
- MCKEE, A. C. & ROBINSON, M. E. 2014. Military-related traumatic brain injury and neurodegeneration. *Alzheimers Dement*, 10, S242-53.
- MCLAY, R. N., KLAM, W. P. & VOLKERT, S. L. 2010. Insomnia is the most commonly reported symptom and predicts other symptoms of post-traumatic stress disorder in U.S. service members returning from military deployments. *Mil Med*, 175, 759-62.
- MENDEZ, M. F., OWENS, E. M., REZA BERENJI, G., PEPPERS, D. C., LIANG, L. J. & LICHT, E. A. 2013. Mild traumatic brain injury from primary blast vs. blunt forces: post-concussion consequences and functional neuroimaging. *NeuroRehabilitation*, 32, 397-407.
- MENG, L., JIANG, J., JIN, C., LIU, J., ZHAO, Y., WANG, W., LI, K. & GONG, Q. 2016. Trauma-specific Grey Matter Alterations in PTSD. *Sci Rep*, 6, 33748.
- MENG, Y., QIU, C., ZHU, H., LAMA, S., LUI, S., GONG, Q. & ZHANG, W. 2014. Anatomical deficits in adult posttraumatic stress disorder: a meta-analysis of voxel-based morphometry studies. *Behav Brain Res*, 270, 307-15.
- MICHAEL, A. P., STOUT, J., ROSKOS, P. T., BOLZENIUS, J., GFELLER, J., MOGUL, D. & BUCHOLZ, R. 2015. Evaluation of Cortical Thickness after Traumatic Brain Injury in Military Veterans. *J Neurotrauma*, 32, 1751-8.
- MICHAEL CHAPPELL, T. O., MARK JENKINSON 2018. *Short introduction to MRI Physics for Neuroimaging Analysis*, Oxford University Press.
- MILLER, D. R., HAYES, J. P., LAFLECHE, G., SALAT, D. H. & VERFAELLIE, M. 2017. White matter abnormalities are associated with overall cognitive status in blast-related mTBI. *Brain Imaging Behav*, 11, 1129-1138.
- MISTRY J., M. N. 2017. Traumatic brain injury in adults. *Royal College of General Practitioners*, 10, 608-613.
- MOORE, D. F., JERUSALEM, A., NYEIN, M., NOELS, L., JAFFEE, M. S. & RADOVITZKY, R. A. 2009. Computational biology - modeling of primary blast effects on the central nervous system. *Neuroimage*, 47 Suppl 2, T10-20.
- MOREY, R. A., HASWELL, C. C., SELGRADE, E. S., MASSOGLIA, D., LIU, C., WEINER, J., MARX, C. E., GROUP, M. W., CERNAK, I. & MCCARTHY, G. 2013. Effects of chronic mild traumatic brain injury on white matter integrity in Iraq and Afghanistan war veterans. *Hum Brain Mapp*, 34, 2986-99.
- MORI, S., OISHI, K., JIANG, H., JIANG, L., LI, X., AKHTER, K., HUA, K., FARIA, A. V., MAHMOOD, A., WOODS, R., TOGA, A. W., PIKE, G. B., NETO, P. R., EVANS, A., ZHANG, J., HUANG, H., MILLER, M. I., VAN ZIJL, P. & MAZZIOTTA, J. 2008. Stereotaxic white matter atlas based on diffusion tensor imaging in an ICBM template. *Neuroimage*, 40, 570-582.
- MU, W., CATENACCIO, E. & LIPTON, M. L. 2017. Neuroimaging in Blast-Related Mild Traumatic Brain Injury. *J Head Trauma Rehabil*, 32, 55-69.
- MUELBL, M. J., SLAKER, M. L., SHAH, A. S., NAWARAWONG, N. N., GERNDT, C. H., BUDDE, M. D., STEMPEL, B. D. & OLSEN, C. M. 2018. Effects of Mild Blast Traumatic Brain Injury on Cognitive- and Addiction-Related Behaviors. *Sci Rep*, 8, 9941.
- MUKHERJEE, P., CHUNG, S. W., BERMAN, J. I., HESS, C. P. & HENRY, R. G. 2008. Diffusion tensor MR imaging and fiber tractography: technical considerations. *AJNR Am J Neuroradiol*, 29, 843-52.

- MURPHY, E. J. & HORROCKS, L. A. 1993. A model for compression trauma: pressure-induced injury in cell cultures. *J Neurotrauma*, 10, 431-44.
- MUTCH, C. A., TALBOTT, J. F. & GEAN, A. 2016. Imaging Evaluation of Acute Traumatic Brain Injury. *Neurosurg Clin N Am*, 27, 409-39.
- NAKAGAWA, A., MANLEY, G. T., GEAN, A. D., OHTANI, K., ARMONDA, R., TSUKAMOTO, A., YAMAMOTO, H., TAKAYAMA, K. & TOMINAGA, T. 2011. Mechanisms of primary blast-induced traumatic brain injury: insights from shock-wave research. *J Neurotrauma*, 28, 1101-19.
- NARAYANA, P. A. 2017. White matter changes in patients with mild traumatic brain injury: MRI perspective. *Concussion*, 2, CNC35.
- NELSON, M. D. & TUMPAP, A. M. 2017. Posttraumatic stress disorder symptom severity is associated with left hippocampal volume reduction: a meta-analytic study. *CNS Spectr*, 22, 363-372.
- NELSON, N. W., ANDERSON, C. R., THURAS, P., KEHLE-FORBES, S. M., ARBISI, P. A., ERBES, C. R. & POLUSNY, M. A. 2015. Factors associated with inconsistency in self-reported mild traumatic brain injury over time among military personnel in Iraq. *Br J Psychiatry*, 206, 237-44.
- NELSON NW, D. N. D., SPONHEIM S.R, ANDERSON C.R. 2015. *Brain Neurotrauma: Molecular, Neuropsychological, and Rehabilitation Aspects.*, Boca Raton (FL), CRC Press/Taylor & Francis.
- NEWSOME, M. R., DURGERIAN, S., MOURANY, L., SCHEIBEL, R. S., LOWE, M. J., BEALL, E. B., KOENIG, K. A., PARSONS, M., TROYANSKAYA, M., REECE, C., WILDE, E., FISCHER, B. L., JONES, S. E., AGARWAL, R., LEVIN, H. S. & RAO, S. M. 2015. Disruption of caudate working memory activation in chronic blast-related traumatic brain injury. *Neuroimage Clin*, 8, 543-53.
- NEWSOME, M. R., MAYER, A. R., LIN, X., TROYANSKAYA, M., JACKSON, G. R., SCHEIBEL, R. S., WALDER, A., SATHIYARAJ, A., WILDE, E. A., MUKHI, S., TAYLOR, B. A. & LEVIN, H. S. 2016. Chronic Effects of Blast-Related TBI on Subcortical Functional Connectivity in Veterans. *J Int Neuropsychol Soc*, 22, 631-42.
- NIOGI, S. N., MUKHERJEE, P., GHAJAR, J., JOHNSON, C., KOLSTER, R. A., SARKAR, R., LEE, H., MEEKER, M., ZIMMERMAN, R. D., MANLEY, G. T. & MCCANDLISS, B. D. 2008a. Extent of microstructural white matter injury in postconcussive syndrome correlates with impaired cognitive reaction time: a 3T diffusion tensor imaging study of mild traumatic brain injury. *AJNR Am J Neuroradiol*, 29, 967-73.
- NIOGI, S. N., MUKHERJEE, P., GHAJAR, J., JOHNSON, C. E., KOLSTER, R., LEE, H., SUH, M., ZIMMERMAN, R. D., MANLEY, G. T. & MCCANDLISS, B. D. 2008b. Structural dissociation of attentional control and memory in adults with and without mild traumatic brain injury. *Brain*, 131, 3209-21.
- NORRIS, J. N., SAMS, R., LUNDBLAD, P., FRANTZ, E. & HARRIS, E. 2014. Blast-related mild traumatic brain injury in the acute phase: acute stress reactions partially mediate the relationship between loss of consciousness and symptoms. *Brain Inj*, 28, 1052-62.
- O. BOTTEMA, B. R. 2018. *Theoretical Kinematics*, Dover Publications.
- O'DOHERTY, D. C., CHITTY, K. M., SADDIQUI, S., BENNETT, M. R. & LAGOPOULOS, J. 2015. A systematic review and meta-analysis of magnetic resonance imaging measurement of structural volumes in posttraumatic stress disorder. *Psychiatry Res*, 232, 1-33.
- O'DOHERTY, D. C. M., TICKELL, A., RYDER, W., CHAN, C., HERMENS, D. F., BENNETT, M. R. & LAGOPOULOS, J. 2017. Frontal and subcortical grey matter reductions in PTSD. *Psychiatry Res Neuroimaging*, 266, 1-9.
- O'DONNELL, L. J. & WESTIN, C. F. 2011. An introduction to diffusion tensor image analysis. *Neurosurg Clin N Am*, 22, 185-96, viii.
- OISHI, K., ZILLES, K., AMUNTS, K., FARIA, A., JIANG, H., LI, X., AKHTER, K., HUA, K., WOODS, R., TOGA, A. W., PIKE, G. B., ROSA-NETO, P., EVANS, A., ZHANG, J., HUANG, H., MILLER, M. I., VAN ZIJL, P. C., MAZZIOTTA, J. & MORI, S. 2008. Human brain white matter atlas: identification and assignment of common anatomical structures in superficial white matter. *Neuroimage*, 43, 447-57.
- OKIE, S. 2005. Traumatic brain injury in the war zone. *N Engl J Med*, 352, 2043-7.
- OMALU, B., HAMMERS, J. L., BAILES, J., HAMILTON, R. L., KAMBOH, M. I., WEBSTER, G. & FITZSIMMONS, R. P. 2011. Chronic traumatic encephalopathy in an Iraqi war veteran with posttraumatic stress disorder who committed suicide. *Neurosurg Focus*, 31, E3.
- OMMAYA, A. K. 1995. Head injury mechanisms and the concept of preventive management: a review and critical synthesis. *J Neurotrauma*, 12, 527-46.
- OMMAYA, A. K. & GENNARELLI, T. A. 1974. Cerebral concussion and traumatic unconsciousness. Correlation of experimental and clinical observations of blunt head injuries. *Brain*, 97, 633-54.
- OWEN, A. M. 2000. The role of the lateral frontal cortex in mnemonic processing: the contribution of functional neuroimaging. *Exp Brain Res*, 133, 33-43.
- PATENAUE, B., SMITH, S.M., KENNEDY, D., AND JENKINSON M. A 2011. Bayesian Model of Shape and Appearance for Subcortical Brain. *NeuroImage*, 56, 907-922.
- PESKIND, E. R., PETRIE, E. C., CROSS, D. J., PAGULAYAN, K., MCCRAW, K., HOFF, D., HART, K., YU, C. E., RASKIND, M. A., COOK, D. G. & MINOSHIMA, S. 2011. Cerebrocerebellar hypometabolism associated with repetitive blast exposure mild traumatic brain injury in 12 Iraq war Veterans with persistent post-concussive symptoms. *Neuroimage*, 54 Suppl 1, S76-82.
- PETRIE, E. C., CROSS, D. J., YARNYKH, V. L., RICHARDS, T., MARTIN, N. M., PAGULAYAN, K., HOFF, D., HART, K., MAYER, C., TARABOCHIA, M., RASKIND, M. A., MINOSHIMA, S. & PESKIND, E. R. 2014. Neuroimaging, behavioral, and psychological sequelae of repetitive combined blast/impact mild traumatic brain injury in Iraq and Afghanistan war veterans. *J Neurotrauma*, 31, 425-36.
- PHIPPS, H., MONDELLO, S., WILSON, A., DITTMER, T., ROHDE, N. N., SCHROEDER, P. J., NICHOLS, J., MCGIRT, C., HOFFMAN, J., TANKSLEY, K., CHOCHAN, M., HEIDERMAN, A., ABOU ABBASS, H., KOBEISSY, F. & HINDS, S. 2020. Characteristics and Impact of U.S. Military Blast-Related Mild Traumatic Brain Injury: A Systematic Review. *Front Neurol*, 11, 559318.
- PIERPAOLI, C. & BASSER, P. J. 1996. Toward a quantitative assessment of diffusion anisotropy. *Magn Reson Med*, 36, 893-906.
- PINTO, V. L., TADI, P. & ADEYINKA, A. 2021. Increased Intracranial Pressure. *StatPearls*. Treasure Island (FL).
- PLAISIER, A., PIETERMAN, K., LEQUIN, M. H., GOVAERT, P., HEEMSKERK, A. M., REISS, I. K., KRESTIN, G. P., LEEMANS, A. & DUDINK, J. 2014. Choice of diffusion tensor estimation approach affects fiber tractography of the fornix in preterm brain. *AJNR Am J Neuroradiol*, 35, 1219-25.

- POGODA, T. K., HENDRICKS, A. M., IVERSON, K. M., STOLZMANN, K. L., KRENGEL, M. H., BAKER, E., METERKO, M. & LEW, H. L. 2012. Multisensory impairment reported by veterans with and without mild traumatic brain injury history. *J Rehabil Res Dev*, 49, 971-84.
- PONSFORD, J. & KINSELLA, G. 1992. Attentional deficits following closed-head injury. *J Clin Exp Neuropsychol*, 14, 822-38.
- PREVENTION, C. F. D. C. A. 2020. *Traumatic Brain Injury & Concussion* [Online]. National Center for Injury Prevention and Control. Available: <https://www.cdc.gov/traumaticbraininjury/index.html> [Accessed].
- PRZEKWAS, A., SOMAYAJI, M. R. & GUPTA, R. K. 2016. Synaptic Mechanisms of Blast-Induced Brain Injury. *Front Neurol*, 7, 2.
- RAJI, C. A., WILLEUMIER, K., TAYLOR, D., TARZWELL, R., NEWBERG, A., HENDERSON, T. A. & AMEN, D. G. 2015. Functional neuroimaging with default mode network regions distinguishes PTSD from TBI in a military veteran population. *Brain Imaging Behav*, 9, 527-34.
- RANGANATH, C. & D'ESPOSITO, M. 2005. Directing the mind's eye: prefrontal, inferior and medial temporal mechanisms for visual working memory. *Curr Opin Neurobiol*, 15, 175-82.
- RATLIFF, W. A., MERVIS, R. F., CITRON, B. A., SCHWARTZ, B., RUBOVITCH, V., SCHREIBER, S. & PICK, C. G. 2020. Effect of mild blast-induced TBI on dendritic architecture of the cortex and hippocampus in the mouse. *Sci Rep*, 10, 2206.
- RESSEL, V., VAN HEDEL, H. J. A., SCHEER, I. & O'GORMAN TUURA, R. 2018. Comparison of DTI analysis methods for clinical research: influence of pre-processing and tract selection methods. *Eur Radiol Exp*, 2, 33.
- REZAEI, A., SALIMI JAZI, M., KARAMI, G. & ZIEJEWSKI, M. 2014. A computational study on brain tissue under blast: primary and tertiary blast injuries. *Int J Numer Method Biomed Eng*, 30, 781-95.
- RIEDY, G., SENSENEY, J. S., LIU, W., OLLINGER, J., SHAM, E., KRAPIVA, P., PATEL, J. B., SMITH, A., YEH, P. H., GRANER, J., NATHAN, D., CABAN, J., FRENCH, L. M., HARPER, J., ESKAY, V., MORISSETTE, J. & OAKES, T. R. 2016. Findings from Structural MR Imaging in Military Traumatic Brain Injury. *Radiology*, 279, 207-15.
- ROBINSON, M. E., CLARK, D. C., MILBERG, W. P., MCGLINCHY, R. E. & SALAT, D. H. 2017. Characterization of Differences in Functional Connectivity Associated with Close-Range Blast Exposure. *J Neurotrauma*, 34, S53-S61.
- ROBINSON, M. E., MCKEE, A. C., SALAT, D. H., RASMUSSEN, A. M., RADIGAN, L. J., CATANA, C., MILBERG, W. P. & MCGLINCHY, R. E. 2019. Positron emission tomography of tau in Iraq and Afghanistan Veterans with blast neurotrauma. *Neuroimage Clin*, 21, 101651.
- ROEBUCK-SPENCER, T. M., VINCENT, A. S., TWILLIE, D. A., LOGAN, B. W., LOPEZ, M., FRIEDL, K. E., GRATE, S. J., SCHLEGEL, R. E. & GILLILAND, K. 2012. Cognitive change associated with self-reported mild traumatic brain injury sustained during the OEF/OIF conflicts. *Clin Neuropsychol*, 26, 473-89.
- ROSENBERG, L. J., EMERY, D. G. & LUCAS, J. H. 2001. Effects of sodium and chloride on neuronal survival after neurite transection. *J Neuropathol Exp Neurol*, 60, 33-48.
- ROSENBERG, L. J. & LUCAS, J. H. 1996. Reduction of NaCl increases survival of mammalian spinal neurons subjected to dendrite transection injury. *Brain Res*, 734, 349-53.
- ROSENFELD, J. V. & FORD, N. L. 2010. Bomb blast, mild traumatic brain injury and psychiatric morbidity: a review. *Injury*, 41, 437-43.
- ROSENFELD, J. V., MCFARLANE, A. C., BRAGGE, P., ARMONDA, R. A., GRIMES, J. B. & LING, G. S. 2013. Blast-related traumatic brain injury. *Lancet Neurol*, 12, 882-93.
- ROSS, D. E. 2011. Review of longitudinal studies of MRI brain volumetry in patients with traumatic brain injury. *Brain Inj*, 25, 1271-8.
- ROY, M. J., FRANCIS, J., FRIEDLANDER, J., BANKS-WILLIAMS, L., LANDE, R. G., TAYLOR, P., BLAIR, J., MCLELLAN, J., LAW, W., TARPLEY, V., PATT, I., YU, H., MALLINGER, A., DIFEDE, J., RIZZO, A. & ROTHBAUM, B. 2010. Improvement in cerebral function with treatment of posttraumatic stress disorder. *Ann N Y Acad Sci*, 1208, 142-9.
- RUFF, R. M. & JURICA, P. 1999. In search of a unified definition for mild traumatic brain injury. *Brain Inj*, 13, 943-52.
- RUSIECKI, J., LEVIN, L. I., WANG, L., BYRNE, C., KRISHNAMURTHY, J., CHEN, L., GALDZICKI, Z. & FRENCH, L. M. 2020. Blast traumatic brain injury and serum inflammatory cytokines: a repeated measures case-control study among U.S. military service members. *J Neuroinflammation*, 17, 20.
- RYAN, L. M. & WARDEN, D. L. 2003. Post concussion syndrome. *Int Rev Psychiatry*, 15, 310-6.
- RYU, J., HORKAYNE-SZAKALY, I., XU, L., PLETNIKOVA, O., LERI, F., EBERHART, C., TRONCOSO, J. C. & KOLIATSOS, V. E. 2014. The problem of axonal injury in the brains of veterans with histories of blast exposure. *Acta Neuropathol Commun*, 2, 153.
- RZIGALINSKI, B. A., LIANG, S., MCKINNEY, J. S., WILLOUGHBY, K. A. & ELLIS, E. F. 1997. Effect of Ca<sup>2+</sup> on in vitro astrocyte injury. *J Neurochem*, 68, 289-96.
- RZIGALINSKI, B. A., WEBER, J. T., WILLOUGHBY, K. A. & ELLIS, E. F. 1998. Intracellular free calcium dynamics in stretch-injured astrocytes. *J Neurochem*, 70, 2377-85.
- S.M.SMITH, G. K., S.JBABDI 2015. *Tract-Based Spatial Statistics and Other Approaches for Cross-Subject Comparison of Local Diffusion MRI Parameters*, Academic Press.
- SAJDA, P. 2006. Machine learning for detection and diagnosis of disease. *Annu Rev Biomed Eng*, 8, 537-65.
- SALJO, A., SVENSSON, B., MAYORGA, M., HAMBERGER, A. & BOLOURI, H. 2009. Low-level blasts raise intracranial pressure and impair cognitive function in rats. *J Neurotrauma*, 26, 1345-52.
- SAUNDERS, G. H. & ECHT, K. V. 2012. Blast exposure and dual sensory impairment: an evidence review and integrated rehabilitation approach. *J Rehabil Res Dev*, 49, 1043-58.
- SAVJANI, R. R., TAYLOR, B. A., ACION, L., WILDE, E. A. & JORGE, R. E. 2017. Accelerated Changes in Cortical Thickness Measurements with Age in Military Service Members with Traumatic Brain Injury. *J Neurotrauma*, 34, 3107-3116.
- SCHEIBEL, R. S., NEWSOME, M. R., TROYANSKAYA, M., LIN, X., STEINBERG, J. L., RADAIDEH, M. & LEVIN, H. S. 2012. Altered brain activation in military personnel with one or more traumatic brain injuries following blast. *J Int Neuropsychol Soc*, 18, 89-100.
- SCHILLING, K. G., NATH, V., HANSEN, C., PARVATHANENI, P., BLABER, J., GAO, Y., NEHER, P., AYDOGAN, D. B., SHI, Y., OCAMPO-PINEDA, M., SCHIAVI, S., DADUCCI, A., GIRARD, G., BARAKOVIC, M., RAFAEL-PATINO, J., ROMASCANO, D., RENSONNET, G., PIZZOLATO, M., BATES, A., FISCHI, E., THIRAN, J. P., CANALES-RODRIGUEZ, E. J., HUANG, C., ZHU, H., ZHONG, L., CABEEN, R., TOGA, A. W., RHEAULT, F., THEAUD, G., HOUDE, J. C., SIDHU, J., CHAMBERLAND, M., WESTIN, C. F., DYRBY, T. B., VERMA, R., RATHI, Y., IRFANOGLU, M. O., THOMAS, C., PIERPAOLI, C., DESCOTEAUX, M., ANDERSON, A. W. & LANDMAN, B. A. 2019. Limits to anatomical accuracy of diffusion tractography using modern approaches. *Neuroimage*, 185, 1-11.



- SCHIMMEL, S. J., ACOSTA, S. & LOZANO, D. 2017. Neuroinflammation in traumatic brain injury: A chronic response to an acute injury. *Brain Circ*, 3, 135-142.
- SCHOENFELD, A. J., DUNN, J. C., BADER, J. O. & BELMONT, P. J., JR. 2013. The nature and extent of war injuries sustained by combat specialty personnel killed and wounded in Afghanistan and Iraq, 2003-2011. *J Trauma Acute Care Surg*, 75, 287-91.
- SCHWAB, K. A., IVINS, B., CRAMER, G., JOHNSON, W., SLUSS-TILLER, M., KILEY, K., LUX, W. & WARDEN, D. 2007. Screening for traumatic brain injury in troops returning from deployment in Afghanistan and Iraq: initial investigation of the usefulness of a short screening tool for traumatic brain injury. *J Head Trauma Rehabil*, 22, 377-89.
- SCHWARTZ, I., TUCHNER, M., TSETER, J., SHOCHINA, M., SHOSHAN, Y., KATZ-LEURER, M. & MEINER, Z. 2008. Cognitive and functional outcomes of terror victims who suffered from traumatic brain injury. *Brain Inj*, 22, 255-63.
- SEELIG, A. D., JACOBSON, I. G., SMITH, B., HOOPER, T. I., BOYKO, E. J., GACKSTETTER, G. D., GEHRMAN, P., MACERA, C. A., SMITH, T. C. & MILLENNIUM COHORT STUDY, T. 2010. Sleep patterns before, during, and after deployment to Iraq and Afghanistan. *Sleep*, 33, 1615-22.
- SHANDERA-OCHSNER, A. L., BERRY, D. T., HARP, J. P., EDMUNDSON, M., GRAUE, L. O., ROACH, A. & HIGH, W. M., JR. 2013. Neuropsychological effects of self-reported deployment-related mild TBI and current PTSD in OIF/OEF veterans. *Clin Neuropsychol*, 27, 881-907.
- SHENTON, M. E., HAMODA, H. M., SCHNEIDERMAN, J. S., BOUIX, S., PASTERNAK, O., RATHI, Y., VU, M. A., PUROHIT, M. P., HELMER, K., KOERTE, I., LIN, A. P., WESTIN, C. F., KIKINIS, R., KUBICKI, M., STERN, R. A. & ZAFONTE, R. 2012. A review of magnetic resonance imaging and diffusion tensor imaging findings in mild traumatic brain injury. *Brain Imaging Behav*, 6, 137-92.
- SHIVELY, S. B., HORKAYNE-SZAKALY, I., JONES, R. V., KELLY, J. P., ARMSTRONG, R. C. & PERL, D. P. 2016. Characterisation of interface astroglial scarring in the human brain after blast exposure: a post-mortem case series. *Lancet Neurol*, 15, 944-953.
- SHIVELY, S. B. & PERL, D. P. 2017. Viewing the Invisible Wound: Novel Lesions Identified in Postmortem Brains of U.S. Service Members With Military Blast Exposure. *Mil Med*, 182, 1461-1463.
- SHU, I. W., ONTON, J. A., O'CONNELL, R. M., SIMMONS, A. N. & MATTHEWS, S. C. 2014. Combat veterans with comorbid PTSD and mild TBI exhibit a greater inhibitory processing ERP from the dorsal anterior cingulate cortex. *Psychiatry Res*, 224, 58-66.
- SIDAROS, A., ENGBERG, A. W., SIDAROS, K., LIPTROT, M. G., HERNING, M., PETERSEN, P., PAULSON, O. B., JERNIGAN, T. L. & ROSTRUP, E. 2008. Diffusion tensor imaging during recovery from severe traumatic brain injury and relation to clinical outcome: a longitudinal study. *Brain*, 131, 559-72.
- SIDAROS, A., SKIMMINGE, A., LIPTROT, M. G., SIDAROS, K., ENGBERG, A. W., HERNING, M., PAULSON, O. B., JERNIGAN, T. L. & ROSTRUP, E. 2009. Long-term global and regional brain volume changes following severe traumatic brain injury: a longitudinal study with clinical correlates. *Neuroimage*, 44, 1-8.
- SILVER, J. M., MCALLISTER, T. W., & YUDOFKY, S. C. 2005. *Textbook of traumatic brain injury*, American Psychiatric Publishing, Inc.
- SIMARD, J. M., PAMPORI, A., KELEDJIAN, K., TOSUN, C., SCHWARTZBAUER, G., IVANOVA, S. & GERZANICH, V. 2014. Exposure of the thorax to a sublethal blast wave causes a hydrodynamic pulse that leads to perivascular inflammation in the brain. *J Neurotrauma*, 31, 1292-304.
- SMITH, S. M. 2002. Fast robust automated brain extraction. *Hum Brain Mapp*, 17, 143-55.
- SMITH, S. M., JENKINSON, M., JOHANSEN-BERG, H., RUECKERT, D., NICHOLS, T. E., MACKAY, C. E., WATKINS, K. E., CICCARELLI, O., CADER, M. Z., MATTHEWS, P. M. & BEHRENS, T. E. 2006. Tract-based spatial statistics: voxelwise analysis of multi-subject diffusion data. *Neuroimage*, 31, 1487-505.
- SNOOK, L., PLEWES, C. & BEAULIEU, C. 2007. Voxel based versus region of interest analysis in diffusion tensor imaging of neurodevelopment. *Neuroimage*, 34, 243-52.
- SOARES, J. M., MARQUES, P., ALVES, V. & SOUSA, N. 2013. A hitchhiker's guide to diffusion tensor imaging. *Front Neurosci*, 7, 31.
- SORG, S. F., DELANO-WOOD, L., LUC, N., SCHIEHSE, D. M., HANSON, K. L., NATION, D. A., LANNI, E., JAK, A. J., LU, K., MELOY, M. J., FRANK, L. R., LOHR, J. B. & BONDI, M. W. 2014. White matter integrity in veterans with mild traumatic brain injury: associations with executive function and loss of consciousness. *J Head Trauma Rehabil*, 29, 21-32.
- SORG, S. F., SCHIEHSE, D. M., BONDI, M. W., LUC, N., CLARK, A. L., JACOBSON, M. W., FRANK, L. R. & DELANO-WOOD, L. 2016. White Matter Microstructural Compromise Is Associated With Cognition But Not Posttraumatic Stress Disorder Symptoms in Military Veterans With Traumatic Brain Injury. *J Head Trauma Rehabil*, 31, 297-308.
- SPIELBERG, J. M., MCGLINCHY, R. E., MILBERG, W. P. & SALAT, D. H. 2015. Brain network disturbance related to posttraumatic stress and traumatic brain injury in veterans. *Biol Psychiatry*, 78, 210-6.
- SPIKMAN, J. M. & VAN DER NAALT, J. 2010. Indices of impaired self-awareness in traumatic brain injury patients with focal frontal lesions and executive deficits: implications for outcome measurement. *J Neurotrauma*, 27, 1195-202.
- SPONHEIM, S. R., MCGUIRE, K. A., KANG, S. S., DAVENPORT, N. D., AVIYENTE, S., BERNAT, E. M. & LIM, K. O. 2011. Evidence of disrupted functional connectivity in the brain after combat-related blast injury. *Neuroimage*, 54 Suppl 1, S21-9.
- STEVEN, A. J., ZHUO, J. & MELHEM, E. R. 2014. Diffusion kurtosis imaging: an emerging technique for evaluating the microstructural environment of the brain. *AJR Am J Roentgenol*, 202, W26-33.
- STOCKER, R. P., CIEPLY, M. A., PAUL, B., KHAN, H., HENRY, L., KONTOS, A. P. & GERMAIN, A. 2014. Combat-related blast exposure and traumatic brain injury influence brain glucose metabolism during REM sleep in military veterans. *Neuroimage*, 99, 207-14.
- STROOP, J. R. 1935. Studies of interference in serial verbal reactions. *Journal of experimental psychology*, 18, 643-662.
- SYDNOR, V. J., BOUIX, S., PASTERNAK, O., HARTL, E., LEVIN-GLEBA, L., REID, B., TRIPODIS, Y., GUENETTE, J. P., KAUFMANN, D., MAKRI, N., FORTIER, C., SALAT, D. H., RATHI, Y., MILBERG, W. P., MCGLINCHY, R. E., SHENTON, M. E. & KOERTE, I. K. 2020. Mild traumatic brain injury impacts associations between limbic system microstructure and post-traumatic stress disorder symptomatology. *Neuroimage Clin*, 26, 102190.
- TABER, K. H., HURLEY, R. A., HASWELL, C. C., ROWLAND, J. A., HURT, S. D., LAMAR, C. D. & MOREY, R. A. 2015. White matter compromise in veterans exposed to primary blast forces. *J Head Trauma Rehabil*, 30, E15-25.
- TATE, D. F., GUSMAN, M., KINI, J., REID, M., VELEZ, C. S., DRENNON, A. M., COOPER, D. B., KENNEDY, J. E., BOWLES, A. O., BIGLER, E. D., LEWIS, J. D., RITTER, J. & YORK, G. E. 2017. Susceptibility Weighted Imaging and White

- Matter Abnormality Findings in Service Members With Persistent Cognitive Symptoms Following Mild Traumatic Brain Injury. *Mil Med*, 182, e1651-e1658.
- TATE, D. F., WADE, B. S., VELEZ, C. S., DRENNON, A. M., BOLZENIUS, J., GUTMAN, B. A., THOMPSON, P. M., LEWIS, J. D., WILDE, E. A., BIGLER, E. D., SHENTON, M. E., RITTER, J. L. & YORK, G. E. 2016. Volumetric and shape analyses of subcortical structures in United States service members with mild traumatic brain injury. *J Neurol*, 263, 2065-79.
- TATE, D. F., YORK, G. E., REID, M. W., COOPER, D. B., JONES, L., ROBIN, D. A., KENNEDY, J. E. & LEWIS, J. 2014. Preliminary findings of cortical thickness abnormalities in blast injured service members and their relationship to clinical findings. *Brain Imaging Behav*, 8, 102-9.
- TAYLOR, P. A. & FORD, C. C. 2009a. Simulation of blast-induced early-time intracranial wave physics leading to traumatic brain injury. *Journal of biomechanical engineering*, 131, 061007.
- TAYLOR, P. A. & FORD, C. C. 2009b. Simulation of blast-induced early-time intracranial wave physics leading to traumatic brain injury. *J Biomech Eng*, 131, 061007.
- TEFERA, G. B., ZHOU, Y., JUNEJA, V. & NARAYANA, P. A. 2013. Evaluation of fiber tracking from subsampled q-space data in diffusion spectrum imaging. *Magn Reson Imaging*, 31, 820-6.
- THOMPSON, J. M., SCOTT, K. C. & DUBINSKY, L. 2008. Battlefield brain: unexplained symptoms and blast-related mild traumatic brain injury. *Can Fam Physician*, 54, 1549-51.
- TOMPKINS, P., TESIRAM, Y., LERNER, M., GONZALEZ, L. P., LIGHTFOOT, S., RABB, C. H. & BRACKETT, D. J. 2013. Brain injury: neuro-inflammation, cognitive deficit, and magnetic resonance imaging in a model of blast induced traumatic brain injury. *J Neurotrauma*, 30, 1888-97.
- TROTTER, B. B., ROBINSON, M. E., MILBERG, W. P., MCGLINCHEY, R. E. & SALAT, D. H. 2015. Military blast exposure, ageing and white matter integrity. *Brain*, 138, 2278-92.
- TWAMLEY, E. W., ALLARD, C. B., THORP, S. R., NORMAN, S. B., HAMI CISELL, S., HUGHES BERARDI, K., GRIMES, E. M. & STEIN, M. B. 2009. Cognitive impairment and functioning in PTSD related to intimate partner violence. *J Int Neuropsychol Soc*, 15, 879-87.
- VAN BODEGOM, M., HOMBERG, J. R. & HENCKENS, M. 2017. Modulation of the Hypothalamic-Pituitary-Adrenal Axis by Early Life Stress Exposure. *Front Cell Neurosci*, 11, 87.
- VAN BOVEN, R. W., HARRINGTON, G. S., HACKNEY, D. B., EBEL, A., GAUGER, G., BREMNER, J. D., D'ESPOSITO, M., DETRE, J. A., HAACKE, E. M., JACK, C. R., JR., JAGUST, W. J., LE BIHAN, D., MATHIS, C. A., MUELLER, S., MUKHERJEE, P., SCHUFF, N., CHEN, A. & WEINER, M. W. 2009. Advances in neuroimaging of traumatic brain injury and posttraumatic stress disorder. *J Rehabil Res Dev*, 46, 717-57.
- VAN HECKE, W., LEEMANS, A., DE BACKER, S., JEURISSEN, B., PARIZEL, P. M. & SIJBERS, J. 2010. Comparing isotropic and anisotropic smoothing for voxel-based DTI analyses: A simulation study. *Hum Brain Mapp*, 31, 98-114.
- VAN ROOIJ, S. J., RADEMAKER, A. R., KENNIS, M., VINK, M., KAHN, R. S. & GEUZE, E. 2014. Impaired right inferior frontal gyrus response to contextual cues in male veterans with PTSD during response inhibition. *J Psychiatry Neurosci*, 39, 330-8.
- VAN ROOIJ, S. J., RADEMAKER, A. R., KENNIS, M., VINK, M., KAHN, R. S. & GEUZE, E. 2015. Neural correlates of trauma-unrelated emotional processing in war veterans with PTSD. *Psychol Med*, 45, 575-87.
- VANDERPLOEG, R. D., BELANGER, H. G. & CURTISS, G. 2009. Mild traumatic brain injury and posttraumatic stress disorder and their associations with health symptoms. *Arch Phys Med Rehabil*, 90, 1084-93.
- VANDERPLOEG, R. D., BELANGER, H. G., HORNER, R. D., SPEHAR, A. M., POWELL-COPE, G., LUTHER, S. L. & SCOTT, S. G. 2012. Health outcomes associated with military deployment: mild traumatic brain injury, blast, trauma, and combat associations in the Florida National Guard. *Arch Phys Med Rehabil*, 93, 1887-95.
- VANDERPLOEG, R. D., CURTISS, G. & BELANGER, H. G. 2005. Long-term neuropsychological outcomes following mild traumatic brain injury. *J Int Neuropsychol Soc*, 11, 228-36.
- VASTERLING, J. J., BRAILEY, K., PROCTOR, S. P., KANE, R., HEEREN, T. & FRANZ, M. 2012. Neuropsychological outcomes of mild traumatic brain injury, post-traumatic stress disorder and depression in Iraq-deployed US Army soldiers. *Br J Psychiatry*, 201, 186-92.
- VASTERLING, J. J. & PROCTOR, S. P. 2011. Understanding the neuropsychological consequences of deployment stress: a public health framework. *J Int Neuropsychol Soc*, 17, 1-6.
- VASTERLING, J. J., PROCTOR, S. P., AMOROSO, P., KANE, R., HEEREN, T. & WHITE, R. F. 2006. Neuropsychological outcomes of army personnel following deployment to the Iraq war. *JAMA*, 296, 519-29.
- VENKATASUBRAMANIAN, P. N., KENI, P., GASTFIELD, R., LI, L., AKSENOV, D., SHERMAN, S. A., BAILES, J., 3RD, SINDELAR, B., FINAN, J. D., LEE, J., BAILES, J. E. & WYRWICZ, A. M. 2020. Diffusion Tensor Imaging Detects Acute and Subacute Changes in Corpus Callosum in Blast-Induced Traumatic Brain Injury. *ASN Neuro*, 12, 1759091420922929.
- VESPA, P., TUBI, M., CLAASSEN, J., BUITRAGO-BLANCO, M., MCARTHUR, D., VELAZQUEZ, A. G., TU, B., PRINS, M. & NUWER, M. 2016. Metabolic crisis occurs with seizures and periodic discharges after brain trauma. *Ann Neurol*, 79, 579-90.
- VYTHILINGAM, M., LUCKENBAUGH, D. A., LAM, T., MORGAN, C. A., 3RD, LIPSCHITZ, D., CHARNEY, D. S., BREMNER, J. D. & SOUTHWICK, S. M. 2005. Smaller head of the hippocampus in Gulf War-related posttraumatic stress disorder. *Psychiatry Res*, 139, 89-99.
- WALTZMAN, D., SOMAN, S., HANTKE, N. C., FAIRCHILD, J. K., KINOSHITA, L. M., WINTERMARK, M., ASHFORD, J. W., YESAVAGE, J., WILLIAMS, L., ADAMSON, M. M. & FURST, A. J. 2017. Altered Microstructural Caudate Integrity in Posttraumatic Stress Disorder but Not Traumatic Brain Injury. *PLoS One*, 12, e0170564.
- WANG, S., PETERSON, D. J., GATENBY, J. C., LI, W., GRABOWSKI, T. J. & MADHYASTHA, T. M. 2017. Evaluation of Field Map and Nonlinear Registration Methods for Correction of Susceptibility Artifacts in Diffusion MRI. *Front Neuroinform*, 11, 17.
- WANG, Y., WEI, Y., OGUNTAYO, S., WILKINS, W., ARUN, P., VALIYAVEETIL, M., SONG, J., LONG, J. B. & NAMBIAR, M. P. 2011. Tightly coupled repetitive blast-induced traumatic brain injury: development and characterization in mice. *J Neurotrauma*, 28, 2171-83.
- WARE, J. B., BIESTER, R. C., WHIPPLE, E., ROBINSON, K. M., ROSS, R. J. & NUCIFORA, P. G. 2016. Combat-related Mild Traumatic Brain Injury: Association between Baseline Diffusion-Tensor Imaging Findings and Long-term Outcomes. *Radiology*, 280, 212-9.
- WECHSLER, D. 1945. A Standardized Memory Scale for Clinical Use. *The Journal of Psychology*, 19, 87-95.
- WERNER, C. & ENGELHARD, K. 2007. Pathophysiology of traumatic brain injury. *Br J Anaesth*, 99, 4-9.

- WOLF, S. J., BEBARTA, V. S., BONNETT, C. J., PONS, P. T. & CANTRILL, S. V. 2009. Blast injuries. *Lancet*, 374, 405-15.
- WORSLEY, K. J., MARRETT, S., NEELIN, P., VANDAL, A. C., FRISTON, K. J. & EVANS, A. C. 1996. A unified statistical approach for determining significant signals in images of cerebral activation. *Hum Brain Mapp*, 4, 58-73.
- WROCKLAGE, K. M., AVERILL, L. A., COBB SCOTT, J., AVERILL, C. L., SCHWEINSBURG, B., TREJO, M., ROY, A., WEISSER, V., KELLY, C., MARTINI, B., HARPAZ-ROTEM, I., SOUTHWICK, S. M., KRYSTAL, J. H. & ABDALLAH, C. G. 2017. Cortical thickness reduction in combat exposed U.S. veterans with and without PTSD. *Eur Neuropsychopharmacol*, 27, 515-525.
- YARIBEYGI, H., PANAH, Y., SAHRAEI, H., JOHNSTON, T. P. & SAHEBKAR, A. 2017. The impact of stress on body function: A review. *EXCLI J*, 16, 1057-1072.
- YEH, P. H., GUAN KOAY, C., WANG, B., MORISSETTE, J., SHAM, E., SENSENEY, J., JOY, D., KUBLI, A., YEH, C. H., ESKAY, V., LIU, W., FRENCH, L. M., OAKES, T. R., RIEDY, G. & OLLINGER, J. 2017. Compromised Neurocircuitry in Chronic Blast-Related Mild Traumatic Brain Injury. *Hum Brain Mapp*, 38, 352-369.
- YEH, P. H., WANG, B., OAKES, T. R., FRENCH, L. M., PAN, H., GRANER, J., LIU, W. & RIEDY, G. 2014. Postconcussional disorder and PTSD symptoms of military-related traumatic brain injury associated with compromised neurocircuitry. *Hum Brain Mapp*, 35, 2652-73.
- YU, X., AZOR, A., SHARP, D. & GHAJARI, M. 2020. Mechanisms of tensile failure of cerebrospinal fluid in blast traumatic brain injury. *Extreme Mechanics Letters*, 38, 100739.
- YURGELUN-TODD, D. A., BUELER, C. E., MCGLADE, E. C., CHURCHWELL, J. C., BRENNER, L. A. & LOPEZ-LARSON, M. P. 2011. Neuroimaging correlates of traumatic brain injury and suicidal behavior. *J Head Trauma Rehabil*, 26, 276-89.
- YURGIL, K. A., BARKAUSKAS, D. A., VASTERLING, J. J., NIEVERGELT, C. M., LARSON, G. E., SCHORK, N. J., LITZ, B. T., NASH, W. P., BAKER, D. G. & MARINE RESILIENCY STUDY, T. 2014. Association between traumatic brain injury and risk of posttraumatic stress disorder in active-duty Marines. *JAMA Psychiatry*, 71, 149-57.
- ZALESKY, A. 2011. Moderating registration misalignment in voxelwise comparisons of DTI data: a performance evaluation of skeleton projection. *Magn Reson Imaging*, 29, 111-25.
- ZHANG, L., YANG, K. H. & KING, A. I. 2004. A proposed injury threshold for mild traumatic brain injury. *J Biomech Eng*, 126, 226-36.
- ZHANG, Y., BRADY, M. & SMITH, S. 2001. Segmentation of brain MR images through a hidden Markov random field model and the expectation-maximization algorithm. *IEEE Trans Med Imaging*, 20, 45-57.
- ZHANG, Y. A. B., M. AND SMITH, S. 2001. Segmentation of brain MR images through a hidden Markov random field model and the expectation-maximization algorithm. *EEE Trans Med Imag*, 20, 45-57.
- ZHOU, Y., QUN, X., QIN, L. D., QIAN, L. J., CAO, W. W. & XU, J. R. 2011. A primary study of diffusion tensor imaging-based histogram analysis in vascular cognitive impairment with no dementia. *Clin Neurol Neurosurg*, 113, 92-7.

# APPENDIX



## A.3. APPENDIX OF CHAPTER 3

### 1.8.9. A.3.1. Code of SSDS

#### Subject Specific Diffusion Statistics (SSDS)

adriana.azor16@imperial.ac.uk

Developed by Adriana Azor

at C3NL, Imperial College London, London, UK

Last update: 20/03/2021

#### Description

This notebook wraps FSL & MRTRIX3 native commands in a pipeline to generate FA summary measures from whole tracts and boundary in native diffusion space

#### Dependencies

- FSL installation
- MRTRIX3 installation
- hpcSubmit (PBS submission script for parallelisation)
- **Input data** Raw DWI & T1w  
**Data organization:**
  - Working directory (with subjects.txt file list of all subjects in analysis)
    - Subject directory
      - DWI
        - Raw diffusion file & bvec, bval
      - T1
        - T1.nii.gz
        - gre\_map\_field.nii.gz (if available)

#### Step 1. Pre-processing of diffusion data

The following cells preprocess raw diffusion data and fit tensor

```
1. subj='cat subject.txt'
2. echo "eddy correcting"
3. eddy_correct "$subj" "$subj"_ec 0; # change to match b0 from scanner
4. echo "create nodif"
5. for i in `cat subjects.txt`
6. do eddy_correct "$i"/DWI/data.nii.gz "$i"/DWI/data_ec.nii.gz 0;
7. fsroi "$i"/DWI/data_ec "$i"/DWI/nodif.nii.gz 0 1;
   # change first value to match b0 from scanner
8. echo "fdt rotate"
9. fdt_rotate_bvecs "$i"/DWI/*_bvec "$i"/DWI/rotated_bvec "$i"/DWI/data_ec.ecclog;
10. echo "bet"
11. bet "$i"/DWI/nodif.nii.gz "$i"/DWI/nodif_brain -f 0.2 -g 0 -m;
   # QA brain extract
12. echo "dtifit"
13. dtifit --data="$i"/DWI/data.nii.gz --out="$i"/DWI/dti --mask="$i"/DWI/nodif_brain_mask bvecs="$i"/DWI/rotated_bvec --bvals="$i"/DWI/"$i".bval -w;
14. done
```

#### Step 2. Setup paths for analysis & setup directories & pre-process data

The following cells setup the current environment for analysis and the directories required

| EDIT HERE: Project Directory, Tract Directory, Standard Directory. Export working directory, tract directory, and standard atlas directory.

```
1. for i in `cat subjects.txt`;
2. do mkdir $(workdir)/"$i"/boundary_mask;
3. mkdir $(workdir)/"$i"/boundary_mask/MASK;
4. mkdir $(workdir)/"$i"/boundary_mask/transform;
5. mkdir $(workdir)/"$i"/boundary_mask/tmp_files
6. cp $(workdir)/"$i"/T1/T1.nii.gz $(workdir)/"$i"/boundary_mask/MASK
7. cp $(workdir)/"$i"/DWI/nodif_brain.nii.gz $(workdir)/"$i"/boundary_mask/
8. cp $(workdir)/"$i"/DWI/nodif.nii.gz $(workdir)/"$i"/boundary_mask/
9. done
10. echo "Directories ready"
11. echo "***** REALIGNING 80 IMAGES *****"
```

```

12. for i in `cat subjects.txt`;
13. do flirt -dof 6 -in ${workdir}/${Si}/boundary_mask/nodif_brain.nii.gz -ref ${workdir}/${Si}/DWI/data.nii.gz -out ${workdir}/${Si}/boundary_mask/nodif_brain.nii.gz -cost
mutualinfo;
14. done
15. echo " ***** Skull stripping of T1 *****"
16. _____
17. for i in `cat subjects.txt`;
18. do bet ${workdir}/${Si}/boundary_mask/MASK/T1.nii.gz ${workdir}/${Si}/boundary_mask/MASK/T1_brain.nii.gz -f 0.2 -B;
19. done

```

### Step 3-a. Registration of T1 to B0 when field map is available

The following cells runs the BBR of T1 to B0 when field map is available. If not, jump to *Step3-b*

```

1. echo " ***** Calculating matrix to move T1 to B0 using BBR *****"
2. _____
3. for i in `cat subjects.txt`;
4. do epi_reg -fmapmag=${workdir}/${Si}/T1/gre_field_mapping.nii --epi=${workdir}/${Si}/boundary_mask/nodif.nii.gz --t1=${workdir}/${Si}/boundary_mask/MASK/T1.nii.gz -
t1brain=${workdir}/${Si}/boundary_mask/MASK/T1_brain.nii.gz --pedir=-y --out=${workdir}/${Si}/boundary_mask/transform/epi_reg;
5. convert_xfm -omat ${workdir}/${Si}/boundary_mask/transform/T1_to_nodif_bbr.mat -inverse ${workdir}/${Si}/boundary_mask/transform/epi_reg.mat
6. flirt -in ${workdir}/${Si}/boundary_mask/MASK/T1.nii.gz -ref ${workdir}/${Si}/boundary_mask/nodif.nii.gz -out ${workdir}/${Si}/boundary_mask/MASK/T1_B0_bbr.nii.gz -
applyxfm -init ${workdir}/${Si}/boundary_mask/transform/T1_to_nodif_bbr.mat
7. done

```

### Step 3-b. Registration of T1 to B0 when field map is not available

The following cells runs the registration of T1 to B0 when field map is not available using BBR. This requires an initial segmentation of the T1 and estimation of a boundary mask that will then be used with a BBR cost function and a standard affine registration.

```

1. echo " ***** Segmentation in T1 and preparation of WM maps for BBR *****"
2. _____
3. for i in `cat subjects.txt`;
4. do 5ttgen -nocrop fsl ${workdir}/${Si}/SSDS/MASK/T1_brain.nii.gz ${workdir}/${Si}/SSDS/MASK/5ttseg.mif -premasked -force;
5. mtrtransform -interp nearest -template ${workdir}/${Si}/SSDS/MASK/T1_brain.nii.gz ${workdir}/${Si}/SSDS/MASK/5ttseg.mif ${workdir}/${Si}/SSDS/MASK/5ttseg2.mif -force;
6. mrconvert -coord 3 2 ${workdir}/${Si}/SSDS/MASK/5ttseg2.mif ${workdir}/${Si}/SSDS/MASK/wmseg.mif -force;
7. mrconvert ${workdir}/${Si}/SSDS/MASK/wmseg.mif ${workdir}/${Si}/SSDS/MASK/wmseg.nii.gz -force
8. done
9. #Boundary-based registration of T1 to B0
10. echo " ***** Calculating matrix to move T1 to B0 using BBR *****"
11. _____
12. for i in `cat subjects.txt`;
13. do
14. fslmaths ${workdir}/${Si}/SSDS/MASK/wmseg.nii.gz -bin ${workdir}/${Si}/SSDS/MASK/wmseg.nii.gz #binarize WM mask
15. flirt -dof 6 -in ${workdir}/${Si}/SSDS/nodif_brain.nii.gz -ref ${workdir}/${Si}/SSDS/MASK/T1_brain.nii.gz -omat ${workdir}/${Si}/SSDS/transform/nodif2T1.mat -interp
nearestneighbour; #estimate initial transform matrix from nodif to T1
16. done
17. for i in `cat subjects.txt`;
18. do flirt -dof 6 -in ${workdir}/${Si}/SSDS/nodif_brain.nii.gz -ref ${workdir}/${Si}/SSDS/MASK/T1_brain.nii.gz -out ${workdir}/${Si}/SSDS/MASK/nodif2T1_brain.nii.gz -wmseg
${workdir}/${Si}/SSDS/MASK/wmseg.nii.gz -init ${workdir}/${Si}/SSDS/transform/nodif2T1.mat -omat ${workdir}/${Si}/SSDS/transform/nodif2T1_bbr.mat -cost bbr -schedule
/usr/local/fsl/etc/flirtsch/bbr.sch;
# estimate transform matrix using BBR from nodif to T1
19. convert_xfm -omat ${workdir}/${Si}/SSDS/transform/T1_to_nodif_bbr.mat -inverse ${workdir}/${Si}/SSDS/transform/nodif2T1_bbr.mat
#reverse matrix to obtain transformation of T1 to nodif
20. flirt -in ${workdir}/${Si}/SSDS/MASK/T1_brain.nii.gz -ref ${workdir}/${Si}/SSDS/nodif_brain.nii.gz -out ${workdir}/${Si}/SSDS/MASK/T1_B0_bbr.nii.gz -applyxfm -init
${workdir}/${Si}/SSDS/transform/T1_to_nodif_bbr.mat
#apply BBR matrix to T1 image to move ot to nodif space and QC

```

21. done

#### Step 4. Now working in diffusion space to estimate a 1-erosion whole-brain boundary map

The following cells runs the segmentation of the T1 brain image in diffusion space before estimating a whole brain boundary mask, a mask of the WM/CSF and WM/GM boundaries. Whole brain boundary is SSDS\_B0. CSF boundary is SSDS\_B0\_csf, and GM boundary is SSDS\_B0\_gm. The last step exports the results in two separate CSV files.

```
1. for i in `cat subjects.txt`;
2. do 5ttgen -nocrop fsl ${workdir}/${Si}/SSDS/MASK/T1_B0_bbr.nii.gz ${workdir}/${Si}/SSDS/MASK/5ttseg_B0.mif -premasked -force;
3. mrtransform -interp nearest -template ${workdir}/${Si}/SSDS/nodif_brain.nii.gz ${workdir}/${Si}/SSDS/MASK/5ttseg_B0.mif ${workdir}/${Si}/SSDS/MASK/5ttseg2_B0.mif -
force;
4. mrconvert -coord 3 2 ${workdir}/${Si}/SSDS/MASK/5ttseg2_B0.mif ${workdir}/${Si}/SSDS/MASK/wmseg_B0.mif -force;
5. mrcalc ${workdir}/${Si}/SSDS/MASK/wmseg_B0.mif 0.5 -gt ${workdir}/${Si}/SSDS/MASK/wmseg_binary_B0.mif -force;
6. maskfilter ${workdir}/${Si}/SSDS/MASK/wmseg_binary_B0.mif connect ${workdir}/${Si}/SSDS/MASK/wmseg_bin_connected_B0.mif -largest -force;
7. maskfilter ${workdir}/${Si}/SSDS/MASK/wmseg_bin_connected_B0.mif erode ${workdir}/${Si}/SSDS/MASK/wmseg_bin_eroded_B0.mif -force;
8. mrcalc ${workdir}/${Si}/SSDS/MASK/wmseg_bin_connected_B0.mif ${workdir}/${Si}/SSDS/MASK/wmseg_bin_eroded_B0.mif -sub
${workdir}/${Si}/SSDS/MASK/wmseg_bin_diff_B0.mif -force;
9. mrconvert ${workdir}/${Si}/SSDS/MASK/wmseg_bin_diff_B0.mif ${workdir}/${Si}/SSDS/MASK/SSDS_B0.nii.gz -force;
10. mrconvert ${workdir}/${Si}/SSDS/MASK/wmseg_B0.mif ${workdir}/${Si}/SSDS/MASK/wmseg_B0.nii.gz -force;
11. fsmaths ${workdir}/${Si}/SSDS/MASK/wmseg_B0.nii.gz -thr 0.99 -bin ${workdir}/${Si}/SSDS/MASK/wmseg_B0.nii.gz ;
12. done
13. echo "BOUNDARY MASKS READY"
```

#### 14. echo "Estimating CSF and GM boundaries in WM map"

```
15. for i in `cat subjects.txt`;
16. do fsmaths ${workdir}/${Si}/SSDS/boundaries_2_B0/csfseg_B0.nii.gz -dilM ${workdir}/${Si}/SSDS/boundaries_2_B0/csfseg_B0_dil.nii.gz
17. fsmaths ${workdir}/${Si}/SSDS/boundaries_2_B0/gmseg_B0.nii.gz -sub ${workdir}/${Si}/SSDS/boundaries_2_B0/csfseg_B0_dil.nii.gz
${workdir}/${Si}/SSDS/boundaries_2_B0/gmseg_B0_nocsf.nii.gz
18. fsmaths ${workdir}/${Si}/SSDS/boundaries_2_B0/gmseg_B0_nocsf.nii.gz -thr 0 -uthr 1 -bin ${workdir}/${Si}/SSDS/boundaries_2_B0/gmseg_B0_nocsf.nii.gz
19. fsmaths ${workdir}/${Si}/SSDS/boundaries_2_B0/SSDS_B0.nii.gz -mas ${workdir}/${Si}/SSDS/boundaries_2_B0/csfseg_B0_dil.nii.gz
${workdir}/${Si}/SSDS/boundaries_2_B0/SSDS_B0_csf.nii.gz
20. fsmaths ${workdir}/${Si}/SSDS/boundaries_2_B0/SSDS_B0_csf.nii.gz -sub ${workdir}/${Si}/SSDS/boundaries_2_B0/SSDS_B0_csf.nii.gz
${workdir}/${Si}/SSDS/boundaries_2_B0/SSDS_B0_gm.nii.gz
21. fsmaths ${workdir}/${Si}/SSDS/boundaries_2_B0/SSDS_B0_gm.nii.gz -thr 0 -uthr 1 -bin ${workdir}/${Si}/SSDS/boundaries_2_B0/SSDS_B0_gm.nii.gz
22. Done

23. for i in `cat subjects.txt`;do stats=`fslstats $(i)/DWI/dti_FA.nii.gz -k ${workdir}/${Si}/SSDS/boundaries_2_B0/SSDS_B0_gm.nii.gz -M`;echo
${workdir}/${Si}/SSDS/boundaries_2_B0/SSDS_B0_gm.nii.gz $(i) $(stats);done>FA_results_GM_boundary.csv;
24. for i in `cat subjects.txt`;do stats=`fslstats $(i)/DWI/dti_FA.nii.gz -k ${workdir}/${Si}/SSDS/boundaries_2_B0/SSDS_B0_csf.nii.gz -M`;echo
${workdir}/${Si}/SSDS/boundaries_2_B0/SSDS_B0_csf.nii.gz $(i) $(stats);done>FA_results_CSF_boundary.csv
```

```
25. for i in `cat subjects.txt`;do stats=`fslstats $(i)/DWI/dti_FA.nii.gz -k ${workdir}/${Si}/SSDS/boundaries_2_B0/SSDS_B0.nii.gz -M`;echo
${workdir}/${Si}/SSDS/boundaries_2_B0/SSDS_B0_csf.nii.gz $(i) $(stats);done>FA_results_boundary.csv
```

#### Step 5. Non-linear registration of MNI152 template to diffusion space

This step creates a non-linear warp to estimate the registration of the template to the native diffusion space. This template will later be used to move the tracts to the diffusion space.

```
1. echo "***** Create transformation matrix to move T1 to JHU - nonlinear *****"
2.

3. for i in `cat subjects.txt`;
4. do flirt -in ${workdir}/${Si}/SSDS/MASK/T1_brain.nii.gz -ref ${standard}/MNI152_T1_1mm_brain.nii.gz -omat ${workdir}/${Si}/SSDS/transform/T1_2_MNI_aff_brain.mat -
interp nearestneighbour;
5. fnirt -in=${workdir}/${Si}/SSDS/MASK/T1_brain.nii.gz --ref=${standard}/MNI152_T1_1mm_brain.nii.gz --iout=${workdir}/${Si}/SSDS/MASK/T1_2_MNI_aff_diff_brain.nii.gz --
aff=${workdir}/${Si}/SSDS/transform/T1_2_MNI_aff_brain.mat --
refmask=/Users/aa6616/Desktop/All_data/My_project/TEDS/Boundaries/MNI152_T1_1mm_brain_mask.nii.gz --
cout=${workdir}/${Si}/SSDS/transform/T1_2_MNI_brain.nii.gz
6. done
7.

8. echo "***** Inverse warp (from T1 -> MNI to MNI -> T1) *****"
9.
```

```

10. for i in `cat subjects.txt`;
11. do inwarp --ref=${workdir}/${Si}/SSDS/MASK/T1_brain.nii.gz --warp=${workdir}/${Si}/SSDS/transform/T1_2_MNI_brain.nii.gz --
    out=${workdir}/${Si}/SSDS/transform/MNI_2_T1_brain.nii.gz;
12. done

```

#### Step 6. Non-linear registration of tracts to diffusion space

This step uses the non-linear warp previously estimated to move the tracts from standard space to native diffusion space. The tracts used are initially eroded. Once registered, they are further thresholded and cross masked with the WM map to ensure exclusion of partial volume

```

1.  echo "Moving JHU tracts to native diffusion"

# Create tract directory in main subject directories
2.  for i in `cat subjects.txt`;
3.  do
4.  for f in `cat ${tractdir}/tracts.txt`;
5.  do mkdir ${workdir}/${Si}/SSDS/tracts_ero/;
6.  cp ${tractdir}/${f}.nii.gz ${workdir}/${Si}/SSDS/tracts_ero/;
7.  done
8.  done

#Warp tracts from MNI to B0 and den tracts
9.  for i in `cat subjects.txt`;
10. do
11. for f in `cat ${tractdir}/tracts.txt`
12. do applywarp --ref=${workdir}/${Si}/SSDS/nodif_brain.nii.gz --in=${tractdir}/${f} --warp=${workdir}/${Si}/SSDS/transform/MNI_2_T1_brain.nii.gz --
    postmat=${workdir}/${Si}/SSDS/transform/T1_to_nodif_bbr.mat --out=${workdir}/${Si}/SSDS/boundaries_2_B0/tracts/${f}_B0 --interp=nn;
13. fslmaths ${workdir}/${Si}/SSDS/MASK/SSDS_B0.nii.gz -mul ${workdir}/${Si}/SSDS/tracts_ero/${f}_B0.nii.gz ${workdir}/${Si}/SSDS/tracts_ero/${f}_edge #cross-mask with
    boundary mask
14. fslmaths ${workdir}/${Si}/SSDS/MASK/wmseg_B0.nii.gz -mul ${workdir}/${Si}/SSDS/tracts_ero/${f}_B0 ${workdir}/${Si}/SSDS/tracts_ero/${f}_B0_WM;
15. fslmaths ${workdir}/${Si}/SSDS/tracts_ero/${f}_B0_WM -thr 0.99 ${workdir}/${Si}/SSDS/tracts_ero/${f}_B0_WM_0.99;
16. fslmaths ${workdir}/${Si}/SSDS/tracts_ero/${f}_B0_WM_0.99 -bin ${workdir}/${Si}/SSDS/tracts_ero/${f}_center;
17. done
18. done

```

#### Step 7. Cleaning up unwanted files

```

1.  echo "moving temporary files to tmp folder"
2.  for i in `cat subjects.txt`;
3.  do mv ${workdir}/${Si}/SSDS/tracts_ero/*T1_bin.nii.gz ${workdir}/${Si}/SSDS/tmp_files
4.  mv ${workdir}/${Si}/SSDS/tracts_ero/*warp.nii.gz ${workdir}/${Si}/SSDS/tmp_files
5.  mv ${workdir}/${Si}/SSDS/tracts_ero/*dil.nii.gz ${workdir}/${Si}/SSDS/tmp_files
6.  mv ${workdir}/${Si}/SSDS/MASK/*.*.mif ${workdir}/${Si}/SSDS/tmp_files
7.  mv ${workdir}/${Si}/SSDS/tracts_ero/*thr* ${workdir}/${Si}/SSDS/tmp_files
8.  mv ${workdir}/${Si}/SSDS/tracts_ero/*bin* ${workdir}/${Si}/SSDS/tmp_files
9.  mv ${workdir}/${Si}/SSDS/tracts_ero/*WM* ${workdir}/${Si}/SSDS/tmp_files
10. mv ${workdir}/${Si}/SSDS/tracts_ero/*sm* ${workdir}/${Si}/SSDS/tmp_files
11. done

```

#### Step 8. Pull data for statistics

This step pulls the mean FA from each estimated tract.

```

1.  echo "*****"
2.  * ALL DONE: *
3.  * NOW EXTRACTING FA VALUES *
4.  *****

5.  for i in `cat subjects.txt`;
6.  do cd ${workdir}/${Si}/SSDS/tracts_ero/ &&
7.  ls *center.nii.gz>> tracts_center.txt

```

```

8. cd $(workdir)
9. done

10. for i in `cat subjects.txt`;do for roi in `cat ${workdir}/${Si}/SSDS/tracts_ero/tracts_center.txt`;do stats=`fslstats $(i)/DWI/dti_FA.nii.gz -k ${workdir}/${Si}/SSDS/tracts_ero/${roi}
-M -S`;echo ${workdir}/${Si}/SSDS/tracts_ero/${roi} ${i} ${stats};done;done>FA_results.csv;
11.
12. echo " * ~~~~~COMPLETED~~~~~ * "
13. done

```

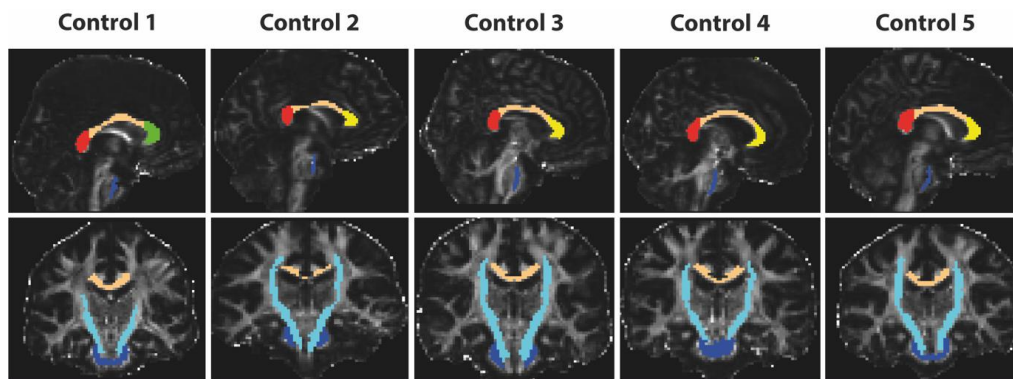
### 1.8.10. A.3.2. Tracts from the JHU atlas

Supplementary Table 1: Tracts from the JHU atlas and their abbreviation.

Abbreviation	Tract	Abbreviation	Tract
AIC-L	Anterior limb of internal capsule L	ML-L	Medial lemniscus L
AIC-R	Anterior limb of internal capsule R	ML-R	Medial lemniscus R
ACR-L	Anterior corona radiata L	MCP	Middle cerebellar peduncle
ACR-R	Anterior corona radiata R	PCT	Pontine Crossing Tract
BCC	Body of corpus callosum	PLIC-L	Posterior limb of internal capsule L
Cerebral Ped L	Cerebral peduncle L	PLIC-R	Posterior limb of internal capsule R
Cerebral Ped R	Cerebral peduncle R	PCR-L	Posterior corona radiata L
CG-L	Cingulum gyrus L	PCR-R	Posterior corona radiata R
CG-R	Cingulum gyrus R	PTR-L	Posterior thalamic radiation L
CGH-L	Cingulum parahippocampal L	PTR-R	Posterior thalamic radiation R
CGH-R	Cingulum parahippocampal R	RIC-L	Retrofrenticular part of internal capsule L
CS-L	Corticospinal L	RIC-R	Retrofrenticular part of internal capsule R
CS-R	Corticospinal R	SCC	Splenium of corpus callosum
EC-L	External capsule L	SS-L	Sagittal Stratum L
EC-R	External capsule R	SS-R	Sagittal Stratum R
FST-L	Fornix stria terminalis L	SCP-L	Superior cerebellar peduncle L
FST-R	Fornix stria terminalis R	SCP-R	Superior cerebellar peduncle R
FC-L	Fornix cres L	SCR-L	Superior corona radiata L
FC-R	Fornix cres R	SCR-R	Superior corona radiata R
Fornix	Fornix	SFOF-L	Superior fronto-occipital fasciculus L

GCC	Genu of Corpus Callosum	SFOF-R	Superior fronto-occipital fasciculus R
IFOF-L	Inferior fronto-occipital fasciculus/ Sagittal stratum ILF IFOF L	SLF-L	Superior longitudinal fasciculus L
IFOF-R	Inferior fronto-occipital fasciculus/ Sagittal stratum ILF IFOF R	SLF-R	Superior longitudinal fasciculus R
ILF-L	Inferior longitudinal fasciculus L	Tapetum L	Tapetum L
ILF-R	Inferior longitudinal fasciculus R	Tapetum R	Tapetum R
ICP-L	Inferior cerebellar peduncle L	UF-L	Uncinate fasciculus L
ICP-R	Inferior cerebellar peduncle R	UF-R	Uncinate fasciculus R

### 1.8.11. A.3.3. Segmentation example



**Supplementary Figure 1: Segmentation of 5 different tracts. Red= splenium of corpus callosum, Orange= body of corpus callosum, Green= genu of corpus callosum, Light Blue= corticospinal tract left and right, Dark Blue= middle cerebellar peduncle. Slices are different for each subject.**

## A.4. APPENDIX OF CHAPTER 4

### 1.8.12. A.4.1. ROI mean FA results

Supplementary Table 2: Mean FA results for all ROI following TBSS, SSDS, and boundary segmentation. nbTBI= non blast TBI, bTBI= blast TBI, BCC= body of corpus callosum, GCC= genu of corpus callosum, SCC= splenium of corpus callosum, MCP= middle cerebellar peduncle, ILF=inferior longitudinal fasciculus, L= left, R= right, WM= white matter, GM= grey matter. Significance values: \*p<0.05, \*\*p<0.01, \*\*\*p<0.001.

	One-way ANOVA	Post-hoc Tukey's HSD		
	F value p value	nbTBI vs Controls	bTBI vs Controls	nbTBI vs bTBI
<b>TBSS</b>				
Anterior limb of internal capsule L	3.16 0.06	0.37	0.06	0.38
Anterior limb of internal capsule R	2.51 0.08	0.27	0.08	0.70
BCC	1.71 0.19	0.33	0.21	0.99
GCC	4.37 <b>0.02 *</b>	<b>0.03 *</b>	<b>0.05 *</b>	0.98
SCC	1.83 0.17	0.17	0.35	0.93
MCP	0.19 0.17	0.67	0.13	0.48
Corticospinal R	1.17 0.19	0.39	0.18	0.86
Corticospinal L	4.27 <b>0.02 *</b>	<b>0.05 *</b>	<b>0.02 *</b>	0.92
Cerebral peduncle L	2.42 0.10	0.36	0.08	0.60
Cerebral peduncle R	2.61 0.08	0.52	0.07	0.37
Cingulum L	1.88 0.16	0.54	0.13	0.57
Cingulum R	1.52 0.23	0.73	0.20	0.51
ILF L	5.00 <b>0.01 *</b>	<b>0.03 *</b>	<b>0.01 *</b>	0.94
ILF R	5.66 <b>0.006 **</b>	<b>0.007 **</b>	<b>0.03 *</b>	0.92
Corona radiata L	5.25 <b>0.008 **</b>	<b>0.02 *</b>	<b>0.02 *</b>	1.00
Corona radiata R	3.30 <b>0.04 *</b>	0.1	0.06	0.93
Uncinate fasciculus L	1.13 0.33	0.61	0.29	0.78
Uncinate fasciculus R	1.10 0.34	0.58	0.31	0.83
Mean FA skeleton	3.50 <b>0.04 *</b>	<b>0.05 *</b>	<b>0.03 *</b>	0.99
<b>SSDS</b>				
Anterior limb of internal capsule L	3.43 <b>0.04 *</b>	0.46	<b>0.03 *</b>	0.31
Anterior limb of internal capsule R	4.57 <b>0.01 *</b>	0.20	<b>0.01 *</b>	0.37
BCC	4.19 <b>0.02 *</b>	0.23	<b>0.02 *</b>	0.4

GCC	3.71 0.01 *	0.03 *	0.03 *	0.80		
SCC	4.48 0.02 *	0.09	0.03 *	0.66		
MCP	5.18 0.009 **	0.99	0.02 *	0.02 *		
Corticospinal R	3.73 0.03 *	0.91	0.04 *	0.08		
Corticospinal L	4.25 0.02 *	0.49	0.01 *	0.17		
Cerebral peduncle L	0.53 0.59	0.73	0.59 0.590518	0.97 0.59684215	0.59684215	0.968421
Cerebral peduncle R	2.00 0.14	0.84	0.14 0.13751	0.34 0.3353772	0.3353772	0.335377
Cingulum L	10.85 < 0.001 ***	<0.001 ***	0.000277***	0.90 0.000277665	0.000277665	0.901665
Cingulum R	5.82 0.005 **	0.040 *	0.005 ** 0.0048156	0.63 0.0048156	0.0048156	0.627513
ILF L	5.02 0.01 *	0.3	0.007 **	0.19		
ILF R	10.53 < 0.001 ***	0.02 *	< 0.001 ***	0.14		
Corona radiata L	7.30 < 0.001 ***	0.12	< 0.001 ***	0.11		
Corona radiata R	8.11 < 0.001 ***	0.16	< 0.001 ***	0.07		
Uncinate fasciculus L	0.77 0.47	0.99	0.50	0.57		
Uncinate fasciculus R	2.48 0.09	0.76	0.08	0.29		
WM Boundary						
Whole brain WM / CSF	2.98 0.05 *	0.07	0.05 *	0.44		
BCC WM / CSF	1.63 0.21	0.96	0.22	0.33		
GCC WM / CSF	0.78 0.46	0.56	0.49	0.99		
SCC WM / CSF	1.81 0.17	0.29	0.19	0.96		
MCP WM / CSF	4.79 0.01 **	0.86	0.02 *	0.04 *		
Whole brain WM / GM	3.43 0.04 *	0.06	0.05 *	0.99		
BCC WM / GM	4.56 0.01 **	0.09	0.01 **	0.67		
GCC WM / GM	3.62 0.03 *	0.08	0.04 **	0.96		
SCC WM / GM	4.36 0.02 *	0.25	0.01 **	0.33		
MCP WM / GM	1.00 0.38	0.86	0.67	0.33		



## A.5. APPENDIX OF CHAPTER 5

### 1.8.13. A.5.1. Effect of clinical characteristics on ROI measures

**Supplementary Table 3: Effect of clinical characteristics on ROI measures within the bTBI group. Presence refers to soldiers with the characteristic, and absence refers to soldiers without the characteristics.**

Hippocampal TCV			
	Presence n (Mean $\pm$ SD)	Absence n (Mean $\pm$ SD)	Unpaired t-test
Microbleed	11 (7.61 $\pm$ 0.50)	8 (7.49 $\pm$ 0.44)	t= 0.54 p= 0.59
Contusion	8 (7.60 $\pm$ 0.47)	11 (7.30 $\pm$ 0.32)	t= 1.66 p= 0.11
Pituitary dysfunction	6 (7.72 $\pm$ 0.36)	13 (7.46 $\pm$ 0.48)	t= 1.18 p= 0.26
Hypogonadism	4 (7.36 $\pm$ 0.42)	15 (7.59 $\pm$ 0.46)	t= 0.90 p= 0.38
Antidepressants	9 (7.61 $\pm$ 0.44)	10 (7.48 $\pm$ 0.48)	t= 0.61 p= 0.55
Opiate	9 (7.62 $\pm$ 0.49)	10 (7.47 $\pm$ 0.43)	t= 0.67 p= 0.51
Limb Amputation	8 (7.40 $\pm$ 0.37)	11 (7.65 $\pm$ 0.50)	t= 1.19 p= 0.25
PTA > 24 hours	13 (7.61 $\pm$ 0.69)	6 (7.68 $\pm$ 0.18)	t= 0.24 p= 0.81
Major organ damage	11 (7.60 $\pm$ 0.72)	8 (7.67 $\pm$ 0.32)	t= 0.25 p= 0.81
Fornix Mean FA			
Microbleed	11 (0.43 $\pm$ 0.08)	8 (0.42 $\pm$ 0.09)	t= 0.26 p= 0.80
Contusion	8 (0.41 $\pm$ 0.10)	11 (0.44 $\pm$ 0.07)	t= 0.77 p= 0.45
Pituitary dysfunction	6 (0.44 $\pm$ 0.07)	13 (0.38 $\pm$ 0.12)	t= 1.13 p= 0.27
Hypogonadism	4 (0.43 $\pm$ 0.10)	15 (0.41 $\pm$ 0.05)	t= 0.57 p= 0.57
Antidepressants	9 (0.42 $\pm$ 0.08)	10 (0.39 $\pm$ 0.10)	t= 0.72 p= 0.48
Opiate	9 (0.41 $\pm$ 0.08)	10 (0.43 $\pm$ 0.10)	t= 0.48 p= 0.64
Limb Amputation	8 (0.44 $\pm$ 0.09)	11 (0.44 $\pm$ 0.07)	t= 0.00 p= 1.00
PTA > 24 hours	13 (0.42 $\pm$ 0.09)	6 (0.43 $\pm$ 0.09)	t= 0.14 p= 0.89
Major organ damage	11 (0.41 $\pm$ 0.09)	8 (0.45 $\pm$ 0.08)	t= 1.08 p= 0.29
Cingulum bilaterally Mean FA			
Microbleed	11 (0.35 $\pm$ 0.08)	8 (0.38 $\pm$ 0.11)	t= 0.69 p= 0.50
Contusion	8 (0.36 $\pm$ 0.06)	11 (0.40 $\pm$ 0.07)	t= 1.30 p= 0.21
Pituitary dysfunction	6 (0.39 $\pm$ 0.09)	13 (0.34 $\pm$ 0.13)	t= 0.84 p= 0.41
Hypogonadism	4	15	t= 0.13

	(0.37 ± 0.11)	(0.38 ± 0.14)	p= 0.90
<b>Antidepressants</b>	9 (0.40 ± 0.06)	10 (0.34 ± 0.11)	t= 1.45 p= 0.16
<b>Opiate</b>	9 (0.41 ± 0.10)	10 (0.33 ± 0.10)	t= 1.74 p= 0.09
<b>Limb Amputation</b>	8 (0.37 ± 0.10)	11 (0.37 ± 0.11)	t= 0.00 p= 1.00
<b>PTA &gt; 24 hours</b>	13 (0.38 ± 0.11)	6 (0.36 ± 0.07)	t= 0.67 p= 0.43
<b>Major organ damage</b>	11 (0.36 ± 0.12)	8 (0.39 ± 0.07)	t= 0.54 p= 0.59

### 1.8.14. A.5.2. Medication Details

**Supplementary Table 4: List of medications used by soldiers. MST: morphine sulphate.**

**Adapted from (Baxter et al., 2013)**

Subjects	Medications
M01	Amitriptyline, Diclofenac, MST, Phenytoin
M02	Diclofenac, Sertraline, Tramadol
M03	Amitriptyline, Erythromycin, Gabapentin
M04	C0-codamol
M05	Diclofenac, Tramadol
M07	None
M08	Diclofenac, Lansoprazole, MST, Paracetamol, Pregabalin, Tramadol
M09	Amitriptyline, MST, Nebido, Pregabalin
M10	Betnovate ointment, Co-codamol
M11	None
M12	Amitriptyline, Diclofenac, Nebido, Pregabalin, Ranitidine, Sildenafil, Tramadol
M13	Amitriptyline, Baclofen, Pregabalin
M14	Amitriptyline, Diclofenac, Fluoxetine, Mirazepine, MST, Paracetamol, Pregabalin, Salbutamol inhaler, Zopiclone
M15	Amitriptyline, Nebido, Pregabalin, Tramadol
M16	Mirtazepine, Paracetamol, Pregabalin, Tramadol, Zopiclone
M17	None
M18	Nebido
M19	Diclofenac, Pregabalin, Ranitidine
M20	Sertraline, Zopiclone

Details of all supplementary methods can be found in (Baxter et al., 2013).

## A.5. APPENDIX OF CHAPTER 6

### 1.8.15. A.5.1. Demographics of TBI patients

Age	Gender	Cause	PTA	Neuroradiological abnormalities
38	M	violence/assault	2 days	Microbleeds
51	F	incident fall	2 days	No
31	M	RTA	90 days	Both
20	M	incident fall	28 days	Microbleeds
36	M	violence/assault	3 days	Contusions
44	M	RTA	90 days	Both
51	M	RTA	several weeks	Both
64	M	RTA	few hours to a day	Contusions
58	M	RTA	1 month	Contusions
34	M	other	6 weeks	Both
45	M	RTA	2 weeks	Microbleeds
20	M	RTA	2 months	Both
52	M	RTA	5 days	Microbleeds
45	M	other	14 days	No
31	M	violence/assault	months	Both
49	M	other	yes but unknown duration	Both
24	M	RTA	14 days	No
52	M	incident fall	21 days	Both
54	M	violence/assault	15 days	Both
26	M	violence/assault	56 days	Contusions
21	F	RTA	35 days	Microbleeds
39	F	incident fall	2 days	Both
47	M	RTA	3 days	Both
22	M	RTA	450 days	Contusions
34	M	incident fall	0 days	Contusions
48	M	RTA	60 days	Contusions
38	M	violence/assault	700 days	No
49	F	violence/assault	10 days	Both
36	F	RTA	120 days	Microbleeds
43	M	RTA	42 days	Contusions
31	M	violence/assault	21 days	Contusions
37	M	incident fall	120 days	Both
33	M	RTA	30 days	Both
35	M	incident fall	7 days	Contusions

33	M	RTA	28 days	Contusions
52	M	violence/assault	4 days	Both
38	M	violence/assault	14 days	Both
31	M	RTA	120 days	Both
24	F	RTA	120 days	Contusions
42	M	RTA	unknown	No
37	M	RTA	4 days	Contusions
6	M	incident fall	4-6 hours	No
57	F	incident fall	1-7 days	Both
54	M	incident fall	2 days	Contusions
39	M	RTA	unknown	Microbleeds
44	M	RTA	6 days	Both
48	M	violence/assault	24-48 hours	No
59	M	RTA	1-7 days	Contusions
37	M	incident fall	1 days	Contusions
26	M	RTA	3 days	Both
24	M	RTA	unknown	Contusions
39	M	violence/assault	3 weeks	Contusions
53	M	incident fall	unknown	Both
29	F	RTA	still in PTA	Both
51	M	unknown	unknown	Both
52	M	Incident fall	24-48 hours	Contusions
57	M	RTA	4 days	Contusions
34	M	unknown	3 days	Contusions
49	F	incident fall	24-48 hours	Microbleeds
39	M	unknown	7 days	Both
44	F	RTA	unknown	Both
49	M	RTA	unknown	Contusions
61	F	RTA	120 days	Contusions
39	F	RTA	unknown	Contusions
49	M	unknown	unknown	No
72	M	unknown	unknown	Both
40	F	RTA	unknown	Contusions
65	M	incident fall	14 days	Contusions
40	M	RTA	42 days	Contusions
54	M	RTA	10 days	Contusions
42	F	RTA	3 days	No
56	F	RTA	several months	Both
40	F	unknown	unknown	Microbleeds
31	M	incident fall	unknown	No
43	M	RTA	unknown	Contusions
39	M	RTA	unknown	No
57	M	RTA	unknown	No

31	F	unknown	unknown	No
38	M	unknown	unknown	No
51	M	incident fall	unknown	Contusions
54	M	RTA	1 days	Both
46	F	incident fall	4 weeks	Contusions
43	M	RTA	no	Microbleeds
55	M	violence/assault	4 days	Contusions
48	M	RTA	no	Contusions

**Supplementary Table 5: TBI demographics. RTA= road traffic accident, M=male, F=female.**

### 1.8.16. A.5.2. Results from SSDS

**Supplementary Table 6: Results from SSDS in TBI (n=85) vs controls(n=100).**

Tract	Controls		TBI	
	Mean	SD	Mean	SD
Anterior corona radiata L	0.44	0.06	0.39	0.05
Anterior corona radiata R	0.44	0.06	0.39	0.05
Anterior limb of internal capsule L	0.64	0.07	0.64	0.07
Anterior limb of internal capsule R	0.63	0.08	0.64	0.06
BCC	0.74	0.06	0.63	0.13
Cerebral peduncle L	0.69	0.07	0.65	0.07
Cerebral peduncle R	0.70	0.06	0.68	0.07
Cingulum CG L	0.58	0.07	0.46	0.13
Cingulum CG R	0.56	0.08	0.46	0.12
Cingulum L	0.52	0.08	0.50	0.08
Cingulum R	0.56	0.08	0.46	0.12
Corticospinal L	0.61	0.04	0.60	0.03
Corticospinal R	0.62	0.04	0.61	0.04
External capsule L	0.55	0.06	0.50	0.07
External capsule R	0.52	0.06	0.47	0.07
Fornix Stria Terminalis L	0.65	0.08	0.57	0.09
Fornix Stria Terminalis R	0.64	0.07	0.57	0.11
GCC	0.59	0.10	0.47	0.13
Inf longitudinal fasc L	0.50	0.05	0.45	0.06
Inf longitudinal fasc R	0.57	0.06	0.52	0.07
Medial lemniscus L	0.52	0.08	0.52	0.09
Medial lemniscus R	0.52	0.08	0.53	0.10
Middle cerebellar peduncle	0.58	0.05	0.59	0.04
Pontine Crossing Tract	0.47	0.05	0.49	0.06
Posterior corona radiata L	0.47	0.03	0.46	0.05
Posterior corona radiata R	0.48	0.04	0.47	0.06
Posterior limb of internal capsule L	0.69	0.05	0.69	0.04
Posterior limb of internal capsule R	0.68	0.05	0.70	0.04
Posterior thalamic radiation L	0.63	0.07	0.69	0.04
Posterior thalamic radiation R	0.64	0.06	0.70	0.04
Retrolenticular internal capsule L	0.64	0.06	0.58	0.08
Retrolenticular internal capsule R	0.61	0.05	0.60	0.08
Inferior fronto-occipital fasciculus L	0.62	0.07	0.61	0.06
Inferior fronto-occipital fasciculus R	0.63	0.07	0.60	0.04
Sagittal Stratum L	0.62	0.07	0.57	0.09
Sagittal Stratum R	0.63	0.07	0.59	0.07
SCC	0.78	0.04	0.57	0.09
Superior cerebellar peduncle L	0.75	0.08	0.59	0.07
Superior cerebellar peduncle R	0.73	0.09	0.68	0.14
Superior corona radiata L	0.51	0.04	0.72	0.08

**Supplementary Table 7: Results from SSDS within the TBI for RTA (n=43) vs other types of injuries (n=42).**

Tract	Other		RTA	
	Mean	SD	Mean	SD
ACR	0.39	0.04	0.39	0.05
AIC	0.64	0.04	0.64	0.06
BCC	0.63	0.13	0.63	0.13
Cerebral ped	0.66	0.05	0.68	0.06
CG	0.47	0.13	0.46	0.12
CS	0.6	0.03	0.61	0.03
EC	0.49	0.06	0.49	0.07
Fornix	0.56	0.09	0.57	0.08
GCC	0.46	0.12	0.48	0.14
IFOF	0.58	0.08	0.58	0.07
ILF	0.48	0.06	0.49	0.05
MCP	0.58	0.05	0.6	0.04
ML	0.52	0.09	0.53	0.1
PCR	0.46	0.04	0.47	0.05
PCT	0.48	0.06	0.49	0.06
PLIC	0.69	0.04	0.7	0.04
PTR	0.59	0.08	0.59	0.07
RIC	0.61	0.05	0.6	0.04
SCC	0.67	0.15	0.68	0.13
SCP	0.71	0.08	0.71	0.08
SCR	0.48	0.05	0.5	0.05
SLF	0.54	0.06	0.56	0.05
SS	0.58	0.08	0.58	0.07

**Supplementary Table 8: Results from SSDS within the TBI for presence of focal injuries (contusions/microbleeds) (n=14) vs no focal injuries (n=71).**

Tract	Neuroradiological abnormalities		No Neuroradiological abnormalities	
	Mean	SD	Mean	SD
ACR	0.39	0.04	0.40	0.04
AIC	0.63	0.05	0.66	0.03
BCC	0.62	0.14	0.68	0.07
Cerebral ped	0.67	0.06	0.67	0.05
CG	0.45	0.12	0.53	0.09
CS	0.60	0.03	0.60	0.03
EC	0.48	0.06	0.53	0.05
Fornix	0.56	0.09	0.62	0.08
GCC	0.47	0.14	0.50	0.10
IFOF	0.57	0.08	0.60	0.07
ILF	0.48	0.06	0.51	0.04
MCP	0.59	0.04	0.58	0.05

<b>ML</b>	0.53	0.09	0.51	0.12
<b>PCR</b>	0.47	0.05	0.46	0.06
<b>PCT</b>	0.49	0.06	0.49	0.05
<b>PLIC</b>	0.70	0.04	0.69	0.03
<b>PTR</b>	0.58	0.08	0.62	0.07
<b>RIC</b>	0.60	0.04	0.62	0.04
<b>SCC</b>	0.67	0.14	0.71	0.11
<b>SCP</b>	0.71	0.08	0.75	0.05
<b>SCR</b>	0.49	0.05	0.48	0.05
<b>SLF</b>	0.55	0.06	0.56	0.05
<b>SS</b>	0.57	0.08	0.60	0.07

### 1.8.17. A.5.3. Decision Tree Statistics for TBI vs Controls

```

CP nsplit rel error  xerror  xstd
1 0.52941176  0 1.0000000 1.0000000 0.08915787
2 0.11764706  1 0.4705882 0.6470588 0.08177174
3 0.05882353  2 0.3529412 0.4852941 0.07446739
4 0.04411765  3 0.2941176 0.4852941 0.07446739
5 0.04000000  5 0.2058824 0.5147059 0.07602098

```

Variable importance

```

BCCeroalignedcenter.nii.gz      CingulumCGR      CingulumR
      19              13              13
      SCC      CingulumCGL      GCC
      12              10              8
FornixStriaTerminalisL      CorticospinalL      Infflongitudinalfascl
      7              3              3
      ExternalcapsuleR      AnteriorcoronaradiataL      AnteriorcoronaradiataR
      3              2              2
PosteriorcoronaradiataL      SuperiorcoronaradiataR      PosteriorthalamicradiationL
      1              1              1
      CerebralpeduncleL      PosteriorcoronaradiataR
      1              1

```

Node number 1: 148 observations, complexity param=0.5294118

predicted class=control expected loss=0.4594595 P(node) =1

class counts: 80 68

probabilities: 0.541 0.459

left son=2 (64 obs) right son=3 (84 obs)

Primary splits:

BCCeroalignedcenter.nii.gz < 0.735815 to the right, improve=25.22780, (0 missing)

CingulumCGL < 0.4941495 to the right, improve=24.53351, (0 missing)

SCC < 0.7563715 to the right, improve=21.23459, (0 missing)

AnteriorcoronaradiataR < 0.4129995 to the right, improve=19.29287, (0 missing)

FornixStriaTerminalisL < 0.640568 to the right, improve=19.24412, (0 missing)

Surrogate splits:

CingulumCGL < 0.5570925 to the right, agree=0.824, adj=0.594, (0 split)

CingulumCGR < 0.5608445 to the right, agree=0.777, adj=0.484, (0 split)

CingulumR < 0.5608445 to the right, agree=0.777, adj=0.484, (0 split)

GCC < 0.561039 to the right, agree=0.777, adj=0.484, (0 split)

SCC < 0.786882 to the right, agree=0.777, adj=0.484, (0 split)

Node number 2: 64 observations, complexity param=0.04411765

predicted class=control expected loss=0.125 P(node) =0.4324324

class counts: 56 8

probabilities: 0.875 0.125

left son=4 (59 obs) right son=5 (5 obs)

Primary splits:

CorticospinalL < 0.5755095 to the right, improve=4.942373, (0 missing)

AnteriorcoronaradiataL < 0.4011345 to the right, improve=3.882828, (0 missing)  
 CorticospinalR < 0.596043 to the right, improve=3.333333, (0 missing)  
 PosteriorcoronaradiataL < 0.4081555 to the right, improve=3.333333, (0 missing)  
 PosteriorcoronaradiataR < 0.4384035 to the right, improve=3.333333, (0 missing)  
 Surrogate splits:  
 PosteriorcoronaradiataL < 0.4011435 to the right, agree=0.953, adj=0.4, (0 split)  
 SuperiorcoronaradiataR < 0.4421085 to the right, agree=0.953, adj=0.4, (0 split)  
 CerebralpeduncleL < 0.6190795 to the right, agree=0.938, adj=0.2, (0 split)  
 PosteriorcoronaradiataR < 0.4152105 to the right, agree=0.938, adj=0.2, (0 split)

Node number 3: 84 observations, complexity param=0.1176471  
 predicted class=TBI expected loss=0.2857143 P(node) =0.5675676  
 class counts: 24 60  
 probabilities: 0.286 0.714  
 left son=6 (24 obs) right son=7 (60 obs)  
 Primary splits:  
 FornixStriaTerminalisL < 0.6377055 to the right, improve=9.752381, (0 missing)  
 SagittalstratumILFIFOFL < 0.5828255 to the right, improve=7.091418, (0 missing)  
 SagittalStratumL < 0.5828255 to the right, improve=7.091418, (0 missing)  
 CingulumCGL < 0.5031265 to the right, improve=6.269388, (0 missing)  
 CingulumCGR < 0.5307165 to the right, improve=6.268159, (0 missing)  
 Surrogate splits:  
 InflongitudinalfascL < 0.5128065 to the right, agree=0.774, adj=0.208, (0 split)  
 CingulumCGR < 0.5534505 to the right, agree=0.762, adj=0.167, (0 split)  
 CingulumR < 0.5534505 to the right, agree=0.762, adj=0.167, (0 split)  
 ExternalcapsuleR < 0.537873 to the right, agree=0.762, adj=0.167, (0 split)  
 PosteriorthalamicradiationL < 0.6703945 to the right, agree=0.762, adj=0.167, (0 split)

Node number 4: 59 observations  
 predicted class=control expected loss=0.06779661 P(node) =0.3986486  
 class counts: 55 4  
 probabilities: 0.932 0.068

Node number 5: 5 observations  
 predicted class=TBI expected loss=0.2 P(node) =0.03378378  
 class counts: 1 4  
 probabilities: 0.200 0.800

Node number 6: 24 observations, complexity param=0.05882353  
 predicted class=control expected loss=0.3333333 P(node) =0.1621622  
 class counts: 16 8  
 probabilities: 0.667 0.333  
 left son=12 (14 obs) right son=13 (10 obs)  
 Primary splits:  
 CingulumCGR < 0.5307165 to the right, improve=4.609524, (0 missing)  
 CingulumR < 0.5307165 to the right, improve=4.609524, (0 missing)  
 SuperiorcoronaradiataL < 0.5517215 to the left, improve=4.266667, (0 missing)  
 AnteriorcoronaradiataL < 0.3932835 to the right, improve=4.000000, (0 missing)  
 FornixStriaTerminalisR < 0.6502575 to the left, improve=3.200000, (0 missing)  
 Surrogate splits:  
 CingulumR < 0.5307165 to the right, agree=1.000, adj=1.0, (0 split)  
 AnteriorcoronaradiataL < 0.396246 to the right, agree=0.875, adj=0.7, (0 split)  
 AnteriorcoronaradiataR < 0.385622 to the right, agree=0.792, adj=0.5, (0 split)  
 BCCeroalignedcenter.nii.gz < 0.6963665 to the right, agree=0.792, adj=0.5, (0 split)  
 ExternalcapsuleR < 0.474758 to the right, agree=0.792, adj=0.5, (0 split)

Node number 7: 60 observations, complexity param=0.04411765  
 predicted class=TBI expected loss=0.1333333 P(node) =0.4054054  
 class counts: 8 52  
 probabilities: 0.133 0.867  
 left son=14 (5 obs) right son=15 (55 obs)  
 Primary splits:  
 SCC < 0.7859165 to the right, improve=4.848485, (0 missing)  
 InflongitudinalfascL < 0.537172 to the right, improve=3.108046, (0 missing)  
 SagittalstratumILFIFOFL < 0.5828255 to the right, improve=2.280460, (0 missing)  
 SagittalStratumL < 0.5828255 to the right, improve=2.280460, (0 missing)  
 CerebralpeduncleL < 0.7411485 to the right, improve=1.796491, (0 missing)



Surrogate splits:  
InflongitudinalfascL < 0.537172 to the right, agree=0.95, adj=0.4, (0 split)

Node number 12: 14 observations  
predicted class=control expected loss=0.07142857 P(node) =0.09459459  
class counts: 13 1  
probabilities: 0.929 0.071

Node number 13: 10 observations  
predicted class=TBI expected loss=0.3 P(node) =0.06756757  
class counts: 3 7  
probabilities: 0.300 0.700

Node number 14: 5 observations  
predicted class=control expected loss=0.2 P(node) =0.03378378  
class counts: 4 1  
probabilities: 0.800 0.200

Node number 15: 55 observations  
predicted class=TBI expected loss=0.07272727 P(node) =0.3716216  
class counts: 4 51  
probabilities: 0.073 0.927

### 1.8.18. A.5.4. Decision Tree Statistics for RTA vs Other Types of Injuries

Node number 1: 69 observations, complexity param=0.2647059  
predicted class=RTA expected loss=0.4927536 P(node) =1  
class counts: 34 35  
probabilities: 0.493 0.507  
left son=2 (53 obs) right son=3 (16 obs)  
Primary splits:  
Cerebralped < 0.7131178 to the left, improve=3.881905, (0 missing)  
SCP < 0.8024382 to the left, improve=3.014976, (0 missing)  
CS < 0.6096095 to the left, improve=2.254658, (0 missing)  
GCC < 0.569744 to the left, improve=1.959420, (0 missing)  
ML < 0.4502735 to the left, improve=1.922578, (0 missing)  
Surrogate splits:  
CS < 0.6410742 to the left, agree=0.812, adj=0.188, (0 split)  
Fornix < 0.6818 to the left, agree=0.812, adj=0.188, (0 split)  
MCP < 0.6580685 to the left, agree=0.812, adj=0.188, (0 split)  
ACR < 0.4561082 to the left, agree=0.797, adj=0.125, (0 split)  
SCC < 0.799411 to the left, agree=0.797, adj=0.125, (0 split)

Node number 2: 53 observations, complexity param=0.1764706  
predicted class=other expected loss=0.4150943 P(node) =0.7681159  
class counts: 31 22  
probabilities: 0.585 0.415  
left son=4 (37 obs) right son=5 (16 obs)  
Primary splits:  
SCP < 0.6738772 to the right, improve=3.401390, (0 missing)  
EC < 0.5044165 to the right, improve=2.478883, (0 missing)  
ILF < 0.5316678 to the right, improve=2.447477, (0 missing)  
SCC < 0.771218 to the right, improve=2.447477, (0 missing)  
PLIC < 0.6764447 to the right, improve=2.196455, (0 missing)  
Surrogate splits:  
RIC < 0.5734102 to the right, agree=0.830, adj=0.438, (0 split)  
IFOF < 0.553174 to the right, agree=0.830, adj=0.438, (0 split)  
SS < 0.553174 to the right, agree=0.830, adj=0.438, (0 split)  
AIC < 0.5879763 to the right, agree=0.811, adj=0.375, (0 split)  
EC < 0.408652 to the right, agree=0.811, adj=0.375, (0 split)

Node number 3: 16 observations  
predicted class=RTA expected loss=0.1875 P(node) =0.2318841  
class counts: 3 13

probabilities: 0.188 0.812

Node number 4: 37 observations, complexity param=0.08823529  
 predicted class=other expected loss=0.2972973 P(node)=0.5362319  
 class counts: 26 11  
 probabilities: 0.703 0.297  
 left son=8 (34 obs) right son=9 (3 obs)  
 Primary splits:  
 SCP < 0.8142445 to the left, improve=3.224165, (0 missing)  
 ILF < 0.4957638 to the left, improve=2.297969, (0 missing)  
 GCC < 0.569744 to the left, improve=2.192218, (0 missing)  
 Fornix < 0.5110372 to the left, improve=1.804287, (0 missing)  
 PCR < 0.432176 to the left, improve=1.804287, (0 missing)

Node number 5: 16 observations, complexity param=0.05882353  
 predicted class=RTA expected loss=0.3125 P(node)=0.2318841  
 class counts: 5 11  
 probabilities: 0.312 0.688  
 left son=10 (9 obs) right son=11 (7 obs)  
 Primary splits:  
 PCT < 0.4983495 to the right, improve=2.430556, (0 missing)  
 AIC < 0.5848405 to the left, improve=2.408333, (0 missing)  
 CG < 0.601576 to the right, improve=2.160714, (0 missing)  
 EC < 0.5049362 to the right, improve=2.160714, (0 missing)  
 ML < 0.4225765 to the left, improve=2.160714, (0 missing)  
 Surrogate splits:  
 AIC < 0.6011248 to the left, agree=0.812, adj=0.571, (0 split)  
 Fornix < 0.4424505 to the right, agree=0.750, adj=0.429, (0 split)  
 GCC < 0.3807665 to the right, agree=0.750, adj=0.429, (0 split)  
 ILF < 0.4914145 to the left, agree=0.750, adj=0.429, (0 split)  
 ML < 0.6118755 to the right, agree=0.750, adj=0.429, (0 split)

Node number 8: 34 observations  
 predicted class=other expected loss=0.2352941 P(node)=0.4927536  
 class counts: 26 8  
 probabilities: 0.765 0.235

Node number 9: 3 observations  
 predicted class=RTA expected loss=0 P(node)=0.04347826  
 class counts: 0 3  
 probabilities: 0.000 1.000

Node number 10: 9 observations, complexity param=0.05882353  
 predicted class=other expected loss=0.4444444 P(node)=0.1304348  
 class counts: 5 4  
 probabilities: 0.556 0.444  
 left son=20 (6 obs) right son=21 (3 obs)  
 Primary splits:  
 SCR < 0.4644008 to the right, improve=2.777778, (0 missing)  
 PTR < 0.5514633 to the right, improve=1.777778, (0 missing)  
 RIC < 0.54381 to the left, improve=1.777778, (0 missing)  
 CG < 0.353939 to the right, improve=1.587302, (0 missing)  
 PCT < 0.5962135 to the left, improve=1.587302, (0 missing)  
 Surrogate splits:  
 CS < 0.5803725 to the right, agree=0.889, adj=0.667, (0 split)  
 PCR < 0.4079322 to the right, agree=0.889, adj=0.667, (0 split)  
 PLIC < 0.6691218 to the right, agree=0.889, adj=0.667, (0 split)  
 SCC < 0.7414 to the left, agree=0.889, adj=0.667, (0 split)  
 ACR < 0.392917 to the right, agree=0.778, adj=0.333, (0 split)

Node number 11: 7 observations  
 predicted class=RTA expected loss=0 P(node)=0.1014493  
 class counts: 0 7  
 probabilities: 0.000 1.000

Node number 20: 6 observations  
 predicted class=other expected loss=0.1666667 P(node)=0.08695652

class counts: 5 1  
probabilities: 0.833 0.167

Node number 21: 3 observations  
predicted class=RTA expected loss=0 P(node) =0.04347826  
class counts: 0 3  
probabilities: 0.000 1.000

## Note from the Author

The bombs stopped 4 years before I was born. It had been 15 years of bloodshed, of bad news, of losing friends, searching for people, souvenirs and pets under the rubbles of what used to be called homes, of walking on the debris of the churches, schools and playgrounds. Our parents came out for the shelters after more than 15 years, with the hope of rebuilding Lebanon, of giving to their children the childhood and youth that had been taken away from them.

Then came our generation, who fell in love with this country, and grew up with the stories of the war. Somehow over the years, the fears of our parents became our drive, and their hopes our dreams. But opportunities were always lacking, and Lebanon never managed to shake off the scars and wounds of the war. We had to leave to find better opportunities, promising to come back home and contribute to the eternal rebuilding of a country still limping. Me? My promise was to fight for children with learning differences, destigmatize neurodiversity, become a neuroscientist and bring some of the experience and knowledge back with me.

When the Covid pandemic hit, I was in the UK alone, in the middle of my PhD studies. My loved ones were on different continents. And when the whole world was struggling with a sanitary problem, the place I call home was hit by its worst economic and financial collapse. I was waiting impatiently for the day I would fly home and hug my family after a long time apart. But suddenly, on the 4<sup>th</sup> of August, at 6.08pm, two days before my scheduled flight, everything went completely silent. The beautiful city of Beirut was hit by yet another tragedy. 217 people lost their life, 7,000 people bled on the streets and more than 300,000 people lost their homes, when the largest non-nuclear explosion in history hit Beirut's port. And then, for the next year and counting, things went from bad to worse, and the country has been enduring one of the worst crises the world has seen in over 150 years.

Although this thesis is about science, and advancing the field, please keep in mind that, for some people like myself, the victims of blasts can be friends, family, and an entire nation. They're people who manage to stay optimistic despite everything, and they're inspiring. I have focused my last 4 years on soldiers, and I believe so much more work is yet to be done, but the forgotten victims are often civilians, and they should be a part of the process. The echoes of the blasts resonate far beyond the initial explosion, and some wounds and scars can never heal. I hope this thesis and my research will be an important part in the overarching aim of giving every survivor of war, terror, explosions or bombing, whether civilian or soldier, a chance at a beautiful life.